STUDIES ON THE IONIC MASS TRANSFER IN THE BOUNDARY LAYER OF A VERTICAL PLANE CATHODE(Dissertation_全文)

AUTHOR(S):

Awakura, Yasuhiro

STUDIES ON THE IONIC MASS TRANSFER IN THE BOUNDARY LAYER OF A VERTICAL PLANE CATHODE

YASUHIRO AWAKURA

1977

STUDIES ON THE IONIC MASS TRANSFER IN THE BOUNDARY LAYER OF A VERTICAL PLANE CATHODE

by

YASUHIRO AWAKURA

Submitted to Kyoto University

in Partial Fulfilment of the Requirements

for the Degree of Doctor of Engineering

ABSTRACT

It was intended in the present work to study the ionic mass transfer and the natural convective flow in the vicinity of the surface of a vertical plane copper cathode during the electrolysis of the unstirred aqueous $CuSO_4$ and $CuSO_4$-H_2SO_4 solutions.

In the first place, the theoretical equations of the ionic mass transfer in the cathodic diffusion layer and the current distribution on the surface of a vertical plane cathode were derived, and the expressions with regard to the maximal velocity of natural convective flow, the concentration difference of ionic species between bulk-electrolyte and cathode surface, the thickness of diffusion layer and the resultant distribution of local cathodic current densities were obtained under various electrolytic conditions.

The velocity profile of upward natural convection along the surface of a vertical plane cathode installed in the unstirred aqueous 0.1M $CuSO_4$, 0.6M $CuSO_4$ and 0.6M $CuSO_4$-1.5M H_2SO_4 solutions was measured. The measurement was made at the cathodic current densities below one half of the cathodic limiting current density where the local current densities are uniform. The maximal velocity of natural convection, u_m, and the distance between cathode surface and the position of the maximal velocity,

τ, increased with the height from the lower edge of cathode. When the cathodic current density was raised, u_m increased and τ decreased at any height on the cathode.

In 0.1M $CuSO_4$ solution, u_m is lower than in 0.6M $CuSO_4$ solution, and it can not be explained from the change of property constants of both solutions. The parameter η which is the ratio of thickness of diffusion layer, δ_1, to τ is larger in 0.1M $CuSO_4$ solution, and it is indicated that δ_1 is larger in this solution because τ is virtually unvaried in both solutions. This larger δ_1-value in 0.1M $CuSO_4$ solution may be attributed to the higher diffusivity of $CuSO_4$ in the solution.

Furthermore, both u_m and τ were lower in 0.6M $CuSO_4$-1.5M H_2SO_4 solution as compared with the aqueous 0.6M $CuSO_4$ solution. The density distribution near the cathode surface in the above two solutions was calculated. From the comparison of the distribution of density in both solutions, it was suggested that the upward natural convection is depressed in the acidified $CuSO_4$ solution by the downward gravitational force due to the accumulated H^+ ion in the outer portion of the diffusion layer.

The concentration profile of $CuSO_4$ in the cathodic diffusion layer which is accompanied by the upward natural convection along the cathode surface was measured by holographic interferometry in aqueous 0.05M and 0.1M $CuSO_4$ solutions, respectively. The measurement was carried out at various heights from the lower edge of cathode. The cathodic current density was also varied.

Experimental results obtained at the current densities far lower than the limiting value were in good agreement with the theoretical value which was derived under the assumption that the distribution of the current density is uniform.

Furthermore the profile of the refractive index in the cathodic diffusion layer of an aqueous solution containing 0.05M $CuSO_4$ and 1.85M H_2SO_4 was measured at various heights from the lower edge of cathode and at various cathodic current densities up to the limiting value. The theoretical expression for the difference of the refractive index between cathode surface and bulk-electrolyte was derived. Experimental results were in good agreement with the theoretical value in the whole region of the cathodic current density up to the limiting value.

Measurement was also made with the aqueous solutions containing 1.85M H_2SO_4 and 0.01, 0.02, 0.03, 0.04 and 0.05M $CuSO_4$, respectively, at their cathodic limiting current densities, and H_2SO_4 concentration at the cathode surface was estimated from the interferogram. The estimated H_2SO_4 concentration was compared with the theoretical value, and it was found that they are fairly well coincident with each other.

Finally, the distribution of local cathodic current densities on a vertical plane cathode was measured with the miniature probes imbedded in the cathode plate. In the electrolysis of aqueous solutions of 0.1M $CuSO_4$-1.0M H_2SO_4 and 0.1M $CuSO_4$-1.85M H_2SO_4, the local cathodic current densities were uniform in the vertical di-

rection at lower average cathodic current densities.

The local current densities decrease along the height from the lower edge of cathode when the average cathodic current density is raised, and it is proportional to the -1/4th power of the height at the cathodic limiting current density. It is in good accordance with the previous works. The theoretical distribution of cathodic current densities in the aqueous solution of 0.1M $CuSO_4$-1.85M H_2SO_4 was calculated, and it was demonstrated that both theoretical and experimental results are in excellent agreement with each other.

From the measurement with the aqueous solutions of 0.1M $CuSO_4$-0.1M H_2SO_4, 0.1M $CuSO_4$-0.01M H_2SO_4 and 0.1M $CuSO_4$, it was revealed that the distribution is uniform in the vertical direction in the region of the average cathodic current density lower than one half of the limiting value. This is due to the lower electric conductivity of the solutions of low acid concentrations. At the cathodic limiting current density, the dependance of the local current densities on the vertical distance from the lower edge of cathode was fairly lower than the theoretical prediction. It is presumably because of the turbulent natural convective flow in the upper portion of the cathode which is caused by the hydrodynamic resistance at the surface of the rough electrodeposit.

ACKNOWLEDGEMENTS

The author is very grateful to his thesis supervisor, Professor Y. Kondo, for the encouragement and counsel given throughout the course of this work.

The author is also thankful to Dr. Z. Asaki for his suggestions during this study, and he wishes to express his thanks to Mr. Y. Takenaka (Kobe Steel, Ltd.), Mr. A. Ebata (Nippon Kokan K. K.), Mr. M. Morita (Mitsui Mining and Smelting Co., Ltd.), Mr. K. Maruoka (Graduate Student, Kyoto University) and Mr. M. Okada (Mitsubishi Corp.) for their earnest assistances in the experimental works for this study.

Dr. H. Majima, Dr. K. Fukuda, Dr. K. Asada and Dr. K. Yamakawa provided valuable insights in our discussion.

He extends a hearty thanks to the laboratory staffs and colleagues for their kind helps and cooperations and to my wife, Mrs. M. Awakura for her neat job of typewriting of the present paper.

CONTENTS

		Page
ABSTRACT		i
ACKNOWLEDGEMENT		v
NOMENCLATURE		x
CHAPTER 1	INTRODUCTION	1
	Reference to Chapter 1	14
CHAPTER 2	THEORETICAL EXPRESSIONS OF CATHODIC CURRENT DISTRIBUTION AND IONIC MASS TRANSFER IN CATHODIC DIFFUSION LAYER	17
2.1	Introduction	17
2.2	Basic Equations	24
2.3	Electrolysis of an Aqueous $CuSO_4$ Solution	31
2.3.1	Electrolysis at the limiting current density	37
2.3.2	Electrolysis at the current densities of uniform distribution on the cathode surface	39
2.3.3	Electrolysis in the intermediate region between the cathodic limiting current density and the uniform current densities	41
2.4	Electrolysis of an Aqueous $CuSO_4$-H_2SO_4 Solution	44
2.4.1	Electrolysis at the limiting current density	47
2.4.2	Electrolysis at the current densities of	

		Page
	uniform distribution on the cathode surface	48
2.4.3	Electrolysis in the intermediate region between the cathodic limiting current density and the uniform current densities	50
	Reference to Chapter 2	51
CHAPTER 3	VELOCITY DISTRIBUTION OF NATURAL CONVECTIVE FLOW IN CATHODIC BOUNDARY LAYER	53
3.1	Introduction	53
3.2	Experimental	57
3.2.1	Experimental arrangement and procedure	57
3.2.2	Experimental results	61
3.3	Discussion	74
3.4	Summary	97
	Reference to Chapter 3	100
CHAPTER 4	CONCENTRATION DISTRIBUTION OF $CuSO_4$ AND H_2SO_4 IN CATHODIC DIFFUSION LAYER	102
4.1	Introduction	102
4.2	Concentration Profile of $CuSO_4$ in Cathodic Diffusion Layer in the Electrolysis of Aqueous $CuSO_4$ Solution	107
4.2.1	Experimental arrangement and procedure	107
4.2.2	Interpretation of interferogram	114

		Page
4.2.3	Experimental results	121
4.2.4	Discussion	126
4.3	Concentration Profiles of $CuSO_4$ and H_2SO_4 in Cathodic Diffusion Layer in the Electrolysis of Aqueous $CuSO_4$-H_2SO_4 Solution	147
4.3.1	Measurement of profile of refractive index in the cathodic diffusion layer	147
4.3.2	Experimental results	148
4.3.3	Discussion	160
4.4	Summary	179
	Reference to Chapter 4	183
CHAPTER 5	MEASUREMENT OF LOCAL CATHODIC CURRENT DENSITIES ON A VERTICAL PLANE CATHODE	186
5.1	Introduction	186
5.2	Experimental Procedure	190
5.3	Experimental Results	204
5.4	Discussion	210
5.5	Summary	227
	Reference to Chapter 5	230
CHAPTER 6	SUMMARY AND CONCLUSION	232

		Page
Appendix A.	Relationship between Concentration Gradients of Cu^{2+} and H^{+} Ions at the Cathode Surface	246
	Reference to Appendix A	250
	Nomenclature to Appendix A	251
Appendix B.	Measurement of Diffusivity of $CuSO_4$ in Aqueous $CuSO_4$ and $CuSO_4$-H_2SO_4 Solutions	253
1.	Introduction	253
2.	Theoretical	254
3.	Experimental	258
3.1	Experimental Apparatus and Procedure	258
3.2	Experimental Results	262
4.	Discussion	269
5.	Summary	283
	Reference to Appendix B	285
	Nomenclature to Appendix B	286
Appendix C.	Dissociation of H_2SO_4	288
	Reference to Appendix C	292
	Nomenclature to Appendix C	293
Appendix D.	Densification Coefficient of H^{+} Ion in the Integrated Navier-Stokes Equation	294
	Nomenclature to Appendix D	296

NOMENCLATURE

A	numerical constant	(-)
A_2, A_4	numerical constants	(-)
A'	numerical constant	(-)
a	degree of dissociation of HSO_4^- ion	(-)
B	numerical constant	(-)
b	distance between cathode and anode	(cm)
C	numerical constant	(-)
$^*c$	concentration of $CuSO_4$ in the bulk-electrolyte	(mol/cm^3)
c	concentration of $CuSO_4$ at a distance y	(mol/cm^3)
Δc	concentration difference of $CuSO_4$ between bulk-electrolyte and cathode surface	(mol/cm^3)
Δc_i	concentration difference of ionic species i between bulk-electrolyte and cathode surface	(mol/cm^3)
c_i	concentration of ionic species i	(mol/cm^3)
$^\circ c_i$	concentration of ionic species i at the cathode	(mol/cm^3)
$^*c_i$	concentration of ionic species i in the bulk-electrolyte	(mol/cm^3)
D	diffusivity	(cm^2/sec)
D_1	diffusivity of $CuSO_4$	(cm^2/sec)
D_2	diffusivity of H_2SO_4	(cm^2/sec)
d	width of cathode	(cm)

E_e	equilibrium electrode potential	(volt)
E_c	cathode potential	(volt)
E_a	anode potential	(volt)
E_1, E_2, E_3, E_4	numerical constants	(-)
E'	$= E_1$	
F	Faraday constant	(= 96,500 coulombs/g-equiv.)
g	gravitational acceleration	(= 980 cm/sec^2)
Gr	Grashof number ($= g\alpha_1 {}^*c_1 H^3/{}^*\nu^2$)	(-)
Gr*	modified Grashof number	
	($= g\alpha_1 {}^*t_2 i_{c,av} x^4/z_1 F {}^*\nu^2 D_1$)	(-)
H	height of vertical plane electrode	(cm)
I	total electric current	(A)
i	current density at a distance y	(A/cm^2)
$i_{c,av}$	average cathodic current density	(A/cm^2)
$i_c(x)$	local current density on the cathode surface	(A/cm^2)
$i_a(x)$	local current density on the anode surface	(A/cm^2)
i_e	exchange current density	(A/cm^2)
i_d	cathodic limiting current density	(A/cm^2)
$i_{d,av}$	average cathodic limiting current density	(A/cm^2)
J_i	mass flux of ionic species i	(mol/sec·cm^2)
k	gradient of refractive index	(1/cm)
k_i	diffusivity of ionic species i	(cm^2/sec)
k_x	local cathodic mass transfer coefficient	

	at a height x	(cm/sec)
k_{av}	average cathodic mass transfer coefficient	(cm/sec)
ℓ	thickness of hydrodynamic boundary layer	(cm)
N	number of fringe shift	(-)
n	refractive index of solution	(-)
n(y)	refractive index of solution at a distance y	(-)
$n_f(y)$	apparent refractive index of solution obtained from interferogram at a distance y	(-)
$^*n$	refractive index of solution in the bulk-electrolyte	(-)
^on	refractive index of solution at the cathode surface	(-)
n_i	refractive index of solution at a distance y_i	(-)
n_o	refractive index of solution at a distance y_o	(-)
Δn	$= {}^*n - {}^on$	(-)
p	optical path length along the beam trajectory	(cm)
R	gas constant	(= 8.314 joule/K•mol)
Sc	Schmidt number ($= {}^*\nu/D_l$)	(-)
Sh_x	local Sherwood number at a height x	

	$(= k_x x/D_l)$	(-)
Sh_{av}	average Sherwood number $(= k_{av} H/D_l)$	(-)
s	integer	(-)
s_i	number of moles of ionic species i which reacts on the cathode surface per one Faraday	(mol/F)
T	absolute temperature	(K)
t	integral variable	(-)
$^*t_i$	transference number of ionic species i in the bulk-electrolyte	(-)
^oU	proportionality constant in the assumed velocity profile	(cm/sec)
u	velocity of upward natural convective flow	(cm/sec)
u_m	maximal velocity of upward natural convective flow	(cm/sec)
u_i	ionic mobility of species i	(cm^2/sec•volt)
V	terminal voltage	(volt)
V´	ohmic potential drop in the electrolyte between cathode and anode	(volt)
v	velocity of natural convective flow in horizontal direction	(cm/sec)
x	height from lower edge of cathode surface	(cm)
y	horizontal distance from cathode surface	(cm)
y_i	horizontal distance between incident point of beam and cathode surface	(cm)

y_o	horizontal distance between exit point of beam and cathode surface	(cm)
Δy	$= y_o - y_i$	(cm)
z	distance perpendicular to x- and y-directions	(cm)
z_i	valency of ionic species i	(g-equiv./mo:
z'	Boltzmann parameter	($cm/sec^{1/2}$)

Greek Letters

α	transfer coefficient	(-)
α_i	densification coefficient of ionic species i ($= d\ln\rho/dc_i$)	(cm^3/mol)
$\beta_p(q,r)$	incomplete β function defined by Eq. (2.34)	
γ	numerical constant	(-)
δ	thickness of diffusion layer	(cm)
δ_i	thickness of diffusion layer of ionic species i	(cm)
ε	numerical parameter	(-)
η	numerical parameter	(-)
Θ_i	$= {}^*c_i - {}^oc_i$	(mol/cm^3)
θ_i	$= {}^*c_i - c_i$	(mol/cm^3)
κ	electric conductivity	(mho/cm)
λ	numerical parameter	(-)
λ'	wavelength	(cm)
$^*\mu$	viscosity of bulk-electrolyte	(g/sec·cm)

ν	kinematic viscosity	(cm^2/sec)
$*\nu$	kinematic viscosity of bulk-electrolyte	(cm^2/sec)
ξ	numerical constant	(-)
ρ	density of solution at a distance y	(g/cm^3)
$*\rho$	density of bulk-electrolyte	(g/cm^3)
σ	ratio of thickness of diffusion layers of H^+ and Cu^{2+} ($= \delta_2/\delta_1$)	(-)
τ	distance between cathode surface and the position of u_m of natural convection	(cm)
$\Phi(a,b,c,d)$	auxiliary function defined by Eq. (2.33)	(-)
ϕ	potential	(volt)
ϕ_c	potential of electrolyte at the cathode surface	(volt)
ϕ_a	potential of electrolyte at the anode surface	(volt)
$\phi_{c,av}$	average potential of electrolyte at the cathode surface	(volt)
ω_1, ω_2	numerical parameters	(-)

subscripts

1	Cu^{2+} ion
2	H^+ ion
3	HSO_4^- ion
4	SO_4^{2-} ion

CHAPTER 1 INTRODUCTION

The electrolytic refining and winning have widely been employed in the hydrometallurgical process for the extraction of common metals such as copper and zinc. High purity copper is obtained from the electrolytic refining process of crude copper manufactured from the pyrometallurgical process of matte smelting and converting. More than half of the total production of metallic zinc in Japan is attributed to the electrolytic winning of zinc from aqueous solution containing zinc sulfate and sulfuric acid.

These processes of electrolytic refining and winning possess an advantage over the pyrometallurgical process that the metals of high purity can easily be obtained at low temperature by applying the electric energy. However, an important engineering problem[1)] in the electrolytic process is the limited productivity of metals per unit area of the electrolytic bath. This is because the electrolytic reaction occurs only on the surface of electrode.

Recently, this problem of lower productivity in the electrolytic process was recognized, and many attempts have been made to

overcome the problem: the electrolytic refining and winning at higher current densities were studied, and they have been brought into practice in various electrolytic plants.[2)]

It is known that the current distribution on the surface of electrode usually becomes uneven when higher current densities are applied. It may cause an undesirable side reaction at the locations of higher current densities: growth of needle-shaped metal on the cathode surface may cause a short-curcuit between both electrodes at the extremely higher current densities.

It is desired that the electrolytic refining and winning are conducted at a current density of uniform distribution to the possible extent in order to avoid the undesirable side reactions. The same requirement is also imposed on the electrolytic plating. From this reason, many theoretical and experimental works have been made on the current distribution on the electrode surface since more than thirty years ago.

Kasper[3)] was the first worker who theoretically studied this problem of current distribution, and his works published in 1940 on the current distribution in the electrolytic bath is regarded as an origin of the electrochemical engineering. He applied the potential theory to obtain the current distribution and calculated the current distribution in the electrolytic bath of various forms by solving the Laplace equation

$$\nabla^2\phi = 0 \qquad (1.1)$$

under the appropriate boundary conditions.

In the investigations of the current distribution based on the potential theory, it is convenient to take account of the following four items.

(1) When a potential is applied between the two electrodes placed in an aqueous solution of uniform composition, the current distribution is primarily determined by the geometrical form of the electrolytic bath and electrode and by their relative arrangement.

(2) The chemical polarization is developed on the surface of both electrodes during the electrolysis.

(3) The potential drop due to the ohmic law is established in the electrolyte.

(4) The composition of the electrolyte is not necessarily uniform within the electrolytic bath.

The calculation made by Kasper for the first time was the current distribution in which only the above-mentioned item 1 was taken into consideration, and it is generally called as the primary current distribution. Thereafter, the primary current distribution for the electrolytic bath and electrode of various geometrical forms and relative arrangements were calculated by many workers[4,5,6] by solving the Laplace equation by means of the Fourier analysis or the conformal mapping under the appropriate boundary conditions. In addition, these results of theoretical calculation have also been compared with the experimental results in which the alternating current was applied.

A direct current is applied in the electrolytic refining, winning and plating, and consequently the chemical polarization is developed on the surface of the electrodes. It was empirically shown[7] that when the direct current is applied, the current distribution on the surface of electrodes becomes different from the above-mentioned primary current distribution: it is more uniform when the magnitude of chemical polarization is comparable with the ohmic potential drop within the bulk-electrolyte or it predominates the potential drop between both electrodes. The current distribution in which the chemical polarization is also taken into consideration is called as the secondary current distribution.

The theoretical secondary current distribution on the surface of electrodes is obtained by solving the Laplace equation under the boundary condition that the potential of the electrolyte at the electrode surface is equal to the potential of the electrode plus the chemical polarization potential which is a function of the current density on the electrode.

Ishizaka et al.[8,9] carried out the theoretical calculation of the secondary current distribution in two cases that the chemical polarization is of the Tafel-type and that it is linear with regard to the applied current density, respectively. Furthermore, they also measured the distribution of the local current densities on the electrode surface in order to identify the results of their theoretical calculations based on the potential theory. Wagner[10] also conducted a theoretical calculation in

order to clarify the effect of chemical polarization on the local concentration of the current at the edge of the electrode.

Furthermore, it is known that the composition of electrolyte is rarely uniform within the electrolytic bath during the electrolysis: it is observed that a thin liquid layer of different composition from the bulk-electrolyte is formed on the surface of electrodes. This thin liquid layer is called as the diffusion layer. When this diffusion layer is taken into consideration, the current distribution on the surface of electrode cannot be obtained by merely taking account of the above items 1 and 2. This current distribution is affected not only by the above-mentioned geometrical factors and chemical polarization but also by the ionic mass transfer between the electrode surface and the bulk-electrolyte.

The electrolytic refining, winning and plating are often conducted on a vertical plane cathode placed in the unstirred or gently stirred electrolyte. Under this electrolytic condition, the ionic concentration in the electrolyte is lowered near the cathode surface due to the electrodeposition. This concentration difference between the bulk-electrolyte and the cathodic diffusion layer yields a lowered density of the electrolyte in the diffusion layer, and it results in an upward natural convective flow along the cathode surface. On the contrary, the downward natural convective flow is developed along the anode surface.

Then the natural convection caused by the concentration dif-

ference should be taken into consideration in the studies of ionic mass transfer in the diffusion layer near the surface of a vertical plane electrode. In addition, it should be noted that the process of the mass transfer in the diffusion layer is composed of the diffusion due to concentration difference and the electric migration due to potential gradient between both electrodes.

When the electrolysis is conducted on the surface of a vertical plane cathode in an unstirred electrolyte, the upward natural convection on the cathode surface plays an important role in the steady progress of electrodeposition.[11,12] Due to the electrodeposition of a metallic ion on the cathode surface, the concentration of the ion is lowered near the cathode surface. Then the ion is supplied from the bulk-electrolyte to the cathode surface, and the electrolysis is continued. If the electrolyte is completely stagnant, the ionic mass transfer from the bulk-electrolyte to the cathode surface consists only of the ionic diffusion and the electric migration. Under this electrolytic condition, the concentration of the reacting ion at the cathode surface becomes very low after only a few minutes from the start of the electrolysis. Then the undesirable side reaction such as the evolution of hydrogen gas may occur on the surface of cathode.

However, it is known that a relatively higher current density can be applied at the steady state without the evolution of hydro-

gen gas when the electrolysis takes place on a vertical plane cathode. This is explained as follows:[11,12] the upward natural convective flow along the cathode surface drags the bulk-electrolyte to the vicinity of the cathode surface, and the growth of the cathodic diffusion layer is depressed below a certain thickness, which results in a shorter length of diffusion path.

It is seen from the above considerations on the electrolysis with a vertical plane cathode that the natural convection along the cathode surface plays an important role not only in the ionic mass transfer near the cathode, but also in the attainment of a relatively higher cathodic current density at the steady state.

Since the vertical plane cathodes are often used in the industrial electrolysis, it is also important from the industrial viewpoint to clarify the mechanism of ionic mass transfer in the cathodic diffusion layer which is accompanied by the natural convection in vertical direction. The ionic mass transfer in the cathodic diffusion layer is also interesting from the theoretical point of view because it is composed not only of the diffusion caused by the concentration gradient but also of the electric migration due to the potential gradient.

Since it was recognized[13,14,15] that the natural convection along the surface of a vertical plane electrode plays an important role in the electrolysis of an unstirred electrolyte, numerous theoretical and experimental studies have been made on the velocity profile of the natural convective flow in the hydrodynamic

(velocity) boundary layer,[16,17] on the concentration profile in the diffusion layer[18,19,20] and on the resultant distribution of local current densities on the electrode surface.[21.22.23.24]

In 1949, Wagner[14] first revealed a theory of the distribution of limiting current density in vertical direction on the surface of a vertical plane copper cathode, which is solely determined by the rate of mass transfer of Cu^{2+} ion in the cathodic diffusion layer. He also measured the average limiting current density on the vertical plane copper cathode of different heights and demonstrated that the experimental results were in excellent agreement with the theory. Thereafter, other workers[21,24] also measured the average cathodic limiting current density on the surface of cathode of various forms and sizes in the electrolysis of the solutions of different composition at various temperatures. The general correlation of the data was represented by the non-dimensional equation in term of the Sherwood, Schmidt and Grashof numbers. These experimental results are in agreement with the theoretical values predicted from the theory of ionic mass transfer in the boundary layer which is accompanied by the free convective flow.

Industrial electrolytic refining, winning and plating are conducted below the cathodic limiting current density. Asada et al.[23] proposed a theoretical procedure of calculating the distribution of the local current densities in vertical direction on a vertical plane cathode which is installed in an unstirred elec-

trolyte. In order to verify the theoretical distribution of the cathodic current densities, Asada weighed the electrodeposited copper after cutting it into slices in horizontal direction. This measurement was made only under a limited experimental conditions, and they are supposed to be insufficient to confirm the validity of the theoretical calculation.

A few experimental studies have been made, on the other hand, to measure the concentration profile of $CuSO_4$ in the diffusion layer near the cathode surface. However, the thickness of this diffusion layer is only about 0.1 cm or less, and the measurement was difficult. Precision of the measurement by applying the freezing method conducted by Brenner[18,19] is supposed to be insufficient. An optical measurement using a technique of the Jamin interferometry was proposed by Ibl.[20] In this measurement, however, the required optical precision imposed on the dimension of the electrolytic cell is so strict that only the electrolytic cell of smaller size can be used because of the difficulties in the preparation: Ibl measured the concentration profile of $CuSO_4$ at a height of only 0.9 cm from the lower edge of the cathode.

Moreover, only very few experimental works[16,18] have been carried out on the velocity profile of the natural convection, though this measurement is indispensable for the theoretical calculations of the ionic mass transfer in the cathodic diffusion layer and the resultant current distribution. It is known

that the kinematic viscosity of aqueous solutions is of a magnitude 10^{-2} cm^2/s, and the diffusivity of solute is 10^{-5} to 10^{-6} cm^2/s, and the thickness of the hydrodynamic boundary layer is fairly larger than the diffusion layer.

The industrial electrolytic refining of copper is conducted in an electrolyte containing $CuSO_4$ and H_2SO_4; sulfuric acid is added to raise the electric conductivity of the electrolyte. During the electrolysis, H^+ ion which is dissociated from the sulfuric acid migrates toward the cathode surface and is accumulated in the cathodic diffusion layer.[21,25] The accumulation of sulfuric acid may affect the natural convective flow and the ionic mass transfer in the cathodic boundary layer.[17,26] With regard to this problem, only a few theoretical studies have recently been made by Newman et al.[17]

From what were mentioned above, it may be said with regard to the electrolysis of the unstirred electrolytes containing $CuSO_4$ and $CuSO_4$ plus H_2SO_4 with the vertical plane cathode that only a few theoretical and experimental works have been carried out on the ionic mass transfer in the cathodic diffusion layer and on the resultant distribution of the local current densities in the region of the current density lower than the limiting value, although much more works have been made at the cathodic limiting current density.

It is intended in the present work to study the ionic mass transfer and the natural convection in the boundary layer near

the surface of a vertical plane copper cathode during the electrolysis of unstirred aqueous $CuSO_4$ and $CuSO_4$-H_2SO_4 solutions. One experimental feature of the present work is that the optical methods are employed to measure the concentration profile and the velocity profile of natural convection in the cathodic boundary layer; by applying these optical techniques, it becomes feasible to conduct the measurements without disturbing the boundary layer. Among them, the holographic interferometry[27,28,29] is employed to measure the concentration profile of $CuSO_4$ in the cathodic diffusion layer. One major experimental advantage of this technique is the employment of common-path interference which is different from the conventional two-beam interference employed in the Jamin[20] and the Mach-Zehnder[30] interferometries. Because of this advantage, it becomes possible to measure the concentration profile along the surface of a taller plane cathode installed in a large electrolytic cell of lower optical precision.

The theoretical equations of the ionic mass transfer in the cathodic diffusion layer and the current distribution on the surface of a vertical plane cathode are derived in Chapter 2. The following plausible assumptions have often been made in the previous works[14,25,31,32] with regard to the velocity profile of natural convection and the concentration profile in the cathodic boundary layer, respectively, in order to derive the theoretical expressions of ionic mass transfer which is accompanied by the natural convection. They are as follows.

velocity profile:

$$u = U_0\left[2\frac{y}{\delta_1} - \left(\frac{y}{\delta_1}\right)^2\right] \quad 0 \leq y \leq \delta_1 \tag{1.2}$$

or

$$u = U_0 \frac{y}{\delta_1}\left[1 - \frac{y}{\delta_1}\right]^2 \quad 0 \leq y \leq \delta_1 \tag{1.3}$$

concentration profile:

$$\theta_1 = \theta_1\left(1 - \frac{y}{\delta_1}\right)^2 \tag{1.4}$$

According to Ibl et al.,[16] however, more sophisticated assumptions are made in the present work concerning the velocity and concentration profiles, and the theoretical expressions are derived on the ionic mass transfer and the distribution of local current densities on a vertical plane cathode placed in the unstirred solutions containing $CuSO_4$ and $CuSO_4$-H_2SO_4.

Next, in Chapter 3, the natural convection along the surface of a vertical plane cathode is measured. From the measurement of the velocity profile, the maximal velocity of the natural convection and the horizontal distance between the cathode surface and the position of the maximal velocity are obtained, and their dependances on the cathodic current density and on the height from the lower edge of cathode are discussed by comparing them with the theoretical values, respectively.

The concentration profiles of $CuSO_4$ and H_2SO_4 in the cathodic diffusion layer are studied in Chapter 4 by applying a technique of holographic interferometry. The correcting procedure

of the optical distortion of the beam due to the concentration gradient in the diffusion layer is also described. The concentration differences of $CuSO_4$ and H_2SO_4 between the cathode surface and the bulk-electrolyte and the thickness of the cathodic diffusion layer are obtained, and their dependances on the cathodic current density and on the height from the lower edge of cathode are discussed by comparing them with the results of theoretical calculation, respectively.

Finally, in Chapter 5 the distribution of the local cathodic current densities is studied. It is measured by using several miniature electrodes imbedded in vertical direction in the host cathode. The experimental results are discussed by comparing the experimental results with the theoretical values. The effect of H_2SO_4 on the distribution of the local cathodic current densities is also discussed.

Reference to Chapter 1

1) S. Yoshizawa: Denki Kagaku, 34 (1966) 355.

2) Y. Kondo: Denki Kagaku, 39 (1971) 1970.

3) C. Kasper: Trans. Electrochem. Soc., 77 (1940) 353, 365; 78 (1940) 131, 147; 82 (1942) 153.

4) S. Ishizaka: Denki Kagaku, 17 (1949), 1, 47; Reps. Govnt. Chem. Ind. Res. Inst., Tokyo, 46 (1952) 341, 350.

5) F. Hine, S. Yoshizawa and S. Okada: J. Appl. Phys., Japan, 22 (1953) 9, 297; J. Electrochem. Soc., 103 (1956) 186; J. Soc. Chem. Ind., Japan, 59 (1956) 875.

6) P. Drossbach: Z. Elektrochem., 56 (1952) 23, 599.

7) S. Ishizaka: Denki Kagaku, 24 (1956) 496.

8) S. Ishizaka: Denki Kagaku, 19 (1951) 55.

9) S. Ishizaka and H. Matsuda: Denki Kagaku, 19 (1951) 89; 20 (1952) 38, 84; 22 (1952) 420.

10) C. Wagner: J. Electrochem. Soc., 99 (1951) 116.

11) R. E. Wilson and H. A. Youtz: Ind. Eng. Chem., 15 (1923) 603.

12) S. Glasstone: Trans. Electrochem. Soc., 59 (1931) 277.

13) J. N. Agar: Discussions Faraday Soc., 1 (1947) 26.

14) C. Wagner: J. Electrochem. Soc., 95 (1949) 161.

15) G. H. Keulegan: J. Res. Nat. Bur. Std., 47 (1951) 2240.

16) N. Ibl and R. H. Müller: Z. Elektrochem., 59 (1955) 671; J. Electrochem. Soc., 105 (1958) 346.

17) J. Selman and J. Newman: J. Electrochem. Soc., 118 (1971) 1070.

18) A. Brenner: Proc. Am. Electroplaters' Soc., (1940) 95; (1941) 28.

19) T. Yannakopoulos and A. Brenner: J. Electrochem. Soc., 105 (1958) 521.

20) N. Ibl, Y. Barrada and G. Trümpler: Helv. Chim. Acta, 37 (1954) 583.

21) C. R. Wilke, M. Eisenberg and C. W. Tobias: J. Electrochem. Soc., 100 (1953) 513; Chem. Eng. Prog., 49 (1953) 663.

22) N. Ibl, W. Rüegg and G. Trümpler: Helv. Chim. Acta, 36 (1953) 1624.

23) K. Asada, F. Hine, S. Yoshizawa and S. Okada: J. Electrochem. Soc., 107 (1960) 242.

24) Y. Maru, S. Ito, S. Oyama and Y. Kondo: Denki Kagaku, 38 (1970) 343.

25) N. Ibl and U. Braun: Chimia, 21 (1967) 395.

26) L. Hsueh and J. Newman: Ind. Eng. Chem. Fund., 10 (1971) 615.

27) C. Knox, R. R. Sayano, E. T. Seo and H. P. Silverman: J. Phys. Chem., 71 (1967) 3102.

28) L. O. Heflinger, R. F. Werker and R. E. Brooks: J. Appl. Phys., 37 (1966) 642.

29) E. Yeager and A. J. Salkind: "Techniques of Electrochemistry", vol.2, p.144, John Wiley and Sons Inc., New York (1973).

30) A. Tuvarusko and L. S. Watkinds: Electrochim. Acta, 14 (1969) 1109.

31) C. R. Wilke, M. Eisenberg and C. R. Tobias: Chem. Eng. Prog.

Symp. Ser., 49 (1953) 513.

32) E. R. G. Eckert: "Introduction to the Transfer of Heat and Mass", p.158, McGraw-Hill, New York (1950).

CHAPTER 2 THEORETICAL EXPRESSIONS OF CATHODIC CURRENT DISTRIBUTION AND IONIC MASS TRANSFER IN CATHODIC DIFFUSION LAYER

2.1 Introduction

It is known regarding a system in which an electrochemical reaction is involved that the processes of mass transfer in the electrolyte take place in addition to the electrode reaction, and they are closely related with each other. Then the theoretical expressions of ionic mass transfer in the cathodic diffusion layer and the current distribution on the cathode surface are to be derived by taking the ohmic potential drop in the solution, the changes of ionic concentrations and natural convective flow near the cathode surface and the cathode reaction into consideration: it is assumed that the solution is unstirred and the convective flow is laminar.

The majority of the previous works concerns the following two simplified electrolytic systems. One is the systems in which the ohmic potential drop in the solution can be neglected. In these systems, the resistance to the ionic mass transfer in

the bulk-electrolyte is neglected, and the ionic mass transfer in the cathodic diffusion layer and the distribution of cathodic current densities are solely determined by the resistance to the mass transfer in the cathodic boundary layer, and the same principles as those applied to the problems of heat transfer and mass transfer in the non-electrolytic solutions have been employed. As one of these systems, the electrolysis of copper conducted at the cathodic limiting current in a solution containing excessive amount of supporting electrolyte like H_2SO_4 is mentioned.[1,2,3] At the cathodic limiting current density, the concentration of Cu^{2+} ion is regarded as being zero at the cathode surface, and the situation is further simplified.

At the current densities far lower than the limiting value, on the other hand, the current distribution on the cathode surface is determined by the ohmic potential drop in the solution and the chemical polarization, and the resistance to the ionic mass transfer in the cathodic boundary layer is neglected. Thus the situation is again simplified. This is another system which many previous workers also investigated. The potential theory developed in the electrostatics and the theory of steady heat conduction have directly been applied.[4,5,6] The electrode kinetics are used as the boundary condition for obtaining the integrated rate equation, and this is different from those encountered in the other applications of the potential theory.

At the intermediate cathodic current densities between the

limiting value and the current densities far lower than this value, on the other hand, the situation becomes more complicated. The diffusional and convective mass transfer of ions is essential, and furthermore, neither the cathode reaction nor the ohmic potential drop in the bulk-electrolyte can be neglected. Thus all these resistances are to be considered[7,8] for deriving the theoretical expressions.

The rate of electrodeposition of an ion on a vertical plane cathode is more or less affected by the rate of convective ionic mass transfer near the cathode surface. Wagner[1] investigated the convective ionic mass transfer under the condition of cathodic limiting current density by applying the theory of boundary layer which was developed in the fluid mechanics. Asada et al.[8] pursued the above-mentioned problem of intermdediate nature in which the electrolysis is conducted at the cathodic current densities moderately lower than the limiting value. They took the ionic mass transfer, the cathode reaction and the ohmic potential drop in the bulk-electrolyte into consideration and combined them by applying the continuity of transfer of electric charge. They calculated the distribution of current densities on the surface of a vertical plane cathode during the electrolysis of an unstirred electrolyte. Electrodes were installed at each end of a rectangular electrolytic cell.

The calculation of convective ionic mass transfer in the cathodic boundary layer toward a vertical plane cathode is usually

carried out with the same procedure as the computation of the rate of heat transfer, since the basic differential equations for both cases are of the similar form.[9] In order to integrate the Navier-Stokes equation and the mass balance equations of ions and electrolyte within the cathodic boundary layer, the arbitrary plausible assumptions[1,8,10,11,12] have been made with regard to the velocity profile of natural convective flow and the concentration profile near the cathode surface. Integration was carried out according to the method proposed by von Kármán and Pohlhausen.[13,14]

The velocity distribution of natural convection of electrolyte near the vertical plane cathode is schematically illustrated in Fig. 2.1. The velocity is zero at the cathode surface, increases until a maximal velocity is reached and then decreases again to zero in the bulk-electrolyte. The comparatively small region near the cathode surface in which the upward natural convective flow primarily occurs is called as the hydrodynamic (or velocity) boundary layer. Similarly, the cathodic diffusion layer is defined as the region in which the ionic concentration is significantly different from the bulk-electrolyte. It is also demonstrated in Fig. 2.1.

The ratio of the path of propagation of a non-uniformity of momentum to the path of propagation of a non-uniformity of concentration is of the order of $(\nu/D)^{1/2}$, or, about 30 for the special case of aqueous solutions. In other words, the thickness

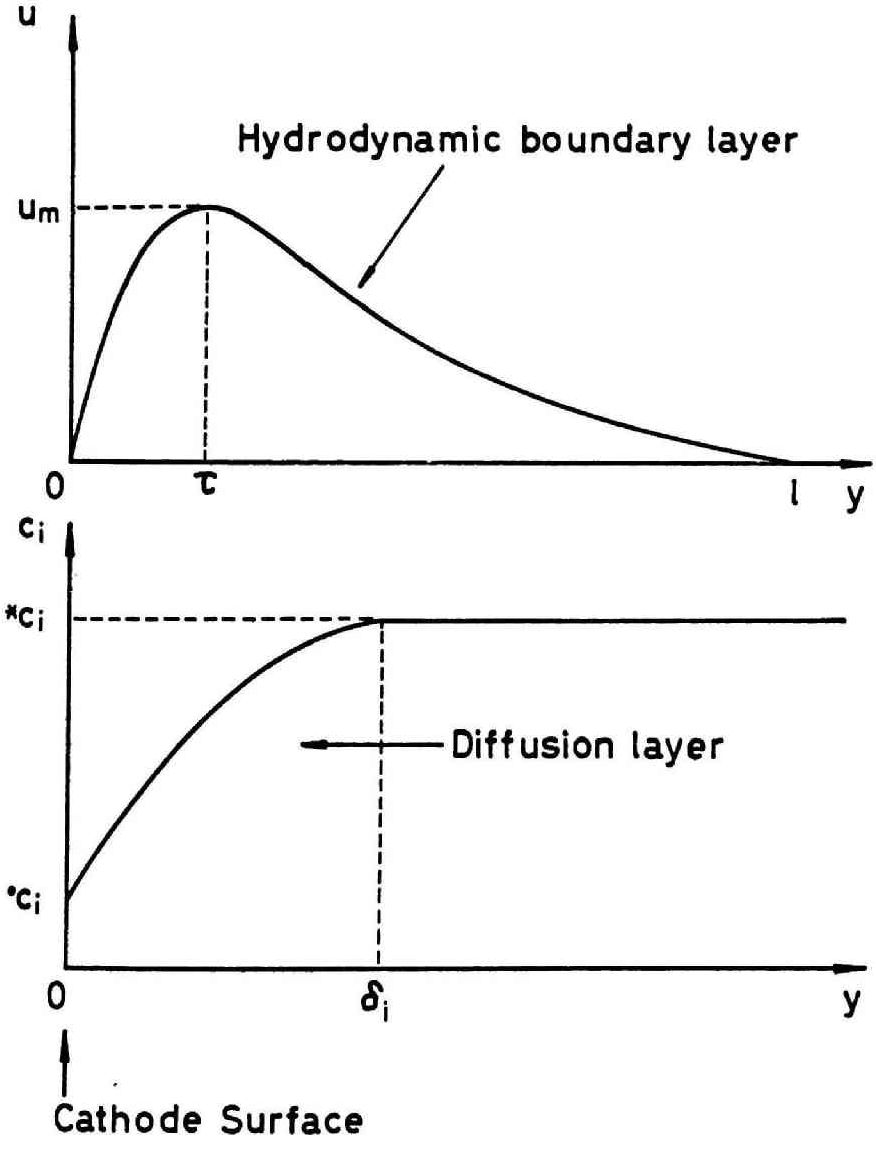

Fig. 2.1 Schematic diagram of velocity and concentration profiles near the cathode surface

of the hydrodynamic boundary layer is expected to be much greater than the thickness of diffusion layer.[1,15] From the similar consideration, the thickness of diffusion layer for a certain ion may be different from those for other ions.

In order to simplify the calculating procedure, the simplified functions have been assumed for the velocity and concentration profiles, respectively, and a plausible assumption that all the thickness of diffusion layer for each ion and of hydrodynamic boundary layer are same was employed by many previous workers.[8,9]

When these over-simplified functions were employed, however, the velocity and concentration profiles in the cathodic boundary layer can not exactly be described, even though it might be possible to explain the dependances of the local cathodic current density and the thickness of diffusion layer on the height from the lower edge of cathode. Furthermore, the actual thickness of the cathodic diffusion layer is much smaller than that of the hydrodynamic boundary layer due to the values of the diffusivity of ions and the kinematic viscosity of the aqueous solution which were mentioned above. Thus, it is desirable to provide a more sophisticated functions for the velocity and concentration profiles in the cathodic boundary layer for the calculation of the ionic mass transfer and the current distribution. In the present work, the generalized functions are used to express the velocity and concentration profiles in the cathodic boundary layer according to Ibl et al.[15] The parameters involved in these

functions were determined from the measured velocity and concentration profiles.

2.2 Basic Equations

A schematic diagram of the ionic mass transfer and the natural convective flow of electrolyte in a rectangular cell containing unstirred electrolyte is illustrated in Fig. 2.2. The vertical plane electrodes of a height H are installed at each end of the cell which is filled with the electrolyte up to the same height as the electrodes. The flux of an ionic species in the electrolyte is caused by the migration in an electric field, the ionic diffusion due to the concentration gradient and the natural convection in the cathodic and anodic boundary layers. It should be noted that the ionic flux in the bulk-electrolyte is due only to the electric migration.

The potential distribution in the rectangular electrolytic cell is schematically demonstrated in Fig. 2.3. The broken line AB'C'D' represents the potential distribution before the start of electrolysis: the lines AB' and C'D' represents the equilibrium electrode potential, respectively. The distribution of potential during the steady electrolysis under an applied terminal voltage V is shown by the line ABCD. The cathodic and anodic over-potentials are expressed as

$$-(AB' - AB) = -(E_c - E_e) = \phi_c(x,0) \tag{2.1}$$

and

$$(DC - D'C') = (E_a - E_e) = V - \phi_a(x,b) \tag{2.2}$$

respectively. In these equations, $\phi_c(x,0)$ and $\phi_a(x,b)$ are the

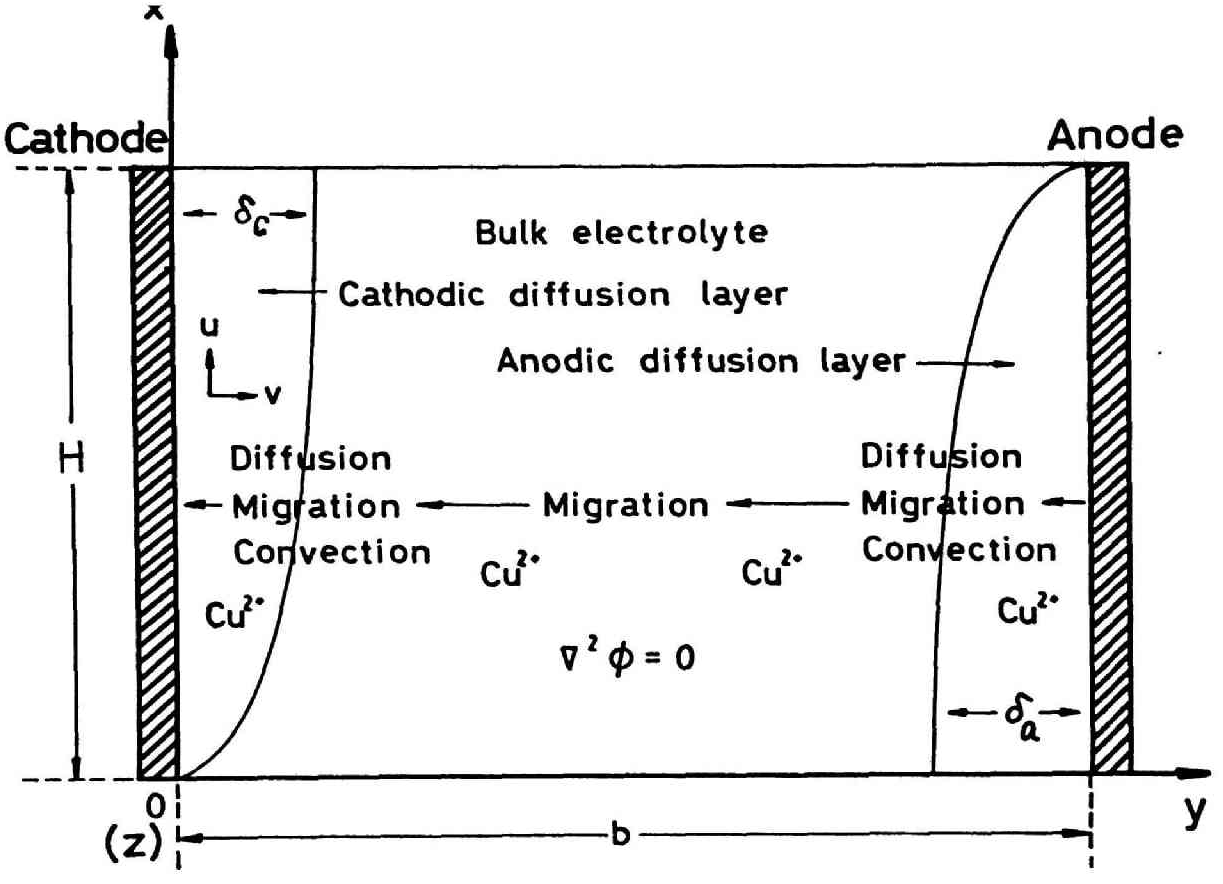

Fig. 2.2 Schematic diagram of ionic mass transfer and natural convection in a rectangular cell containing unstirred electrolyte

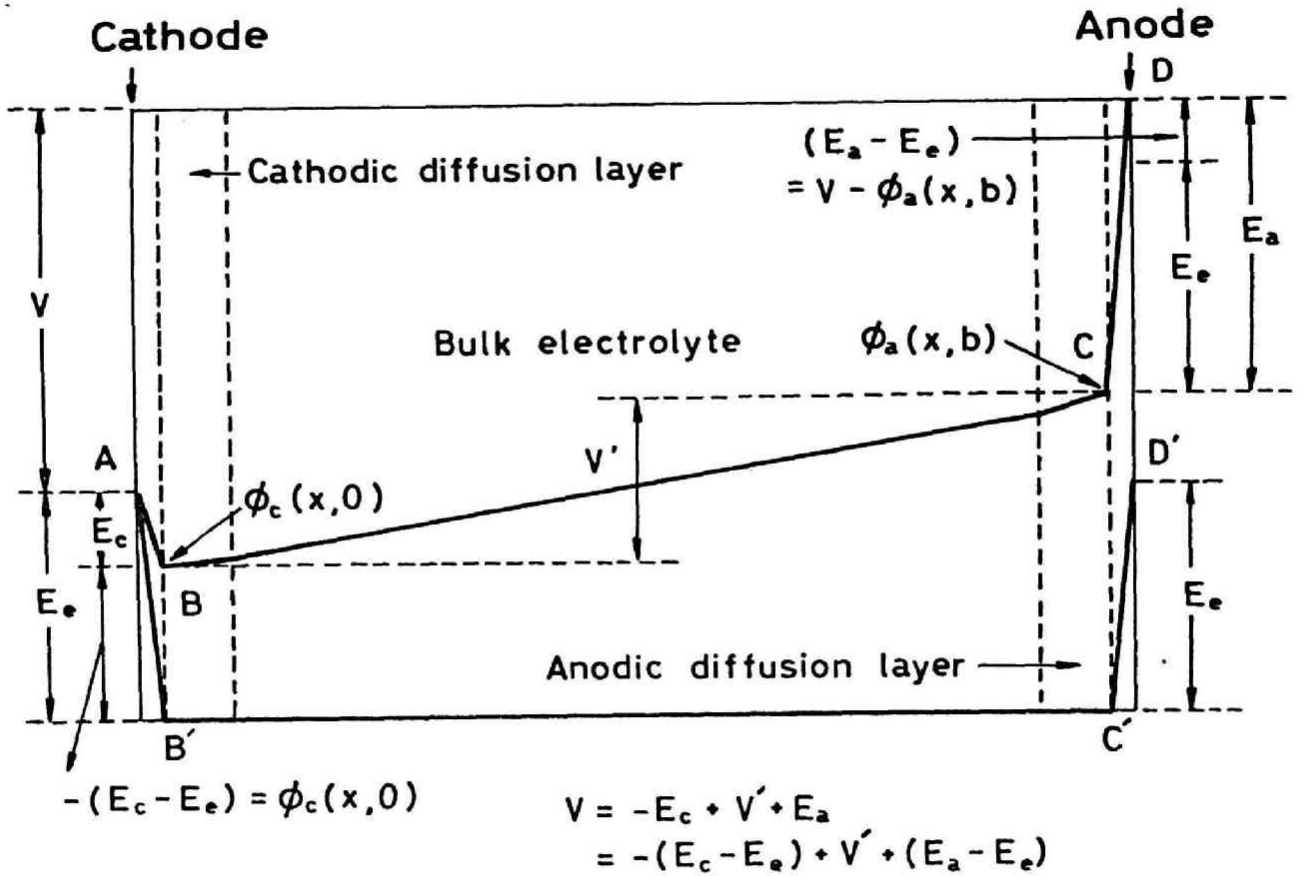

Fig. 2.3 Schematic diagram of potential distribution in a rectangular cell

potentials of electrolyte at the cathode and anode surfaces, respectively. The notations x and y are the distance in vertical and horizontal directions as shown in Fig. 2.2, respectively. The origin is located at the lower edge of cathode surface. Furthermore, the notation V' in the diagram represents the ohmic potential drop in the electrolyte in which the concentration overpotentials at the surface of both electrodes are involved.

In order to obtain the resultant equations of ionic mass transfer and current distribution on the cathode surface, the equations regarding the natural convective flow, the ionic mass transfer and the charge transfer are to be solved simultaneously together with the rate equation of electrode reaction. Assuming that the width of electrodes is infinite and the electrolysis is conducted at the steady state, these basic equations are described as follows.

With regard to the motion of electrolyte within the hydrodynamic boundary layer, the velocity of natural convective flow is determined from the Navier-Stokes equation and the continuity equation.[12] They are

$$\rho\left(u\frac{\partial u}{\partial x} + v\frac{\partial u}{\partial y}\right) = -g(\rho - {}^*\rho) + {}^*\mu\left(\frac{\partial^2 u}{\partial y^2}\right) \tag{2.3}$$

and

$$\frac{\partial u}{\partial x} + \frac{\partial v}{\partial y} = 0 \tag{2.4}$$

respectively.

With regard to the ionic mass transfer, the mass balance of

an ionic species i at the steady state within an infinitesimal volume element yields the following differential conservation equation.

$$-k_i \frac{\partial^2 c_i}{\partial y^2} - u_i \frac{\partial}{\partial y}\left(c_i \frac{\partial \phi}{\partial y}\right) - u \frac{\partial c_i}{\partial x} - v \frac{\partial c_i}{\partial y} = 0 \qquad (2.5)$$

To a very good approximation, the electrolyte is presumed to be electrically neutral and

$$\sum_i z_i c_i = 0 \qquad (2.6)$$

except for the diffuse part of the double layer formed adjacent to the interface between the electrode and the electrolyte.[7]

The current density in the electrolyte is determined by the motion of charged ionic species. A charge balance for all ionic species within an infinitesimal volume element leads to the following equation.

$$F \sum_i z_i k_i \nabla^2 c_i + \kappa \nabla^2 \phi = 0 \qquad (2.7)$$

Since the thickness of diffusion layer near the electrode surface is far smaller than the distance between both electrodes, it can be said from Eq. (2.7) that the potential distribution in the electrolyte is given by the following Laplace equation:

$$\frac{\partial^2 \phi}{\partial x^2} + \frac{\partial^2 \phi}{\partial y^2} = 0 \qquad (2.8)$$

Euqation (2.8) is valid when the gradient of the diffusion potential is neglected as compared with the ohmic potential drop, and the electric conductivity, κ, is constant within the electro-

lyte.[7,8]

For the rectangular cell in which the vertical plane electrodes are installed at both end, the boundary condition of Eq. (2.8) on the surface of each electrode is expressed as

$$y = 0 \quad \text{and} \quad y = b, \qquad i = \kappa(\partial\phi/\partial y) \tag{2.9}$$

where b is the distance between both electrodes. Another boundary condition at the bottom and at the surface of the electrolyte is as follows.

$$x = 0 \quad \text{and} \quad x = H, \qquad \partial\phi/\partial x = 0 \tag{2.10}$$

Equation (2.8) is solved under the boundary conditions of Eq. (2.9) and (2.10) by applying a technique of Fourier analysis. The origin of the potential ϕ is chosen to satisfy the following relationship.

$$\left.\begin{aligned} \phi_c(x,0) &= -(E_c - E_e) \\ \phi_a(x,b) &= V - (E_a - E_e) \end{aligned}\right\} \tag{2.11}$$

where V is the applied terminal voltage. Equation (2.11) is self-consistent when the potential drop within the electrode material is neglected and the equilibrium emf of the cell is null.[8]

Then the solution of the Laplace equation (2.8) is obtained as follows:

$$\phi(x,y) = \phi_{c,av} + \frac{i_{c,av}}{\kappa}y - \frac{2}{\pi\kappa}\sum_{s=1}^{\infty}\left(\frac{1}{s}\right)\frac{\cos\frac{s\pi}{H}x}{\sinh\left(\frac{s\pi}{H}b\right)} \times\left[\cosh\frac{s\pi(b-y)}{H}\int_0^H i_c(t)\cos\frac{s\pi}{H}t\,dt - \cosh\frac{s\pi}{H}y\int_0^H i_a(t)\cos\frac{s\pi}{H}t\,dt\right] \tag{2.12}$$

Assuming that the distance between electrodes is infinite, we have

$$\phi(x,y) = \phi_{c,av} + \frac{i_{c,av}}{\kappa} y - \frac{2}{\pi\kappa} \sum_{s=1}^{\infty} \left(\frac{1}{s}\right) \cos\frac{s\pi}{H} x \int_0^H i_c(t) \cos\frac{s\pi}{H} t\, dt \qquad (2.13)$$

2.3 Electrolysis of an Aqueous $CuSO_4$ Solution

Theoretical derivation of the resultant equations of ionic mass transfer and current distribution on the cathode surface during the steady electrolysis of an aqueous $CuSO_4$ solution is important as the basis for the theoretical investigations, though the electrolysis of aqueous $CuSO_4$ solution is rarely employed in the industries.

Integration of Eq. (2.3) concerning the upward natural convective flow along the cathode surface under the boundary conditions of

$$\left.\begin{aligned} &y = 0,\ u = 0 \text{ and } v = 0 \\ &y = \ell,\ u = 0 \text{ and } (\partial u/\partial y) = 0 \end{aligned}\right\} \tag{2.14}$$

together with Eq. (2.4) yields

$$\frac{d}{dx}\int_0^{\ell} u^2 dy = -g\int_0^{\ell}\frac{\rho - {}^*\rho}{{}^*\rho}\,dy - {}^*\nu\left(\frac{du}{dy}\right)_{y=0} \tag{2.15}$$

The following approximation with which the density of electrolyte is related to the composition may be valid.[1)]

$$\frac{\rho - {}^*\rho}{{}^*\rho} = \sum_i \alpha_i (c_i - {}^*c_i) \tag{2.16}$$

where

$$\alpha_i = \frac{\partial \ln \rho}{\partial c_i} \tag{2.17}$$

The parameter α_i is called as the densification coefficient for the species i in the electrolyte. In the aqueous $CuSO_4$ solu-

tion, the density is dependent solely on the concentration of Cu^{2+} ion due to the electroneutrality in the solution. Then the integrated Navier-Stokes equation is rewritten as:

$$\frac{d}{dx}\int_0^{\ell} u^2 dy = -\alpha_1 g \int_0^{\ell} (c_1 - {}^*c_1) dy - {}^*\nu\left(\frac{du}{dy}\right)_{y=0} \tag{2.18}$$

Next, the integration of Eq. (2.5) regarding the mass balance of Cu^{2+} ion under the boundary conditions of

$$\left.\begin{aligned} y = 0, \quad & c_1 = {}^oc_1 \\ y = \delta_1, \quad & c_1 = {}^*c_1 \end{aligned}\right\} \tag{2.19}$$

yields

$$\frac{d}{dx}\int_0^{\delta_1} uc_1 dy = -[J_1]_0^{\delta_1} \tag{2.20}$$

where J_1 is the mass flux of Cu^{2+} ion along the y-direction. It is demonstrated as

$$J_1 = -k_1\left(\frac{\partial c_1}{\partial y}\right) - c_1 u_1 \left(\frac{\partial \phi}{\partial y}\right) + vc_1 \tag{2.21}$$

Since the thickness of the diffusion layer is far thinner than the distance between both electrodes, the term of potential gradient, $(\partial\phi/\partial y)$, in Eq. (2.21) can be expressed by the term of ionic concentration[8] under the assumption that the electric force line is parallel to the y-axis in the cathodic diffusion layer, which implies that the current density, i, is constant along this axis. Then the right-hand side of Eq. (2.20) is written as

$$-[J_1]_0^{\delta_1} = J_{1,y=0} - J_{1,y=\delta_1}$$

$$= \frac{i}{z_1 F} + {}^*c_1 u_1 \left(\frac{d\phi}{dy}\right)_{y=\delta_1} - ({}^*vc_1)_{y=\delta_1} \qquad (2.22)$$

because the mass flux of Cu^{2+} ion on the cathode surface (y=0) is expressed as the local cathodic current density and the concentration gradient of Cu^{2+} ion is zero at $y=\delta_1$. Furthermore, the current density at $y=\delta_1$ is related to the mass flux of all ionic species as follows.

$$i = F(\Sigma_i z_i J_i)_{y=\delta_1}$$

$$= -F(\Sigma_i z_i {}^*c_i u_i)\left(\frac{d\phi}{dy}\right)_{y=\delta_1} + (vF\Sigma_i z_i {}^*c_i)_{y=\delta_1} \qquad (2.23)$$

Since the second term on the right-hand side of Eq. (2.23) is eliminated due to the electroneutrality of the solution, we have the following equation with regard to the potential gradient at $y=\delta_1$.

$$\left(\frac{d\phi}{dy}\right)_{y=\delta_1} = -\frac{i}{z_1 F} \frac{z_1}{\sum_i z_i {}^*c_i u_i} \qquad (2.24)$$

On the other hand, the integration of Eq. (2.4) yields the following equation

$$(v{}^*c_1)_{y=\delta_1} = -\frac{d}{dx}\int_0^{\delta_1} {}^*c_1 u dy \qquad (2.25)$$

By substituting Eq. (2.24) and (2.25) in Eq. (2.22), we have

$$-[J_1]_0^{\delta_1} = \frac{i}{z_1 F} - \frac{i}{z_1 F} \frac{z_1 {}^*c_1 u_1}{\sum_i z_i {}^*c_i u_i} + \frac{d}{dx}\int_0^{\delta_1} {}^*c_1 u dy \qquad (2.26)$$

Furthermore, the transference number of ionic species i is defined[16] as

$$t_i = \frac{z_i c_i u_i'}{\sum_i z_i c_i u_i'} \tag{2.27}$$

Equation (2.27) is substituted in Eq. (2.26), and the substitution of the resultant equation in Eq. (2.20) yields

$$\frac{d}{dx}\int_0^{\delta_1} u(c_1 - {}^*c_1)dy = \frac{i'(1-{}^*t_1)}{z_1 F} \tag{2.28}$$

In order to further integrate Eq. (2.18) and (2.28) which are the integrated Navier-Stokes equation and the mass balance equation of Cu^{2+} ion, respectively, it is assumed according to Ibl[15] that the concentration profile of $CuSO_4$ in the diffusion layer and the velocity profile of upward natural convective flow in the hydrodynamic boundary layer are expressed by the following equations:

$$\theta_1 = \Theta_1\left(1 - \frac{y}{\delta_1}\right)^{\omega_1} \tag{2.29}$$

and

$$u = \frac{u_m}{\lambda - 1}\left[\lambda\frac{y}{\tau} - \left(\frac{y}{\tau}\right)^{\lambda}\right] \qquad \text{for } 0 \leqq y \leqq \tau$$

$$u = u_m\left[1 - \frac{y-\tau}{\varepsilon\tau}\right] \qquad \text{for } \tau \leqq y \leqq (\varepsilon+1)\tau \tag{2.30}$$

respectively. In these equations, $\theta_1 = {}^*c_1 - c_1$, $\Theta_1 = {}^*c_1 - {}^\circ c_1$, $\delta_1 = \eta\tau$ and $\ell = (\varepsilon+1)\tau$.

Substitution of Eq. (2.29) and (2.30) in Eq. (2.18) and (2.28) yields upon integration

$$0 = \left(\frac{\alpha_1 g}{\omega_1 + 1}\right)\delta_1\Theta_1 - \left(\frac{{}^*\nu\,\eta\,\lambda}{\lambda - 1}\right)\frac{u_m}{\delta_1} \tag{2.31}$$

and

$$\frac{\Phi(\omega_1, \eta, \lambda, \varepsilon)}{\eta(\lambda - 1)}\frac{d}{dx}(u_m\Theta_1\delta_1) = \frac{i'(1 - {}^*t_1)}{z_1 F} \tag{2.32}$$

respectively. The term on the left-hand side of Eq. (2.18) is much smaller than each term on the right-hand side of the same equation,[1,15] and it was omitted in Eq. (2.31). The notation $\Phi(a,b,c,d)$ in Eq. (2.32) is

$$\Phi(a,b,c,d) = \frac{c(b-1)^{a+2}}{b^a(a+1)(a+2)}\left[\left(\frac{b}{b-1}\right)^{a+2} - \frac{c-1}{dc} - \frac{a+2}{c(b-1)} - 1\right]$$

$$- b^{c+1}\beta_{1/b}(c+1,\ a+1) \tag{2.33}$$

and

$$\beta_p(q,r) = \int_0^p t^{q-1}(1 - t)^{r-1}dt \tag{2.34}$$

By eliminating u_m from Eq. (2.31) and (2.32), we have

$$\frac{\Phi(\omega_1, \eta, \lambda, \varepsilon)}{(\omega_1 + 1)\eta^2\lambda}\frac{\alpha_1 g}{{}^*\nu}\frac{d}{dx}(\delta_1^3\,\theta_1^2) = \frac{i'(1 - {}^*t_1)}{z_1 F} \tag{2.35}$$

The mass transfer equations of Cu^{2+} ion and SO_4^{2-} ion at the cathode surface, on the other hand, are written as[17]

$$\frac{i}{z_1 F} = k_1\left(\frac{dc}{dy}\right)_{y=0} + cu_1\left(\frac{d\phi}{dy}\right)_{y=0} \tag{2.36}$$

and

$$0 = k_2\left(\frac{dc}{dy}\right)_{y=0} - cu_2\left(\frac{d\phi}{dy}\right)_{y=0} \tag{2.37}$$

respectively. The first and second terms on the right-hand side of Eq. (2.36) and (2.37) represent the rate of mass transfer due to diffusion and migration, respectively. After eliminating the term $(d\phi/dy)_{y=0}$ in Eq. (2.36) and (2.37) which represents the potential gradient at the cathode surface, we have

$$\frac{i^{*}t_2}{z_1 F} = D_1\left(\frac{dc}{dy}\right)_{y=0} \tag{2.38}$$

where

$$^{*}t_2 = 1 - {}^{*}t_1 = \frac{u_2}{u_1 + u_2} \tag{2.39}$$

and

$$D_1 = \frac{k_2 u_1 + k_1 u_2}{u_1 + u_2} \tag{2.40}$$

The concentration of $CuSO_4$, c, is equal to the concentration of Cu^{2+} ion, c_1. Then substitution of Eq. (2.29) in Eq. (2.38) yields

$$\frac{\omega_1 D_1 \Theta_1}{\delta_1} = \frac{i^{*}t_2}{z_1 F} \tag{2.41}$$

It is noted that Eq. (2.35) and (2.41) are the basic equations of mass transfer in the cathodic diffusion layer which is accompanied by the upward natural convection.

The solution of the simultaneous Eq. (2.35) and (2.41) under the assumption that $\Theta_1 = {}^{*}c_1$, for example, represents the distribution of the local current densities in vertical direction and the thickness of the diffusion layer at the cathodic limiting current density. The solution under the assumption that the cur-

rent density, i, is uniform in vertical direction on the cathode surface, on the other hand, is related to the electrolysis at the current densities far lower than the limiting value. Furthermore, by combining Eq. (2.35) and (2.41) with the solution of the Laplace equation in the form of $\nabla^2\phi = 0$ under the appropriate boundary conditions which represent the potential distribution within the electrolytic cell and with the rate equation of the electrode reaction, it becomes possible to obtain the general solution which holds in the region of intermediate cathodic current densities.

2.3.1 Electrolysis at the limiting current density

In the electrolysis at the cathodic limiting current density, the concentration of Cu^{2+} ion, ${}^{\circ}c_1$, is nearly equal to zero at the cathode surface,[1,2] and the calculation is simplified. By eliminating i from Eq. (2.35) and (2.41), and employing the relationship of $\theta_1 = {}^{*}c_1$, we have

$$\frac{\Phi(\omega_1, \eta, \lambda, \varepsilon)}{(\omega_1+1)\eta^2\lambda}\frac{\alpha_1 g}{{}^{*}\nu}\,{}^{*}c_1\frac{d}{dx}\delta_1^3 = \frac{\omega_1 D_1}{\delta_1} \tag{2.42}$$

The integration of Eq. (2.42) under the boundary conditions of

$$\left.\begin{aligned} x = 0, \quad & \delta_1 = 0 \\ x = x, \quad & \delta_1 = \delta_1 \end{aligned}\right\} \tag{2.43}$$

yields

$$\delta_1 = \eta E_1 \left(\frac{4 D_1 {}^*\nu}{3 g \alpha_1 {}^* c_1} \right)^{1/4} x^{1/4} \tag{2.44}$$

and

$$i_d = \frac{z_1 F D_1}{{}^*t_z} \frac{\omega_1}{\eta E_1} \left(\frac{3 g \alpha_1}{4 D_1 {}^*\nu} \right)^{1/4} {}^*c_1^{\,5/4} x^{-1/4} \tag{2.45}$$

where

$$E_1 = \left[\frac{(\omega_1 + 1) \omega_1 \lambda}{\Phi(\omega_1, \eta, \lambda, \varepsilon) \eta^2} \right]^{1/4} \tag{2.46}$$

The average cathodic limiting current density over the cathode height, H, is obtained from Eq. (2.45) as

$$i_{d,av} = \frac{4 z_1 F D_1}{3 {}^*t_z} \frac{\omega_1}{\eta E_1} \left(\frac{3 g \alpha_1}{4 D_1 {}^*\nu} \right)^{1/4} {}^*c_1^{\,5/4} H^{-1/4} \tag{2.47}$$

Furthermore, the Grashof number [3] of

$$Gr = \frac{g \alpha_1 {}^* c_1 H^3}{{}^*\nu^2} \tag{2.48}$$

and the average Sherwood number[3] in the form of

$$Sh_{av} = \frac{k_{av} H}{D_1} \tag{2.49}$$

where the average mass transfer coefficient, k_{av}, over the whole surface of the cathode is defined as

$$\frac{i_{d,av} {}^* t_z}{z_1 F} = k_{av} {}^* c_1 \tag{2.50}$$

are employed together with the Schmidt number of

$$Sc = \frac{{}^*\nu}{D_1} \tag{2.51}$$

and we have

$$Sh_{av} = 1.24 \frac{\omega_1}{\eta E_1} (Sc \cdot Gr)^{1/4} \tag{2.52}$$

2.3.2 Electrolysis at the current densities of uniform distribution on the cathode surface

When the cathodic current density is far lower than the limiting value, it is presumed that the local current densities are regarded as being equal from bottom to top of the cathode surface: it was observed[18,19] that the current density is virtually uniform when it is lower than about one-half of the limiting value. Under this condition of i = const, the following expressions of the concentration difference in the cathodic diffusion layer and its thickness are obtained from Eq. (2.35) and (2.41) as

$$\Delta c = \Theta_1 = \frac{\eta E_2}{\omega_1} \frac{* I_2}{z_1 F D_1} \left(\frac{z_1 F * \nu D_1^2}{g \alpha_1 * t_2} \right)^{1/5} i^{4/5} x^{1/5} \tag{2.53}$$

and

$$\delta_1 = \eta E_2 \left(\frac{z_1 F * \nu D_1^2}{g \alpha_1 * t_2} \right)^{1/5} i^{-1/5} x^{1/5} \tag{2.54}$$

where

$$E_2 = \left[\frac{\omega_1^2 (\omega_1 + 1) \lambda}{\Phi(\omega_1, \eta, \lambda, \varepsilon) \eta^3} \right]^{1/5} \tag{2.55}$$

respectively. Furthermore, the modified Grashof number[15] in the form of

$$Gr^* = \frac{g \alpha_1 * t_2 i' x^4}{z_1 F * \nu^2 D_1} \tag{2.56}$$

and the Sherwood number[2] of

$$Sh_x = \frac{k_x \cdot x}{D_1} \tag{2.57}$$

where the mass transfer coefficient, k_x, is defined as

$$\frac{i^* t_2}{z_1 F} = k_x \Delta c \tag{2.58}$$

are employed together with the Schmidt number of Eq. (2.51), and Eq. (2.53) and (2.54) are rewritten as

$$Sh_x = \frac{\omega_1}{\eta E_2} (Sc \cdot Gr^*)^{1/5} \tag{2.59}$$

and

$$\frac{\delta_1}{x} = \eta E_2 (Sc \cdot Gr^*)^{-1/5} \tag{2.60}$$

respectively.

With regard to the maximal velocity of the natural convective flow, on the other hand, Eq. (2.53) and (2.54) are substituted in Eq. (2.31), and we have

$$u_m = (\lambda - 1) A_2 \left(\frac{g \alpha_1^* t_2}{z_1 F^* \nu} \right)^{2/5} D^{1/5} i^{2/5} x^{3/5} \tag{2.61}$$

where

$$A_2 = \left[\frac{\eta \omega_1}{\Phi^3(\omega_1, \eta, \lambda, \varepsilon) \lambda^2 (\omega_1 + 1)^2} \right]^{1/5} \tag{2.62}$$

Furthermore, the distance between the position of the maximal velocity, u_m, and the cathode surface is obtained from Eq. (2.54) as

$$\tau = E_2 \left(\frac{z_1 F^* \nu D_1^2}{g \alpha_1^* t_2} \right)^{1/5} i^{-1/5} x^{1/5} \tag{2.63}$$

Equations (2.61) and (2.63) are rewritten as the following non-dimensional equations by using the modified Grashof number and Schmidt number defined above.

$$\frac{u_m x}{D_1} = A_2(Sc \cdot Gr^*)^{2/5} \tag{2.64}$$

and

$$\frac{\tau}{x} = E_2(Sc \cdot Gr^*)^{-1/5} \tag{2.65}$$

respectively.

2.3.3 Electrolysis in the intermediate region between the cathodic limiting current density and the uniform current densities

Presuming that the cathodic current density at a height x, $i_c(x)$, is known, the thickness of cathodic diffusion layer at the height x, $\delta_1(x)$, is obtained from Eq. (2.35) and (2.41) as

$$\delta_1(x) = \eta \cdot E_2 \cdot \left(\frac{z_1 F {}^*\nu D_1^2}{g\alpha_1 {}^* t_z}\right)^{1/5} \left\{ i_c(x)^{-2} \int_0^x i_c(t)dt \right\}^{1/5} \tag{2.66}$$

The rate equation of the cathode reaction is represented as

$$i_c(x) = i_e \left\{ \left(\frac{{}^o c_1}{{}^* c_1}\right) \exp\left(-\frac{\alpha z_1 F(E_c - E_e)}{RT}\right) - \exp\left(\frac{(1-\alpha) z_1 F(E_c - E_e)}{RT}\right) \right\} \tag{2.67}$$

By eliminating $^o c$ from Eq. (2.67) and (2.41), and substituting Eq. (2.11) in the resultant equation, we have

$$i_c(x) = \frac{i_e\left\{\exp\left(\frac{\alpha z_1 F\phi(x,0)}{RT}\right) - \exp\left(-\frac{(1-\alpha)z_1 F\phi(x,0)}{RT}\right)\right\}}{1 + \frac{i_e * t_2}{\omega_1 z_1 F D_1 * c_1}\delta_1(x)\exp\left(\frac{\alpha_1 z_1 F\phi(x,0)}{RT}\right)} \qquad (2.68)$$

When it is assumed that the distance between both electrodes is sufficiently large, $\phi(x,0)$ is obtained from Eq. (2.13) as follows.

$$\phi(x,0) = \phi(x,0)_{av} - \frac{2}{\pi k}\sum_{s=1}^{\infty}\left(\frac{1}{s}\right)\cos\frac{s\pi}{H}x\int_0^H i_c(t)\cos\frac{s\pi}{H}t\,dt \qquad (2.69)$$

Thus, the thickness of cathodic diffusion layer, $\delta_1(x)$, and the distribution of current density on the cathode surface, $i_c(x)$, are obtained by solving the simultaneous Eq. (2.66), (2.68) and (2.69): calculation was conducted by employing a technique of successive approximation.[8] An example of the steps of the successive approximation is as follows:

Step 1: A certain value of $\phi(x,0)_{av}$ is given together with the temperature and the composition of the electrolyte as the electrolytic conditions, instead of the terminal voltage V.

Step 2: Assuming an appropriate value of $i_c(x)$, $\phi(x,0)$ and $\delta_1(x)$ are calculated from Eq. (2.69) and (2.66), respectively.

Step 3: New set of numerical values of current distribution, $i_c(x)$, is calculated with Eq. (2.68) by employing the numerical values of $\phi(x,0)$ and $\delta_1(x)$ calculated in the step 2.

Step 4: These new values of $i_c(x)$ are employed, and the calculations of the above steps 2 and 3 are repeated.

This successive calculation is continued until the consistent current distribution, $i_c(x)$, is obtained within a predetermined critical range. Substituting these values of $i_c(x)$ in Eq. (2.66), the thickness of cathodic diffusion layer, $\delta_l(x)$, is obtained.

2.4 Electrolysis of an Aqueous $CuSO_4$-H_2SO_4 Solution

The industrial electrolytic refining and plating of copper are often conducted in an unstirred or gently stirred electrolyte containing $CuSO_4$ and H_2SO_4, and it is important to derive the resultant theoretical expressions of the ionic mass transfer in the cathodic diffusion layer and the current distribution on the cathode surface. The ionic mass transfer in this mixed electrolyte is also of theoretical interest because of the presence of an indifferent electrolyte of H_2SO_4 which does not take part in the cathode reaction.

It is assumed in the following theoretical derivation that the dissociation of $CuSO_4$ and the first stage dissociation of H_2SO_4 into H^+ and HSO_4^- are complete in the electrolyte and the second stage dissociation of HSO_4^- into H^+ and SO_4^{2-} is incomplete: the latter dissociation is determined by the second stage dissociation constant K_2. It is also assumed that the electrolyte contains an excessive amount of H_2SO_4. Then the density of the electrolyte is expressed by using the concentrations of Cu^{2+} and H^+ ions because of the electrical neutrality in the solution and the dissociation equilibrium of HSO_4^-.

The integrated Navier-Stokes equation is derived as

$$\frac{d}{dx}\int_0^{\ell} u^2 dy = \alpha_1 g \int_0^{\ell} (c_1 - {}^*c_1)dy + \alpha_2 g \int_0^{\ell} (c_2 - {}^*c_2)dy - {}^*\nu\left(\frac{dv}{dy}\right) \qquad (2.70)$$

from Eq. (2.15). The subscripts 1 and 2 in this equation denote Cu^{2+} ion and H^{+} ion, respectively.

Furthermore, the mass balance equations of Cu^{2+} ion and H^{+} ion are written as

$$\frac{d}{dx}\int_0^{\delta_1} u(c_1 - {}^*c_1)dy = \frac{i(1-{}^*t_1)}{z_1 F} = -k_1\left(\frac{dc_1}{dy}\right)_{y=0} \tag{2.71}$$

and

$$\frac{d}{dx}\int_0^{\delta_2} u(c_2 - {}^*c_2)dy = -\frac{i\,{}^*t_2}{z_2 F} \tag{2.72}$$

respectively. In order to integrate Eq. (2.70) to (2.72), Eq. (2.29) and (2.30) are again employed to demonstrate the velocity profile of natural convection and the concentration profile of Cu^{2+} ion, respectively. The concentration of H^{+} ion is expressed by the following equation.

$$\theta_2 = \Theta_2\left(1 - \frac{y}{\sigma\eta\tau}\right)^{\omega_2} \qquad 0 \leq y \leq \delta_2 \tag{2.73}$$

In this equation, $\theta_2 = {}^*c_2 - c_2$, $\Theta_2 = {}^*c_2 - {}^\circ c_2$ and $\sigma = \delta_2/\delta_1$.

Substitution of Eq. (2.29), (2.30) and (2.73) in Eq. (2.70) yields

$$0 = \left(\frac{\alpha_1 g}{\omega_1+1}\right)\delta_1\Theta_1 + \left(\frac{\alpha_2 g}{\omega_2+1}\right)\delta_2\Theta_2 - \left(\frac{\eta\lambda^*\nu}{\lambda-1}\right)\frac{u_m}{\delta_1} \tag{2.74}$$

Similarly, substitution of Eq. (2.29) and (2.30) in Eq. (2.72) yields

$$\frac{\Phi(\omega_1,\eta,\lambda,\varepsilon)}{\eta(\lambda-1)}\frac{d}{dx}(u_m\theta_1\delta_1) = \frac{i(1-*t_1)}{z_1F} \tag{2.75}$$

We also have from Eq. (2.30), (2.73) and (2.72)

$$\frac{\Phi(\omega_2,\sigma\eta,\lambda,\varepsilon)}{\sigma\eta(\lambda-1)}\frac{d}{dx}(u_m\theta_2\delta_2) = -\frac{i*t_2}{z_2F} \tag{2.76}$$

When the concentration of H_2SO_4 is sufficiently high, the following approximation holds (see Appendix A).

$$\left(\frac{d\theta_2}{dy}\right)_{y=0} = -\gamma\left(\frac{d\theta_1}{dy}\right)_{y=0} \tag{2.77}$$

where

$$\gamma = \frac{(1+a)^{\circ}C_2}{2(1+a)^{\circ}C_1+(1+2a)^{\circ}C_2} \tag{2.78}$$

and the notation a in this equation demonstrates the degree of dissociation of HSO_4^-.

From Eq. (2.29) and (2.73), we have

$$\theta_2 = -\gamma\sigma\frac{\omega_1}{\omega_2}\theta_1 \tag{2.79}$$

Substitution of Eq. (2.79) in Eq. (2.75) and (2.76) yields

$$\sigma\Phi(\omega_2,\sigma\eta,\lambda,\varepsilon) = -\frac{z_1*t_2}{\gamma z_2(1-*t_1)}\Phi(\omega_1,\eta,\lambda,\varepsilon) \tag{2.80}$$

The parameters ω_1, ω_2, η, λ, ε and σ are involved in this equation and the parameter σ is determined when the former five parameters are given.

By eliminating u_m and θ_2 from Eq. (2.74), (2.75) and (2.79), we have

$$\frac{\Phi(\omega_1,\eta,\lambda,\varepsilon)}{\eta^2\lambda}\frac{\xi g}{{}^*\nu}\frac{d}{dx}(\delta_1^3\,\theta_1^2) = \frac{i(1-{}^*t_1)}{z_1F} \tag{2.81}$$

where

$$\xi = \omega_1\left[\frac{\alpha_1}{\omega_1(\omega_1+1)} - \gamma\sigma^2\frac{\alpha_2}{\omega_2(\omega_2+1)}\right] \tag{2.82}$$

Furthermore, substitution of Eq. (2.29) in the right-hand side of Eq. (2.71) yields

$$\frac{\omega_1 k_1}{\delta_1}\theta_1 = \frac{i(1-{}^*t_1)}{z_1F} \tag{2.83}$$

Equations (2.81) and (2.83) are the basic equation of ionic mass transfer in the cathodic diffusion layer which is accompanied by the upward natural convection in the electrolyte containing $CuSO_4$ and H_2SO_4.

2.4.1 Electrolysis at the limiting current density

When the electrolysis takes place at the cathodic limiting current density, the concentration of Cu^{2+} ion at the cathode surface is regarded as being zero.[1,2] Then the following equation is derived from Eq. (2.81) and (2.83).

$$\frac{\Phi(\omega_1,\eta,\lambda,\varepsilon)}{\eta^2\lambda}\frac{\xi g}{{}^*\nu}{}^*c\frac{d}{dx}\delta_1^3 = \frac{\omega_1 k_1}{\delta_1} \tag{2.84}$$

Integration of Eq. (2.84) under the boundary conditions of Eq. (2.43) yields

$$\delta_1 = \eta E_3 \left(\frac{4 k_1 {}^*\nu}{3 g \xi {}^*c_1} \right)^{1/4} x^{1/4} \tag{2.85}$$

By substituting Eq. (2.85) in Eq. (2.83), we also have

$$i_d = \frac{z_1 F k_1}{(1 - {}^*t_1)} \cdot \frac{\omega_1}{\eta E_3} \cdot \left(\frac{4 k_1 {}^*\nu}{3 g \xi {}^*c} \right)^{1/4} {}^*c_1^{5/4} x^{-1/4} \tag{2.86}$$

where

$$E_3 = \left[\frac{\omega_1 \lambda}{\Phi(\omega_1, \eta, \lambda, \varepsilon) \eta^2} \right]^{1/4} \tag{2.87}$$

Furthermore, the cathodic average limiting current density over the whole cathode height is

$$i_{d,av} = \frac{4}{3} \frac{z_1 k_1 F}{(1 - {}^*t_1)} \frac{\omega_1}{\eta E_3} \left(\frac{3 g \xi}{4 k_1 {}^*\nu} \right)^{1/4} {}^*c_1^{5/4} H^{1/4} \tag{2.88}$$

2.4.2 Electrolysis at the current densities of uniform distribution on the cathode surface

When the electrolysis is conducted at the current densities far lower than the limiting value, the local current densities are regarded as being equal along the height of the cathode.[18,19] Under this condition, the following expressions concerning the concentration difference, Θ_1, and the thickness of the diffusion layer, δ_1, are obtained from Eq. (2.81) and (2.83) as

$$\Delta c_1 = \theta_1 = \frac{\eta E_4}{\omega_1} \frac{(1-*t_1)}{z_1 F k_1} \cdot \left(\frac{z_1 F *\nu k_1^2}{g \xi (1-*t_1)} \right)^{1/5} \cdot i^{4/5} x^{1/5} \qquad (2.89)$$

and

$$\delta_1 = \eta E_4 \left(\frac{z_1 F *\nu k_1^2}{g \xi (1-*t_1)} \right)^{1/5} i^{-1/5} x^{1/5} \qquad (2.90)$$

respectively, where

$$E_4 = \left[\frac{\omega_1^2 \lambda}{\Phi(\omega_1, \eta, \lambda, \epsilon)\, \eta^3} \right]^{1/5} \qquad (2.91)$$

On the other hand, the substitution of Eq. (2.89) and (2.90) in Eq. (2.74) yields the expression of the maximal velocity of the upward natural convective flow along the cathode surface. It is

$$u_m = (\lambda - 1) A_4 \left(\frac{g \xi (1-*t_1)}{z_1 F *\nu} \right)^{2/5} k_1^{1/5} i^{2/5} x^{3/5} \qquad (2.92)$$

where

$$A_4 = \left[\frac{\eta \omega_1}{\Phi^3(\omega_1, \eta, \lambda, \epsilon)\, \lambda^2} \right]^{1/5} \qquad (2.93)$$

The distance between the position of the maximal velocity and the cathode surface is derived from Eq. (2.90) as

$$\tau = E_4 \left(\frac{z_1 F *\nu k_1^2}{g \xi (1-*t_1)} \right)^{1/5} i^{-1/5} x^{1/5} \qquad (2.94)$$

2.4.3 Electrolysis in the intermediate region between the cathodic limiting current density and the uniform current densities

With the similar procedure mentioned in 2.3.3, the expression of the thickness of the cathodic diffusion layer, the rate equation of the cathode reaction and the equation of the cathodic potential, $\phi(x,0)$, are derived. They are

$$\delta_1(x) = \eta E_4 \left(\frac{z_1 F *_1 \nu k_1^{z}}{g z (1-*t_1)}\right)^{1/5} \cdot \{i_c(x)^{-2} \int_0^{x} i_c(t)dt\}^{1/5} \qquad (2.95)$$

$$i_c(x) = \frac{i_e \left\{ \exp\left(\frac{\alpha z_1 F \phi(x,0)}{RT}\right) - \exp\left(-\frac{(1-\alpha) z_1 F \phi(x,0)}{RT}\right)\right\}}{1 + \frac{\lambda e (1-*t_1)}{\omega_1 z_1 F k_1 * c_1} \delta_1(x) \exp\left(\frac{\alpha z_1 F \phi(x,0)}{RT}\right)} \qquad (2.96)$$

and

$$\phi(x,0) = \phi_{av}(x,0) - \frac{2}{\pi K} \sum_{s=1}^{\infty} \left(\frac{1}{s}\right) \cos \frac{s\pi}{H} x \int_0^{H} i_c(t) \cos \frac{s\pi}{H} t\, dt \qquad (2.69)$$

respectively. The technique of successive approximation mentioned in 2.3.3 is also applied for calculating the thickness of cathodic diffusion layer, $\delta_1(x)$, and the distribution of current densities on the cathode surface, $i_c(x)$.

Reference to Chapter 2

1) C. Wagner: J. Electrochem. Soc., 95 (1949) 161.

2) C. R. Wilke, M. Eisenberg and C. M. Tobias: J. Electrochem. Soc., 100 (1953) 513.

3) N. Ibl: Electrochim. Acta, 1 (1959) 3.

4) C. Kasper: Trans. Electrochem. Soc., 77 (1940) 353, 365; 78 (1940) 131, 147; 82 (1942) 153.

5) S. Ishizaka: Denki Kagaku, 17 (1949) 1, 47; Reps. Govnt. Ind. Res. Inst., Tokyo, 46 (1952) 341, 350.

6) F. Hine, S. Yoshizawa and S. Okada: J. Appl. Phys., Japan, 22 (1953) 9, 297; J. Electrochem. Soc., 103 (1956) 186; J. Soc. Chem. Ind., Japan, 59 (1956) 875.

7) J. Newman: UCRL-16665, December, (1966)

8) K. Asada, F. Hine, S. Yoshizawa and S. Okada: J. Electrochem. Soc., 107 (1960) 242.

9) R. B. Bird, W. E. Stewart and E. N. Lightfoot: "Transport Phenomena", p.608, John Wiley and Sons, New York (1962).

10) N. Ibl and U. Braun: Chimia, 21 (1967) 395.

11) C. R. Wilke, M. Eisenberg and C. R. Tobias: Chem. Eng. Prog. Symp. Ser., 49 (1953) 513.

12) E. R. G. Eckert: "Introduction to the Transfer of Heat and Mass", p.158, McGraw-Hill, New York (1950).

13) Th. von Karman: Z. angew. Math. Mech., 1 (1921) 233.

14) K. Pohlhausen: Z. angew. Math. Mech., 1 (1921) 252.

15) N. Ibl and R. H. Müller: J. Electrochem. Soc., 105 (1958) 346.

16) E. A. Moelwyn-Hughes: "Physical Chemistry", p.864, Pergamon Press, New York (1961).

17) G. H. Keulegan: J. Res. Nat. Bur. Std., 47 (1951) 2240.

18) C. Wagner: J. Electrochem. Soc., 104 (1957) 129.

19) N. Ibl, W. Rüegg and G. Trümpler: Helv. Chim. Acta, 36 (1953) 1624.

CHAPTER 3 VELOCITY DISTRIBUTION OF NATURAL CONVECTIVE FLOW IN CATHODIC BOUNDARY LAYER

3.1 Introduction

It is indispensable to study the velocity profile of natural convective flow along the surface of a vertical plane cathode placed in the unstirred electrolyte for clarifying the distribution of the current densities, because the industrial electrolytic refining and plating of copper are often conducted in the unstirred or gently stirred electrolyte containing $CuSO_4$ and H_2SO_4.

In the procedure of applying the von Kármán-Pohlhausen method for obtaining the natural convective flow and the ionic mass transfer near the cathode surface, the concentration profile of an ion in the cathodic diffusion layer has often been approximated as[1,2,3,4]

$$\theta_i = \theta_i(1 - \frac{y}{\delta})^2 \qquad (3.1)$$

Regarding the velocity distribution of the natural convective flow in the cathodic hydrodynamic boundary layer, on the other hand, the following approximations have been made by the previous workers.[1,2,3,4] They are

$$u = U_o[2\frac{y}{\delta} - (\frac{y}{\delta})^2] \qquad \text{for } 0 \leqq y \leqq \delta \qquad (3.2)$$

and

$$u = U_o\frac{y}{\delta}(1 - \frac{y}{\delta})^2 \qquad \text{for } 0 \leqq y \leqq \delta \qquad (3.3)$$

As seen in Eq. (3.2), for example, it was postulated that the velocity increases to the maximum at the outer edge of the diffusion layer ($y = \delta$) and it decreases to zero at $y = 2\delta$. Thus it is indicated in Eq. (3.2) that the thickness of the hydrodynamic boundary layer is twice larger than the diffusion layer. According to Eq. (3.3), on the other hand, the velocity reaches to the maximum at $y = \delta/3$ and decreases to zero at $y = \delta$: it is postulated that the thickness of diffusion layer and hydrodynamic boundary layer are equal.

When either Eq. (3.2) or Eq. (3.3) is employed in the theoretical calculation according to the von Kármán-Pohlhausen method, the same results are obtained with regard to the dependances of the maximal velocity of natural convection, the ionic concentration difference between bulk-electrolyte and cathode surface, and the limiting current densities upon the height from the lower edge of cathode. The same dependances are also obtained with regard to the maximal velocity of natural convection and the ionic concentration difference upon the cathodic current density. However, the maximal velocity calculated by Eq. (3.2) is more than twice larger than the calculated value due to Eq. (3.3) when a uniform concentration is assumed in vertical direction on the

cathode surface. The cathodic current densities are also affected by the assumed velocity profiles. Substantially different values of the maximal velocities are obtained in the case of uniform local current densities along the cathode surface, which depend on whether Eq. (3.2) or Eq. (3.3) is assumed.

On the other hand, it was revealed from the theoretical considerations by Wagner[1] that it is very likely that the thickness of hydrodynamic boundary layer is much larger than the diffusion layer. This was later confirmed by the experimental studies of Ibl et al.[5] They also found that the calculated maximal velocity and the limiting current density both due to Eq. (3.3) are in much better coincidence with the experimental data than Eq. (3.2)[6] is assumed: it seems strange that an unsubstitutional assumption of Eq. (3.3) leads to a better agreement with the experimental results.

In order to obtain a better insight about the influence of the assumptions on the velocity and concentration profiles upon the theoretical calculation, Ibl et al.[6] further calculated the maximal velocity of the natural convective flow by using the generalized functions of velocity and concentration profiles in the forms of Eq. (2.29) and Eq. (2.30), respectively. They also measured the velocity profile of natural convective flow during the electrolysis of aqueous 0.6M $CuSO_4$ solution by applying the dark field method, and compared the experimental results with theoretical calculation.

Based on the above-mentioned considerations, the velocity profile of natural convective flow along the cathode surface is studied in the present work during the electrolysis of the aqueous 0.6M and 0.1M $CuSO_4$ solutions. Experimental results are compared with the theoretical calculation and with the experimetnal results obtained by Ibl et al.[6] The effects of $CuSO_4$ concentration on the velocity profile are also considered. Furthermore, the velocity profile of natural convective flow is measured with a solution containing 0.6M $CuSO_4$ and 1.5M H_2SO_4, and the effects of H_2SO_4 on the velocity profile are examined.

3.2 Experimental

3.2.1 Experimental Arrangement and Procedure

The velocity profile of upward natural convective flow along the cathode surface was measured by filming the motion of colophonium particles dragged along by the convective flow with a cinecamera. The experimental arrangement is schematically illustrated in Fig. 3.1. A helium-neon gas laser emitter of 10 mW output was used as the light source. The emitted beam was enlarged to a parallel beam of about 1.2 cm in diameter by an expander E and lens L_1 (f = 200 mm), and was transmitted into the electrolytic cell near the cathode surface. The silhouette of suspended colophonium particles was filmed with a Bolex H 16 reflex cinecamera. By using a lens L_2 (f = 200 mm), the silhouette near the cathode surface was magnified about 10 times on the film.

The electrolytic cell is demonstrated in Fig. 3.2. The inner dimension of the cell was 0.7 cm thick, 5.8 cm wide, and 20 cm high. Both anode and cathode are copper bar 0.5 cm square and 26 cm long. Except for the portion on the facing surface of both electrodes between the height of 3 and 17 cm from the lower edge of cathode, the remaining part was insulated by coating PVC resin.

In order to obtain the exact velocity profile from the motion of colophonium particles, it was essential to install the cathode

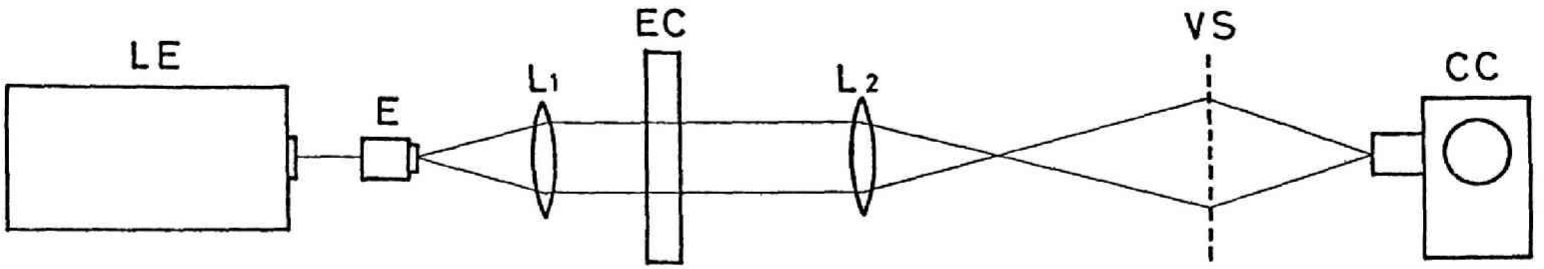

LE: Laser Emitter
E: Expander
L_1, L_2: Lenses
EC: Electrolytic Cell
CC: Cinecamera
VS: Virtual Screen

Fig. 3.1 Experimental arrangement

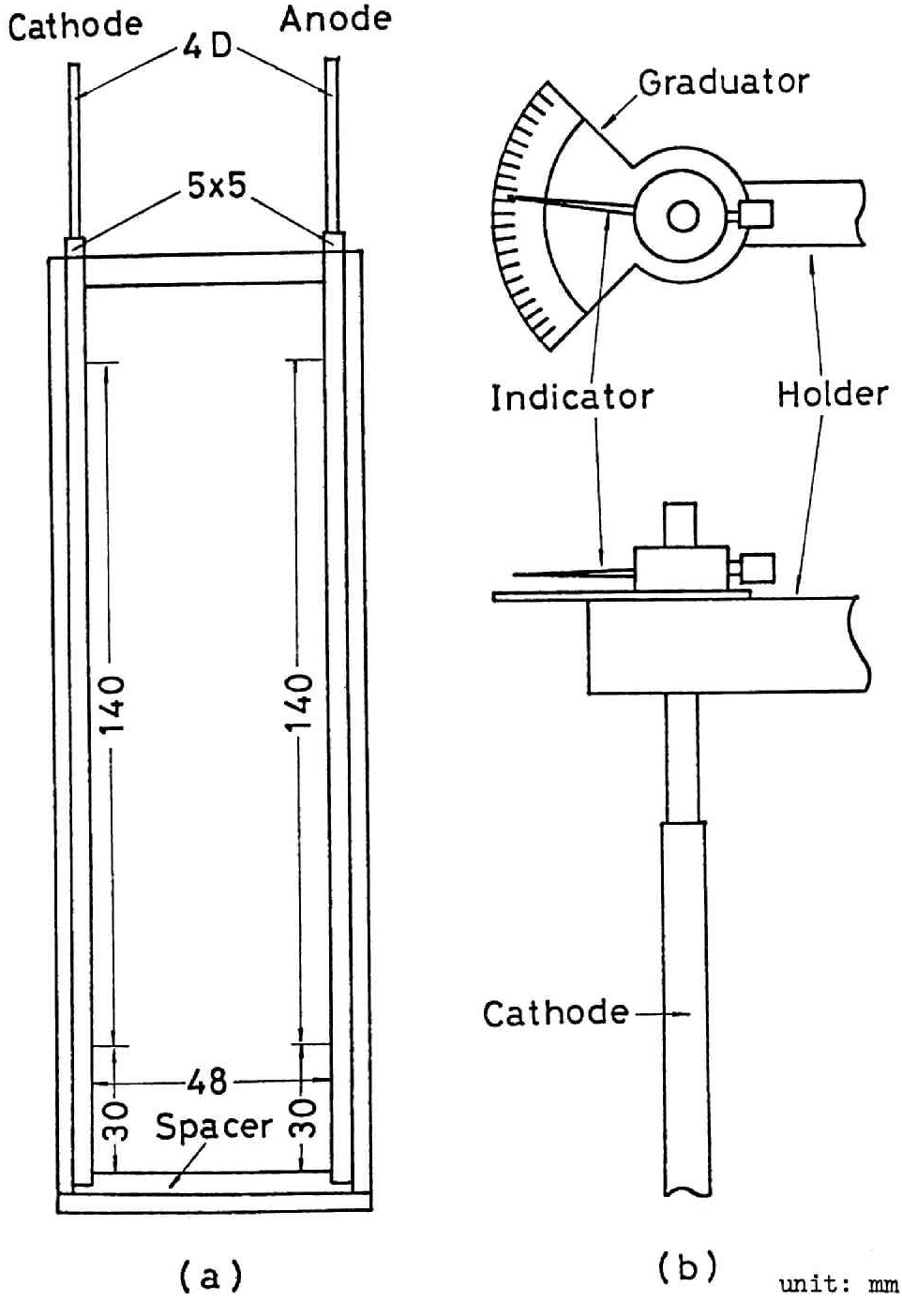

Fig. 3.2 Electrolytic cell and cathode holder

surface parallel to the incident beam. In order to realize this, a revolvable cathode holder was employed, and after the cell wall on the light-entrance side was adjusted to be at right angles to the incident beam, the cathode was gently revolved and maintained at a position where the enlarged silhouette of the cathode surface on the screen VS recedes farthest. The focus of the cinecamera was fixed at the middle point of the cell thickness because the optical distortion is minimal which is caused by the gradient of refractive index established in the cathodic diffusion layer during the electrolysis.[7] It is also thought that the effect of cell wall on the natural convective flow is minimal at this point.

All measurements were carried out at 23° ± 1°C. Colophonium particles of about 10 μm size were poured into the electrolyte. With completely stagnant conditions, the electrolysis was started, and the steady state regarding the natural convection was attained within 20 minutes. After this period was passed, the motion of colophonium particles was filmed. By comparing the position of the same particle on the films exposed in an interval of a few seconds, the transferred distance of the particle in vertical direction was measured and the velocity of natural convective flow was obtained. Measurements were conducted below the cathodic current density of 4 mA/cm^2, which is far lower than the limiting value, and the local cathodic current densities were regarded as being uniform throughout the cathode surface.[8,9]

Analytical reagent grade $CuSO_4 \cdot 5H_2O$, H_2SO_4 and deionized water were used, and the aqueous $CuSO_4$ and $CuSO_4$-H_2SO_4 solutions were prepared. Colophonium particles of about 10 μm size were prepared by sedimentation and centrifugation. A micro-photograph of colophonium particles is shown in Fig. 3.3.

3.2.2 Experimental Results

A. Aqueous $CuSO_4$ solution

The measured velocity profiles of natural convection in aqueous 0.6M $CuSO_4$ and o.1M $CuSO_4$ solutions are demonstrated in Fig. 3.4 and 3.5 and in Fig. 3.6 to 3.8, respectively.

The velocity profiles in the former solution at the heights of 1.5, 2.5, 7 and 11 cm from the lower edge of cathode are summarized in Fig. 3.4. The average cathodic current density was maintained at 1 mA/cm^2. As seen in this figure, u_m and τ increase with the height, and the hydrodynamic boundary layer grows downstream. The velocity profiles in the same solution at the average cathodic current densities of 0.05, 0.1, 0.5, 1 and 3 mA/cm^2 at a height of 7 cm are demonstrated in Fig. 3.5. It is clear from this figure that u_m increases and τ decreases when the cathodic current density is increased. Furthermore, from the comparison of Fig. 3.4 and 3.5 with the corresponding experimental results of Ibl et al.[6] it was revealed that both velocity

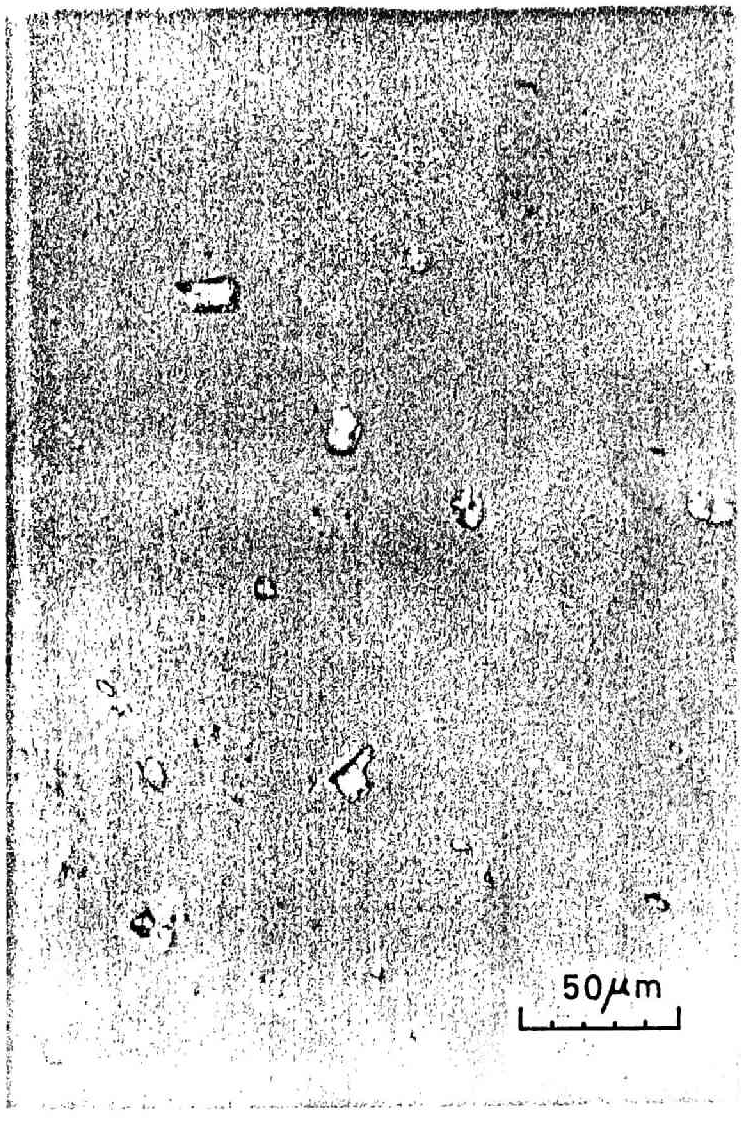

Fig. 3.3 Micro-photograph of colophonium particles

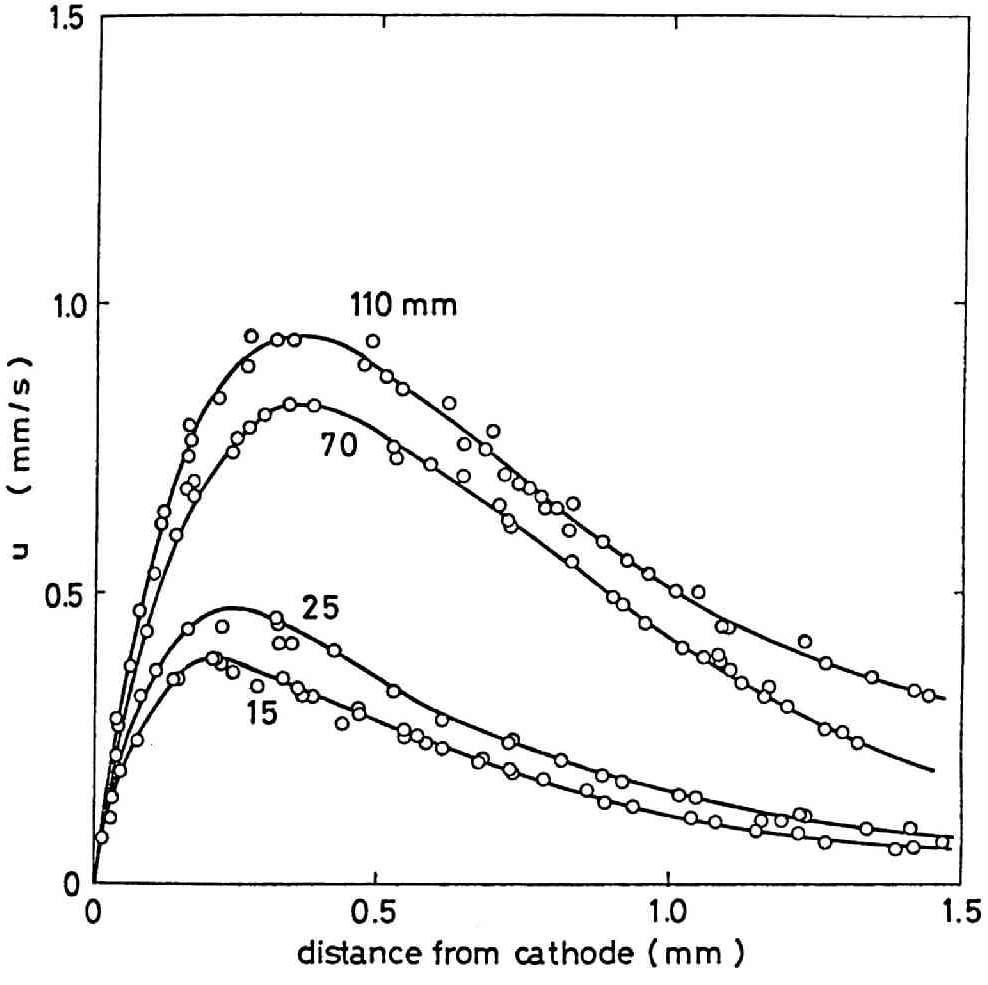

Fig. 3.4 Velocity profiles at a current density of 1 mA/cm^2 in 0.6M $CuSO_4$ solution

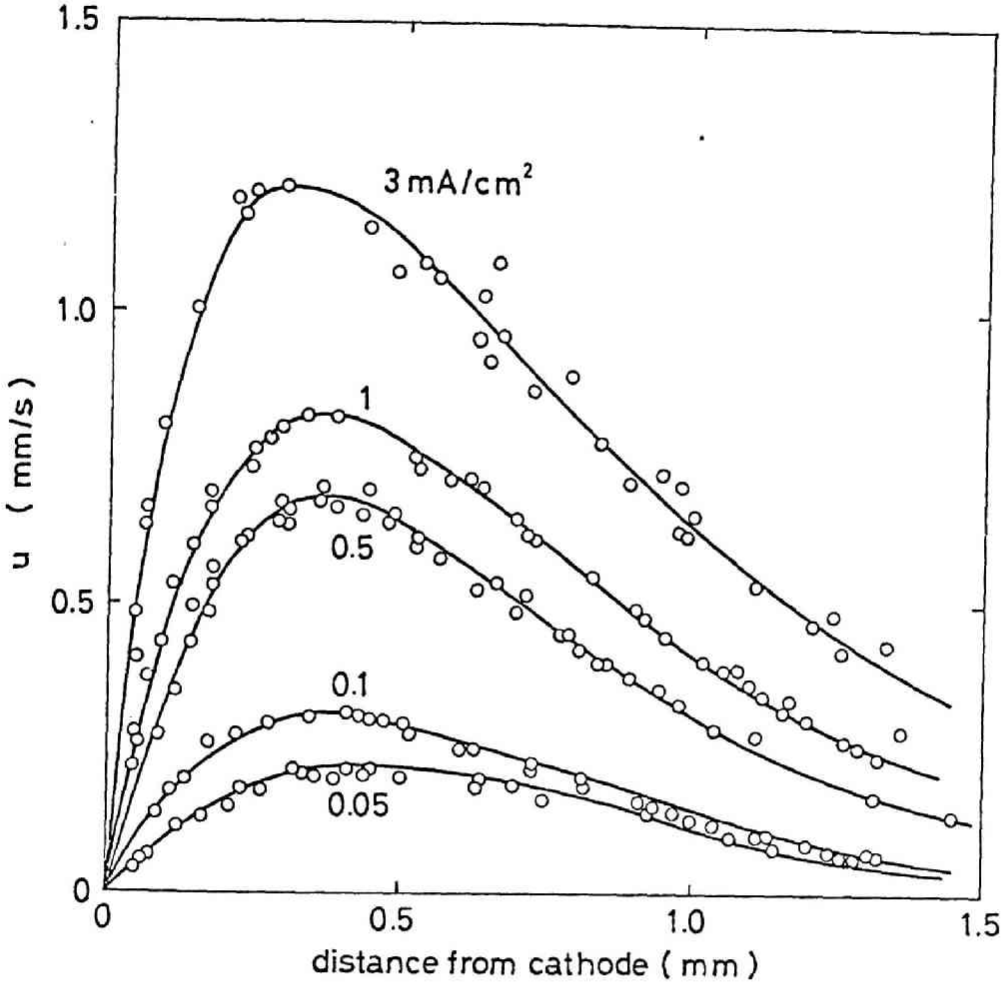

Fig. 3.5 Velocity profiles at a height of 7 cm in 0.6M $CuSO_4$ solution

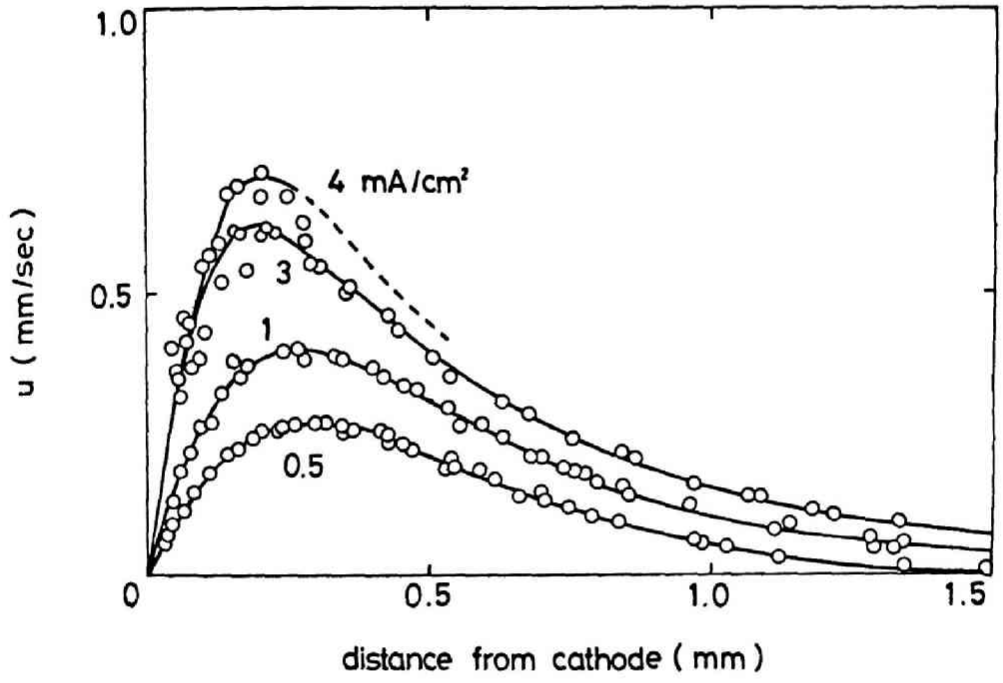

Fig. 3.6 Velocity profiles at a height of 2.5 cm in 0.1M $CuSO_4$ solution

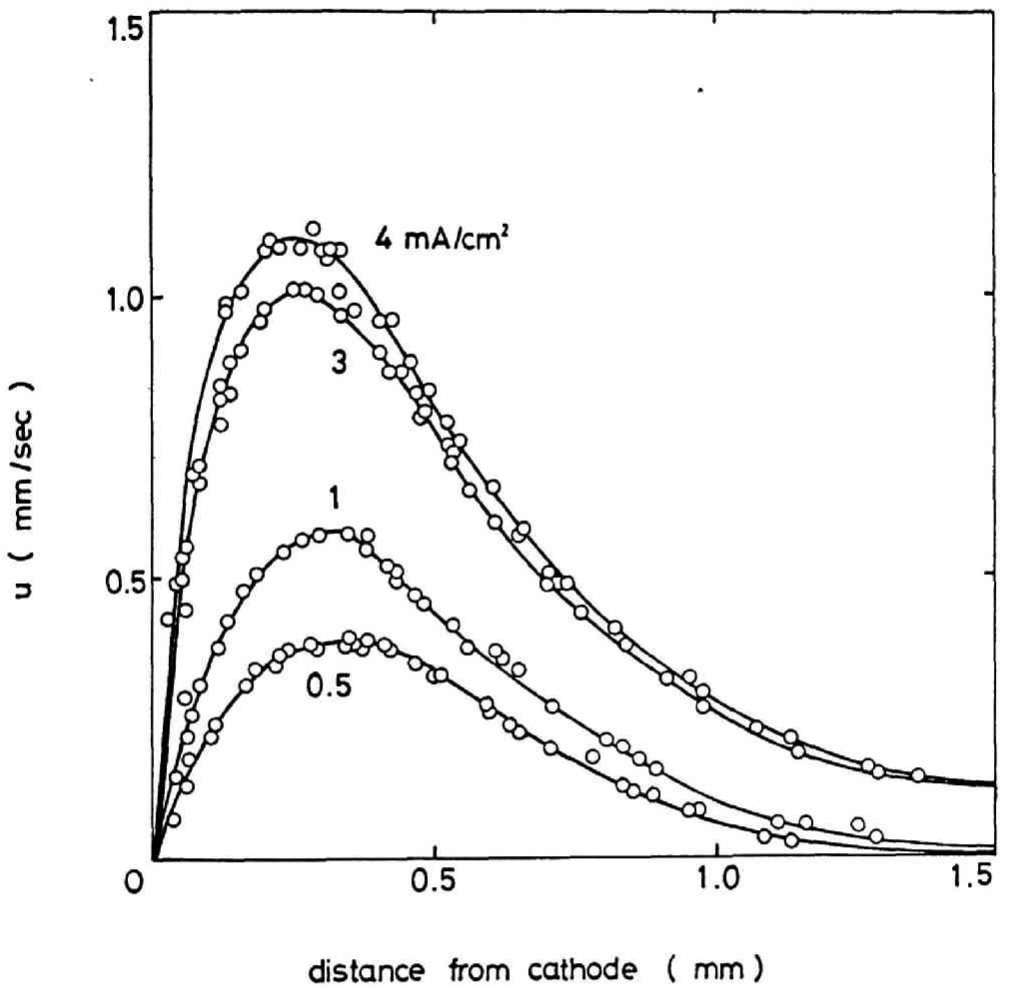

Fig. 3.7 Velocity profiles at a height of 7 cm in 0.1M $CuSO_4$ solution

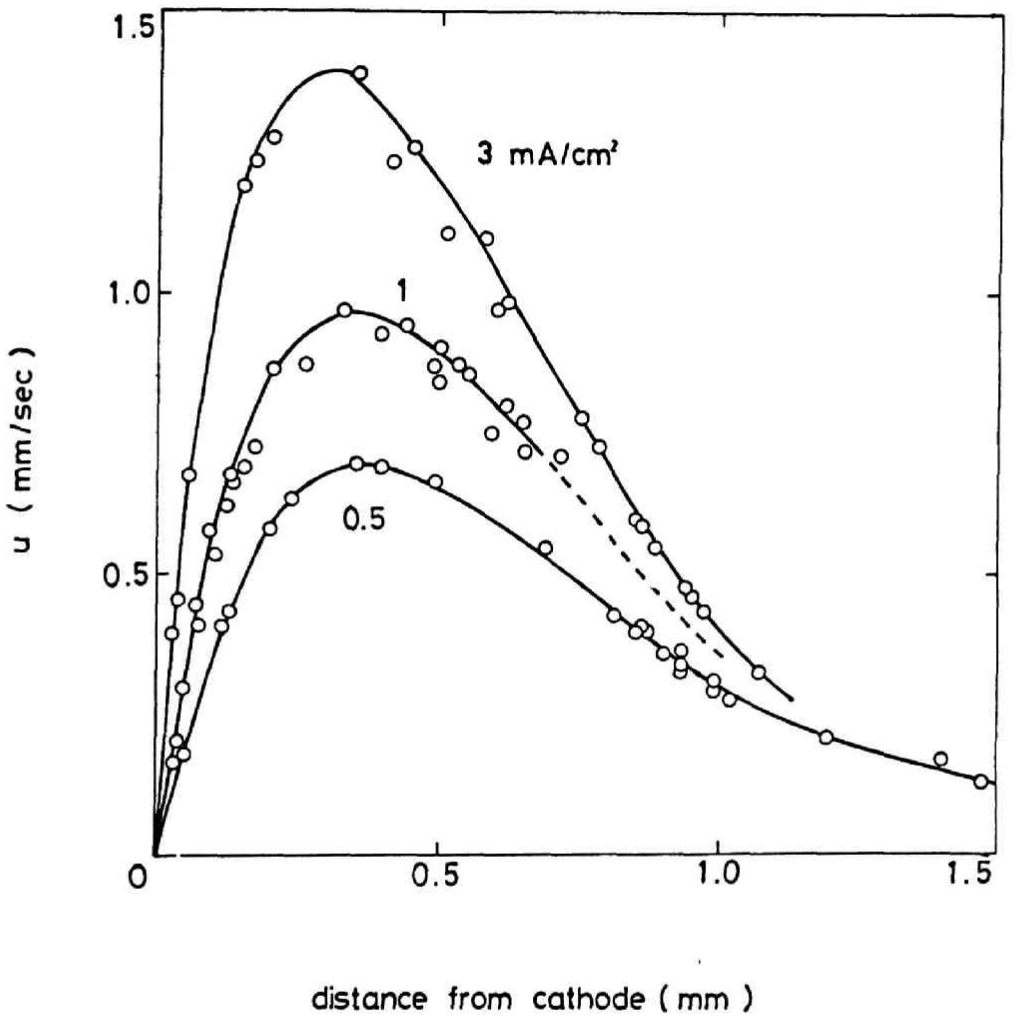

Fig. 3.8 Velocity profiles at a height of 11 cm in 0.1M $CuSO_4$ solution

profiles are in excellent coincidence with each other within the horizontal distance between 0 and τ, though the experimental results obtained in the present work are somewhat lower than Ibl et al. in the outer region beyond τ.

The measurement of velocity profile in the aqueous 0.1M $CuSO_4$ solution was conducted at the average cathodic current densities of 0.5, 1, 3 and 4 mA/cm^2 at the heights of 2.5, 7 and 11 cm from the lower edge of cathode surface, respectively, and they are demonstrated in Fig. 3.6 to 3.8. It is again seen in these figures that both u_m and τ increase with the height from the lower edge of cathode and that u_m increases and τ decreases when the average cathodic current density increases. The former variation of natural convection indicates that the hydrodynamic boundary layer grows downstream. The latter variation is, on the other hand, due to the increased difference in the density of solution between bulk-electrolyte and diffusion layer at higher current densities. It was also observed that the convective flow becomes slightly turbulent at the height above 11 cm from the lower edge of cathode when the average cathodic current density higher than 4 mA/cm^2 is applied.

By comparing u_m and τ in aqueous 0.1M $CuSO_4$ solution with those in aqueous 0.6M $CuSO_4$ solution, it was found that u_m is evidently lower in 0.1M $CuSO_4$ solution, although no significant difference was found in τ-values.

The reproducibility of the velocity profile measurement was

good in the inner portion of the hydrodynamic boundary layer between y = 0 and τ. However, it became fairly poor in the outer portion of y > τ. The natural convection in this outer portion is much more affected by the possible motion of the bulk-electrolyte.

B. Aqueous $CuSO_4$-H_2SO_4 solution

The measured velocity profiles of the natural convection in 0.6M $CuSO_4$-1.5M H_2SO_4 solution are demonstrated in Fig. 3.9 to 3.12. The measurement was carried out at the heights of 1.5, 2.5, 7 and 11 cm from the lower edge of cathode at the average cathodic current densities of 0.05, 0.1, 0.5, 1 and 3 mA/cm^2, respectively. It is seen in these figures that similar tendencies regarding the current density and height were observed as in the aqueous $CuSO_4$ solutions. Furthermore, a more precise comparison revealed that u_m and τ are lower in the acidified solution than in the aqueous $CuSO_4$ solution under the same electrolytic conditions.

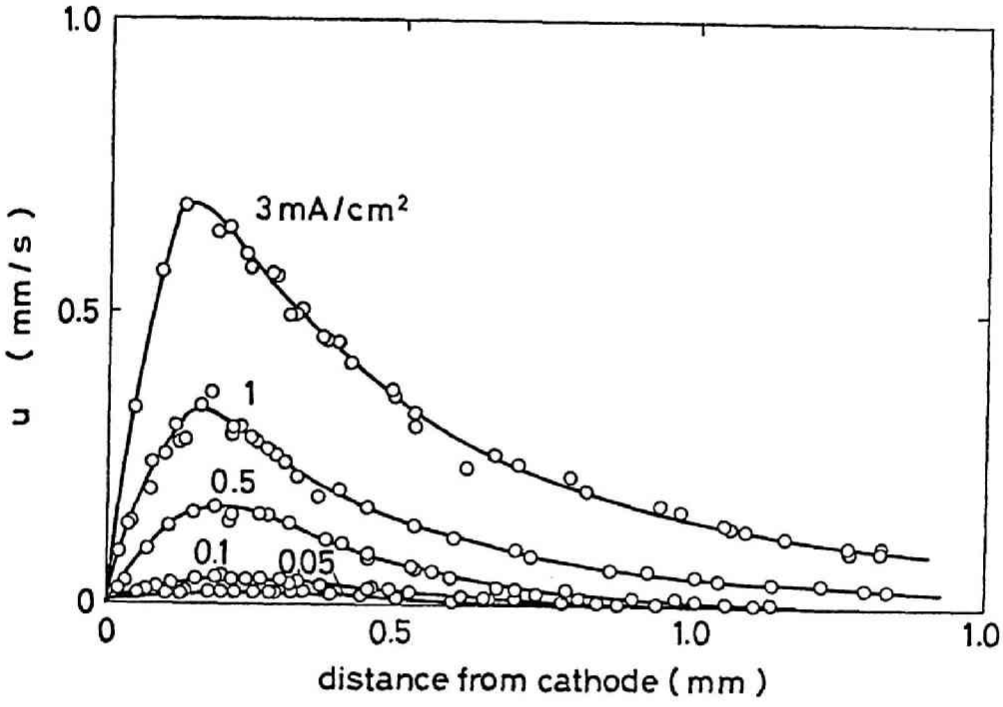

Fig. 3.9 Velocity profiles at a height of 1.5 cm in 0.6M $CuSO_4$-1.5M H_2SO_4 solution

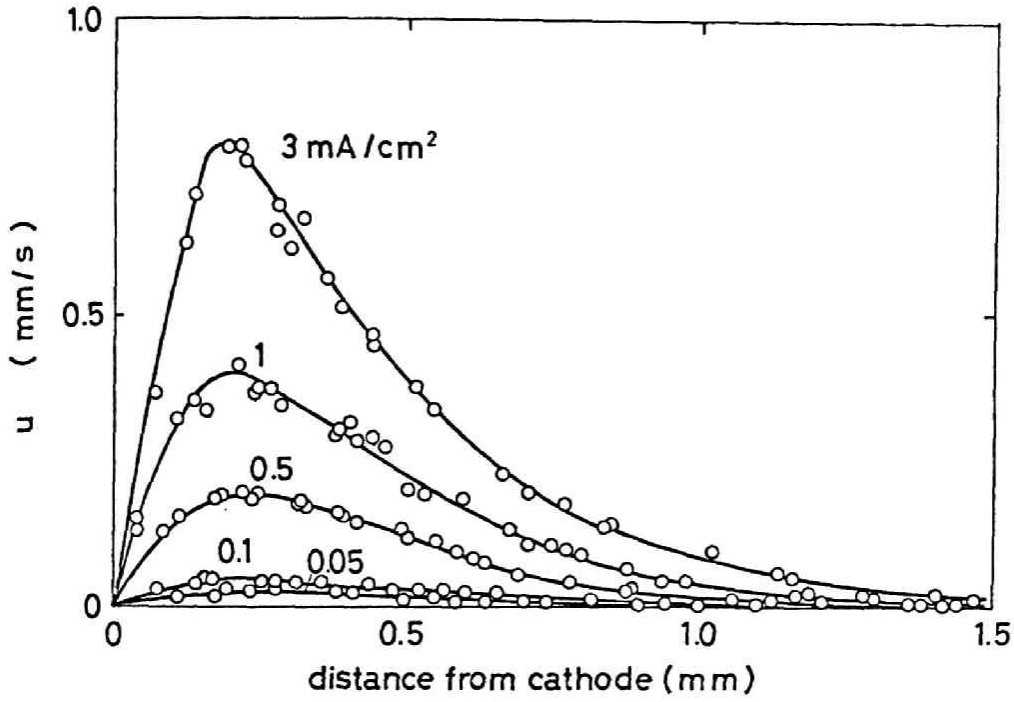

Fig. 3.10 Velocity profiles at a height of 2.5 cm in 0.6M $CuSO_4$-1.5M H_2SO_4 solution

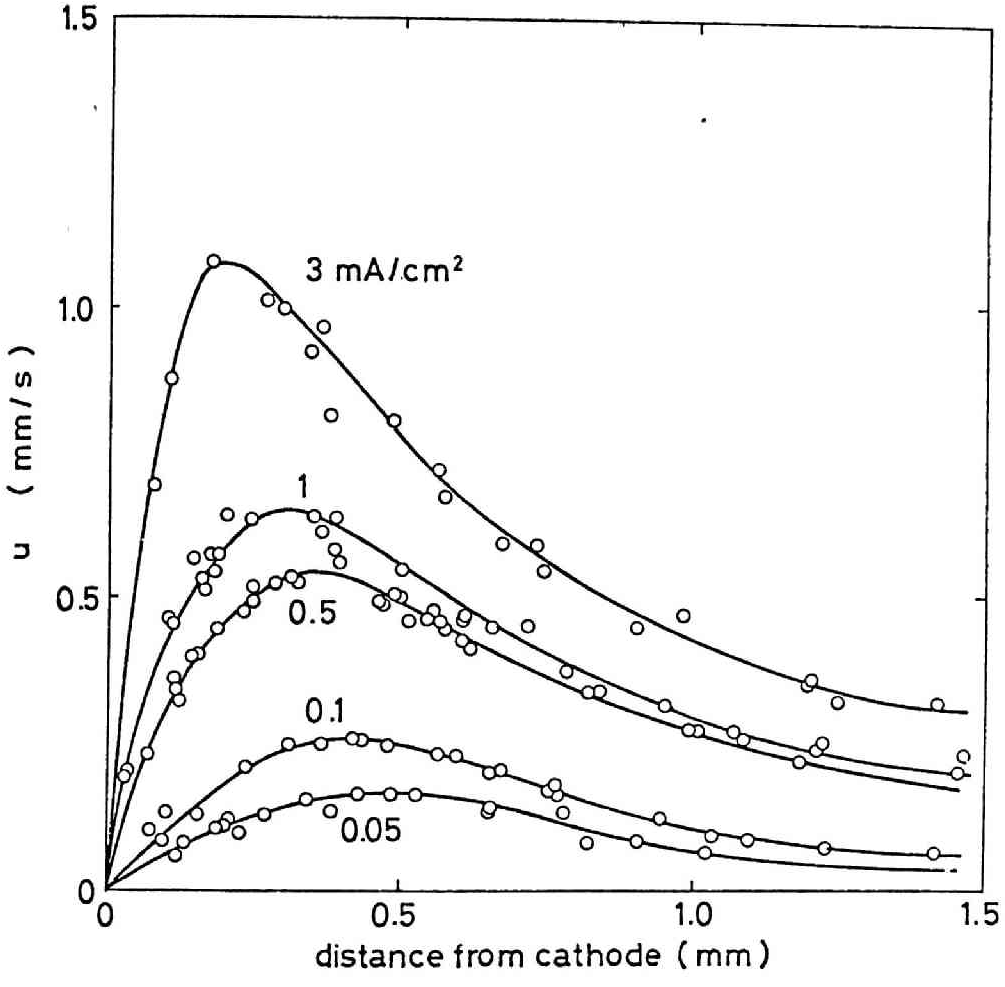

Fig. 3.11 Velocity profiles at a height of 7 cm in 0.6M $CuSO_4$-1.5M H_2SO_4 solution

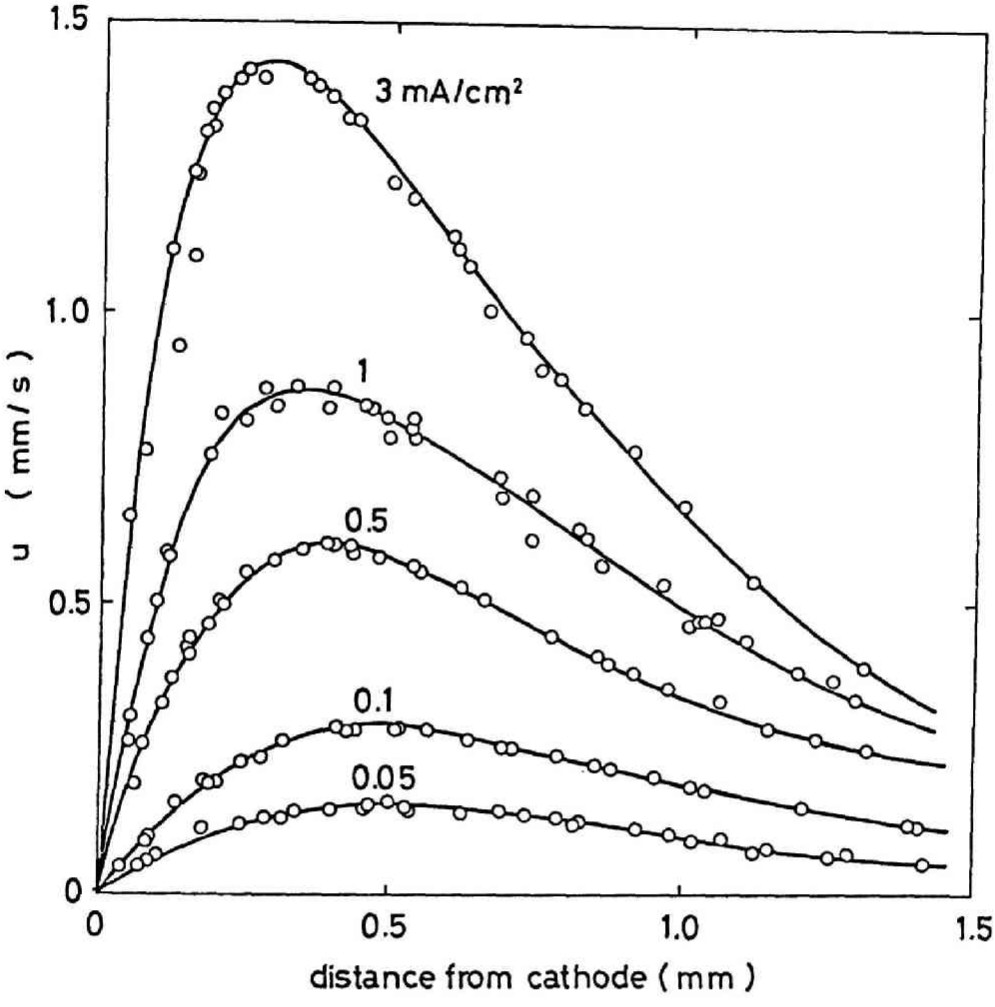

Fig. 3.12 Velocity profiles at a height of 11 cm in 0.6M $CuSO_4$-1.5M H_2SO_4 solution

3.3 Discussion

In the first place, the measured natural convection in the aqueous 0.6M $CuSO_4$ solution was compared with the experimental results of Ibl et al.[6] In order to achieve this comparison, the dimension of the electrolytic cell used in the present work was chosen to be the same as Ibl et al.[6] The property constants of the electrolytes[10-16] used in the following calculations are summarized in Table 3.1. Diffusivity of $CuSO_4$ was measured by a modified Lamm scale method using moiré pattern (see Appendix B).

The dimensionless $u_m x/D_1$ and τ/x in the aqueous 0.6M $CuSO_4$ solution were calculated from the measured u_m and τ shown in Fig. 3.4 and 3.5, and $\log(u_m x/D_1)$ and $\log(\tau/x)$ were plotted against $\log(Sc \cdot Gr^*)$ in Fig. 3.13 and 3.14, respectively. Assuming that the slopes of the regression lines are 2/5 and -1/5 from Eq. (2.64) and (2.65), respectively, the intercepts at $\log(Sc \cdot Gr^*) = 0$ were calculated by the least squares method. The parameters A_2 and E_2 in Eq. (2.64) and (2.65) were found to be $A_2 = 1.09$ and $E_2 = 1.45$ with the aqueous 0.6M $CuSO_4$ solution, respectively, which are in good agreement with $A_2 = 1.04$ and $E_2 = 1.63$ obtained by Ibl et al.[6], respectively.

Furthermore, Ibl et al.[6] determined the parameters appearing in Eq. (2.29) and (2.30) as $\omega_1 = 2.3$, $\lambda = 1.7$, $\eta = 2.1$ and $\varepsilon = 10$. In order to ascertain the λ-value, u/u_m was plotted against y/τ

Table 3.1 Property constants used in the calculation

	0.6M $CuSO_4$ solution	0.1M $CuSO_4$ solution
z_1	1	1
D_1 (cm^2/sec)	4.5×10^{-6}*	6.0×10^{-6}*
*ν (cm^2/sec)[6,10]	1.33×10^{-2}	1.022×10^{-2}
α_1[6,11]	140	151.5
*t_1[11,12]	0.29	0.357

* see Appendix B

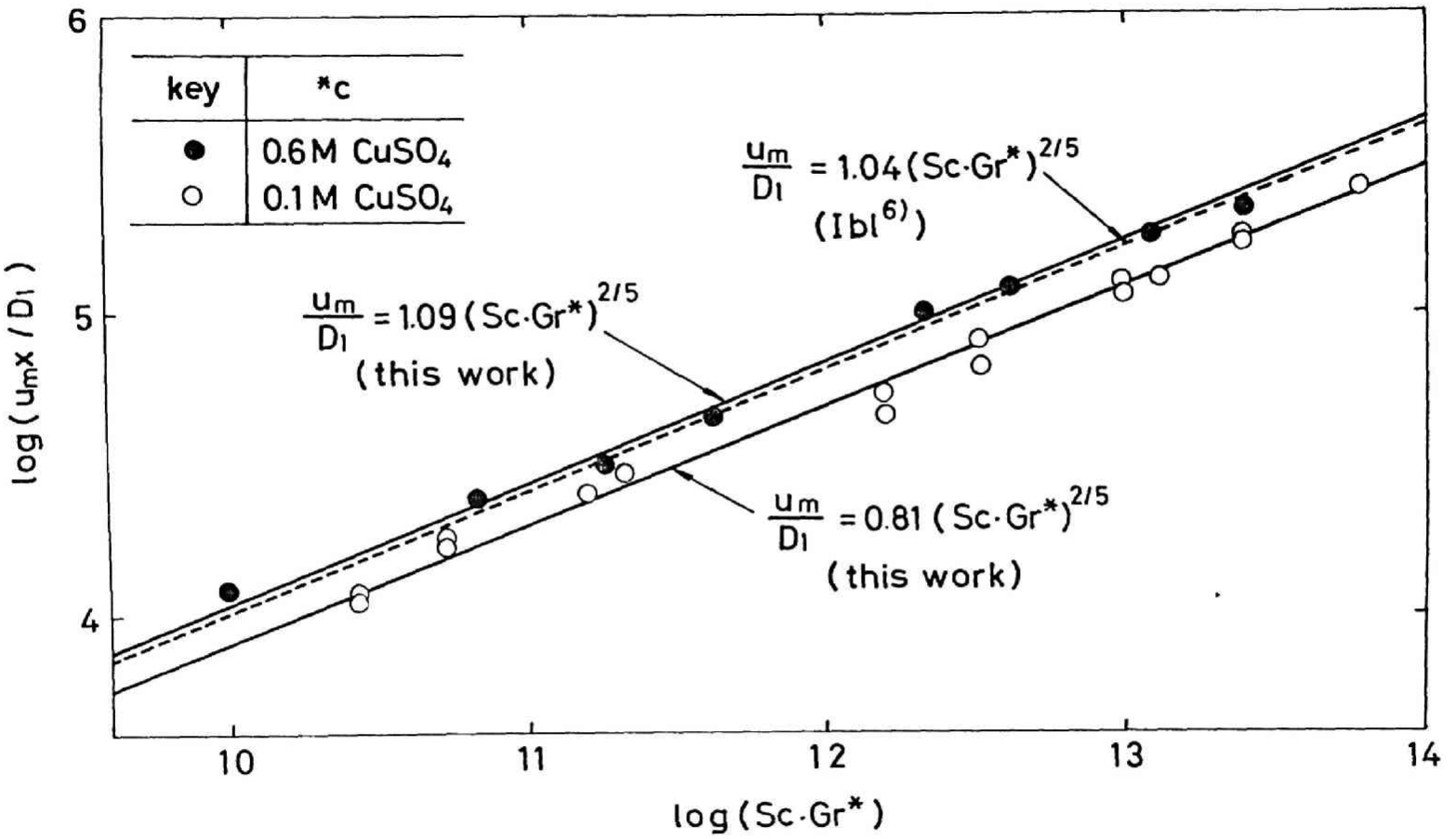

Fig. 3.13 General correlation of maximal velocity in 0.6M $CuSO_4$ and 0.1M $CuSO_4$ solutions

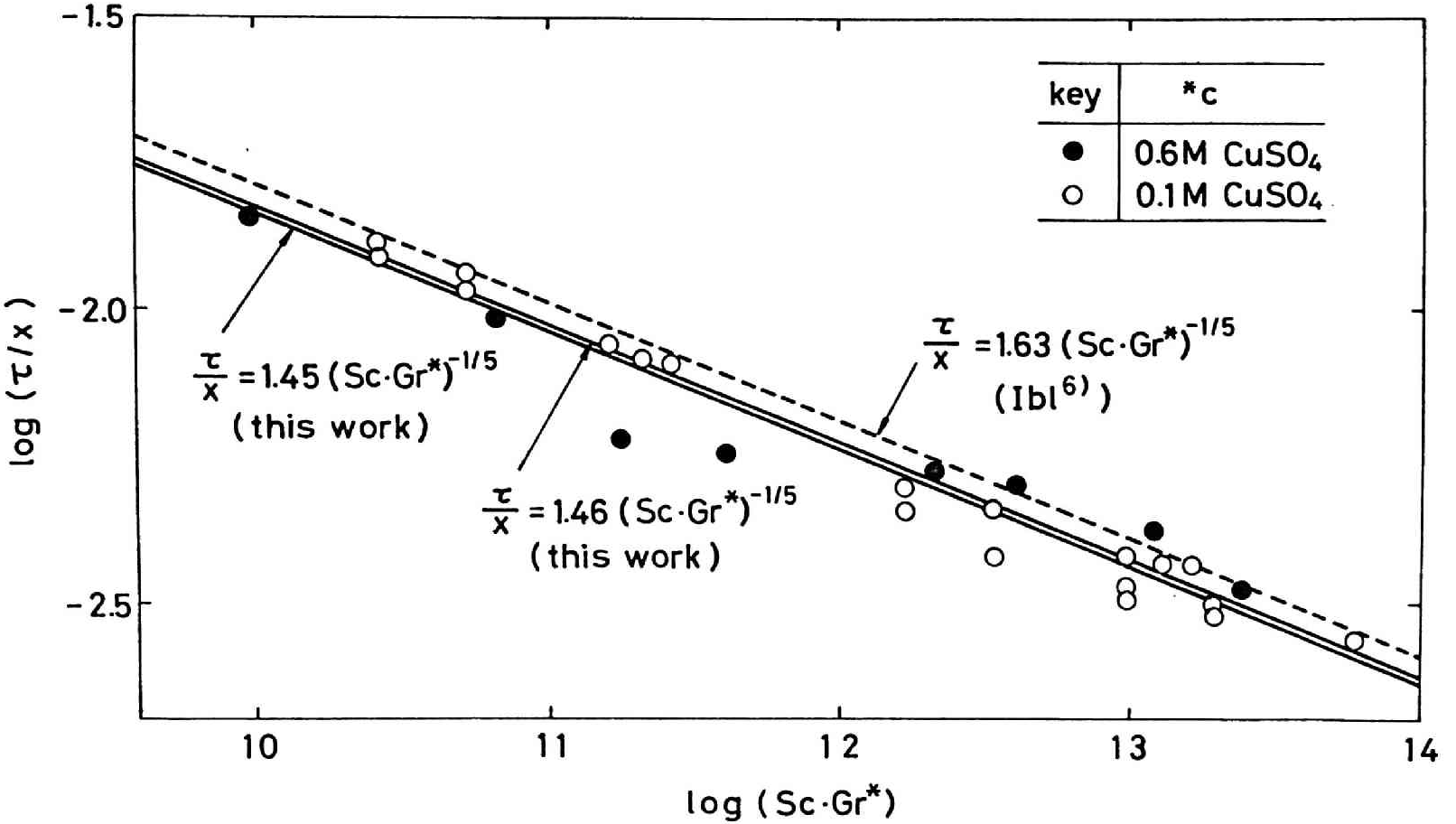

Fig. 3.14 General correlation of distance between cathode surface and the position of maximal velocity in 0.6M $CuSO_4$ and 0.1M $CuSO_4$ solutions

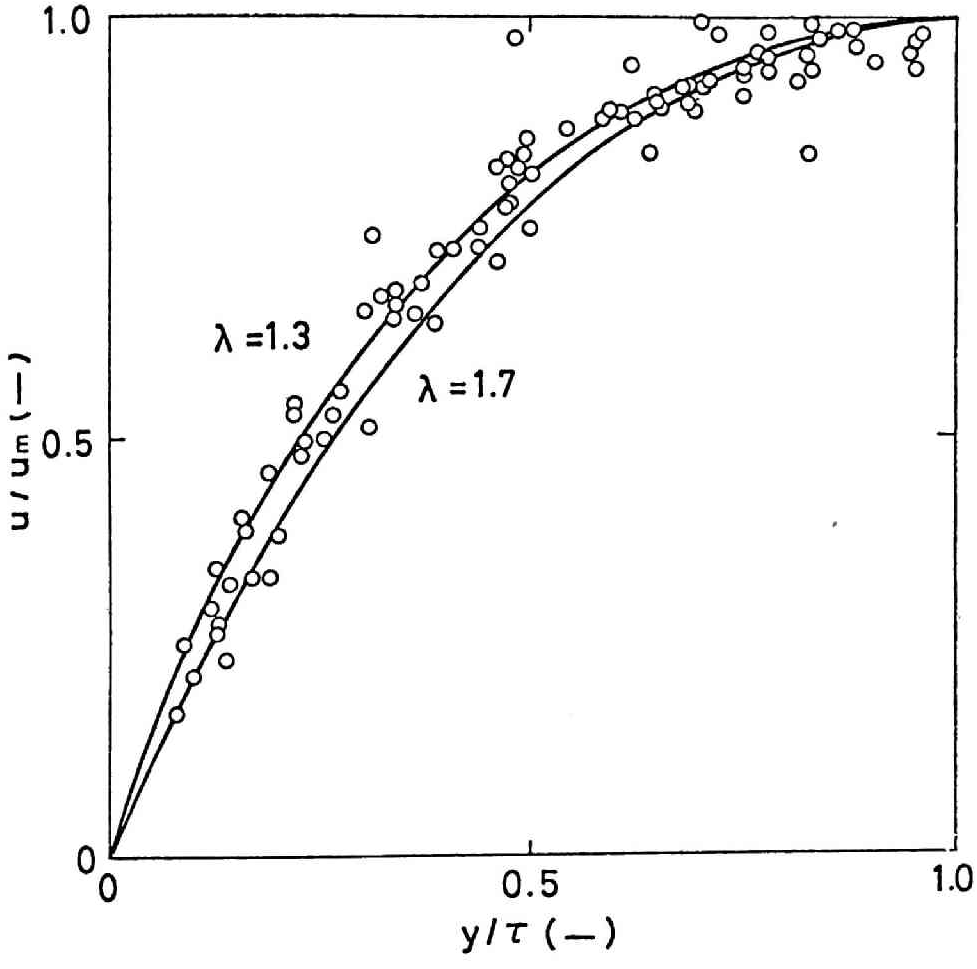

Fig. 3.15 Plot of u/u_m versus y/τ in 0.6M $CuSO_4$ solution

in Fig. 3.15. According to Eq. (2.30), the plot of u/u_m against y/τ within the distance τ from the cathode surface composes an identical curve. Though the plot in Fig. 3.15 is somewhat scattered, it can be said that all of the experimental data virtually cluster around a single curve. The best fitted λ-value was obtained as 1.3. The numerical value of 1.7 obtained by Ibl et al.[6] is also within the variation of the experimental data.

In the next place, the natural convection in the aqueous 0.1M $CuSO_4$ solution is examined. From the experimental values of u_m and τ obtained from Fig. 3.6 to 3.8 and the property constants of the electrolyte demonstrated in Table 3.1, $\log(u_m x/D_1)$ and $\log(\tau/x)$ were calculated, and they were plotted against $\log(Sc \cdot Gr^*)$ in Fig. 3.13 and 3.14, respectively, together with the experimental results with the aqueous 0.6M $CuSO_4$ solution. As seen in these figures, the experimental data obtained with the aqueous 0.1M $CuSO_4$ solution also satisfy the prediction from the theory: $(u_m x/D_1)$ and (τ/x) are proportional to the 2/5th and -1/5th power of $(Sc \cdot Gr^*)$, respectively. Presuming that the slope of the regression line is 2/5 and -1/5, respectively, the intercepts A_2 and E_2 of Eq. (2.64) and (2.65) at $\log(Sc \cdot Gr^*) = 0$ were calculated by the least squares method. They are

$$A_2 = 0.81 \quad \text{and} \quad E_2 = 1.46$$

When they are compared with the numerical values of $A_2 = 1.09$ and $E_2 = 1.45$ obtained with the aqueous 0.6M $CuSO_4$ solution and with $A_2 = 1.04$ and $E_2 = 1.63$ obtained by Ibl et al.,[6] it may be said

that E_2-values are fairly well coincident with each other within the experimental error. On the other hand, A_2-value obtained in the aqueous 0.1M $CuSO_4$ solution is evidently lower than the other two values obtained with aqueous 0.6M $CuSO_4$ solution. Since the experimental error in the measurement of u_m is fairly minor as compared with τ, it may not be appropriate to presume that this difference in A_2-values is due to the experimental error. The following considerations were made.

When the property constants of aqueous 0.1M $CuSO_4$ solution are compared with 0.6M $CuSO_4$ solution shown in Table 3.1, D_1, α_1 and $*t_1$ are higher and ν is lower in 0.1M $CuSO_4$ solution. Presuming that the parameters in Eq. (2.29) and (2.30) are unvaried in both solutions, it was disclosed from the calculation that u_m in 0.1M $CuSO_4$ solution is about 10 percent higher than that in 0.6M $CuSO_4$ solution, which is contrary to the experimental result of Fig. 3.13.

Then it is supposed that the parameters in Eq. (2.29) and (2.30) are affected by the change of $CuSO_4$ concentration, and it was tried to determine the parameters so as to fit the obtained values of A_2 (= 0.81) and E_2 (= 1.46), respectively. Among the parameters, ε which influences the slope of velocity profile in the outer portion of hydrodynamic boundary layer has no significant effect on the estimation of u_m and τ,[6] and it was assumed to be 10. Furthermore, the parameter ω_1 which determines the concentration profile of $CuSO_4$ was assumed to be 2.3 from the ex-

perimental results which will be mentioned in Chapter 4. Then the other parameters λ and η were varied at an interval of 0.1 in the region of 1.0 to 2.9 and 1.2 to 4.1, respectively, and A_2- and E_2-values were calculated using each combination of these two parameters. Thus the combinations of parameters which yield the values of A_2 and E_2 coincident with 0.81 and 1.46, respectively, were pursued. The results are summarized in Table 3.2. As seen in this table, several combinations of λ and η were obtained with which the above requirements were satisfied. In these combinations, λ-value is 1.4 to 1.5 and η-value is 2.5 to 2.7.

Then the appropriateness of these numerical values were examined. With regard to λ-value, the experimental values of (u/u_m) in the inner portion of the hydrodynamic boundary layer $(0 \leqq y \leqq \tau)$ were calculated from Fig. 3.6 to 3.8, and they were plotted against (y/τ) in Fig. 3.16. According to Eq. (2.30), this plot composes an identical curve. Though the experimental plot in Fig. 3.16 is somewhat scattered, it may be said that all of the experimental data virtually cluster around a single curve, and the above-mentioned λ-values are in the middle of experimental data. With 0.6M $CuSO_4$ solution, the λ-value was obtained at 1.3 in the present work, and Ibl et al.[6] obtained 1.7. They are also within the variation of the present experimental data.

The numerical values of η shown in Table 3.2, on the other hand, are about 1.2 to 1.3 times larger than η-value of 2.1 obtained by Ibl et al.[6] with 0.6M $CuSO_4$ solution. Since τ-value

Table 3.2 Estimated parameters which are fitted to the experimental data

ω_1	λ	η	ε	A_2	E_2
2.3	1.4	2.5	10.0	0.791	1.498
2.3	1.5	2.5	10.0	0.848	1.456
2.3	1.5	2.6	10.0	0.828	1.408
2.3	1.5	2.7	10.0	0.810	1.363
Experimental data obtained from Fig. 3.13 and 3.14, respectively				0.81	1.46

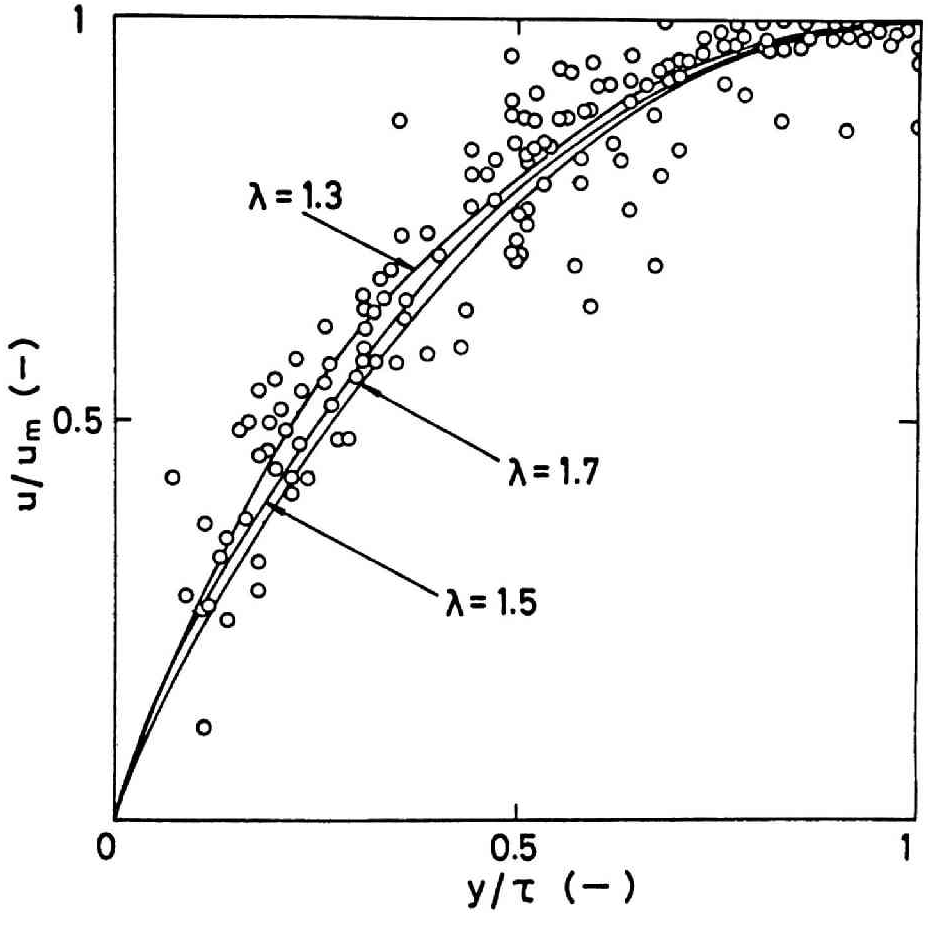

Fig. 3.16 Plot of u/u_m versus y/τ in 0.1M $CuSO_4$ solution

obtained with 0.1M $CuSO_4$ solution is coincident within the experimental error with those of the present work and Ibl et al.[6] both obtained with 0.6M $CuSO_4$ solution, it is indicated that the thickness of cathodic diffusion layer in aqueous 0.1M $CuSO_4$ solution is 1.2 to 1.3 times larger than that in 0.6M $CuSO_4$ solution.

In order to verify this presumption, the following calculation was made. From Eq. (2.41), we have

$$\delta_1 = \left(\frac{\omega_1 z_1 F}{i}\right) \frac{D_1 \Theta_1}{(1-*t_1)} \tag{3.4}$$

Presuming that the parameter ω_1 is unvaried in aqueous 0.1M and 0.6M $CuSO_4$ solutions, the term, $(\omega_1 z_1 F/i)$ on the right-hand side of this equation is constant at a given cathodic current density.

From the experimental results of holographic interferometry which will be described in Chapter 4, the concentration difference of $CuSO_4$ between bulk-electrolyte and cathode surface, Θ_1, in the aqueous 0.1M $CuSO_4$ solution is less than 0.05M under the present experimental conditions. This value of Θ_1 may also be valid in aqueous 0.6M $CuSO_4$ solution. The diffusivity of $CuSO_4$ at the average concentration of 0.075M and 0.575M in the diffusion layer of these aqueous solutions is 6.42×10^{-6} cm^2/sec and 4.45×10^{-6} cm^2/sec, respectively (see Appendix B). As seen in Table 3.1, the variation of transference number of Cu^{2+} ion due to the difference in $CuSO_4$ concentration in the diffusion layer may be omitted.[11,12] Then the ratio of thickness of the diffusion layer in aqueous 0.1M and 0.6M $CuSO_4$ solutions is calculated as

follows.

$$\frac{\delta_1(0.1M)}{\delta_1(0.6M)} = \frac{6.42 \times 10^{-6} \times 0.05 \times (1 - 0.29)}{4.45 \times 10^{-6} \times 0.05 \times (1 - 0.36)}$$

$$= 1.6$$

Though this value is slightly higher than the above-mentioned value of 1.2 to 1.3, it may be said that the lower u_m-values in aqueous 0.1M $CuSO_4$ solution than in 0.6M $CuSO_4$ solution are attributed to the higher η-value in the former solution which is mainly due to the higher diffusivity of $CuSO_4$ in this solution.

Then the considerations were directed to the natural convection in the solution containing $CuSO_4$ and H_2SO_4. By comparing Eq. (2.92) with Eq. (2.61) and Eq. (2.94) with Eq. (2.63), respectively, it is seen that the term α_1 in Eq. (2.61) and (2.63) of the aqueous $CuSO_4$ solution was essentially replaced with the term ξ in Eq. (2.92) and (2.94) of the aqueous solution containing $CuSO_4$ and H_2SO_4. The term ξ which is represented by Eq. (2.82) indicates that the concentration gradient of H^+ ion in the cathodic diffusion layer has an inverse effect on the natural convection as compared with Cu^{2+} ion. Thus Eq. (2.29) and (2.94) involve an additional parameter σ, and it is not possible to rewrite them into the dimensionless expressions. Instead, it is desirable to transform these equations into the forms of

$$u_m x = A' \left(\frac{g \xi^3 (1 - *t_1)}{z_1 F * \nu} \right)^{2/5} k_1^{1/5} (ix^4)^{2/5} \qquad (3.5)$$

where

$$A' = (\lambda - 1)\left[\frac{\eta\omega_1}{\Phi^3(\omega_1, \eta, \lambda, \varepsilon)\lambda^2}\right]^{1/5} \tag{3.6}$$

and

$$\tau/x = E' \left(\frac{z_1 F^* \nu k_1^2}{g\xi(1-^*t_1)}\right)^{1/5} (ix^4)^{-1/5} \tag{3.7}$$

where

$$E' = E_4 \tag{3.8}$$

respectively.

The numerical values u_m and τ were obtained from Fig. 3.9 to 3.12, and $\log(u_m x)$ and $\log(\tau/x)$ were plotted against $\log(ix^4)$ in Fig. 3.17 and 3.18, respectively. The slopes of regression lines were assumed to be 2/5 and -1/5 from Eq. (3.5) and (3.7), and the intercepts were calculated and demonstrated in Fig. 3.17 and 3.18, respectively. It is clear from these diagrams that u_m and τ becomes lower in the acidified solution.

The parameters ω_1, ω_2, η, λ and ε were determined so as to fit to the obtained intercepts of

$$A'[g\xi(1 - {}^*t_1)/z_1 F^* \nu]^{2/5} k_1^{1/5}$$

and

$$E'[z_1 F^* \nu k_1^2 / g\xi(1 - {}^*t)]^{1/5}$$

respectively. The property constants of electrolyte used in the calculation are summarized in Table 3.3. With regard to the diffusivity of Cu^{2+} ion, the diffusivity of $CuSO_4$ in 0.6M $CuSO_4$-1.85M H_2SO_4 solution was employed in the calculation (see

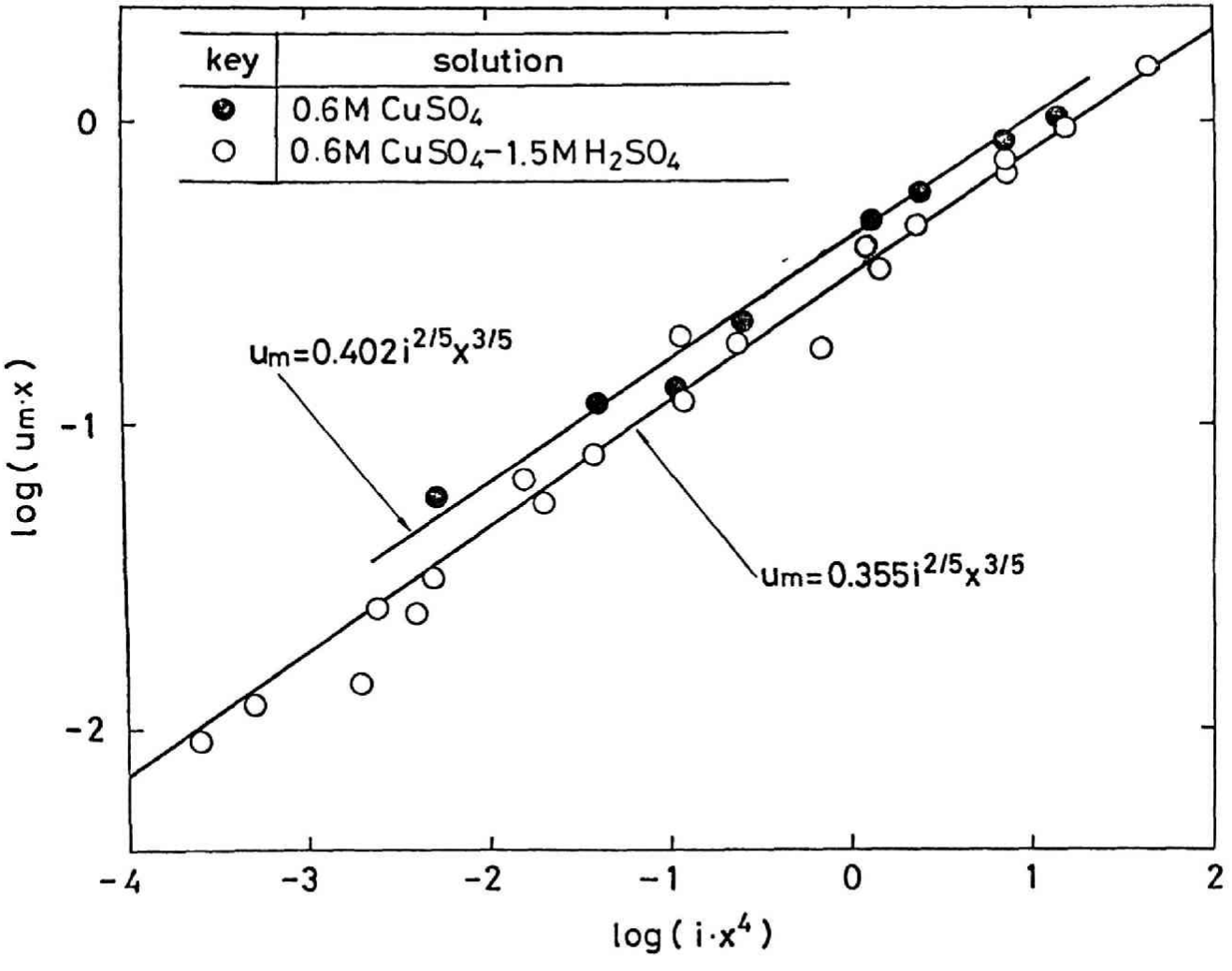

Fig. 3.17 General correlation of the maximal velocitv

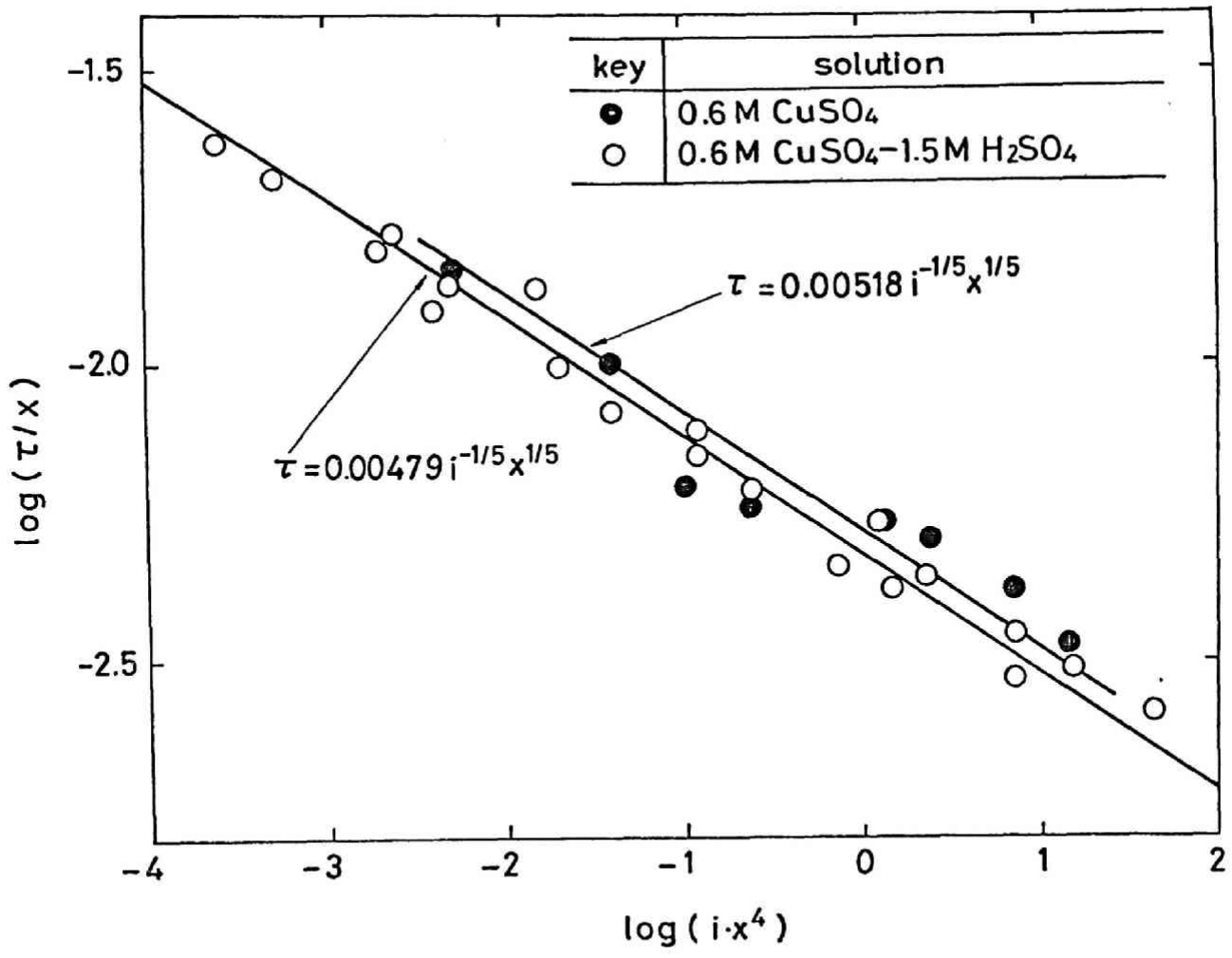

Fig. 3.18 General correlation of the distance between cathode surface and the position of maximal velocity

Table 3.3 Property constants of 0.6M $CuSO_4$-1.5M H_2SO_4 solution used in the calculation

k_l (cm^2/sec)	4.75×10^{-6}*
*ν (cm^2/sec)[13]	1.40×10^{-2}
α_1 (cm^3/mol)[14]	120.6
α_2 (cm^3/mol)[14]	41.6**
*t_1 (-)[15,16]	0.044
*t_2 (-)[15,16]	0.73
a (-)	0.29

* see Appendix B
** see Appendix D

Appendix B). Among these parameters, ε has no significant effect on the estimation of u_m and τ[6], and it was presumed to be 10. It was also assumed that ω_1 is equal to ω_2 as the first approximation. Degree of the second stage dissociation of H_2SO_4 in this solution, a, was presumed to be 0.29 (see Appendix C). Regarding the parameters ω_1, λ and η, they were varied at an interval of 0.05 in the regions of 2.0-3.0, 1.2-3.0 and 1.4-3.0, respectively, and the above-mentioned intercepts of Eq. (3.5) and (3.7) were calculated using each combination of these four parameters. The combinations of parameters which yield the calculated intercepts coincident with the experimental ones were pursued. The results are summarized in Table 3.4.

As seen in this table, several combinations of parameters were obtained with which the above requirement was satisfied. It is seen that the fitted σ-value is 1.54 in these calculations. The diffusivity of H^+ ion is higher than Cu^{2+} ion and the diffusion layer of H^+ ion is thicker. Then σ is higher than unity. On the other hand, the term ξ in Eq. (3.5) and (3.7) is positive, and σ is less than 2.22. The above σ-value is within these two limitations. Ibl et al.[17] obtained σ-value of 1.5 from the theoretical calculation under the experimental conditions of Brenner[18] assuming that H_2SO_4 is completely dissociated into $2H^+ + SO_4^{2-}$.

The λ-value shown in Table 3.4 is 2.90 and 2.95. In order to examine the appropriateness of this numerical value, u/u_m

Table 3.4 Estimated parameters which are fitted to the experimental data

No.	ω_1	λ	η	ε	σ	$u_m/i^{2/5}x^{3/5}$	$\tau/i^{-1/5}x^{1/5}$
1	2.10	2.95	2.50	10	1.54	0.344	0.00479
2	2.15	2.95	2.50	10	1.54	0.348	0.00487
3	2.20	2.95	2.55	10	1.54	0.348	0.00487
4	2.20	2.95	2.60	10	1.54	0.343	0.00479
5	2.25	2.95	2.60	10	1.54	0.347	0.00486
6	2.25	2.95	2.65	10	1.54	0.342	0.00479
7	2.30	2.90	2.65	10	1.54	0.345	0.00487
8	2.30	2.95	2.65	10	1.54	0.347	0.00847
9	2.30	2.95	2.70	10	1.54	0.343	0.00479
10	2.35	2.95	2.70	10	1.54	0.347	0.00486
11	2.35	2.95	2.75	10	1.54	0.341	0.00479
12	2.40	2.95	2.75	10	1.54	0.345	0.00486
13	2.45	2.95	2.80	10	1.54	0.345	0.00486
Experimental data obtained from Fig. 3.17 and 3.18, respectively						0.355	0.00479

within the distance τ shown in Fig. 3.9 through 3.12 were plotted against y/τ in Fig. 3.19. The majority of the experimental data is located between the curves of $\lambda = 1.3$ and 3.0, and the obtained λ-values may be appropriate though they are rather close to the upper limit of the experimental values.

It was already mentioned that both u_m and τ are reduced when H_2SO_4 is added to the solution, and the reasons of the reduced τ-value were pursued. Among the property constants shown in Table 3.3, the difference in kinematic viscosity between the aqueous 0.6M $CuSO_4$ and 0.6M $CuSO_4$-1.85M H_2SO_4 solutions is minor, and the lowered u_m and τ in the acidified solution cannot be ascribed solely to the rise of the kinematic viscosity. Selman and Newman[18,19] calculated the velocity profile of the natural convective flow in the cathodic boundary layer at the limiting current densities in the solutions containing $CuSO_4$ and excessive amount of H_2SO_4, and they indicated that the velocity profile was affected by the accumulated H^+ ion in the cathodic diffusion layer which migrates from the bulk-electrolyte.

The concentration profile of H^+ ion in the diffusion layer is inverse to the profile of Cu^{2+} ion, and the solution density in the cathodic boundary layer is determined by the concentrations of H^+ and Cu^{2+} ions. The terms of buoyancy force in the integrated Navier-Stokes equation are affected by the density of the solution. Based on this thought, the density distribution near the cathode surface was calculated at a height of 7 cm from

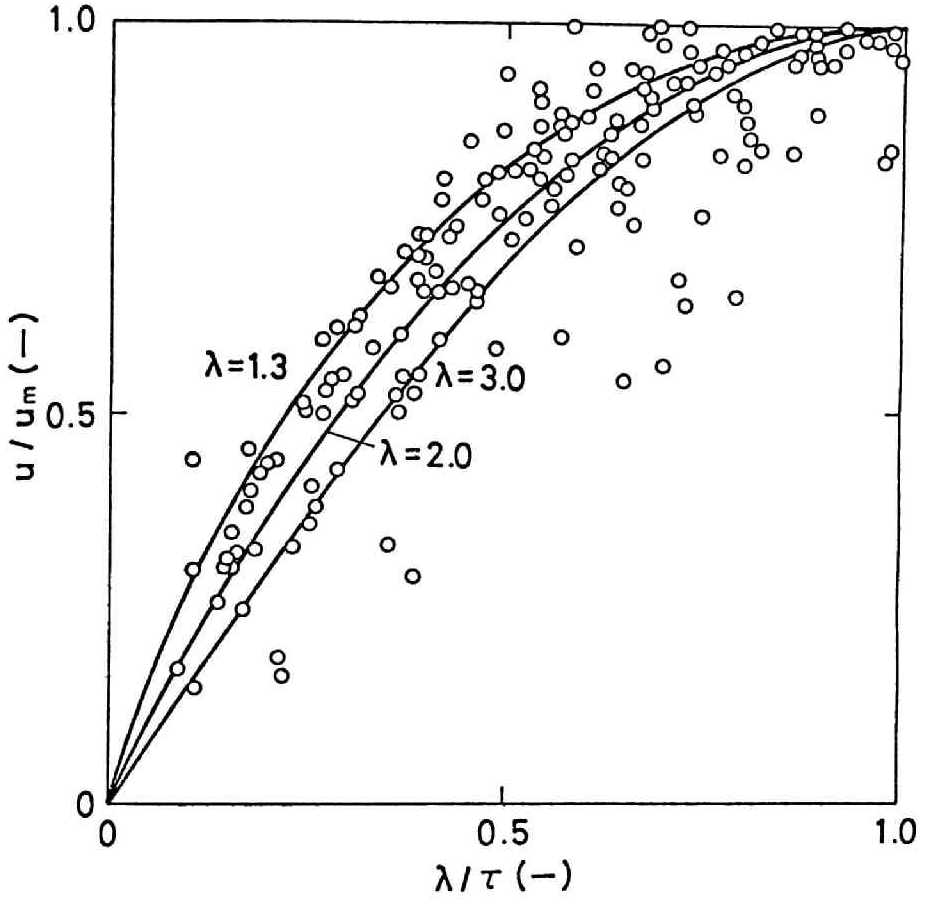

Fig. 3.19 Plot of u/u_m versus y/τ in 0.6M $CuSO_4$-1.5M H_2SO_4 solution

the lower edge of cathode and at a current density of 1 mA/cm^2.

With regard to the aqueous solution containing only $CuSO_4$, the parameters determined by Ibl[6] were employed: they were substituted in Eq. (2.63) and we obtained $\tau = 0.0343$ cm. The density distribution is expressed as

$$\frac{\Delta\rho}{*\rho} = \alpha_1\theta_1 = \alpha_1\theta_1\left(1 - \frac{y}{\eta\tau}\right)^{\omega_1}$$

$$= 0.00337\left(1 - \frac{y}{0.072}\right)^{2.3} \tag{3.9}$$

because

$$\theta_1 = \frac{\eta\tau i(1-*t_1)}{\omega_1 z_1 F D_1} = 0.0000241 \text{ mol/cm}^3 \tag{3.10}$$

The calculated density profile is demonstrated with dots in Fig. 3.20.

With regard to the solution containing both $CuSO_4$ and H_2SO_4, the parameters shown on the eighth line of Table 3.4 were substituted in Eq. (2.94), and $\tau = 0.0282$ cm was obtained. The expression of density distribution is

$$\frac{\Delta\rho}{*\rho} = \alpha_1\theta_1 + \alpha_2\theta_2$$

$$= \alpha_1\theta_1\left(1 - \frac{y}{\eta\tau}\right)^{\omega_1} + \alpha_2\theta_2\left(1 - \frac{y}{\sigma\eta\tau}\right)^{\omega_2} \tag{3.11}$$

Since the thickness of diffusion layers of Cu^{2+} and H^+ ions are given by $\eta\tau$ and $\sigma\eta\tau$, respectively, we have from Eq. (2.83)

$$\theta_1 = 0.0000344 \text{ mol/cm}^3 \tag{3.12}$$

Then

$$\frac{\Delta\rho}{*\rho} = \alpha_1\theta_1\left(1 - \frac{y}{\eta\tau}\right)^{\omega_1} - \gamma\sigma\alpha_2\theta_1\left(1 - \frac{y}{\sigma\eta\tau}\right)^{\omega_1}$$

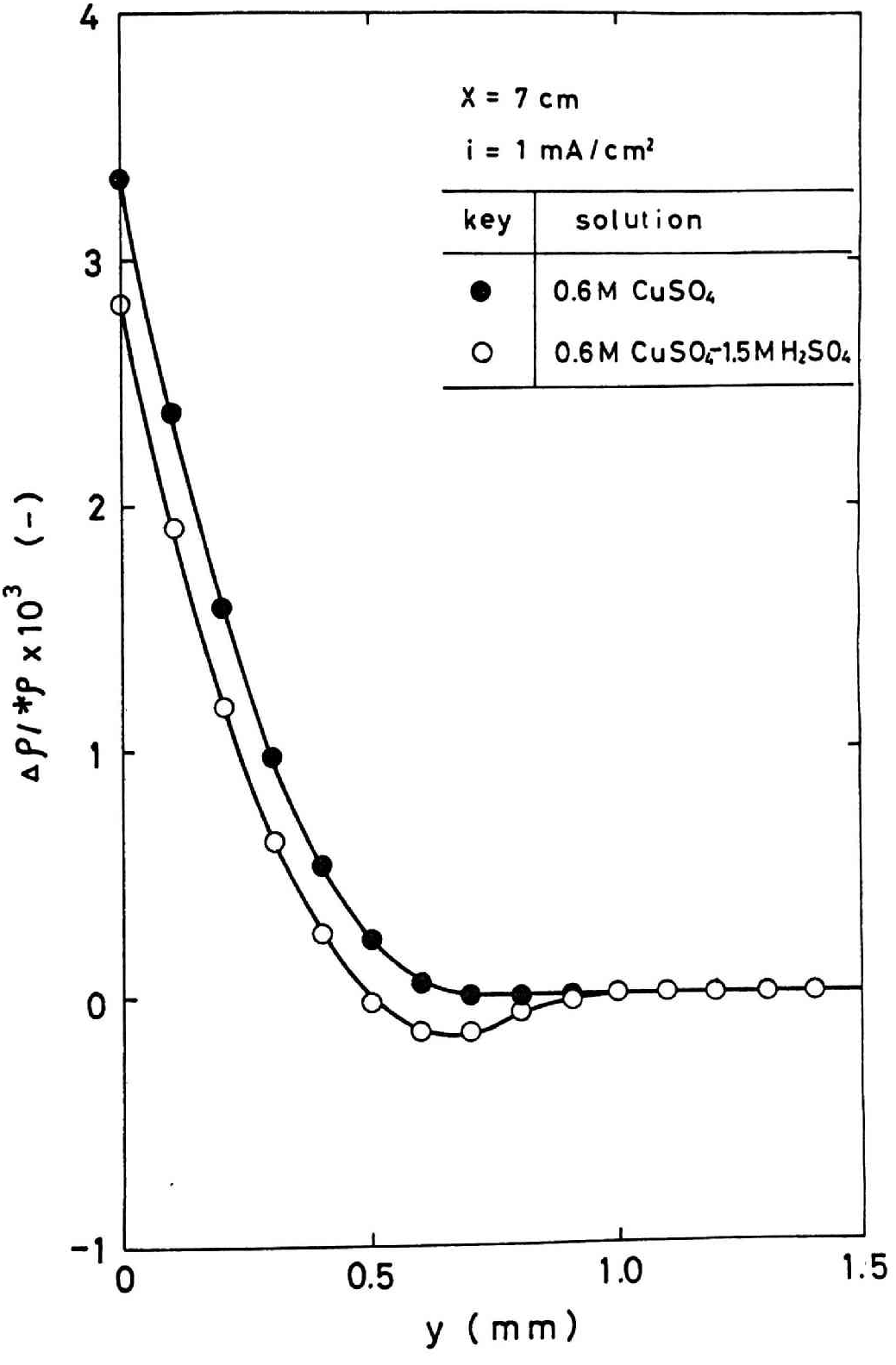

Fig. 3.20 Density profile at x = 7 cm and i = 1 mA/cm^2

$$= 0.00414\left(1 - \frac{y}{0.076}\right)^{2.3} - 0.0019\left(1 - \frac{y}{0.117}\right)^{2.3}$$

$$(0 \leqq y \leqq 0.076 \text{ cm}) \qquad (3.13)$$

and

$$\frac{\Delta\rho}{{}^{*}\rho} = -\gamma\sigma\alpha_2\theta_1\left(1 - \frac{y}{\sigma\eta\tau}\right)^{\omega_1}$$

$$= -0.00119\left(1 - \frac{y}{0.117}\right)^{2.3} \qquad (3.14)$$

$$(0.076 \text{ cm} \leqq y \leqq 0.117 \text{ cm})$$

respectively. It is also demonstrated with circles in Fig. 3.20.

By comparing these two curves shown in Fig. 3.20, it is clear that $\Delta\rho/{}^{*}\rho$ in the aqueous 0.6M $CuSO_4$ solution is positive and the buoyancy force acts in the upward direction in the whole region of the diffusion layer. On the other hand, the sign of $\Delta\rho/{}^{*}\rho$ changes from positive to negative within the diffusion layer in the aqueous 0.6M $CuSO_4$-1.85M H_2SO_4 solution: the direction of the force is downward in the region of ca. 0.05 cm $\leqq$ y $\leqq$ ca. 0.12 cm. Thus the upward natural convection is depressed by the gravitational force caused by the accumulated H^+ ion, and τ is thought to be reduced in the acidified solution.

3.4 Summary

Along the surface of a vertical plane cathode installed in an unstirred electrolyte, natural convection occurs in the upward direction. It is caused by the concentration gradient of cations in the diffusion layer. The rate of mass transfer of cations across the diffusion layer and the distribution of the local cathodic current densities are affected by this natural convective flow.

The velocity profile of the natural convective flow was measured in the aqueous solutions containing $CuSO_4$ and H_2SO_4: small colophonium particles were suspended in the solution and the motion of the particles dragged along by the convective flow near the cathode surface was filmed with a cinecamera. The measurement was carried out at 23° ± 1°C with the aqueous solutions of 0.6M $CuSO_4$, 0.1M $CuSO_4$ and 0.6M $CuSO_4$-1.5M H_2SO_4, respectively, at various heights from the lower edge of cathode at the cathodic current densities below 4 mA/cm^2 where the vertical distribution of the local current densities is presumed to be uniform.

It was revealed from the experimental results with the aqueous $CuSO_4$ solutions that the non-dimensional theoretical correlations between $u_m x/D_1$ and $(Sc \cdot Gr^*)$ and between τ/x and $(Sc \cdot Gr^*)$ are satisfied under the experimental conditions of uniform distribution of cathodic current densities in the vertical direction, respectively. The maximal velocity, u_m, and the distance be-

tween the cathode surface and the position of u_m, τ, in the aqueous 0.6M $CuSO_4$ solution were in good agreement with the experimental results obtained by Ibl et al.[6)]

Furthermore, the experimental results with the aqueous 0.1M $CuSO_4$ solution were compared with those obtained with aqueous 0.6M $CuSO_4$ solution, and the effects of $CuSO_4$ concentration on the velocity profile were pursued. In the 0.1M $CuSO_4$ solution, u_m is lower. This is clear from Fig. 3.13 in which $\log(u_m x/D_1)$ was plotted against $\log(Sc \cdot Gr^*)$. The lower u_m in 0.1M $CuSO_4$ solution was not able to be explained from the difference of property constants of the two solutions. The parameters ε, ω, and λ are unvaried in these two solutions, and the parameter $\eta(= \delta_1/\tau)$ is larger in 0.1M $CuSO_4$ solution. Since τ is virtually unvaried in both solutions, the higher value of η in 0.1M $CuSO_4$ solution may indicate that the thickness of diffusion layer is larger in this solution. From the calculation, it was revealed that the larger δ-value in 0.1M $CuSO_4$ solution is mainly attributed to the higher diffusivity of $CuSO_4$ in this solution.

Next, the experimental results with the aqueous 0.6M $CuSO_4$-1.85M H_2SO_4 solution was found to satisfy the theoretical expressions of u_m and τ in the solutions containing $CuSO_4$ and H_2SO_4 which were derived in Chapter 2. The parameters involved in these equations were determined according to the procedure proposed by Ibl. In this calculation the incomplete dissociation of H_2SO_4 was taken into consideration, and the ratio of the thickness of

diffusion layers of H^+ ion and Cu^{2+} ion was obtained at 1.54, which is an important parameter in the considerations of the ionic mass transfer in the cathodic diffusion layer of the aqueous $CuSO_4$-H_2SO_4 solution. From the comparison of velocity profiles in aqueous 0.6M $CuSO_4$ and 0.6M $CuSO_4$-1.5M H_2SO_4 solutions, it was revealed that both u_m and τ are reduced in the latter solution containing $CuSO_4$ and H_2SO_4. In order to clarify the reduced τ-value in the solution containing $CuSO_4$ and H_2SO_4, a calculation was carried out. It was presumed in this calculation that the change of kinematic viscosity of solutions has no virtual effect on the change of τ-value. In both solutions containing $CuSO_4$ and $CuSO_4$-H_2SO_4, the density distributions in the cathodic diffusion layer were calculated, respectively, and it was disclosed that $\Delta\rho/^*\rho$ is positive in the whole region of the diffusion layer in the former aqueous solution. On the contrary, $\Delta\rho/^*\rho$ changes from positive to negative in the diffusion layer of the latter solution because of the inverse concentration profile of H^+ ion. Thus the upward natural convection is thought to be depressed by the negative $\Delta\rho/^*\rho$ in the outer portion of the cathodic diffusion layer.

Reference to Chapter 3

1) C. Wagner: J. Electrochem. Soc., 95 (1949) 161.

2) C. R. Wilke, C. W. Tobias and M. Eisenberg: Chem. Eng. Prog., 49 (1953) 663.

3) E. M. Sparrow: Nat. Advisory Comm. Aeronaut. Tech. Not., 3508, July (1955).

4) E. R. G. Eckert: "Introduction to the Transfer of Heat and Mass", p. 158ff. McGraw-Hill Book Co., New York (1950).

5) N. Ibl and R. H. Müller: Z. Elektrochem., 59 (1955) 671.

6) N. Ibl and R. H. Müller: J. Electrochem. Soc., 105 (1958) 346.

7) R. H. Müller: "Advances in Electrochemistry and Electrochemical Engineering", vol. 9, p. 281, John Wiley and Sons Inc., New York (1973).

8) N. Ibl, W. Rüegg and G. Trümpler: Helb. Chim. Acta, 36 (1953) 1624.

9) C. Wagner: J. Electrochem. Soc., 104 (1957) 129.

10) "International Critical Tables of Numerical Data, Physics, Chemistry and Technology" ed. by E. Washburn, vol. 3, p. 67 and vol. 5, p. 14, McGraw-Hill Book Co., New York (1929).

11) N. Ibl, Y. Barrada and G. Trümpler: Helv. Chim. Acta, 37 (1954) 583.

12) H. Landolt: "Landolt-Börnstein Zahlenwert und Funktionen und Physik, Chemie, Astronomie, Geophysik und Technik", 1104, Springer, Berlin (1964).

13) M. Eisenberg, C. W. Tobias and C. R. Wilke: J. Electrochem. Soc., 103, (1956) 413.

14) K. Asada, F. Hine, S. Yoshizawa and S. Okada: J. Electrochem. Soc., 107 (1960) 242.

15) R. A. Robinson and R. H. Stokes: "Electrolyte Solutions", p. 465, Butterworths, London (1959).

16) E. A. Moelwyn-Hughes: "Physical Chemistry", p. 859, Pergamon Press, Oxford (1962).

17) N. Ibl and U. Braun: Chimia, 21 (1967) 395.

18) A. Brenner: Proc. Educational Sessions of 29th Annual Convention, Am. Electroplaters Soc., 28 (1941).

19) J. R. Selman and J. Newman: J. Electrochem. Soc., 118 (1971) 1070.

20) J. R. Selman and J. Newman: UCRL-20322, January (1971).

CHAPTER 4 CONCENTRATION DISTRIBUTION OF $CuSO_4$ AND H_2SO_4 IN CATHODIC DIFFUSION LAYER

4.1 Introduction

It was mentioned in Chapter 1 that the concentration of ionic species near the cathode surface becomes different from the bulk-electrolyte along with the progress of electrolysis, and the cathodic diffusion layer is formed. When the electrolysis takes place on a vertical plane cathode installed in an unstirred aqueous solution, upward natural convective flow occurs along the cathode surface due to the concentration difference of ionic species between the cathodic diffusion layer and the bulk-electrolyte. The resultant convective ionic mass transfer in this diffusion layer affects the rate of electrodeposition: for example, the distribution of the local current densities in vertical direction on the cathode surface is determined solely by the ionic mass transfer in the cathodic diffusion layer when the applied current is at the limiting value. The cathodic concentration polarization is often caused by the decrease of concentration of the reacting ionic species near the cathode surface.

In the industrial electrolytic refining and plating, an excessive amount of supporting electrolyte such as H_2SO_4 is usually added to raise the conductivity, and H_2SO_4 is dissociated into H^+, HSO_4^- and SO_4^{2-} ions among which H^+ ion migrates toward the cathode surface due to the applied potential gradient between both electrodes. The concentration profile of H^+ ion is established in the cathodic diffusion layer, and it also affects the natural convective flow along the cathode surface. Consequently, the ionic mass transfer of the reacting species in the cathodic diffusion layer is affected by the accumulation of H_2SO_4 in this layer. It is important to measure the concentration profiles of the reacting species and H^+ ion in the cathodic diffusion layer.

Many experimental works have been carried out on the cathodic diffusion layer by measuring the current-potential curve. The thickness of the Nernst diffusion layer[1)] can easily be calculated from the cathodic limiting current density obtained from the current-potential curve. However, this thickness is merely the average thickness of the cathodic diffusion layer in which the local gradient of concentration is assumed to be equal in vertical direction along the height of the cathode surface: it is not possible to obtain the actual thickness of the cathodic diffusion layer from the measurement of the current-potential curve. It is also clear that this measurement does not offer any information about the cathodic diffusion layer at the current densities below the limiting value.

A few experimental studies have been made, on the other hand, to directly measure the concentration profile of $CuSO_4$ in the diffusion layer near the cathode surface. However, the thickness of this diffusion layer is about 0.1 cm or less, and the measurement was very difficult. Read and Graham,[2] for example, tried to determine the composition of the cathodic diffusion layer by sucking the solution from this layer with a small glass capillary. Brenner[3,4] also measured the concentration profile in the cathodic diffusion layer by rapidly freezing the solution, shaving it into thin slices parallel to the cathode surface and analyzing them. However the cathodic diffusion layer was disturbed in both measurements of the concentration profile, and the measuring precision was insufficient.

An optical method using a technique of Jamin interferometry was proposed by Ibl et al.[5,6] Thereafter, Tvarusko et al.[7,8] conducted the measurements of the concentration profile and the diffusion layer thickness at an unsteady state by applying Mach-Zehnder interferometry with a laser emitter as the light source. The optical methods of Jamin and Mach-Zehnder interferometries have an advantage that the measurement of the concentration profile in the cathodic diffusion layer is carried out without disturbing the thin liquid layer. When these techniques are employed, however, the optical precision imposed on the electrolytic cell is so strict that only the cells of smaller sizes can be used because of the difficulty in the preparation. Thus Ibl et al.

measured the concentration profile of $CuSO_4$ at a height of only 0.9 cm from the lower edge of the cathode installed in a small electrolytic cell. Tvarusko et al. also employed the vertical plane cathode of only 1.7 cm height for the measurements of the thickness of cathodic diffusion layer and the concentration difference between bulk-electrolyte and cathode surface.

Holographic interferometry[9,10,11] is employed in the present work to measure the concentration profile of $CuSO_4$ in the cathodic diffusion layer during the electrolysis of aqueous $CuSO_4$ solutions. The same technique is also employed to measure the profile of refractive index of the solution in the cathodic diffusion layer in the electrolysis of $CuSO_4$-H_2SO_4 aqueous solutions. One major experimental advantage of this technique is the employment of common path interference which is different from the conventional two-beam interference used in the above-mentioned Jamin and Mach-Zehnder interferometries. Because of this advantage, it becomes possible to measure the concentration profile along the surface of a taller plane cathode installed in a large electrolytic cell of lower optical precision.

The concentration gradient of $CuSO_4$ in the cathodic diffusion layer yields the gradient of refractive index of the solution, and the incident beam which passes through the cathodic diffusion layer is deflected due to the gradient of the refractive index. Then the obtained interferogram is distorted due to the deflection of the incident beam. In order to obtain the accurate concen-

tration profile from the interferogram, this optical distortion has to be corrected when the gradient of refractive index is relatively large.

The optical distortion due to the deflection of the incident beam was sometimes not taken into consideration in the previous works.[5,6,7,8] A correcting procedure is proposed in the present work assuming that the change of refractive index in the cathodic diffusion layer between the incident and exit points of the beam on the inner wall of the electrolytic cell is approximated to be linear.

4.2 Concentration Profile of $CuSO_4$ in Cathodic Diffusion Layer in the Electrolysis of Aqueous $CuSO_4$ Solution

4.2.1 Experimental Arrangement and Procedure

Holography is a novel photographic technique which was invented by Gabor[12] in 1947. This technique was further improved and developed by Leith et al.[13] by using a laser emitter as the coherent light source after the invention of the laser emitter by Maiman in 1960.

In the conventional photographic technique, the two-dimensional image of an object is focused on a film plane by using a lens system. On the contrary, in the holographic technique the wave front of light from the object is recorded on a photographic plate. The lenses for focusing the image is not always necessary. The image of the object is easily reconstructed from the developed photographic plate. As seen in Fig. 4.1, the coherent beam from a laser emitter is separated into two beams. One beam is emitted on the object O which is to be recorded, and the reflected beam from the object is transmitted to the photographic plate Ph. The reflected beam from the object is called as the object beam. Another beam which is called as the reference beam is reflected on a mirror M and directly transmitted to the same photographic plate. The developed photographic plate is called as a hologram. It contains all optical informations about the object

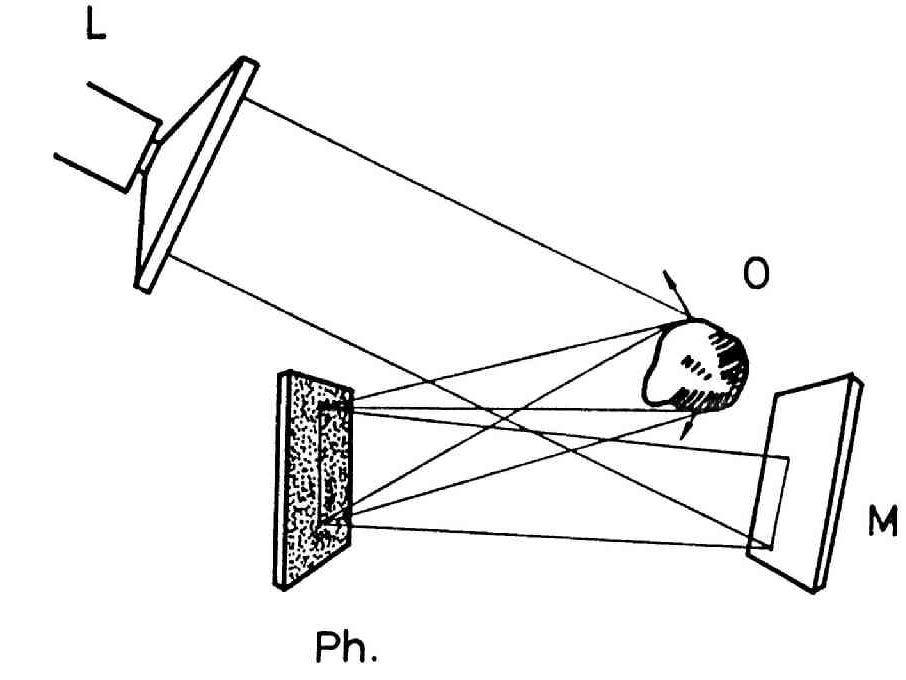

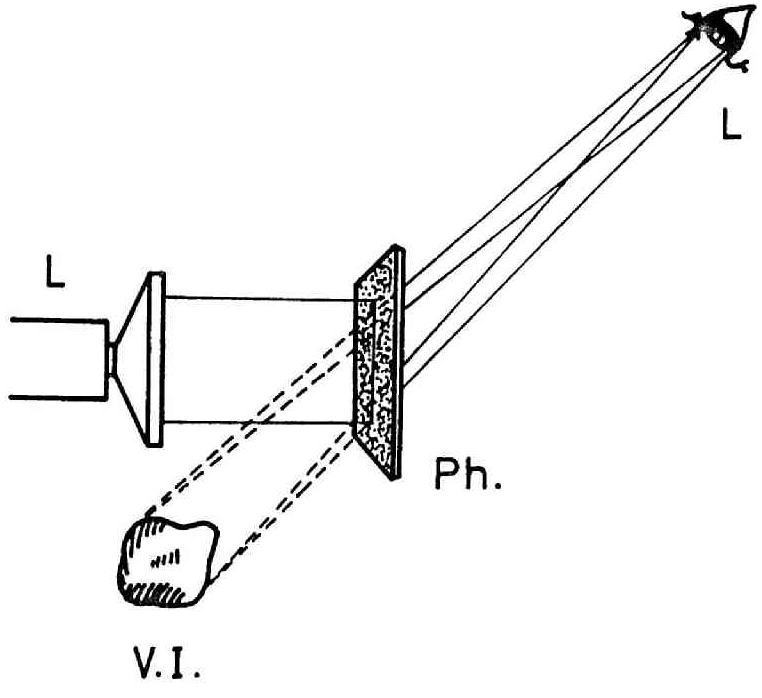

Fig. 4.1 Schematic illustration for making a hologram and reconstructing an image from the hologram

in the form of fine and complicated interference fringes which are produced by the interference between the two coherent object and reference beams on the photographic plate.

The informations recorded in the hologram can easily be taken out by emitting a coherent beam from the light source of laser emitter. The wave front of light from the object is reconstructed: it is the same as the wave front of light diverging from the object when the hologram was made. This reconstructed image of the object is not distinguishable from the original object, and it is three-dimensional and possesses the same contrast and parallax as the original object. The reconstructed image from the hologram is visible and can also be recorded by camera.

Holographic interferometry[14,15,16] is based on the fact that the phase information of light from the object can be recorded in and reconstructed from the hologram. It is known that there are three main procedures of producing a holographic interferogram.[17] They are called as double exposure, time-average and real-time holographic interferometries. Among these procedures, the real-time holographic interferometry is thought to be the most versatile and suitable for the chemical applications, and the concentration profiles of $CuSO_4$ in the cathodic diffusion layer were measured in the present work by using this technique.

The experimental arrangement in the present work is schematically illustrated in Fig. 4.2. A helium-neon gas laser emitter L of 10 mW output was used as the light source. The laser

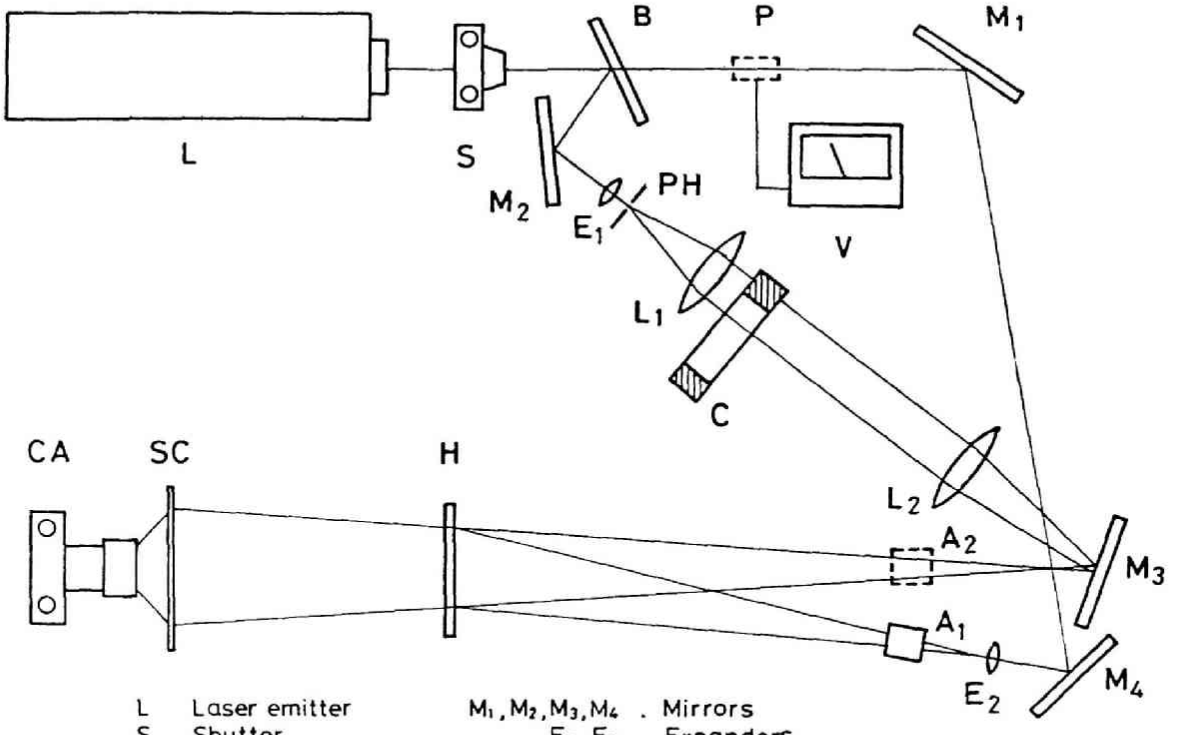

Fig. 4.2 Holographic interferometer

beam was split into two beams by a half-mirror B. A reference beam was reflected on the mirrors M_1 and M_4 and expanded by a lens E_2 (objective lens of a microscope, magnification x 10), and the beam intensity was adjusted by an attenuation polarizer A. Then it was transmitted to a photographic plate H. Another object beam was collimated to a diameter of 1.2 cm by a objective lens of a microscope E_1 (magnification x 5) and a lens L_2 (f = 200 mm). After passing through the vicinity of the cathode surface in the electrolytic cell C, it was joined with the reference beam on the same photographic plate: the image of the vicinity of the cathode surface was magnified about fifteen diameters and the back edge of the cathode surface facing the camera was focused on the screen SC by a lens L_2 (f = 200 mm). After the photographic plate was developed, the hologram was reset at the same position on the frame of the plate holder. With the reference beam incident on this hologram, the wave front of the beam which passed through the electrolytic cell is reconstructed. By superimposing the reconstructed wave front with the wave front of the beam which passed through the electrolytic cell, parallel interference fringes are easily obtained on the screen. Then the reconstructed and real images of the cathode surface were exactly superimposed by finely adjusting a rack and pinion mechanism mounted on the plate holder within an error of 10 μm. When the electrolysis was started, these interference fringes were shifted due to the concentration gradient in the cathodic diffusion layer, and they were

filmed with a camera. The real silhouette of the cathode surface obtained on the screen appears to be advanced to the solution side of the solution-cathode interface after the start of the electrolysis. This is due to the gradient of refractive index formed in the cathodic diffusion layer. However, the position of the cathode surface in the reconstructed image from the hologram does not change during the electrolysis, and this position was taken as the origin of horizontal distance from the cathode surface.

In order to eliminate any vibration during the measurement, all optical instruments except the camera shown in Fig. 4.2 were installed on a heavy steel table ridden on a truck with four tires. Furthermore, each tire was fixed on the bricks placed in a sand box. By employing this system for absorbing the vibration, almost all of the vibrations were elimiated.

The electrolytic cell is illustrated in Fig. 4.3. The inner dimension of the cell was 0.7 cm thick, 13 cm wide, and 10 cm high. The copper electrodes were 0.47 cm square and 16 cm long, and the effective area of the electrodes was $0.47 \times 9.0\ cm^2$. The distance between both electrodes was maintained at 10 cm. As already mentioned, the thickness of the cathodic diffusion layer is less than about 0.1 cm, and it was essential to install the cathode surface exactly parallel to the incident beam. In order to realize this, a revolvable cathode holder shown in Fig. 4.3 was employed. After the cell wall on the light-entrance

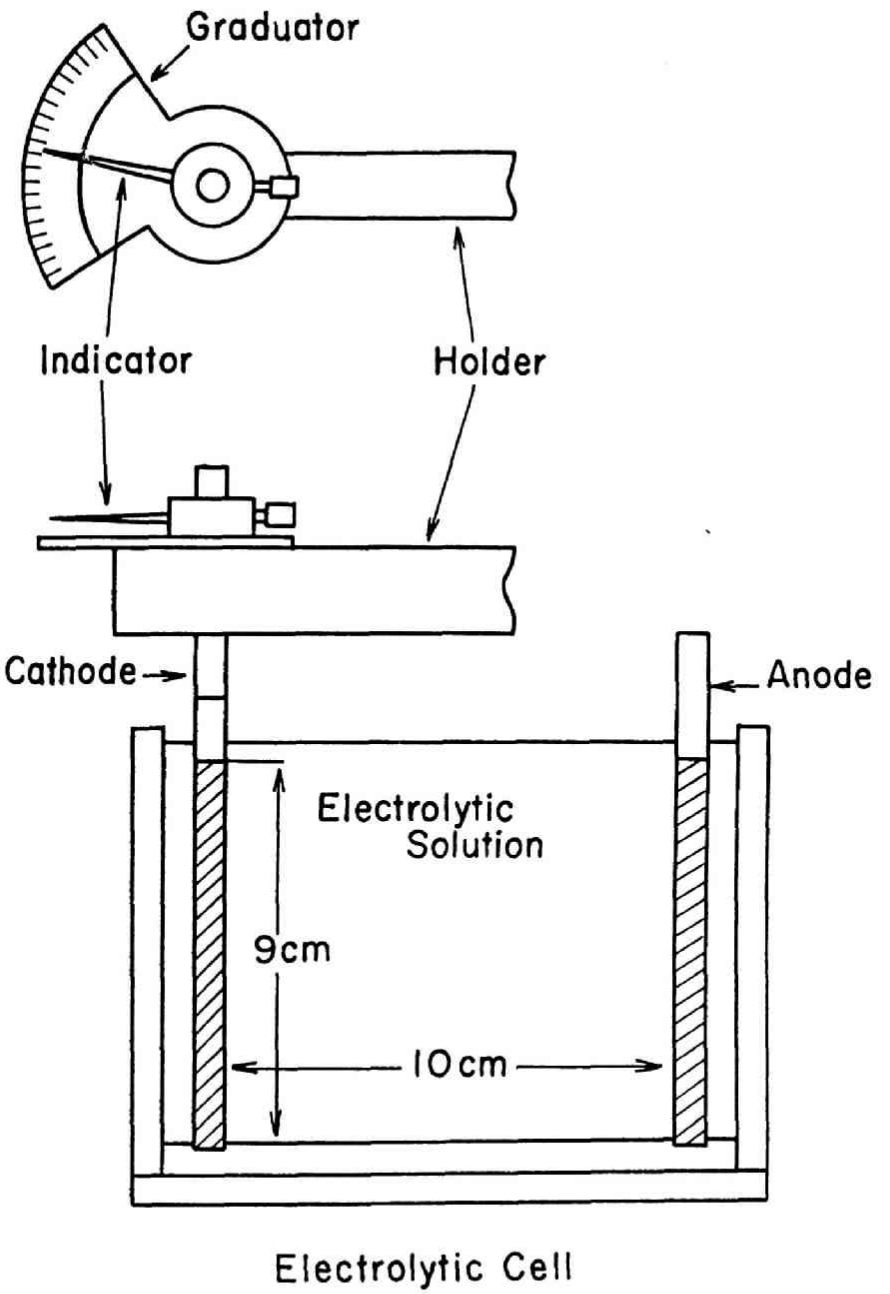

Fig. 4.3 Electrolytic cell and cathode holder

side was adjusted to be at right angles to the incident beam, the cathode was gently revolved and maintained at a position where the enlarged silhouette of the cathode surface on the screen recedes farthest.

Analytical reagent grade $CuSO_4 \cdot 5H_2O$ and deionized water were used, and the aqueous $CuSO_4$ solution was prepared. A photographic plate of spectroscopic quality is required for filming the holographic interferogram. The photographic plate SCIENTIA 10E75 (Agfa-Gevart) was employed in the present work. It has a resolving power of 1000 lines/mm, and the ASA rating is less than 5 (50 erg/cm^2). The exposed photographic plate was developed and fixed with ATOMAL and G-334 (Agfa-Gevart), respectively.

4.2.2 Interpretation of Interferogram

The relationship between the change of the refractive index of the solution and the fringe shift on the interferogram is generally given as[5]

$$\frac{(n' - n)d}{\lambda'} = N \qquad (4.1)$$

When the incident beam is transmitted into a solution having a varying refractive index, however, the true profile of the refractive index is not obtained from Eq. (4.1).[12,13] This is because the incident beam is deflected in the cathodic diffusion layer toward the direction of higher refractive index[8] as shown

in Fig. 4.4. Thus the profile of the refractive index calculated from Eq. (4.1), $n_f(y)$, does not represent the true profile. In order to obtain the true profile of the refractive index in the cathodic diffusion layer, this optical distortion should be corrected. The following correcting procedure is proposed.

The correction involves the estimation of the deflection of the incident beam, Δy, in the diffusion layer and the estimation of the position of a point where the true refractive index of the solution is equal to the apparent refractive index at the exit point of the beam, $n_f(y_o)$. Only one approximation in this correction is that the change of refractive index between the incident and exit points of the beam is regarded as being linear as shown in Fig. 4.4.

Under this approximation, the expressions of the optical path length and the deflection of incident beam which passes through the solution near the cathode surface are given by Müller.[12] They are

$$p = \frac{n_i \alpha}{2} - \frac{n_i^2}{4k} \sinh\left(\frac{2k\alpha}{n_i}\right) \tag{4.2}$$

$$\Delta y = y_o - y_i = -\frac{n_i}{k} - \frac{n_i}{k} \cosh\left(\frac{k\alpha}{n_i}\right) \tag{4.3}$$

respectively. Approximation of these equations yields

$$p = n_i d + \frac{1}{3!} \frac{2}{n_i} k^2 d^3 \tag{4.4}$$

$$\Delta y = \frac{k\alpha^2}{2! n_i} \tag{4.5}$$

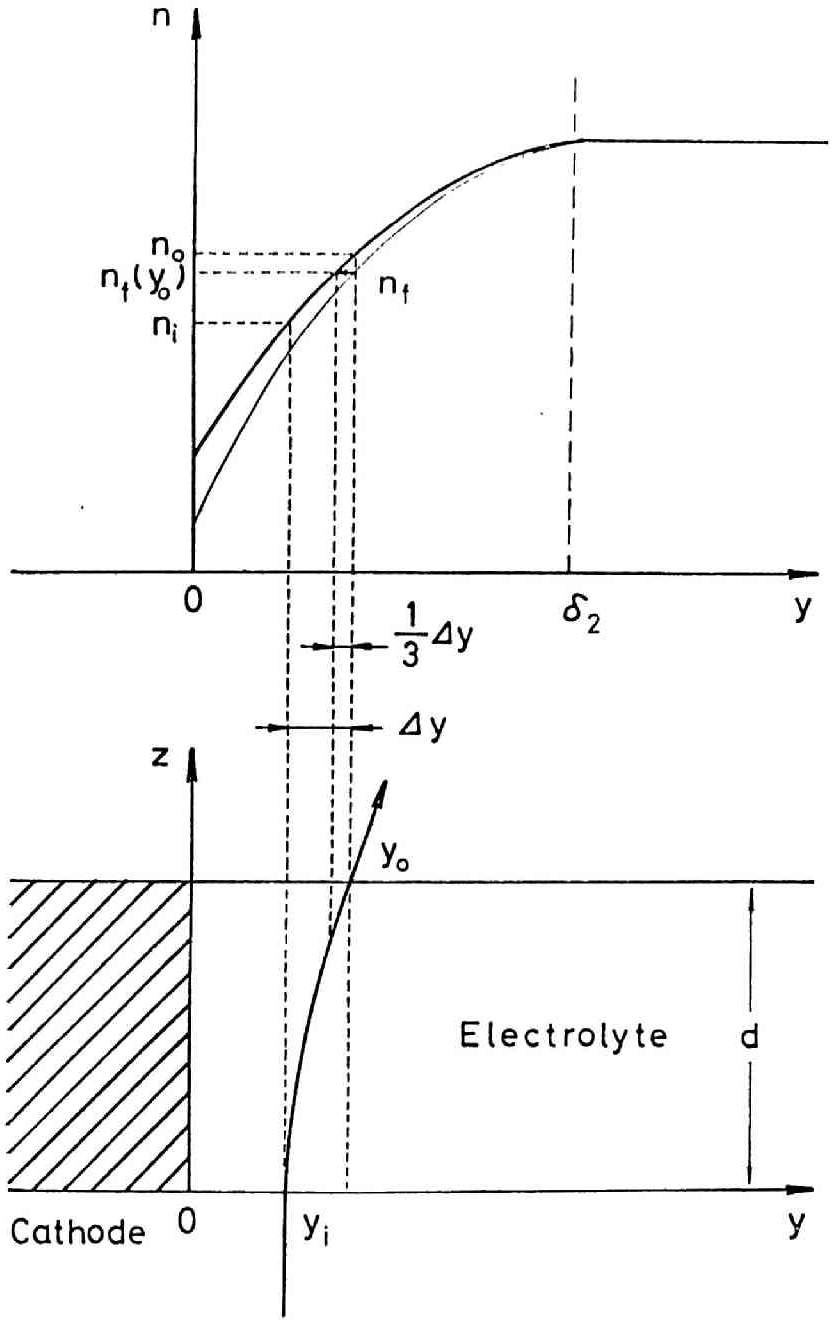

Fig. 4.4 Schematic illustrations of beam deflection and correction of refractive index

The apparent refractive index at the exit point of the beam, $n_f(y_o)$, calculated by Eq. (4.1) is equal to the ratio of optical path length and width of the cathode, p/d, and the following equation is obtained.

$$n_f(y_o) = \frac{p}{d} = n_i + \frac{1}{3!}\frac{2}{n_i}k^2d^2 \qquad (4.6)$$

It is expected from Eq. (4.5) that the deflection of the incident beam in the diffusion layer is about 50 μm or less, and it is far less than the thickness of the cathodic diffusion layer which is about 500 μm in the present work. It may be reasonable to approximate that the change of refractive index is linear within the whole region of beam deflection, Δy. Then the refractive index of the solution in the vicinity of the incident point of the beam can be expressed as follows.

$$n = n_i + k(y - y_i) \qquad (4.7)$$

By equating Eq. (4.6) and (4.7), we obtain the position of a point where the true refractive index, n, is equal to $n_f(y_o)$. It is

$$n_i + k(y - y_i) = n_i + \frac{1}{3!}\frac{2}{n_i}k^2d^2 \qquad (4.8)$$

or

$$y - y_i = \frac{k}{3n_i}d^2 \qquad (4.9)$$

By comparing $(y - y_i)$ with Δy of Eq. (4.5), we have

$$\frac{y - y_i}{\Delta y} = \frac{2}{3} \qquad (4.10)$$

It can be said that $n_f(y_o)$ becomes equal to n at a point of $\{y_i + (2/3)\Delta y\}$ or $\{y_o - (1/3)\Delta y\}$ under the assumption of linear change of refractive index between y_i and y_o.

Under the assumption of linear change of refractive index, Mizushina et al.[14] proposed the following calculating procedure for the beam deflection within the diffusion layer from the apparent profile of the refractive index. When the direction of the incident beam is at right angles to the inner wall of the electrolytic cell, the beam trajectory within the diffusion layer is expressed by the following differential equation.[15]

$$\left(\frac{dy}{dz}\right)^2 + 1 = \left[\frac{n(y)}{n(y_i)}\right]^2 \tag{4.11}$$

where $n(y_i)$ is the refractive index at the incident point of the beam. Integration of Eq. (4.11) under the boundary conditions of

$$\left.\begin{aligned} y &= y_i \qquad z = 0 \\ y &= y_o \qquad z = d \end{aligned}\right\} \tag{4.12}$$

yields

$$\int_0^d dz = \int_{y_i}^{y_o} \frac{n(y_i)}{\sqrt{[n(y)]^2 - [n(y_i)]^2}}\, dy \tag{4.13}$$

The left-hand side of this equation represents the width of the cathode, and the right-hand side can be integrated under the assumption of linear change of the refractive index. Thus the following equation is obtained.

$$d = \frac{n(y_i)}{\left(\frac{dn(y)}{dy}\right)_{y=y_i}} \ln\left[\frac{n(y_o)+\sqrt{[n(y_o)]^2-[n(y)]^2}}{n(y_i)}\right] \tag{4.14}$$

The refractive indeces $n(y_i)$ and $n(y_o)$ are sufficiently close with each other, and the substitution of an approximate relationship of

$$n(y_o) + n(y_i) = 2n_f(y_o) \tag{4.15}$$

in Eq. (4.14) yields

$$\left(\frac{dn(y)}{dy}\right)_{y=y_i} = \frac{n(y_o) - n(y_i) + \sqrt{2n_f(y_o)[n(y_o) - n(y_i)]}}{d} \tag{4.16}$$

Furthermore, the deflection of the incident beam in the diffusion layer is expressed as

$$\Delta y = \frac{n(y_o) - n(y_i)}{\left(\frac{dn(y)}{dy}\right)_{y=y_i}} \tag{4.17}$$

From the definition of the optical path length of incident beam in the diffusion layer, we have

$$p = \int_{y_i}^{y_o} n(y) \sqrt{1 + \left(\frac{dz}{dy}\right)^2}\, dy \tag{4.18}$$

Substitutions of Eq. (4.11) in Eq. (4.18) and the resultant equation in Eq. (4.6) yield

$$n_f(y_o) = \frac{1}{d} \int_{y_i}^{y_o} \frac{[n(y)]^2}{\sqrt{[n(y)]^2-[n(y_i)]^2}}\, dy \tag{4.19}$$

Differentiation of this equation with y_o further yields

$$\frac{d n_f(y_o)}{dy_o} = \frac{1}{d}\sqrt{[n(y_o)]^2 - [n(y_i)]^2} \qquad (4.20)$$

From Eq. (4.15), we have

$$n(y_o) - n(y_i) = \frac{\left[d \frac{d n_f(y_o)}{dy}\right]^2}{2 n_f(y_o)} \qquad (4.21)$$

Then the deflection of the incident beam in the cathodic diffusion layer is calculated by using Eq. (4.16), (4.17) and (4.21) where the gradient of the apparent refractive index, $[dn_f(y_o)/dy_o]$, is obtained from the interferogram. In the calculation of $[dn_f(y_o)/dy_o]$, the measured $n_f(y_o)$ was expressed by the second order equation of y_o by applying the least squares method. Then the correction of the profile of refractive index is completed by transferring $n_f(y_o)$ to a position of $(y_o - 1/3\Delta y)$ in the direction toward the cathode surface.

It is known that the pattern of interferogram is significantly affected by the position of the plane of focus on the cathode surface. According to Müller,[12] the optical distortion on the interferogram is minimal when the middle point of the cathode width is chosen as the plane of focus, although it is rather difficult to exactly determine the plane of focus at this point. Müller et al.[16] also attempted the theoretical analysis of the light deflection in an optical arrangement where the plane of

focus is placed on the front edge of the cathode surface facing the light source. This is a good procedure for correcting the light deflection when a large optical distortion is present in the solution due to the gradient of refractive index. However, the back edge of the cathode was chosen in the present work as the plane of focus according to the conventional method which was employed by many previous workers.[5-8] This is because the gradient of refractive index in the cathodic diffusion layer is thought to be fairly minor under the present electrolytic conditions. The correcting procedure proposed in the present work for the light deflection is appropriate when the gradient of refractive index in the diffusion layer is moderate and the change of refractive index between the incident and exit points of the beam is approximated to be linear.

4.2.3 Experimental Results

The experimental conditions are summarized in Table 4.1. The measurements were carried out at 23° ± 1°C. The current-potential curves were obtained with the solutions shown in Table 4.1, and they are illustrated in Fig. 4.5. As the reference electrode for measuring the cathode potential, an enameled copper wire of 0.18 cm in diameter was used. The average cathodic current densities where the concentration profiles were measured are also shown in the figure. It is seen that the applied

Table 4.1 Experimental conditions

Electrolyte	0.05M and 0.1M $CuSO_4$ aqueous solutions
Distance from lower edge of cathode (cm)	1, 2, 4 and 8
Average cathodic current density (mA/cm^2)	0.473, 0.946, 1.42, 1.84, 2.29, 2.76, 3.65 and 4.60

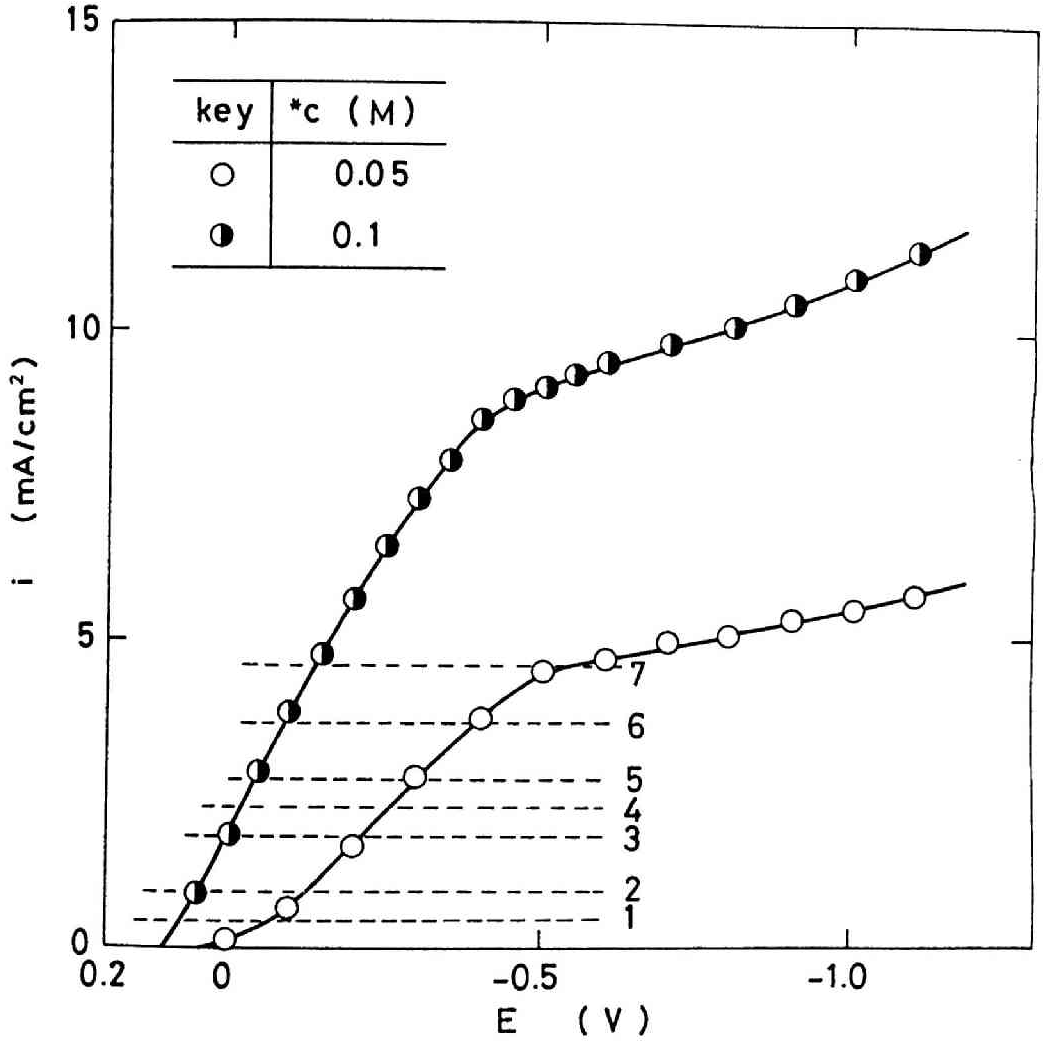

No.	1	2	3	4	5	6	7
i (mA/cm²)	0.473	0.946	1.84	2.29	2.76	3.65	4.60

Fig. 4.5 Current-potential curve

current densities ranged up to the limiting value in the solution of 0.05M $CuSO_4$ and they were below one-half of the limiting value in the solution of 0.1M $CuSO_4$.

A few examples of the holographic interferogram are demonstrated in Fig. 4.6. A holographic interferogram near the cathode surface before the start of electrolysis is shown in Fig. 4.6(a). The horizontal interference fringes in this figure were employed as the reference for measuring the concentration profile. Figures 4.6(b) through (d) demonstrate the interferograms of 0.05M $CuSO_4$ solution at an average cathodic current density of 1.84 mA/cm^2. The measuring height was varied at 1, 4 and 8 cm from the lower edge of the cathode, respectively. They were filmed after 10 min had elapsed from the start of electrolysis: it was observed that the diffusion layer is at the steady state. As seen in these figures, the thickness of the diffusion layer increases in the upper portion of the cathode. This is due to the growth of the upward natural convective flow along the cathode surface.

From these holographic interferograms, the apparent profiles of refractive index in the cathodic diffusion layer were calculated by using Eq. (4.1), and the true profiles of refractive index were obtained by correcting them according to the procedure mentioned in 4.2.2. Furthermore, from the regression of the refractive index, n, upon $CuSO_4$ concentration, c, in the solution the concentration profiles of $CuSO_4$ were calculated. The re-

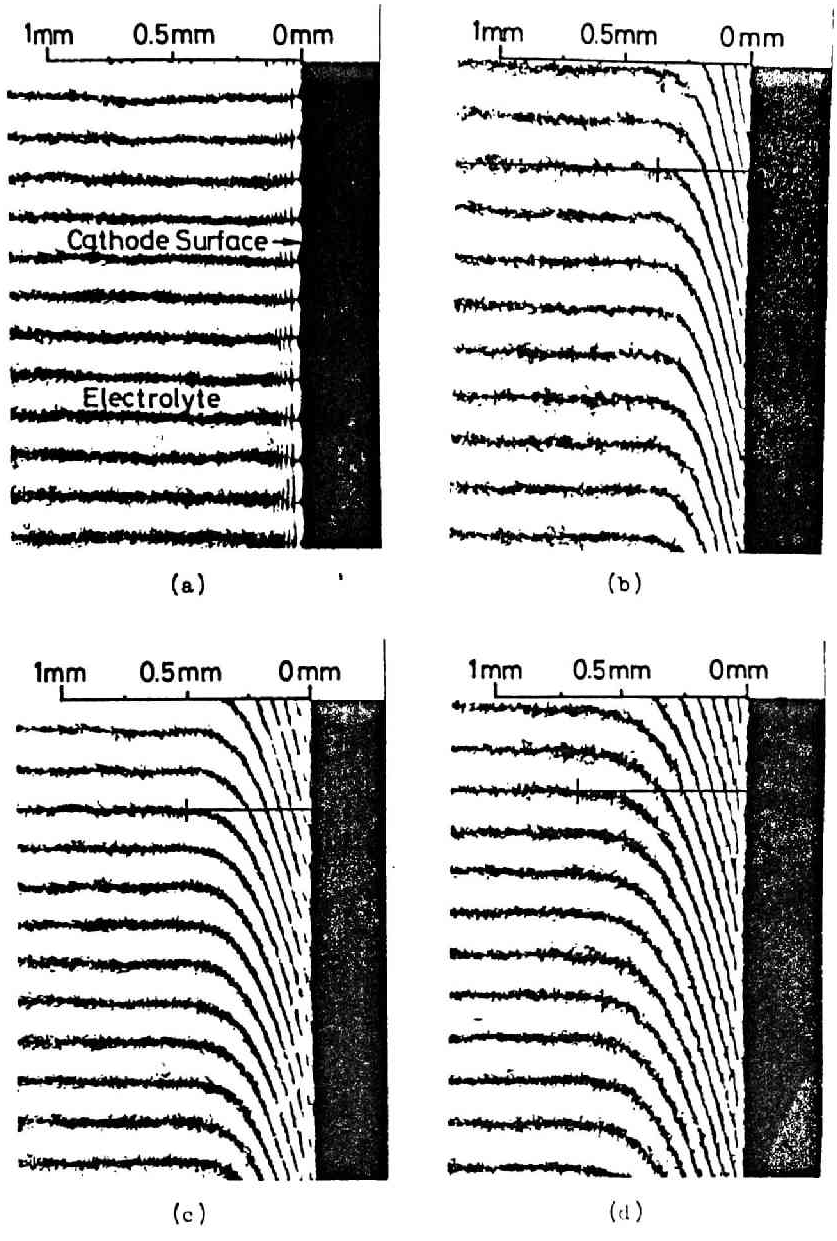

Fig. 4.6 Holographic interferograms of cathodic diffusion layer:
(a) before the start of electrolysis,
(b) x = 1 cm, (c) x = 4 cm, and
(d) x = 8 cm during the electrolysis of 0.05M $CuSO_4$ solution at i = 1.84 mA/cm^2

fractive index of the aqueous solution containing $CuSO_4$ at various concentrations was measured at 23° ± 1°C by using the Abbé refractometer. The regression is expressed as

$$n = 1.3330 + 28.44c \qquad (4.22)$$

in a region below the concentration of 0.5M $CuSO_4$.

A few examples of the corrected concentration profile are demonstrated in Fig. 4.7. They were obtained with 0.05M $CuSO_4$ solution at a height of 4 cm. The uncorrected concentration profiles at each current density are also shown. It is seen in this figure that $CuSO_4$ concentration at the cathode surface is lowered and the thickness of the diffusion layer decreases when the average cathodic current density is raised. Furthermore it is seen that the above-mentioned correction becomes significant when the concentration graident is steeper.

4.2.4 Discussion

In order to calculate the theoretical concentration difference and the thickness of the diffusion layer by Eq. (2.35) and (2.54), respectively, both of which were derived under the assumption that the vertical distribution of cathodic current densities is uniform on the cathode surface, it is necessary to obtain the numerical values of the parameters involved in these equation.

The parameter ω which influences the concentration profile of $CuSO_4$ was determined as follows. Logarithm of (θ_1/θ_1) in

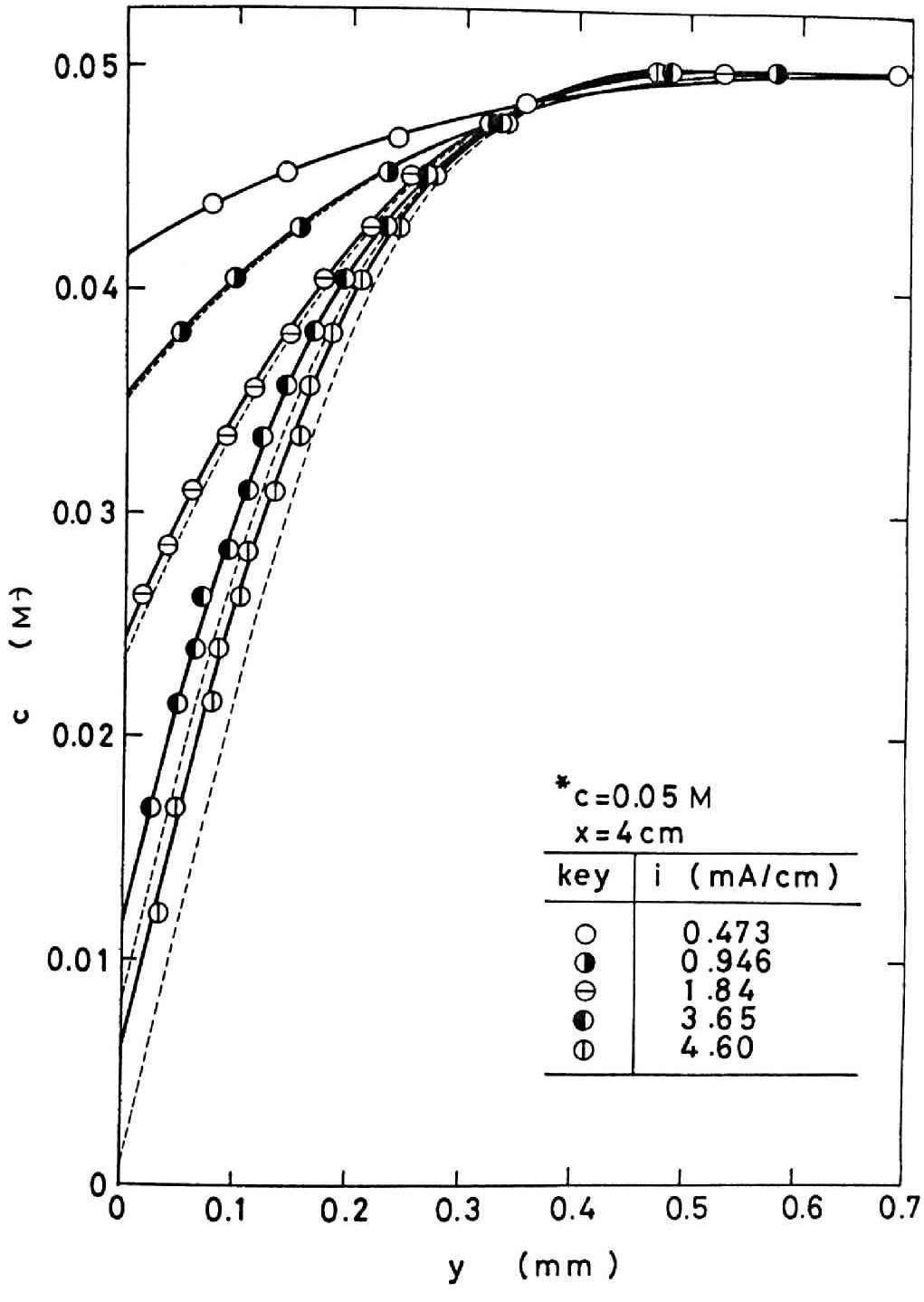

Fig. 4.7 Concentration profile of $CuSO_4$ in the cathodic diffusion layer (Broken lines are the uncorrected concentration profiles)

0.05M and 0.1M $CuSO_4$ solutions was plotted against $\log(1 - y/\delta_1)$ in Fig. 4.8 and 4.9 according to Eq. (2.29), respectively. As seen in Fig. 4.8, the majority of the experimental data are scattered in the region between the slopes of 2.0 and 3.0, and the ω value for 0.05M $CuSO_4$ solution was determined as 2.39 by the least squares method. From the similar procedure it was estimated to be 2.31 for 0.1M $CuSO_4$ solution. Ibl et al.[16] obtained the numerical value of 2.3 from the interferometric measurement in 0.6M $CuSO_4$ solution at a height of 0.9 cm.

The other parameters λ, ε and η involved in Eq. (2.30) which influence the velocity profile of natural convection were presumed to be 1.5, 10 and 2.5, respectively, from the measurement of natural convective flow in 0.1M $CuSO_4$ solution mentioned in Chapter 3.

In order to examine the validity of Eq. (2.53) and (2.54), logarithmic concentration difference between bulk-electrolyte and cathode surface, log Δc, was plotted against logarithmic average cathodic current density, and Fig. 4.10 and 4.11 were obtained for the solutions of 0.05M and 0.1M $CuSO_4$, respectively. As seen in these figures, the slope of all straight lines is 4/5 which is equal to the theoretical value derived from Eq. (2.53).

The dependance of log Δc on the logarithmic height from the lower edge of the cathode was also examined: log Δc in the solutions of 0.05M and 0.1M $CuSO_4$ was plotted against log x in Fig. 4.12 and 4.13, respectively. By comparing the experimental

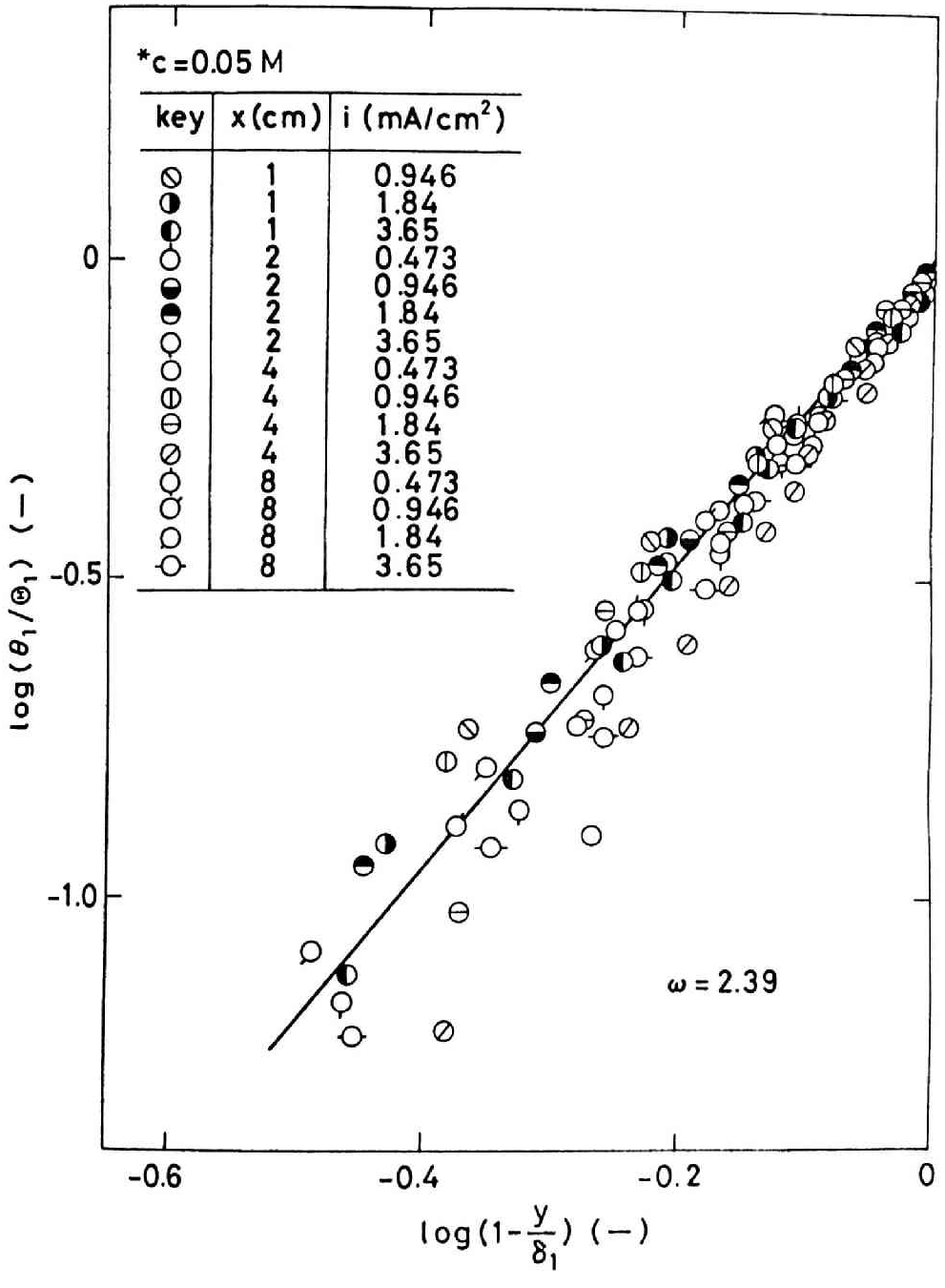

Fig. 4.8 Plot of $\log(\theta_1/\Theta_1)$ vs. $\log(1 - y/\delta_1)$ with aqueous 0.05M $CuSO_4$ solution

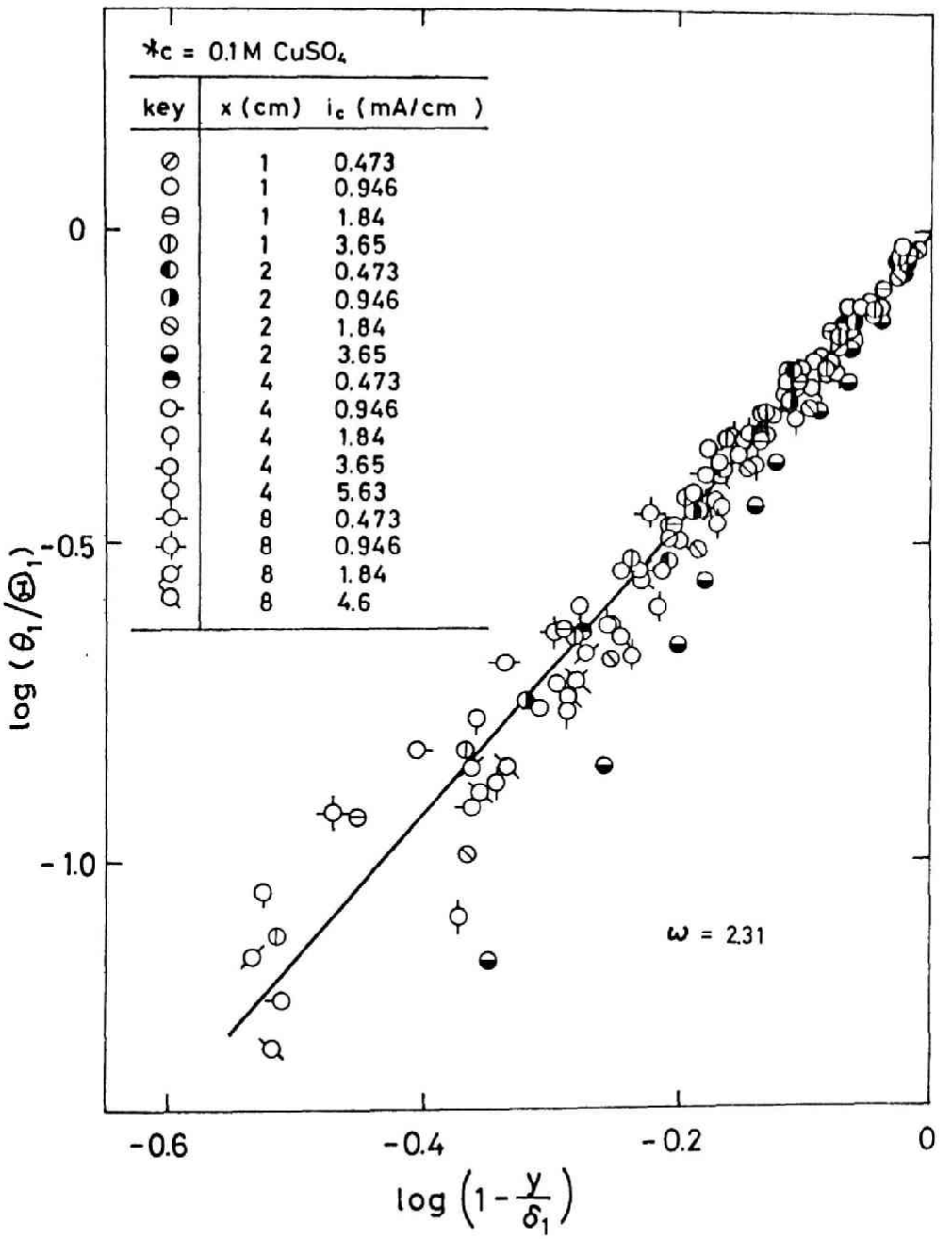

Fig. 4.9 Plot of $\log(\theta_1/\Theta_1)$ vs. $\log(1 - y/\delta_1)$ with aqueous 0.1M $CuSO_4$ solution

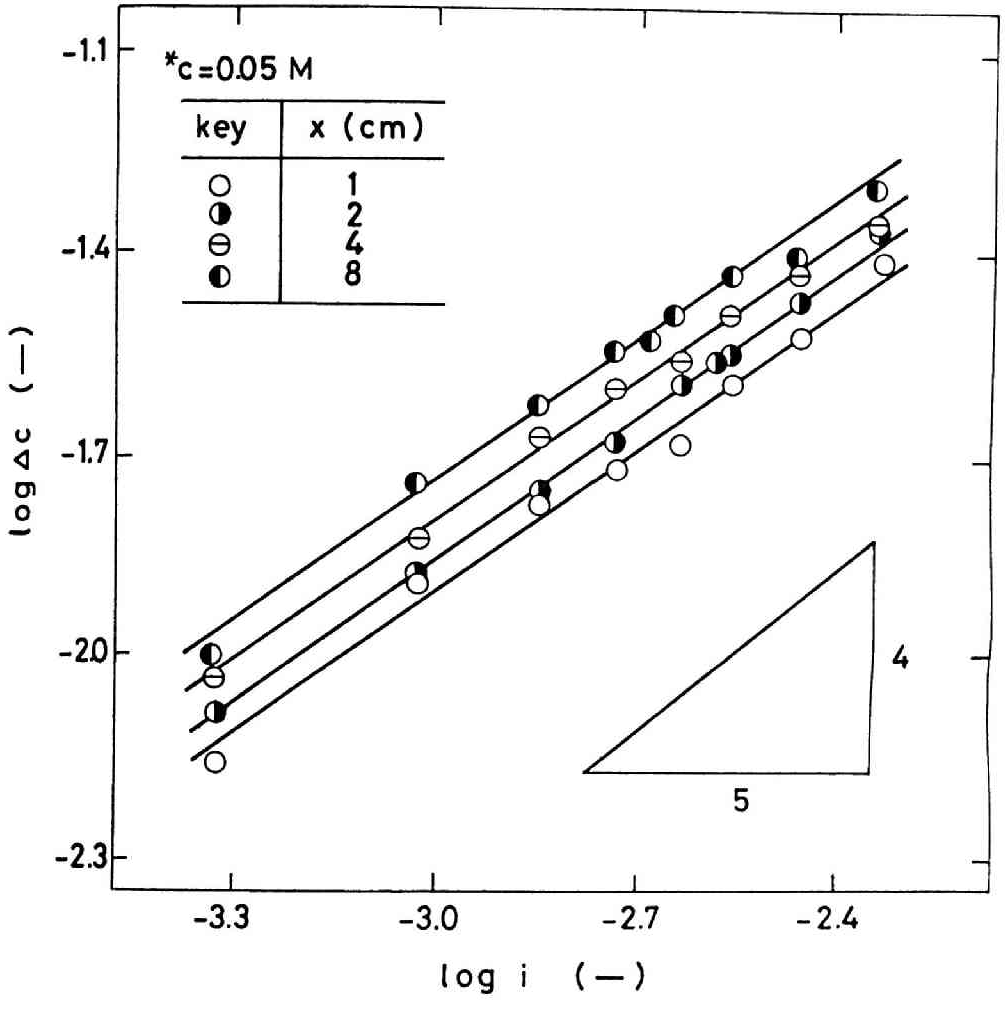

Fig. 4.10 Relationship between concentration difference and average cathodic current density with aqueous 0.05M $CuSO_4$ solution

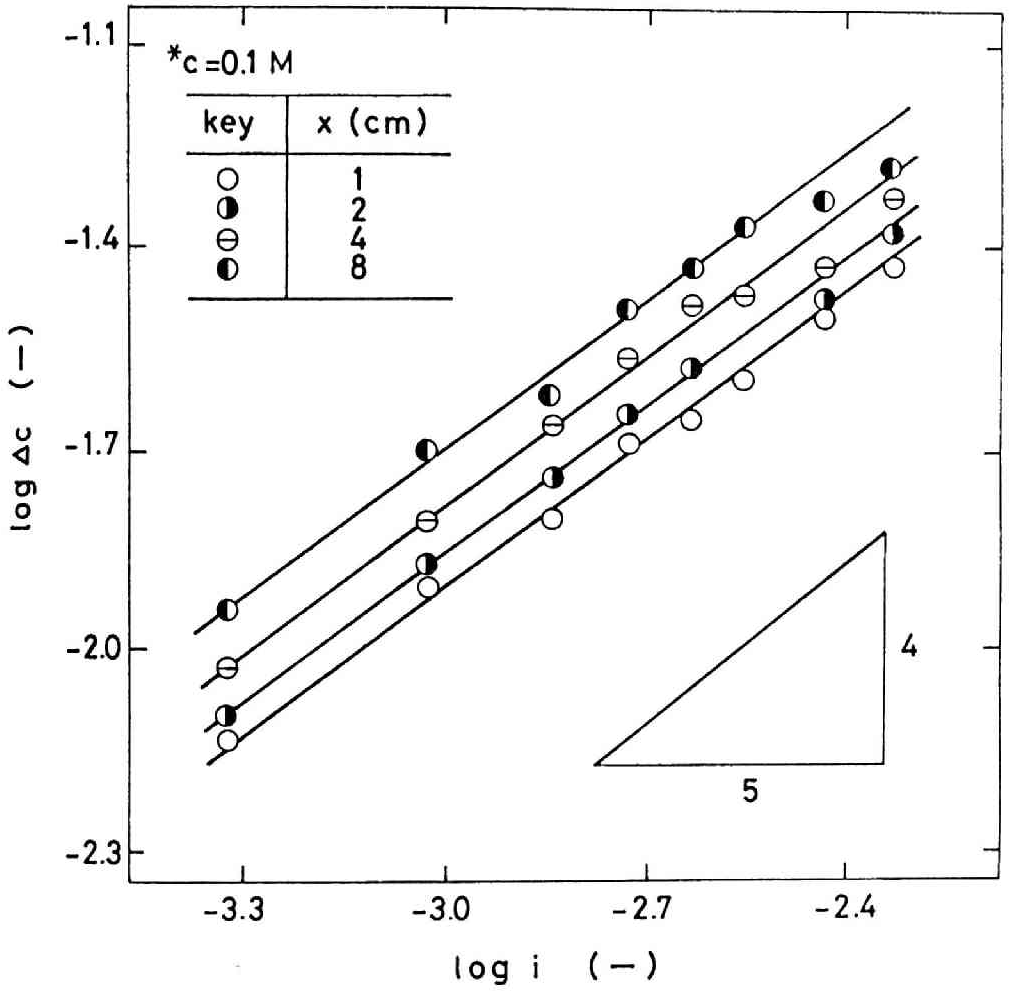

Fig. 4.11 Relationship between concentration difference and average cathodic current density with aqueous 0.1M $CuSO_4$ solution

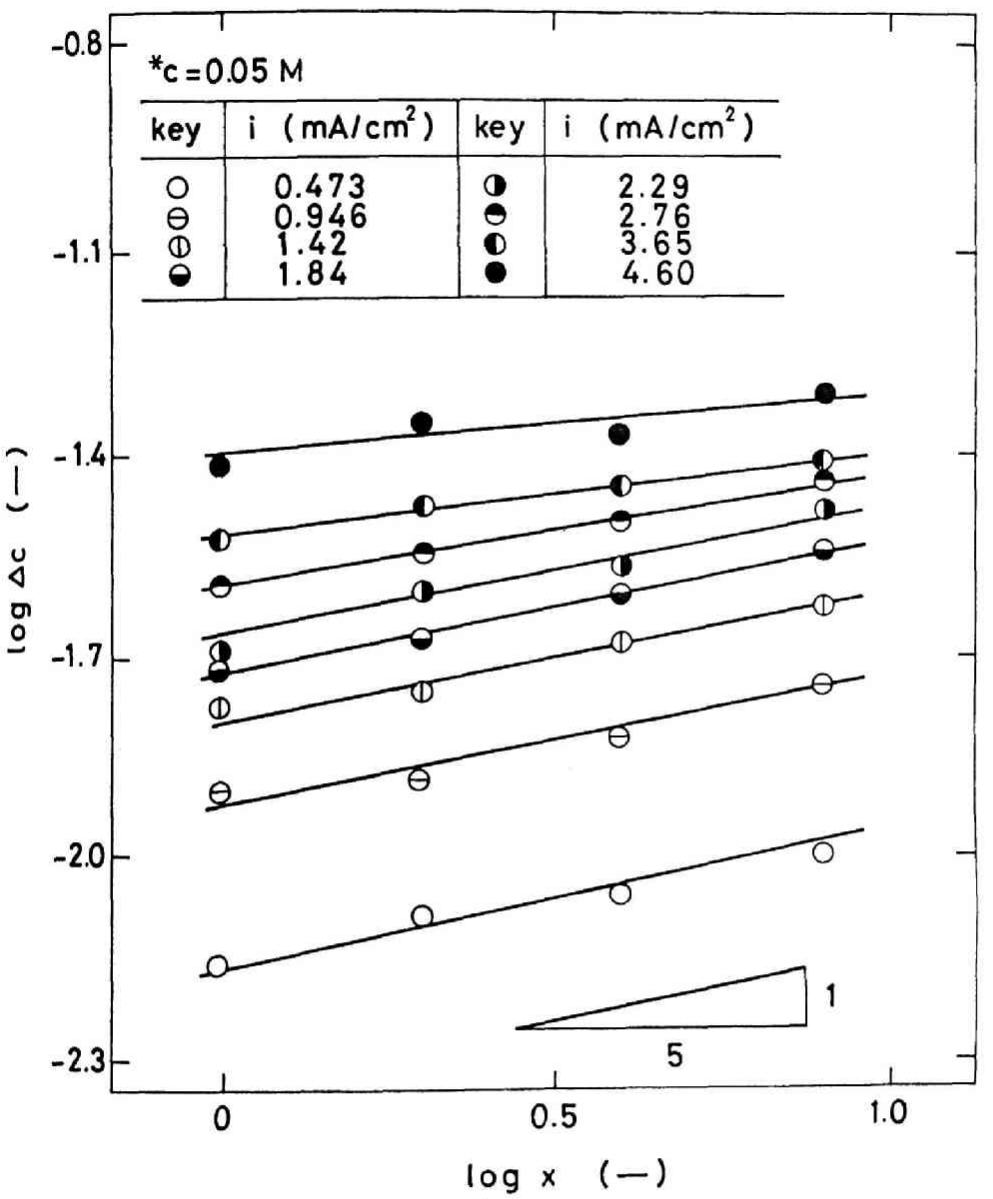

Fig. 4.12 Relationship between concentration difference and height from lower edge of cathode with aqueous 0.05M $CuSO_4$ solution

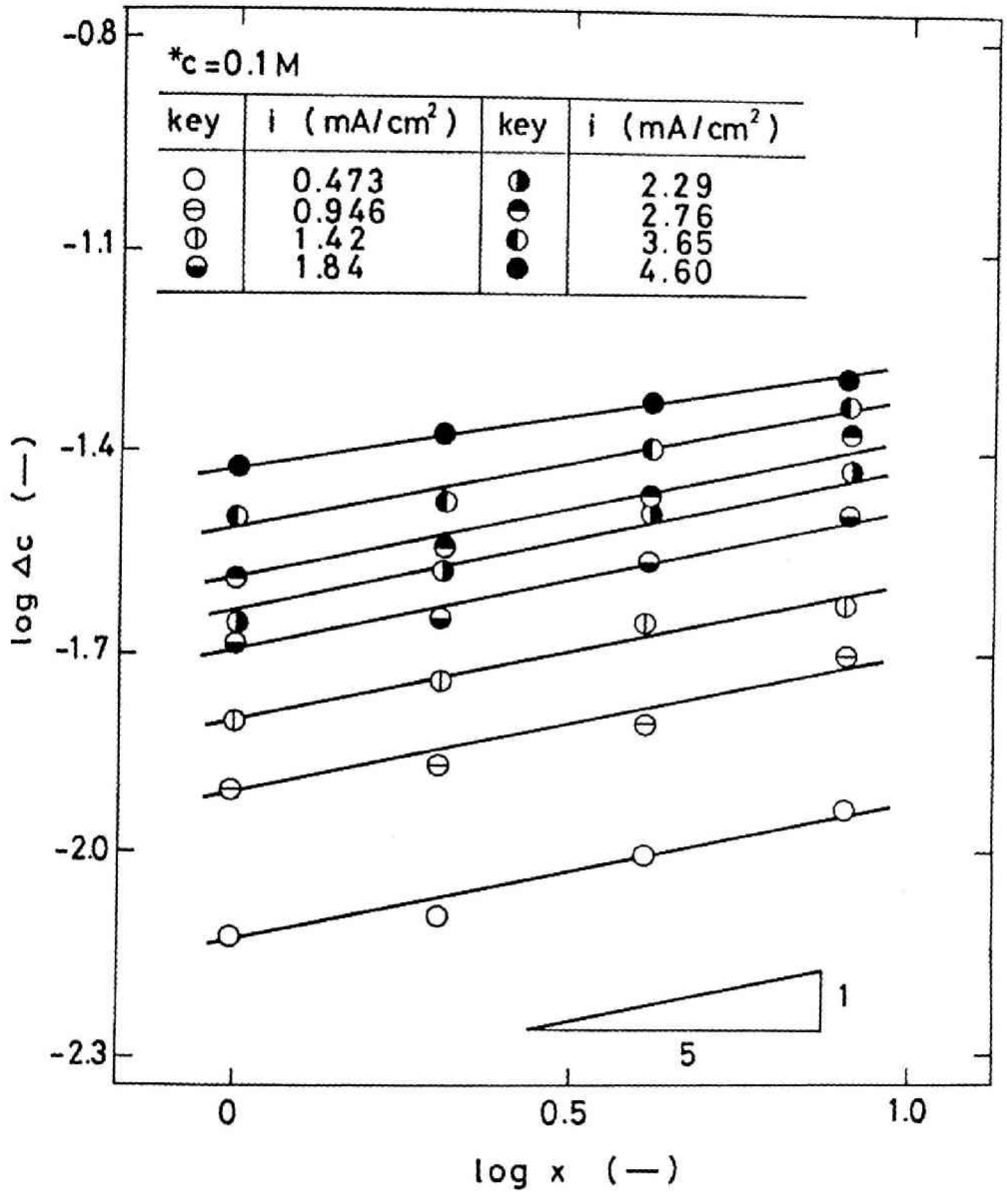

Fig. 4.13 Relationship between concentration difference and height from lower edge of cathode with aqueous 0.1M $CuSO_4$ solution

slopes with the theoretical value of 1/5 from Eq. (4.53), it is seen that the measured slopes in Fig. 4.12 are equal to 1/5 when the average current density is below 2.76 mA/cm^2, and the slope decreases when the average current density becomes higher than 3.65 mA/cm^2. This may suggest that the local cathodic current densities is not uniform in vertical direction above 3.65 mA/cm^2. By comparing Fig. 4.13 with Fig. 4.12, it was revealed that the slopes in Fig. 4.13 are nearly equal to the theoretical value of 1/5 up to the current density of 4.6 mA/cm^2. This is due to the relatively lower applied current densities than the limiting value in the aqueous 0.1M $CuSO_4$ solution.

The dimensionless numbers of Sh_x, Gr* and Sc were calculated by using the experimental data and property constants mentioned in Table 4.2. They are summarized in Table 4.3 and 4.4, respectively. Furthermore, $\log(Sh_x)$ was plotted against $\log(Sc \cdot Gr^*)$ in Fig. 4.14. The theoretical value was calculated from Eq. (2.59) and it is also shown in the same figure. It is seen that the experimental results obtained at the lower current densities are in fairly good agreement with the theoretical value.

The theoretical relationship demonstrated in Eq. (2.54) was also examined. Logarithmic thickness of the diffusion layer in 0.05M and 0.1M $CuSO_4$ solutions was plotted against the logarithmic average current density in Fig. 4.15 and 4.16, respectively. It is seen in these figures that the slopes in the region of the lower current densities is in fairly good agreement with the the-

Table 4.2 Parameters used in the calculation

		0.05M $CuSO_4$ solution	0.1M $CuSO_4$ solution
z_1	(-)	2	2
D_1	(cm^2/sec)	6.5×10^{-6}*	6.0×10^{-6}*
*ν	(cm^2/sec)	1.043×10^{-2}	1.022×10^{-2}
α_1	(cm^3/mol)	151.5	151.5
t_2	(-)	0.643	0.643

* see Appendix B

Table 4.3 The experimental data and the dimensionless numbers of Sh_x, Gr* and Sc with aqueous 0.05M $CuSO_4$ solution

No.	x	i	^oc	Δc	δ_l	Sh_x	$\delta_l/x \times 10^{-2}$	Sc x 10^3	Gr* x 10^8
(-)	(cm)	(mA/cm^2)	(M)	(M)	(mm)	(-)	(-)	(-)	(-)
1	1	0.473	0.0429	0.0071	0.454	34.15	4.54	1.57	0.00344
2	1	0.946	0.0373	0.0127	0.394	38.18	3.94	1.57	0.00688
3	1	1.42	0.0328	0.0172	0.374	42.32	3.74	1.57	0.01032
4	1	1.84	0.0309	0.0191	0.346	49.38	3.46	1.57	0.01338
5	1	2.29	0.0289	0.0211	0.377	55.63	3.77	1.57	0.01665
6	1	2.76	0.0243	0.0257	0.362	55.05	3.62	1.57	0.02007
7	1	3.65	0.0194	0.0306	0.366	61.14	3.66	1.57	0.02654
8	1	4.60	0.0128	0.0372	0.340	63.39	3.40	1.57	0.03440
9	2	0.473	0.0417	0.0083	0.665	58.42	3.33	1.57	0.05502
10	2	0.946	0.0371	0.0129	0.512	75.18	2.56	1.57	0.1100
11	2	1.42	0.0324	0.0176	0.451	82.72	2.26	1.57	0.1652
12	2	1.84	0.0276	0.0224	0.474	84.21	2.37	1.57	0.2140
13	2	2.29	0.0238	0.0262	0.459	89.61	2.30	1.57	0.2664
14	2	2.76	0.0209	0.0291	0.464	97.24	2.32	1.57	0.3210
15	2	3.65	0.0143	0.0357	0.469	104.8	2.35	1.57	0.4257
16	2	4.60	0.0061	0.0439	0.446	107.4	2.23	1.57	0.5351
17	4	0.473	0.0399	0.0101	0.746	96.02	1.87	1.57	0.8803
18	4	0.946	0.0346	0.0154	0.568	125.9	1.42	1.57	1.761
19	4	1.42	0.0281	0.0219	0.600	132.9	1.50	1.57	2.643
20	4	1.84	0.0251	0.0249	0.574	151.5	1.44	1.57	3.424
21	4	2.76	0.0177	0.0324	0.559	174.7	1.40	1.57	5.137
22	4	3.65	0.0137	0.0363	0.551	206.2	1.38	1.57	6.793
23	4	4.60	0.0094	0.0406	0.546	232.3	1.34	1.57	8.561
24	4	0.473	0.0416	0.0084		115.5		1.57	0.8803
25	4	0.946	0.0356	0.0144		134.7		1.57	1.761
26	4	1.42	0.0288	0.0212		137.3		1.57	2.643
27	4	1.84	0.0246	0.0254		148.5		1.57	3.424
28	4	2.29	0.0225	0.0275		170.7		1.57	4.262
29	4	2.76	0.0173	0.0327		173.1		1.57	5.137
30	4	3.65	0.0123	0.0377		198.5		1.57	6.793
31	4	4.60	0.0050	0.0450		209.6		1.57	8.561
32	8	0.473	0.0404	0.0096	0.761	202.0	0.951	1.57	14.08
33	8	0.946	0.0322	0.0178	0.671	217.9	0.839	1.57	28.17
34	8	1.42	0.0257	0.0243	0.616	239.6	0.770	1.57	42.28
35	8	1.84	0.0212	0.0288	0.607	261.9	0.758	1.57	54.79
36	8	2.29	0.0162	0.0338	0.611	277.8	0.734	1.57	68.19
37	8	2.76	0.0122	0.0378	0.576	299.4	0.720	1.57	82.19
38	8	3.65	0.0096	0.0404	0.596	370.5	0.745	1.57	108.7
39	8	4.60	0.00	0.05	0.573	377.3	0.716	1.57	136.9

Table 4.4 The experimental data and the dimensionless numbers of Sh_x, Gr^* and Sc with aqueous 0.1M $CuSO_4$ solution

No.	x	i	c_o	Δc	δ_l	Sh_x	$\delta_l/x \times 10^{-2}$	$Sc \times 10^3$	$Gr^* \times 10^8$
(-)	(cm)	(mA/cm^2)	(M)	(M)	(mm)	(-)	(-)	(-)	(-)
1	1	0.473	0.0926	0.0074	0.524	35.49	5.24	1.74	0.00357
2	1	0.946	0.0868	0.0132	0.432	39.80	4.32	1.74	0.00714
3	1	1.42	0.0838	0.0162	0.378	48.67	3.78	1.74	0.01072
4	1	1.84	0.0773	0.0227	0.358	45.01	3.58	1.74	0.01892
5	1	2.29	0.0775	0.0225	0.361	56.52	3.61	1.74	0.01729
6	1	2.76	0.0740	0.0260	0.341	58.95	3.41	1.74	0.02084
7	1	3.65	0.0658	0.0342	0.348	59.26	3.48	1.74	0.02756
8	1	4.60	0.0653	0.0347	0.311	73.61	3.11	1.74	0.03473
9	1	7.33			0.305		3.05	1.74	0.05534
10	2	0.473	0.0922	0.0078	0.546	67.35	2.73	1.74	0.05714
11	2	0.946	0.0864	0.0136	0.490	77.25	2.45	1.74	0.1142
12	2	1.42	0.0818	0.0182	0.460	86.65	2.40	1.74	0.1715
13	2	1.84	0.0774	0.0224	0.430	90.42	2.15	1.74	0.2223
14	2	2.29	0.0725	0.0275	0.450	92.48	2.25	1.74	0.2766
15	2	2.76	0.0710	0.0290	0.413	105.7	2.07	1.74	0.3334
16	2	3.65	0.0660	0.0340	0.418	119.2	2.09	1.74	0.4409
17	2	4.60	0.0559	0.0441	0.421	115.8	2.11	1.74	0.5557
18	2	5.63			0.394		1.97	1.74	0.6801
19	2	7.33			0.380		1.90	1.74	0.8855
20	4	0.473	0.0899	0.0101	0.706	104.0	1.77	1.74	0.9142
21	4	0.946	0.0844	0.0154	0.571	134.7	1.48	1.74	1.828
22	4	1.42	0.0775	0.0225	0.510	140.2	1.28	1.74	2.745
23	4	1.84	0.0720	0.0280	0.492	145.9	1.23	1.74	3.556
24	4	2.29	0.0671	0.0329	0.505	154.6	1.26	1.74	4.426
25	4	2.76	0.0651	0.0349	0.476	175.7	1.19	1.74	5.335
26	4	3.65	0.0577	0.0423	0.460	191.7	1.15	1.74	7.055
27	4	4.60	0.0497	0.0503	0.511	203.1	1.28	1.74	8.891
28	4	5.63			0.468		1.17	1.74	10.88
29	4	7.33			0.476		1.19	1.74	14.17
30	8	0.473	0.0886	0.0114	0.797	184.3	0.996	1.74	14.53
31	8	0.946	0.0800	0.0200	0.625	210.1	0.781	1.74	29.25
32	8	1.42	0.0760	0.0240	0.633	262.8	0.791	1.74	43.91
33	8	1.84	0.0672	0.0328	0.636	249.2	0.795	1.74	56.90
34	8	2.29	0.0619	0.0381	0.625	267.0	0.781	1.74	70.82
35	8	2.76	0.0573	0.0427	0.608	287.1	0.760	1.74	85.35
36	8	3.65	0.0526	0.0474	0.595	342.1	0.744	1.74	112.9
37	8	4.60	0.0485	0.0515	0.603	396.8	0.754	1.74	142.3
38	8	5.63			0.562		0.703	1.74	174.1
39	8	7.33			0.531		0.664	1.74	226.7

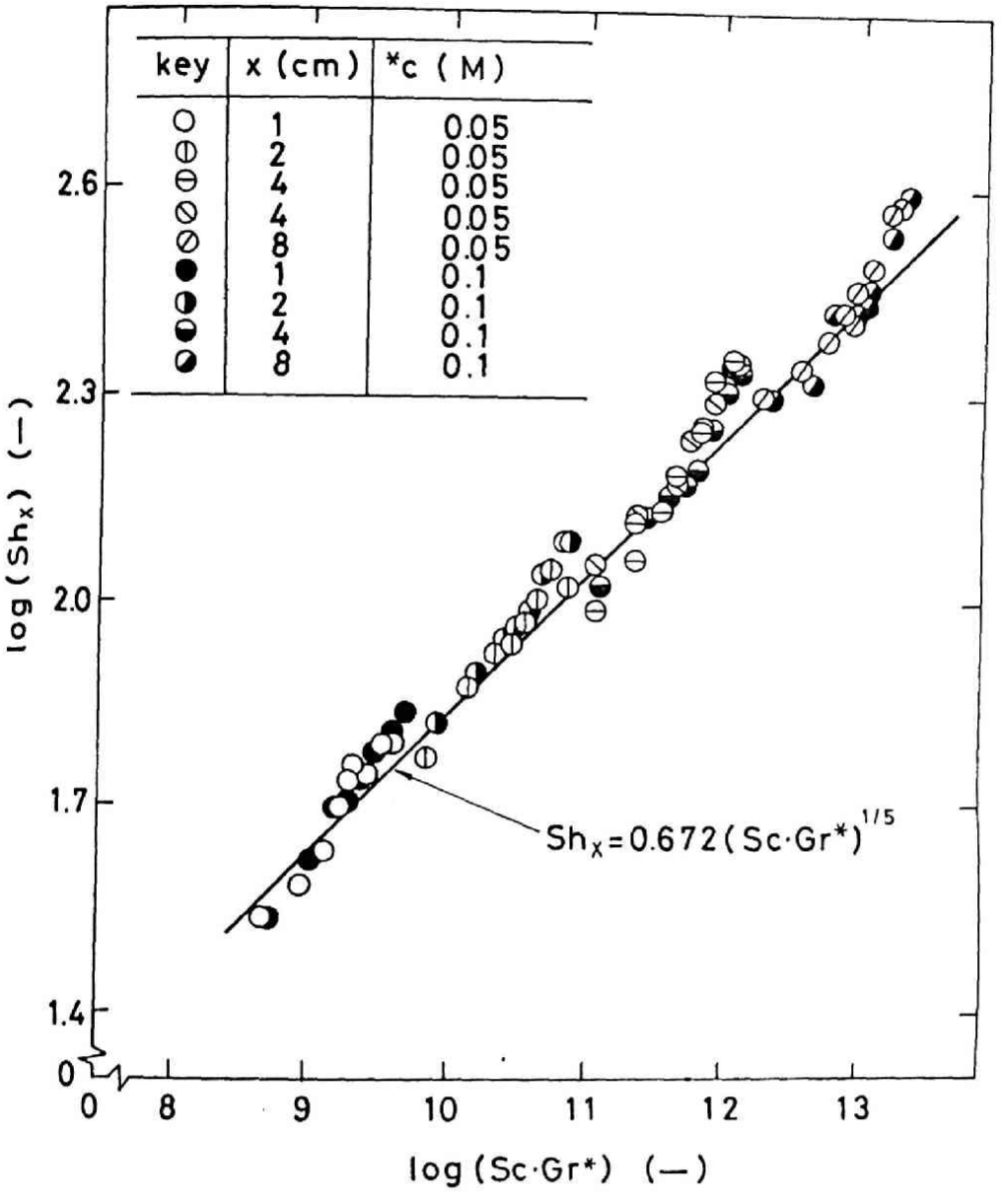

Fig. 4.14 Plot of $\log(Sh_x)$ vs. $\log(Sc \cdot Gr^*)$

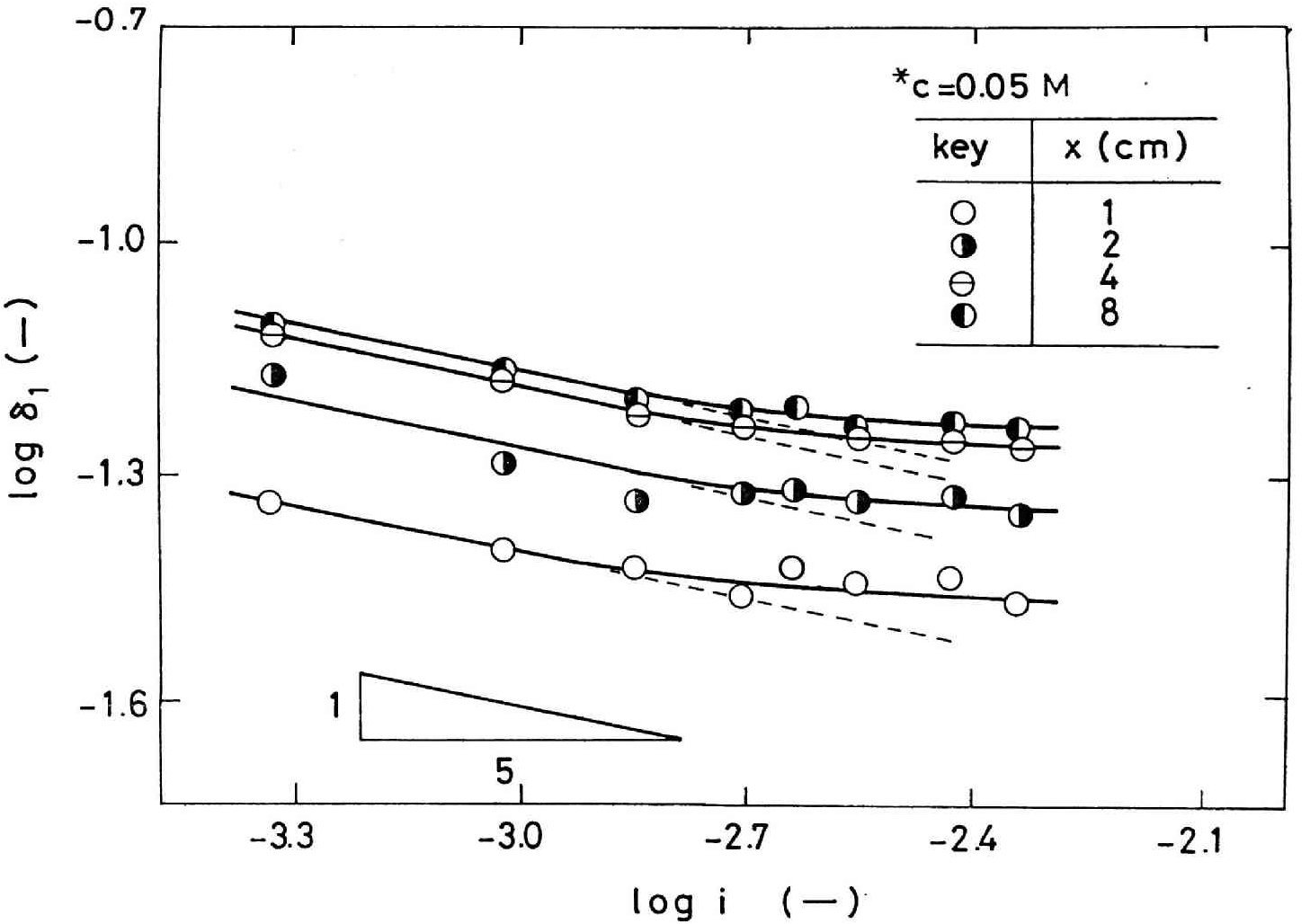

Fig. 4.15 Relationship between thickness of cathodic diffusion layer and average current density with aqueous 0.05M $CuSO_4$ solution

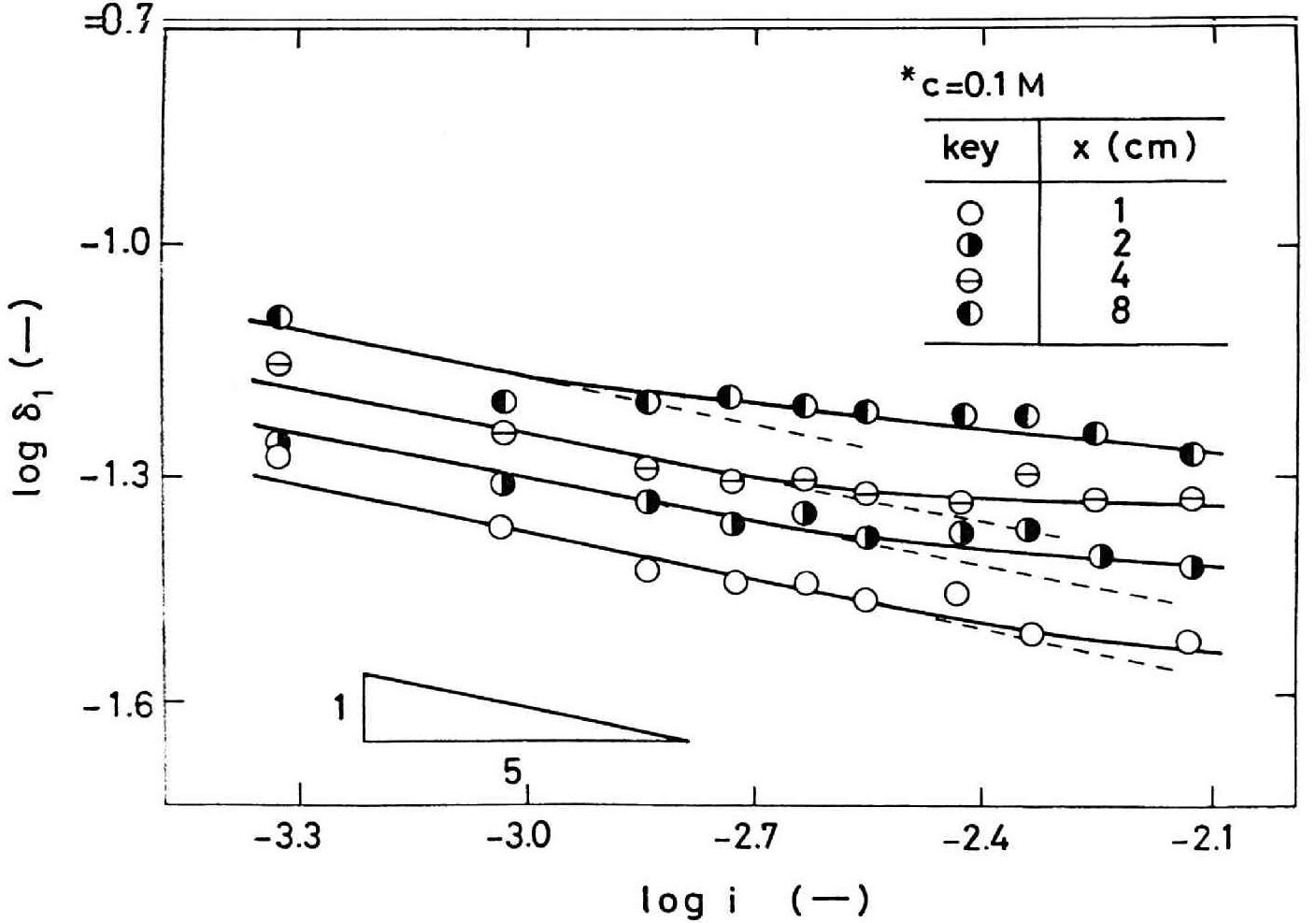

Fig. 4.16 Relationship between thickness of cathodic diffusion layer and average current density with aqueous 0.1M $CuSO_4$ solution

oretical value of -1/5, and the slopes decrease at higher current densities. From a theoretical calculation of the thickness of cathodic diffusion layer under the boundary condition of ${}^{o}c_1 =$ const. which is valid, for example, at the cathodic limiting current density, it was revealed[17] that δ_1 are constant at various current densities. Furthermore it is seen from a comparison of Fig. 4.16 with Fig. 4.15 that the theoretical slope of -1/5 is maintained up to higher current densities in 0.1M $CuSO_4$ solution in which the cathodic limiting current density is higher.

In order to determine the dependance of the thickness of diffusion layer on the height from the lower edge of cathode surface, the logarithmic thickness measured in both solutions of 0.05M and 0.1M $CuSO_4$ was plotted against log x, and Fig. 4.17 and 4.18 were obtained, respectively. The theoretical slope of the straight line is 1/5 from Eq. (4.54). In these figures, this linear relationship is fairly well satisfied. The dispersion of δ_1 values is thought to be related to the lower precision in the measurement of diffusion layer thickness.

In order to compare the measured and theoretical thickness of the diffusion layer, the experimental value of $\log(\delta_1/x)$ was plotted against $\log(Sc \cdot Gr^*)$ in Fig. 4.19. The parameters and property constants were substituted in Eq. (2.60), and the theoretical value is also shown in the same figure. As seen in this figure, the experimental results may be explained by Eq. (2.60), although the experimental data shown in this figure are

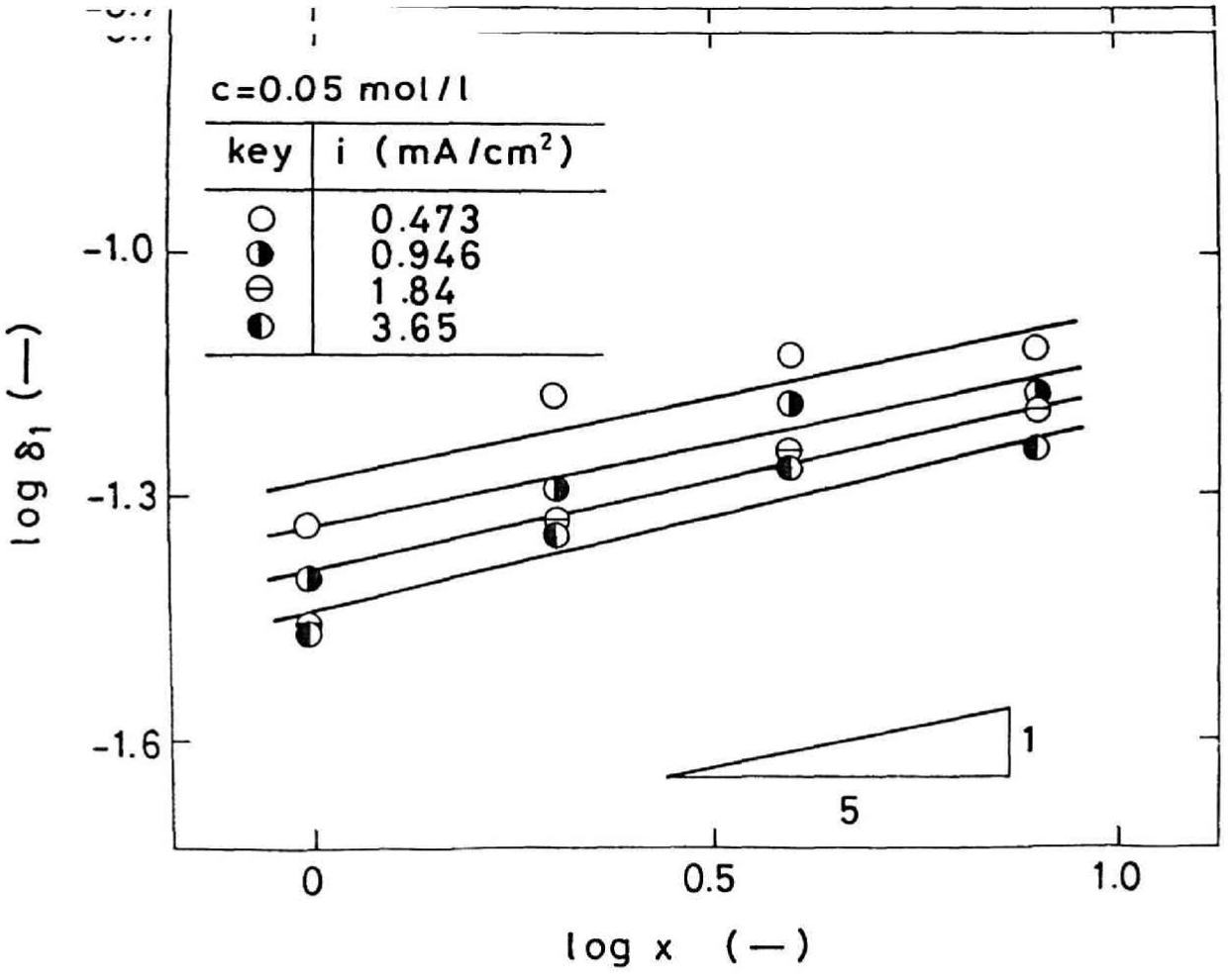

Fig. 4.17 Relationship between thickness of cathode diffusion layer and height from lower edge of cathode with aqueous 0.05M $CuSO_4$ solution

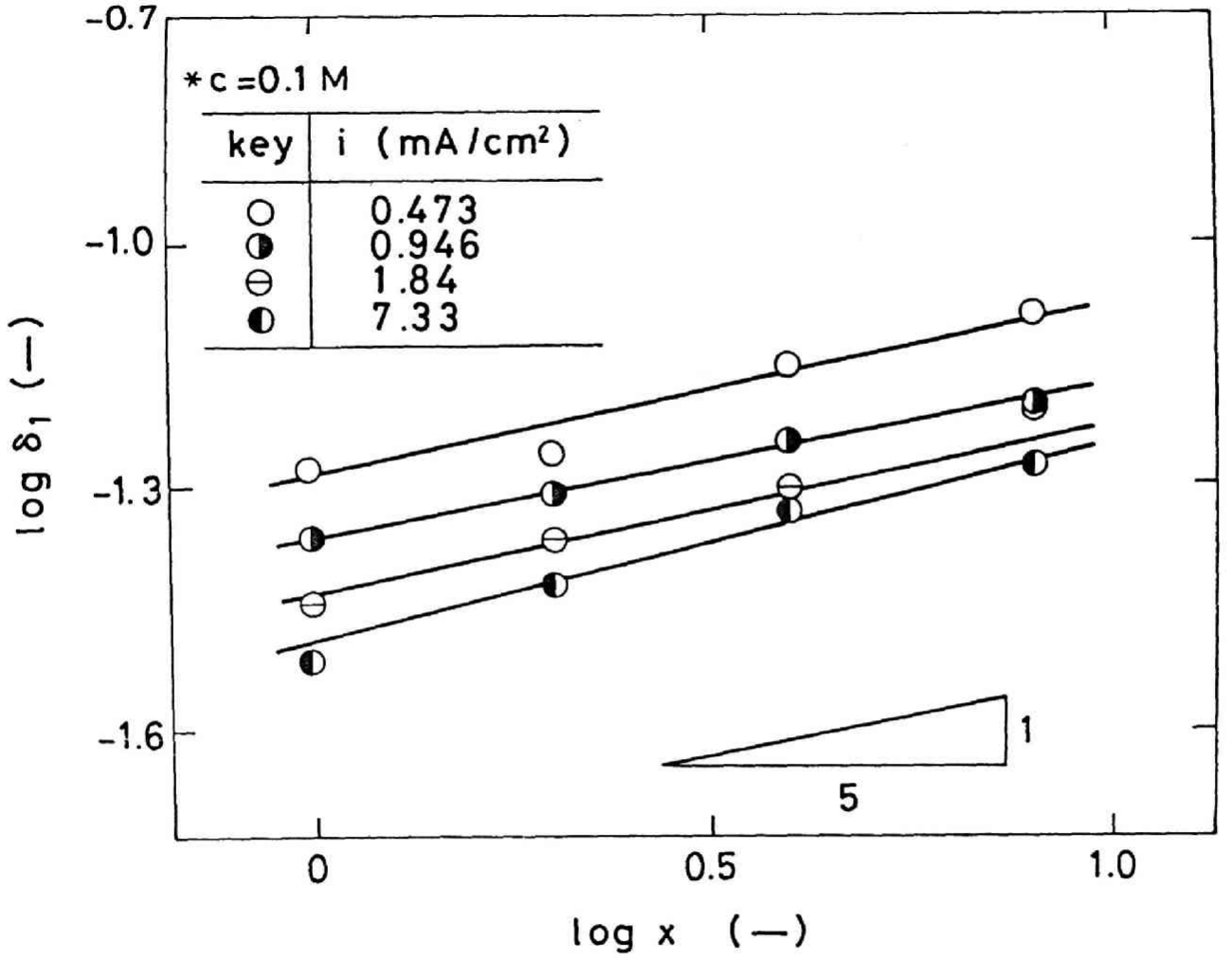

Fig. 4.18 Relationship between thickness of cathode diffusion layer and height from lower edge of cathode with aqueous 0.1M $CuSO_4$ solution

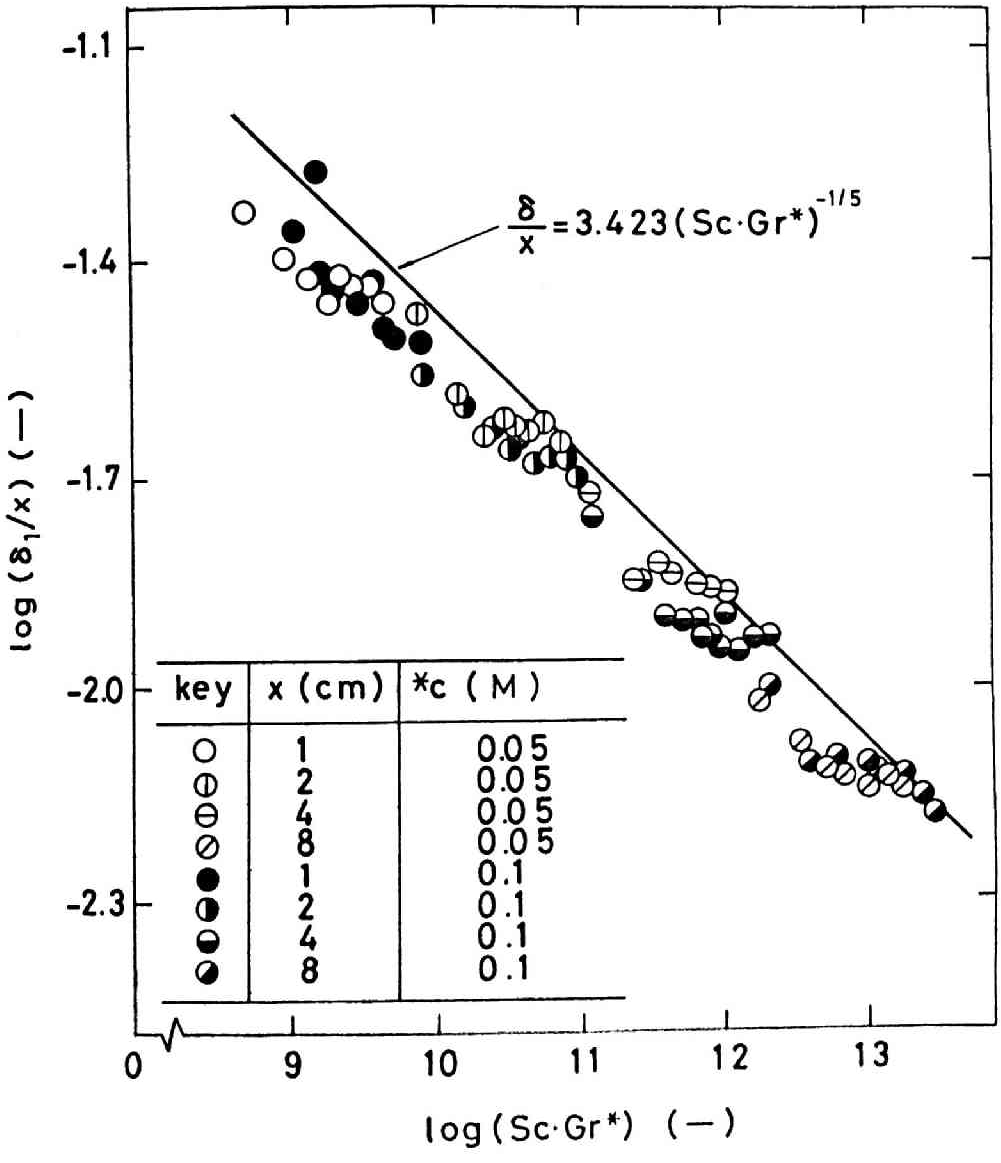

Fig. 4.19 Plot of $\log(\delta_1/x)$ vs. $\log(Sc \cdot Gr^*)$

somewhat lower than the corresponding theoretical value.

4.3 Concentration Profiles of $CuSO_4$ and H_2SO_4 in Cathodic Diffusion Layer in the Electrolysis of Aqueous $CuSO_4$-H_2SO_4 Solution

4.3.1 Measurement of profile of refractive index in the cathodic diffusion layer

The industrial electrolytic refining and plating of copper are often conducted in the unstirred or gently stirred solutions containing $CuSO_4$ and H_2SO_4. It is important to study the concentration profiles of both components in the cathodic diffusion layer. A few experimental studies[7,8] have been made to measure the thickness of cathodic diffusion layer during the unsteady electrolysis of $CuSO_4$-H_2SO_4 solution by using the Mach-Zehnder interferometry. However, the thickness of this diffusion layer determined by the interferometric methods may not have any definite physical meaning for the ionic mass transfer of Cu^{2+} ion in the $CuSO_4$-H_2SO_4 solutions, because the thickness of the diffusion layer of Cu^{2+} ion is different from H^+ ion as mentioned in Chapter 1. Furthermore, very few discussions have been made on the profile of refractive index in the cathodic diffusion layer measured by the interferometric methods in the previous papers.[7,8] This is because the refractive index of the solution in the cathodic diffusion layer is dependent on both concentrations of $CuSO_4$ and H_2SO_4 and each concentration profile can not be separately

determined by the interferometric methods.

As the first step towards the clarification of the concentration profiles of Cu^{2+} and H^{+} ions, the measurement of the profile of refractive index in the cathodic diffusion layer was attempted in the present work by applying a technique of holographic interferometry. The experimental results were compared with the theoretical values.

It is known, on the other hand, that the concentration of $CuSO_4$ is very close to zero at the cathode surface at the cathodic limiting current density.[18,19] Then the refractive index of the solution at the cathode surface at the cathodic limiting current density is dependent solely on the H_2SO_4 concentration. The concentration of H_2SO_4 at the cathode surface was estimated from the holographic interferograms obtained at the cathodic limiting current, and the results were also compared with the theoretical values.

4.3.2 Experimental results

The profile of the refractive index in the cathodic diffusion layer was measured by holographic interferometry using the same electrode and electrolytic cell as mentioned in 4.2.1. Analytical reagent grade $CuSO_4 \cdot 5H_2O$, H_2SO_4 and deionized water were used, and the aqueous solutions containing $CuSO_4$ and H_2SO_4 were made up. The measurement was conducted at 23° ± 1°C.

First, the measurement was carried out below the limiting current. The experimental conditions are given in Table 4.5. A solution of 1.85M H_2SO_4 and 0.05M $CuSO_4$ was used, and the holographic interferograms were obtained at various heights from the lower edge of the cathode at the current densities up to the limiting value. From the current-potential curve shown in Fig. 4.20, it is seen that the average cathodic limiting current density of this solution of 1.85M H_2SO_4 and 0.05M $CuSO_4$ is 1.96 mA/cm^2. The applied cathodic current densities included 8 values up to the limiting value. A few examples of holographic interferogram are demonstrated in Fig. 4.21. A holographic interferogram near the cathode surface before the start of electrolysis is shown in Fig. 4.21(a). Figures 4.21(b) through (d) are the interferograms of 0.05M $CuSO_4$-1.85M H_2SO_4 solution during the electrolysis at an average cathodic current density of 1.66 mA/cm^2 at the heights of 1, 4 and 8 cm from the lower edge of the cathode, respectively. They were filmed after 10 min had elapsed from the start of electrolysis: it was observed that the electrolysis is at the steady state. It is seen from these figures that the thickness of diffusion layer increases in the upper portion of cathode due to the growth of the upward natural convective flow.

Next, the profile of refractive index in the cathodic diffusion layer was measured at the cathodic limiting current densities with the solutions containing 1.85M H_2SO_4 and 0.01, 0.02,

Table 4.5 Experimental conditions

Electrolyte	0.05M $CuSO_4$-1.85M H_2SO_4
Distance from the lower edge of cathode (cm)	1.0, 2.0, 4.0, 8.0
Average cathodic current density (mA/cm^2)	0.236, 0.473, 0.709, 0.946 1.18, 1.42, 1.65, 1.96*

* Cathodic limiting current density

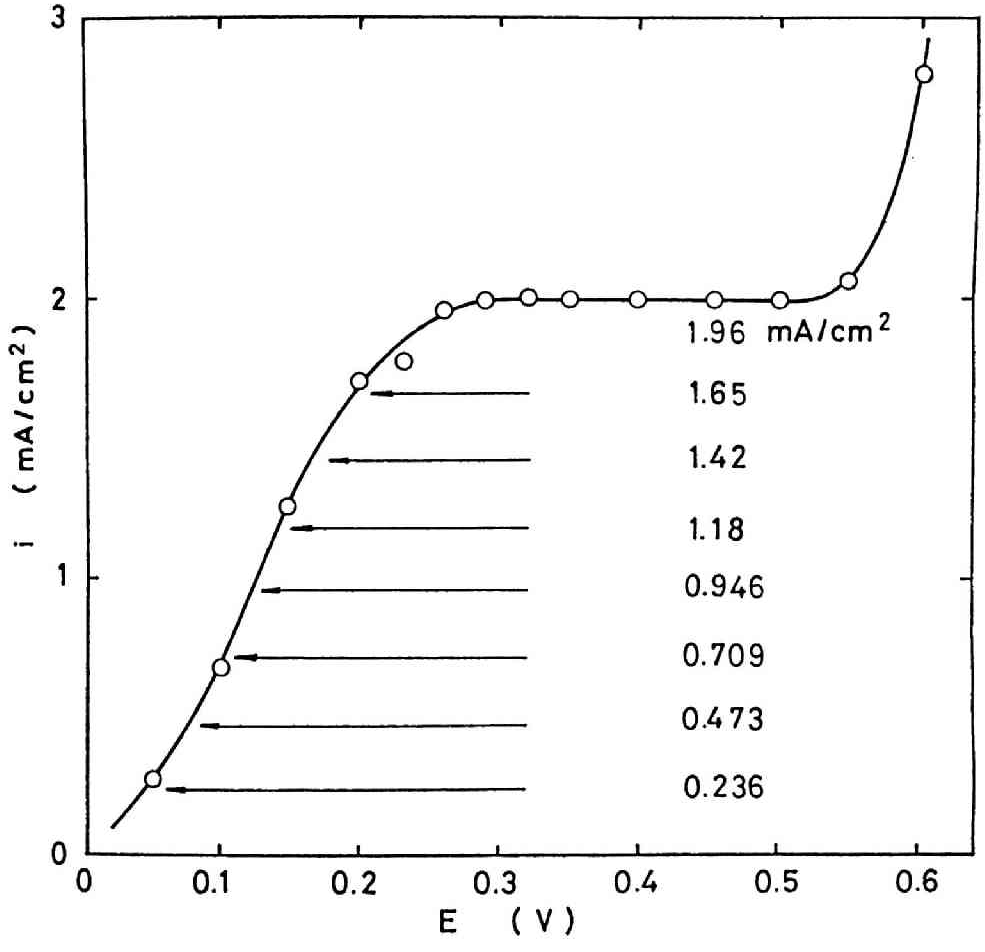

Fig. 4.20 Current potential curve with 0.05M $CuSO_4$-1.85M H_2SO_4 solution

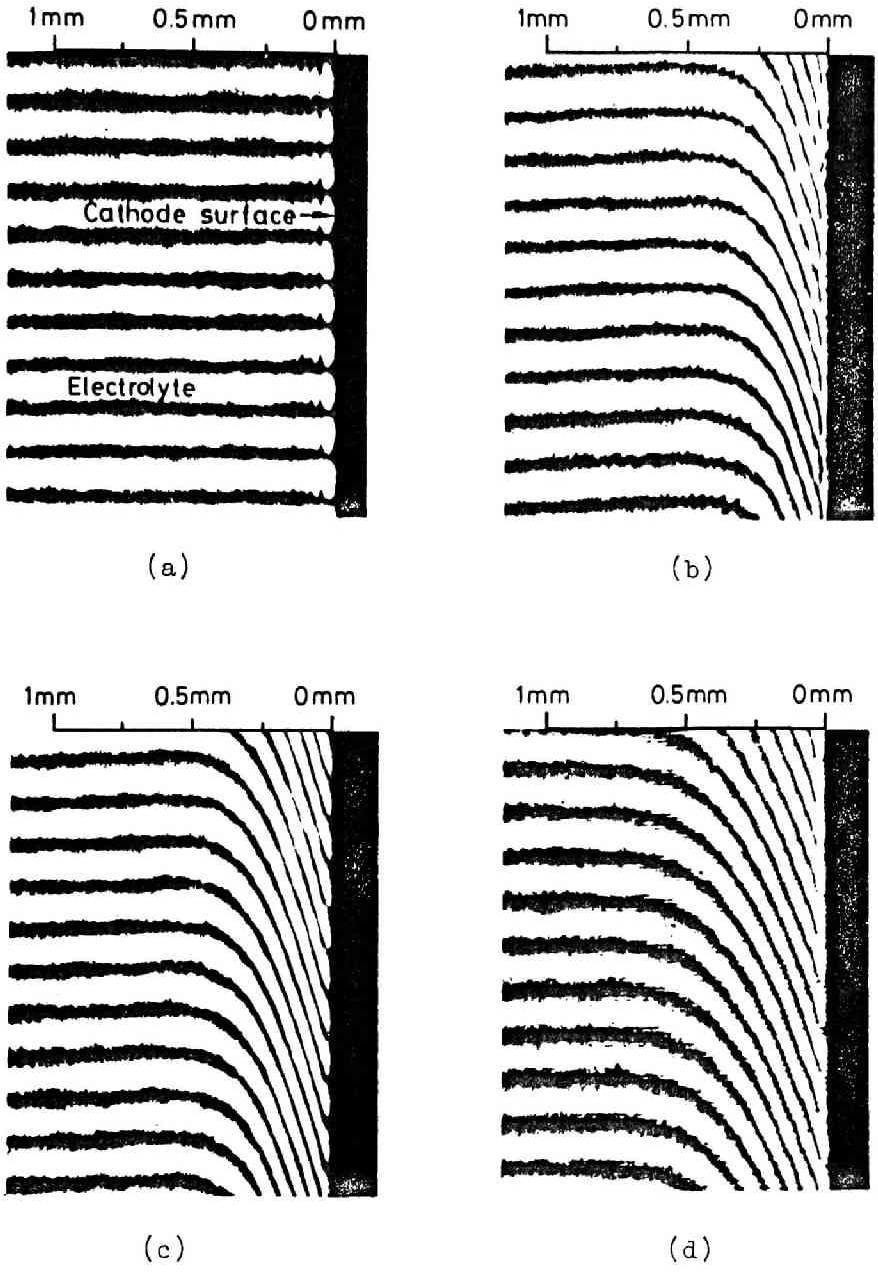

Fig. 4.21 Holographic interferograms of cathodic diffusion layer
(a) before the start of electrolysis
(b) x = 1 cm, (c) x = 4 cm, (d) x = 8 cm
during the electrolysis of 0.05M $CuSO_4$-1.85M H_2SO_4
solution at i = 1.66 mA/cm^2

0.03, 0.04 and 0.05M $CuSO_4$, respectively. Prior to the measurement of the profile of refractive index in the cathodic diffusion layer, the current-potential curve was measured with each solution and they are shown in Fig. 4.22. Based on these results, the electrolysis at the limiting current was conducted under the experimental condition that the cathode potential against the reference electrode was maintained at 300 mV. The measurement was conducted at a height of 4 cm from the lower edge of cathode. Holographic interferograms are illustrated in Fig. 4.23. Figures 4.23(a) through (d) are the interferograms of the cathodic diffusion layer of the solutions of 0.02M $CuSO_4$-1.85M H_2SO_4, 0.03M $CuSO_4$-1.85M H_2SO_4, 0.04M $CuSO_4$-1.85M H_2SO_4 and 0.05M $CuSO_4$-1.85M H_2SO_4 at their limiting current densities of 0.683, 0.910, 1.57 and 1.96 mA/cm^2, respectively. They were filmed at the steady state after 10 min had elapsed from the start of electrolysis.

From these holographic interferograms, the profiles of refractive index in the cathodic diffusion layer were calculated by Eq. (4.1) and corrected according to the procedure mentioned in 4.2.2. Several examples of the corrected profile of refractive index are demonstrated in Fig. 4.24 and 4.25, respectively.

The profiles of the refractive index shown in Fig. 4.24 were obtained with the solution containing 0.05M $CuSO_4$ and 1.85M H_2SO_4 at a height of 4 cm from the lower edge of the cathode. The cathodic current density was varied between 0.236 and 1.96 mA/cm^2.

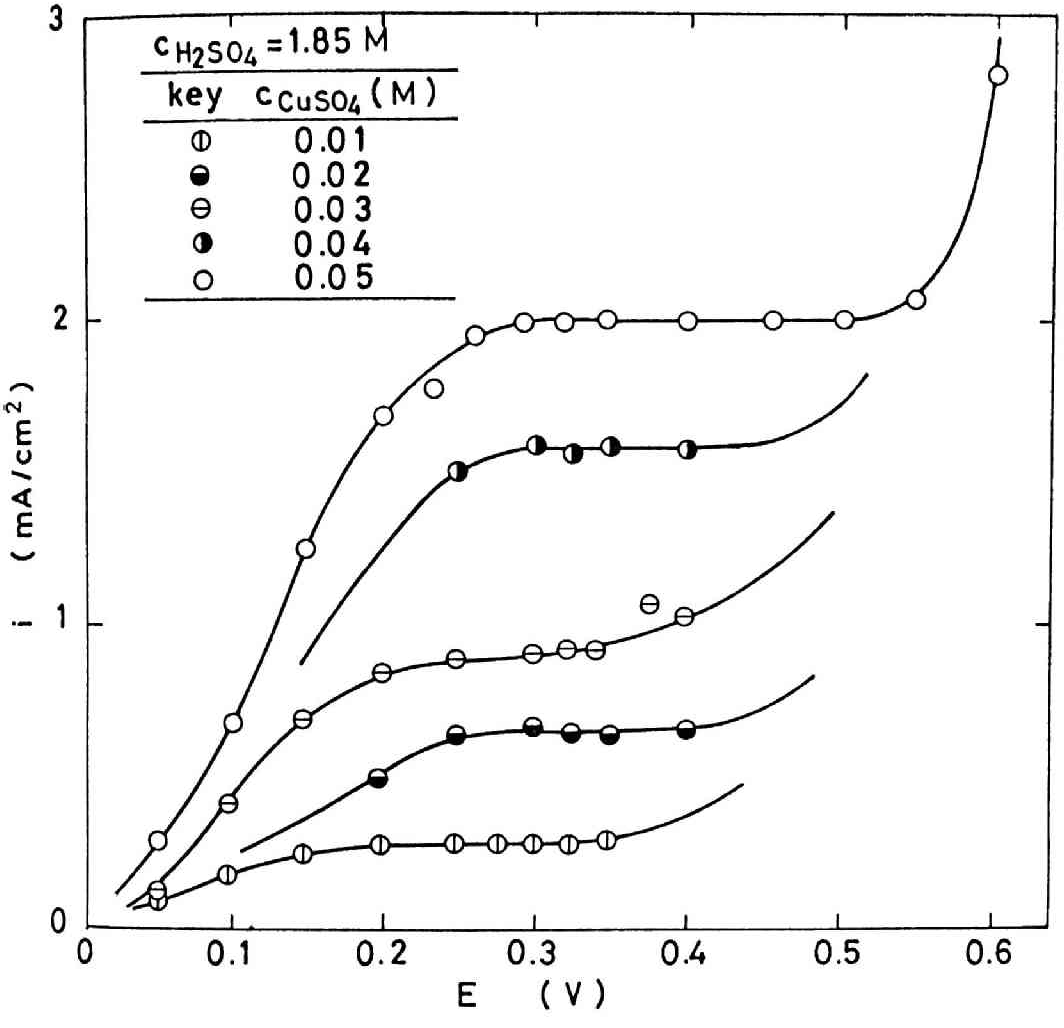

Fig. 4.22 Current-potential curves for each solution

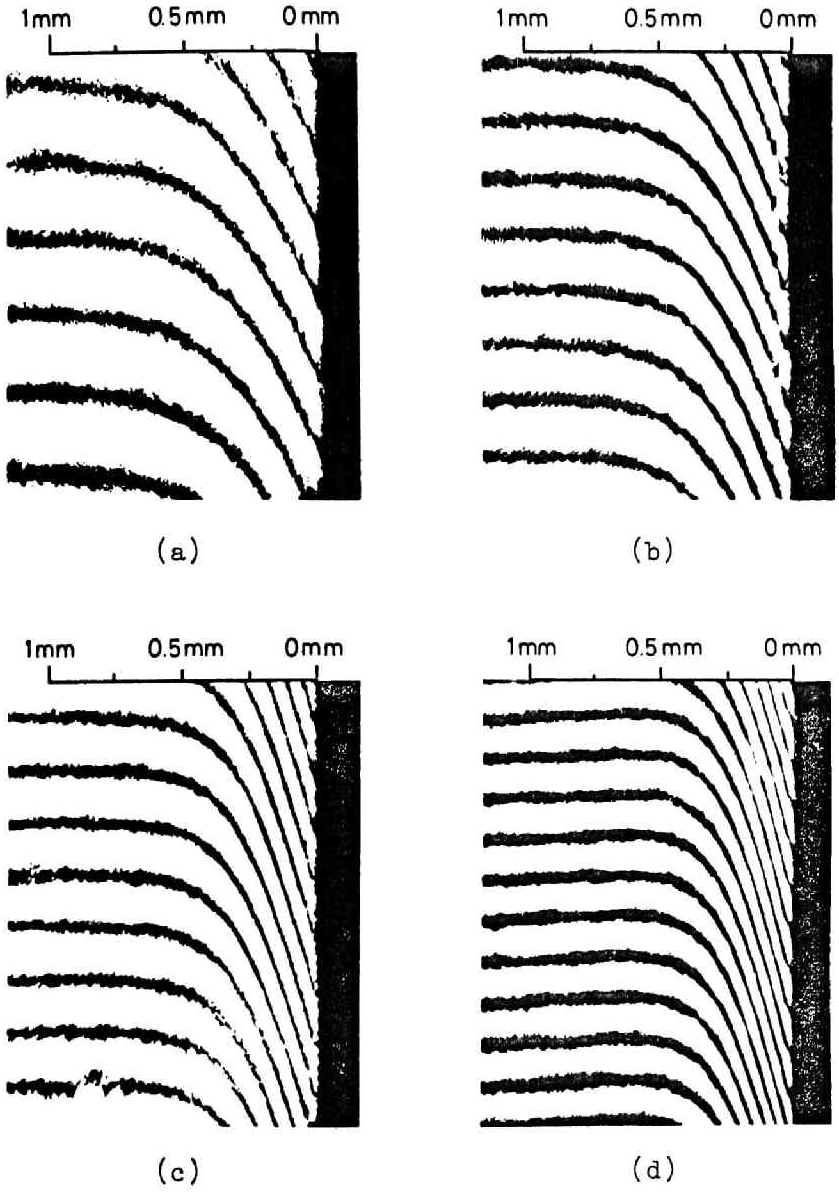

ig. 4.23 Holographic interferograms of the cathodic diffusion layer at x = 4 cm with the solutions of (a) 0.02M $CuSO_4$-1.85M H_2SO_4, (b) 0.03M $CuSO_4$-1.85M H_2SO_4, (c) 0.04M $CuSO_4$-1.85M H_2SO_4, and (d) 0.05M $CuSO_4$-1.85M H_2SO_4 at their limiting current densities of 0.683, 0.910, 1.57 and 1.96 mA/cm^2, respectively.

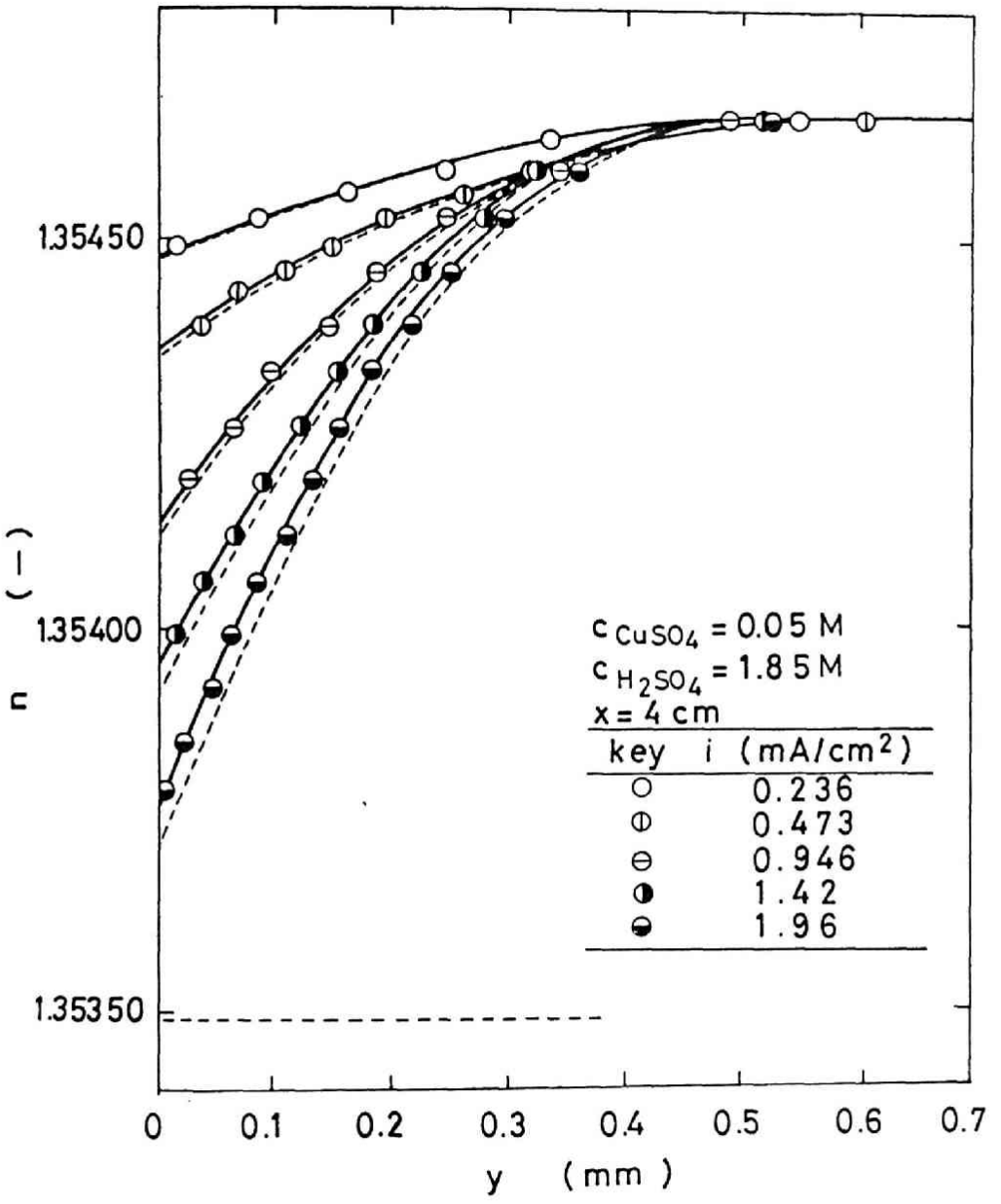

Fig. 4.24 Corrected profiles of refractive index in the cathiduc diffusion layer

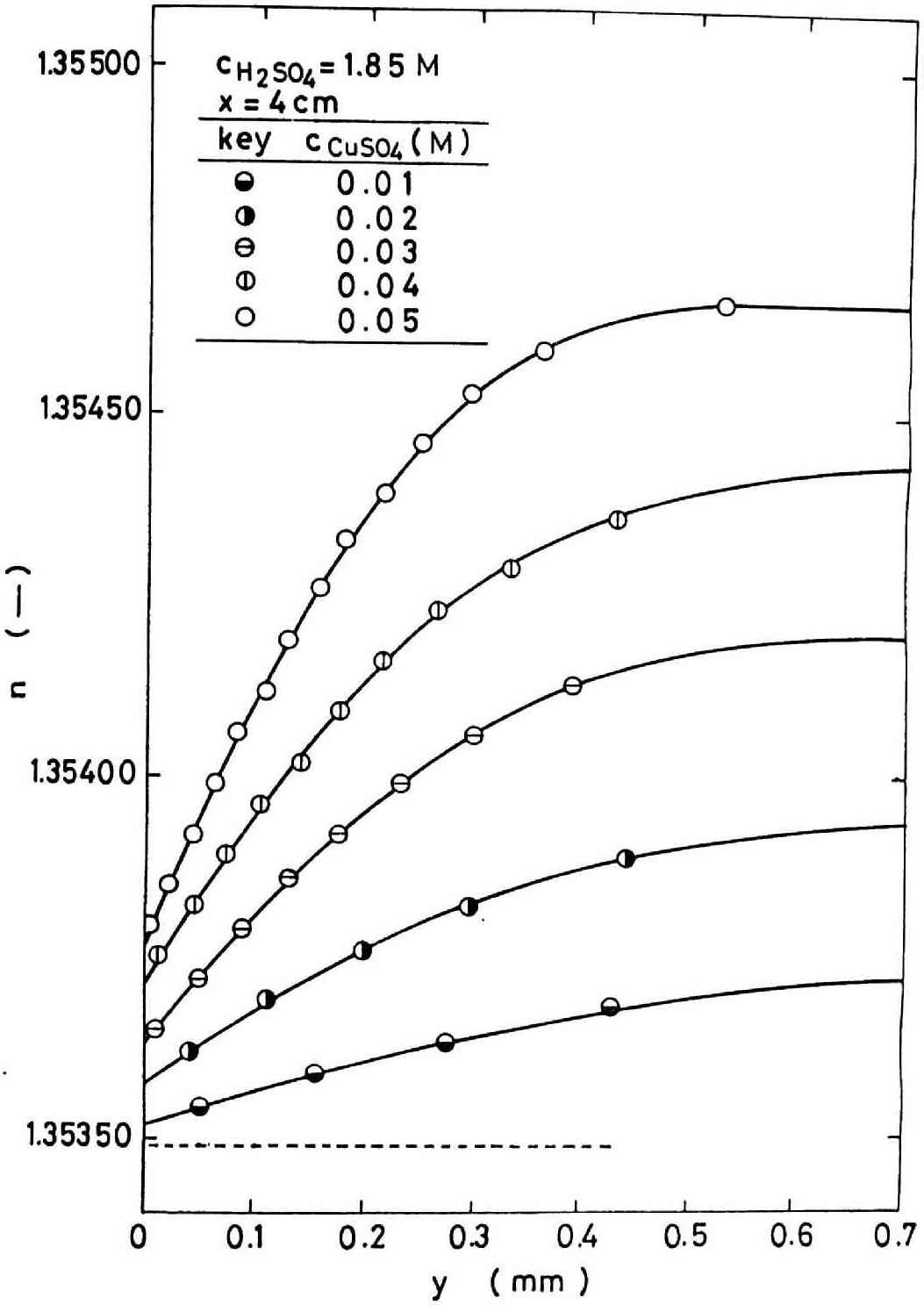

Fig. 4.25 Corrected profiles of refractive index in the cathodic diffusion layer at the limiting current density

The uncorrected profiles of the refractive index are also shown in the same figure. As seen in this figure, the refractive index at the cathode surface becomes lower when the average cathodic current density is raised. It is also seen that the previously mentioned correction for the optical distortion becomes more significant when the slope of the refractive index is steeper. The experimental data obtained with 0.05M $CuSO_4$-1.85M H_2SO_4 solution were summarized in Table 4.6.

The corrected profiles of the refractive index at the limiting current densities in the solutions containing 1.85M H_2SO_4 and 0.01, 0.02, 0.03, 0.04 and 0.05M $CuSO_4$ are demonstrated in Fig. 4.25, respectively. It is seen in this figure that the refractive index of the solution at the cathode surface decreases when the concentration of $CuSO_4$ in the bulk-electrolyte is lower. The horizontal broken lines at 1.35349 in Fig. 4.24 and 4.25 represent the refractive index of the aqueous 1.85M H_2SO_4 solution, respectively. As seen in Fig. 4.25, the numerical values of refractive index at the cathode surface of the solutions at their limiting current densities are higher than that of 1.85M H_2SO_4 solution: it is indicated that H_2SO_4 is accumulated in the cathodic diffusion layer due to the migration of H^+ ion in the electric field between both electrodes.

Table 4.6 The refractive index at the cathode surface with aqueous 0.05M $CuSO_4$-1.85M H_2SO_4 solution

No. (-)	x (cm)	i (mA/cm^2)	^{o}n (-)	Δn (-)	log x (-)	log i (-)	log Δn (-)
1	1	0.236	1.35453	0.00013	0.0000	-0.627	-3.886
2	1	0.473	1.35440	0.00026	0.0000	-0.325	-3.585
3	1	0.709	1.35429	0.00037	0.0000	-0.149	-3.432
4	1	0.946	1.35427	0.00039	0.0000	-0.024	-3.409
5	1	1.18	1.35411	0.00055	0.0000	0.072	-3.260
6	1	1.42	1.35397	0.00069	0.0000	0.152	-3.161
7	1	1.65	1.35395	0.00071	0.0000	0.217	-3.146
8	1	1.96	1.35380	0.00086	0.0000	0.292	-3.063
9	1	0.236	1.35453	0.00013	0.0000	-0.627	-3.886
10	1	0.473	1.35443	0.00023	0.0000	-0.327	-3.638
11	1	0.709	1.35436	0.00030	0.0000	-0.149	-3.523
12	1	0.946	1.35427	0.00039	0.0000	-0.024	-3.409
13	1	1.18	1.35417	0.00049	0.0000	0.072	-3.310
14	1	1.42	1.35405	0.00061	0.0000	0.152	-3.215
15	1	1.65	1.35394	0.00072	0.0000	0.217	-3.143
16	1	1.96	1.35379	0.00087	0.0000	0.292	-3.060
17	2	0.236	1.35448	0.00018	0.3010	-0.627	-3.745
18	2	0.236	1.35449	0.00017	0.3010	-0.627	-3.770
19	2	0.473	1.35436	0.00030	0.3010	-0.325	-3.523
20	2	0.473	1.35436	0.00030	0.3010	-0.325	-3.523
21	2	0.709	1.35429	0.00037	0.3010	-0.149	-3.432
22	2	0.946	1.35422	0.00044	0.3010	-0.024	-3.357
23	2	1.18	1.35411	0.00055	0.3010	0.072	-3.260
24	2	1.42	1.35406	0.00060	0.3010	0.152	-3.222
25	2	1.65	1.35391	0.00075	0.3010	0.217	-3.125
26	2	1.96	1.35380	0.00086	0.3010	0.292	-3.066
27	2	0.236	1.35453	0.00013	0.3010	-0.627	-3.886
28	2	0.473	1.35443	0.00023	0.3010	-0.325	-3.638
29	2	0.709	1.35429	0.00037	0.3010	-0.149	-3.432
30	2	0.946	1.35418	0.00048	0.3010	-0.024	-3.319
31	2	1.18	1.35410	0.00056	0.3010	0.072	-3.252
32	2	1.42	1.35403	0.00063	0.3010	0.152	-3.201
33	2	1.65	1.35393	0.00073	0.3010	0.217	-3.137
34	2	1.96	1.35378	0.00088	0.3010	0.292	-3.056
35	4	0.236	1.35448	0.00018	0.6021	-0.627	-3.745
36	4	0.473	1.35435	0.00031	0.6021	-0.325	-3.509
37	4	0.709	1.35423	0.00043	0.6021	-0.149	-3.367
38	4	0.946	1.35413	0.00053	0.6021	-0.024	-3.276
39	4	1.18	1.35400	0.00066	0.6021	0.072	-3.180
40	4	1.42	1.35393	0.00073	0.6021	0.152	-3.137
41	4	1.65	1.35383	0.00083	0.6021	0.217	-3.081
42	4	1.96	1.35375	0.00091	0.6021	0.292	-3.041
43	8	0.236	1.35448	0.00018	0.9031	-0.627	-3.745
44	8	0.236	1.35446	0.00020	0.9031	-0.627	-3.699
45	8	0.473	1.35432	0.00034	0.9031	-0.325	-3.469
46	8	0.709	1.35419	0.00047	0.9031	-0.149	-3.328
47	8	0.946	1.35411	0.00055	0.9031	-0.024	-0.260
48	8	1.18	1.35402	0.00064	0.9031	0.072	-3.194
49	8	1.42	1.35396	0.00070	0.9031	0.152	-3.155
50	8	1.65	1.35382	0.00084	0.9031	0.217	-3.076
51	8	1.96	1.35372	0.00094	0.9031	0.292	-3.027

4.3.3 Discussion

The profile of the refractive index in the cathodic diffusion layer was measured with the solution containing 1.85M H_2SO_4 and 0.05M $CuSO_4$. In order to investigate the dependances of the difference of refractive index between cathode surface and bulk-electrolyte on the average cathodic current density and on the height from the lower edge of cathode, Eq. (2.89) which was previously derived in 2.4.2 under the condition of uniform cathodic current density was used. It is as below.

$$\Delta c_1 = \theta_1 = \frac{\eta E_4}{\omega_1} \frac{(1-*t_1)}{z_1 F k_1} \left\{ \frac{z_1 F^* \nu k_1^2}{g \xi (1-*t_1)} \right\}^{1/5} i^{4/5} x^{1/5} \qquad (2.89)$$

In addition, the concentration difference of H^+ ion, θ_2, between cathode surface and bulk-electrolyte was related to θ_1 in the form of Eq. (2.79). It is

$$\theta_2 = -\gamma\sigma \frac{\omega_1}{\omega_2} \theta_1 \qquad (2.79)$$

where

$$\sigma = \frac{\delta_2}{\delta_1} \qquad (4.23)$$

The notation σ in this equation represents the ratio of the thickness of cathodic diffusion layers of H^+ ion to Cu^{2+} ion. Its numerical value is slightly higher than unity.[18)]

The refractive index of the solution is related not only to Cu^{2+} ion concentration but also to H^+ ion concentration. When

the refractive index is expressed by a linear equation of

$$n = A + Bc_1 + Cc_2 \tag{4.24}$$

where c_1 and c_2 are the concentrations of $CuSO_4$ and H_2SO_4, respectively, the difference of refractive index between cathode surface and bulk-electrolyte, Δn, is expressed from Eq. (2.79) and (4.24) as

$$\begin{aligned}\Delta n &= {}^*n - n \\ &= B\theta_1 + \frac{1}{1+a} C\theta_2 \\ &= \left(B - \frac{\gamma\sigma\omega_1}{(1+a)\omega_1} C\right)\theta_1\end{aligned} \tag{4.25}$$

where the notation a represents the degree of the second stage dissociation of H_2SO_4. Substitution of Eq. (2.89) in Eq. (4.25) yields

$$\Delta n = \left(B - \frac{\gamma\sigma\omega_1}{(1+a)\omega_2} C\right) \frac{\eta E_4}{\omega_1} \frac{(1-{}^*t_1)}{z_1 F k_1} \left\{\frac{z_1 F {}^*\nu k_1^2}{g \frac{z}{2}(1-{}^*t_1)}\right\}^{1/5} \cdot i^{4/5} x^{1/5} \tag{4.26}$$

It is expected from this equation that Δn is proportional to $i^{4/5}$ and $x^{1/5}$, respectively. The refractive index of the aqueous solutions containing $CuSO_4$ and H_2SO_4 at various concentrations was measured at 23° ± 1°C by using the Abbé refractometer. They are as shown in Fig. 4.26. It is seen in this figure that the variation of refractive index in these solutions is linear with regard to both $CuSO_4$ and H_2SO_4 concentrations in the regions of 0 to 0.27M $CuSO_4$ and 0.8 to 2.0M H_2SO_4, respectively. The regression of the refractive index upon the concentrations of $CuSO_4$

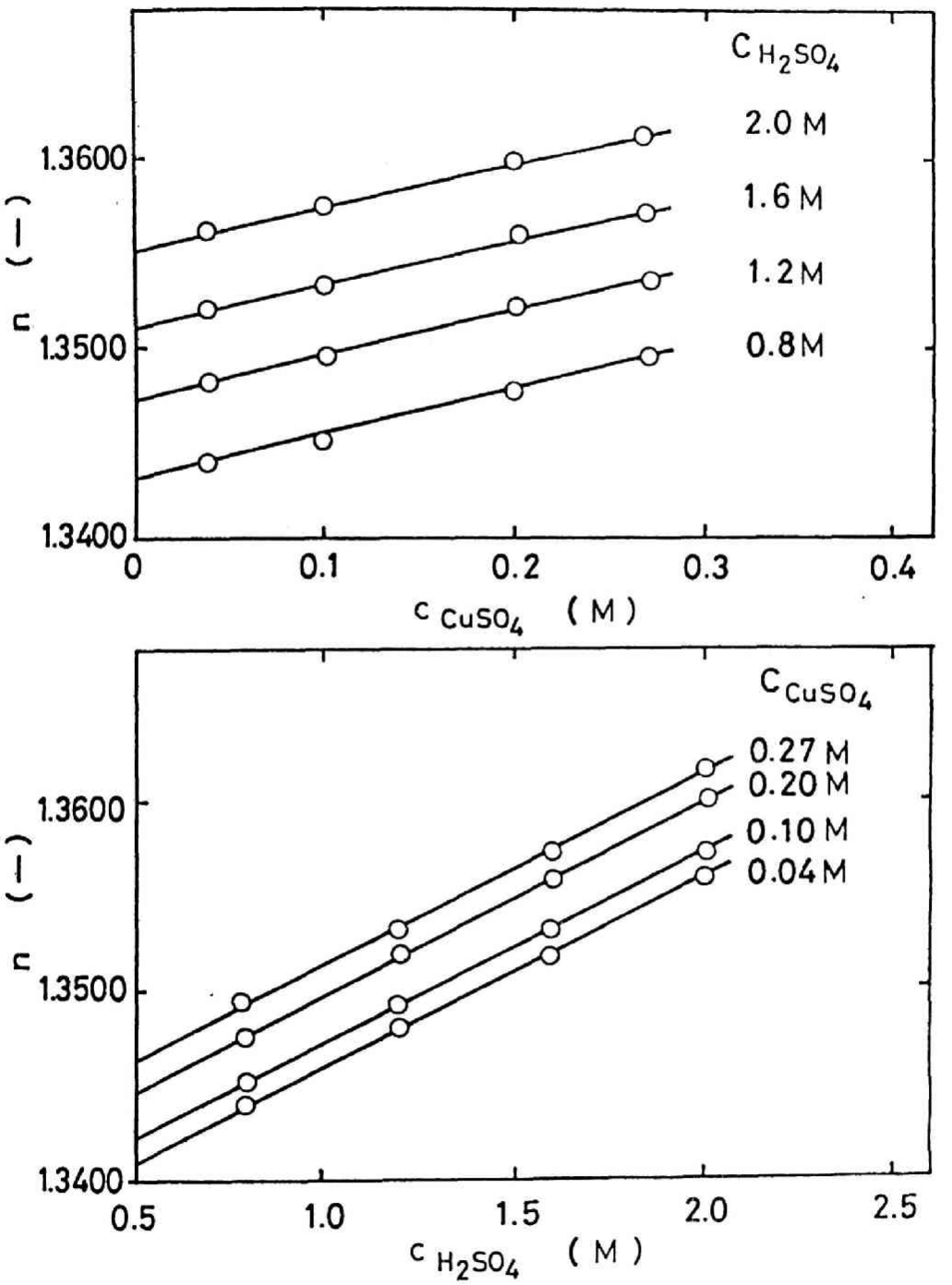

Fig. 4.26 Refractive index of $CuSO_4$-H_2SO_4 aqueous solutions

and H_2SO_4 was calculated by the least squares method. It is

$$n = 1.3348 + 23.447c_1 + 10.075c_2 \qquad (4.27)$$

The dependances of Δn on the average cathodic current density and on the height from the lower edge of cathode were examined: the measured log Δn of the solution containing 1.85M H_2SO_4 and 0.05M $CuSO_4$ was plotted against the logarithmic average cathodic current density, and they are demonstrated in Fig. 4.27. As seen in this figure, the slope of straight lines was obtained at 4/5, which is equal to the theoretical value of Eq. (4.26) when the cathodic current density is lower than the half-value of the limiting current density. Above this half-value, on the other hand, Δn values start to converge into a fixed value at the limiting current density.

Next, log Δn was plotted against log x and demonstrated in Fig. 4.28. By comparing the experimental slopes with the theoretical value of 1/5, it is clear that the experimental slopes are equal to 1/5 at the current densities lower than the half-value of the limiting current density. They start to decrease when the average current density is raised above this half-value: it is virtually null at the cathodic limiting current density of 1.96 mA/cm^2. These experimental results may suggest that the local cathodic current density is not uniform in vertical direction above the half-value of the cathodic limiting current density.[20,21,22)]

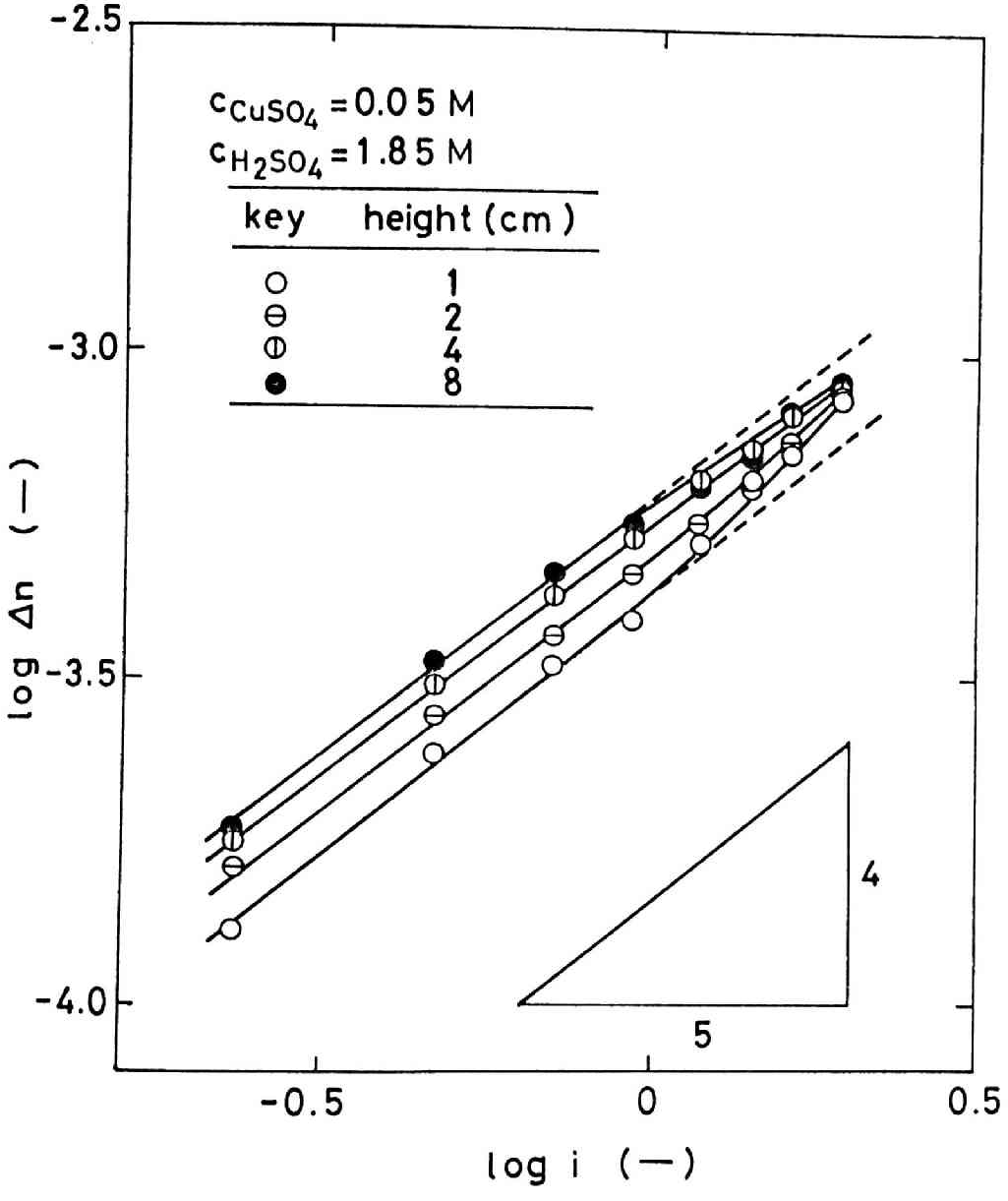

Fig. 4.27 Relationship between refractive index difference and average cathodic current density

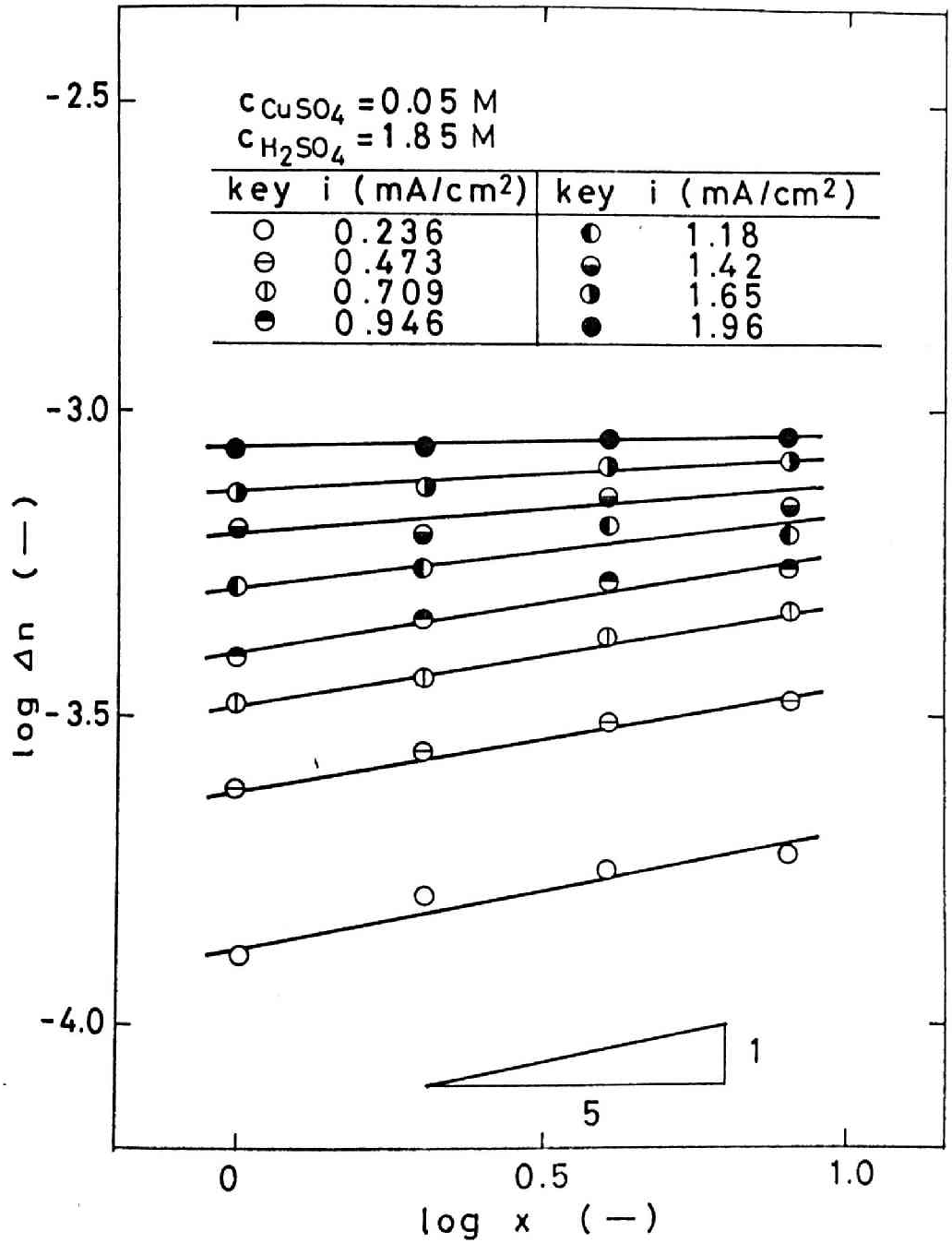

Fig. 4.28 Relationship between refractive index difference and height from lower edge of cathode

Furthermore, the Δn values were calculated from the following equation in which it was assumed that ω_1 is equal to ω_2.

$$\Delta n = \left(B - \frac{\gamma\sigma}{1+a} C \right) \frac{\eta E_4}{\omega_1} \frac{(1-*t_1)}{z_1 F k_1} \left\{ \frac{z_1 F^* \nu k_1^2}{g^2 (1-*t_1)} \right\}^{1/5} \times \left\{ i^3(x) \int_0^x i(x)\, dx \right\}^{1/5} \qquad (4.28)$$

This equation was derived from Eq. (2.83), (2.95) and (4.25). It is valid in the wide range of cathodic current densities between very low current density and the limiting value. The distribution of the local current densities, i(x) at the cathode surface which is necessary to obtain Δn by Eq. (4.28) were first calculated from Eq. (2.95), (2.96) and (2.69) by employing a technique of successive approximation. Then, the Δn values were obtained by substituting i(x) in Eq. (4.28), and they were compared with the measured values. The property constants and transport parameters employed in the calculation are demonstrated in Table 4.7. Among these numerical values, the kinematic viscosity of the solution, ν, was obtained by measuring the viscosity and density of the solution because no data were available in the literature. The diffusivity of Cu^{2+} ion was referred to Appendix B. Furthermore the values of parameters σ and η are 1.54 and 2.65, respectively, in aqueous 0.6M $CuSO_4$-1.5M H_2SO_4 solution, and they were estimated to be 1.18 and 3.45 in 0.05M $CuSO_4$-1.85M H_2SO_4 solution, respectively, because the diffusivity of

Table 4.7 Propoerty constants used in the calculation

k_1	(cm^2/sec)	5.92×10^{-6}*
*t_1	(-)[24,25,26]	0.0033
ν	(cm^2/sec)	1.1148×10^{-2}
α_1	(cm^3/mol)[22]	125
α_2	(cm^3/mol)[22]	40.9**
σ	(-)	1.18
ω	(-)	2.30
η	(-)	3.45
a	(-)	0.31***

* see Appendix B
** see Appendix D
*** see Appendix C

Cu^{2+} ion at the average concentration of 0.025M $CuSO_4$ and 1.85M H_2SO_4 in the diffusion layer of the aqueous 0.05M $CuSO_4$-1.85M H_2SO_4 solution is 1.25 times larger than in 0.6M $CuSO_4$-1.5M H_2SO_4 solution and the term of $(1 - *t_1)$ in the former solution is 1.04 times larger than the latter solution. The degree of the second stage dissociation of H_2SO_4 is 0.31 (see Appendix C).

The results were summarized in Table 4.8. It can be said from this table that the measured values are fairly well coincident with the calculated values over the whole range of the cathodic current densities, though the calculated values are slightly lower than the measured ones. It is also seen that the ratio of the measured values to the calculated values is nearly constant and it is 1.17. This may suggest that Eq. (4.28) explains the dependances of Δn on the cathodic current density and on the height from the lower edge of cathode and also that the difference between the measured and calculated values is caused by the uncertainty in the estimation of the property constants used in the calculation such as the diffusivity of Cu^{2+} ion.

Following this, the difference of the refractive index between cathode surface and bulk-electrolyte at the cathodic limiting current density was pursued: the solutions whose H_2SO_4 concentration is maintained at 1.85M were used. The logarithmic average limiting current density, $\log i_{d,av}$, obtained with each of these solutions was plotted against the logarithmic $CuSO_4$ concentration, and it is demonstrated in Fig. 4.29. According to

Table 4.8 Refractive index difference in the cathodic diffusion layer of aqueous solution containing 1.85M H_2SO_4 and 0.05M $CuSO_4$

x (cm) / $\frac{\Delta n}{i}$ x 10^4 (mA/cm^2)	1		2		4		8	
	meas.	calc.	meas.	calc.	meas.	calc.	meas.	calc.
0.236	1.31	1.11	1.63	1.28	1.79	1.43	1.84	1.68
0.473	2.43	2.02	2.78	2.28	3.11	2.53	3.40	2.85
0.709	3.35	2.90	3.71	3.18	4.33	3.40	4.72	3.83
0.946	3.93	3.76	4.62	4.02	5.28	4.41	5.56	4.87
1.18	5.24	4.62	5.58	4.84	6.59	5.28	6.38	5.59
1.42	6.54	5.50	6.28	5.78	7.32	6.09	7.00	6.36
1.65	7.15	6.36	7.47	6.60	8.27	6.83	8.39	7.02
1.96	8.62	7.66	8.70	7.69	9.12	7.74	9.37	7.77

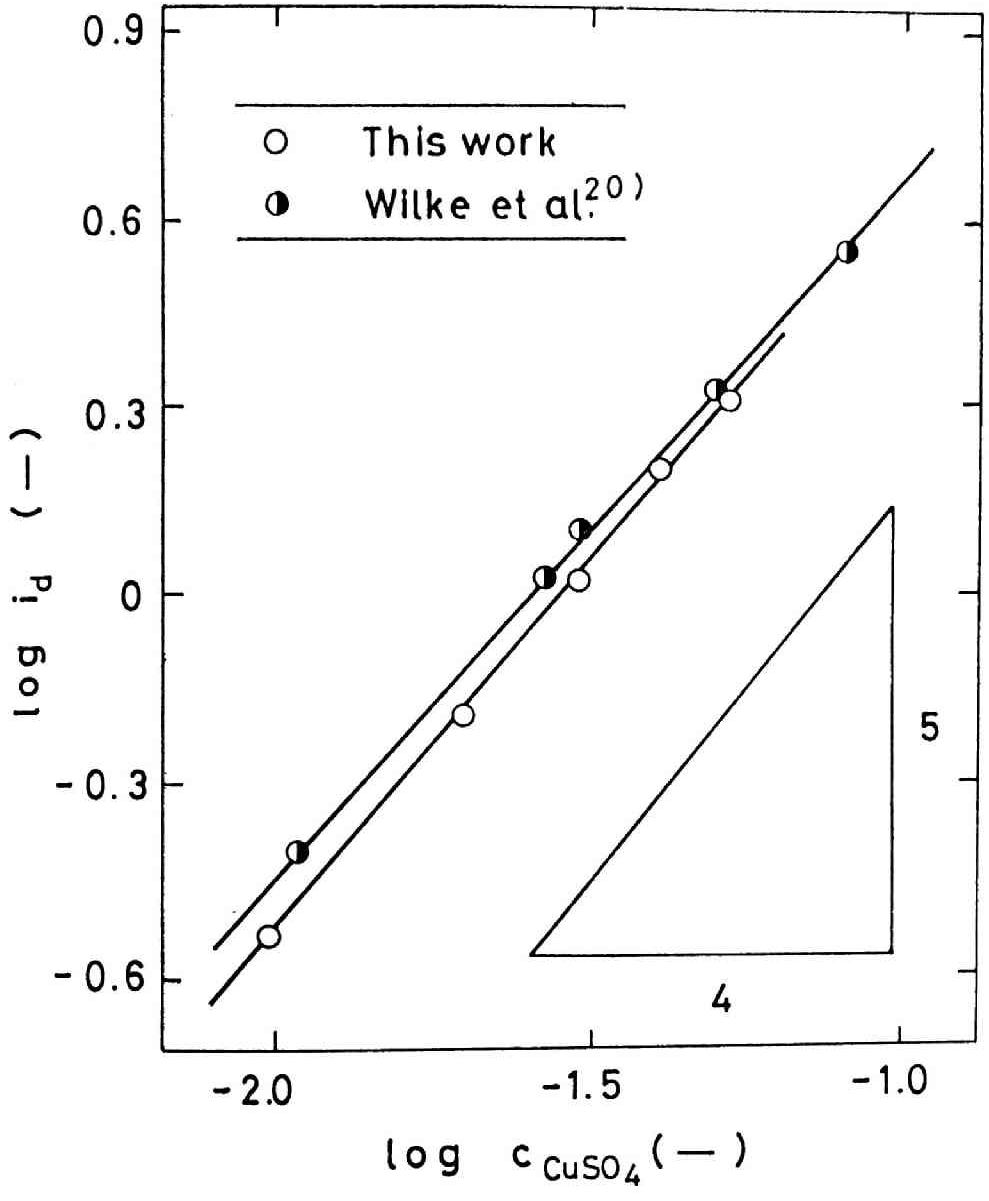

Fig. 4.29 Relationship between cathodic limiting current density and concentration of $CuSO_4$ in the bulk-electrolyte

Eq. (2.88), the average cathodic limiting current density is proportional in the first approximation to the 5/4th power of $CuSO_4$ concentration in the bulk-electrolyte. As seen in Fig. 4.29, this theoretical relationship is satisfied.

For comparison, furthermore, the experimental results obtained by Wilke et al.[20] were applied. That is, Wilke's results where a vertical plane cathode of 7.6 cm height and width which is much wider than in the present work was used and the temperature was maintained at about 23°C were plotted in Fig. 4.30 in addition to the experimental data obtained in the present work. It is seen in this figure that the experimental results in the present work agree fairly well with Wilke's Nu'-Gr-Sc correlation concerning the average cathodic limiting current density. It is also observed in this figure that the effects of side wall of the electrolytic cell used in the present work on the limiting current are neglected. The property constants and transport parameters employed in this calculation of Nu'-Gr-Sc correlation are summarized in Table 4.9. The notations H and $i_{d,av}$ are the cathode height and the average cathodic limiting current density, respectively. The density and viscosity of the solution were measured in the present work, and the diffusivity of Cu^{2+} ion at the average concentation in the diffusion layer of each solution was referred to Appendix B. The variation of α_1 with the composition of the solution is not significant.

As mentioned before, $CuSO_4$ concentration at the cathode sur-

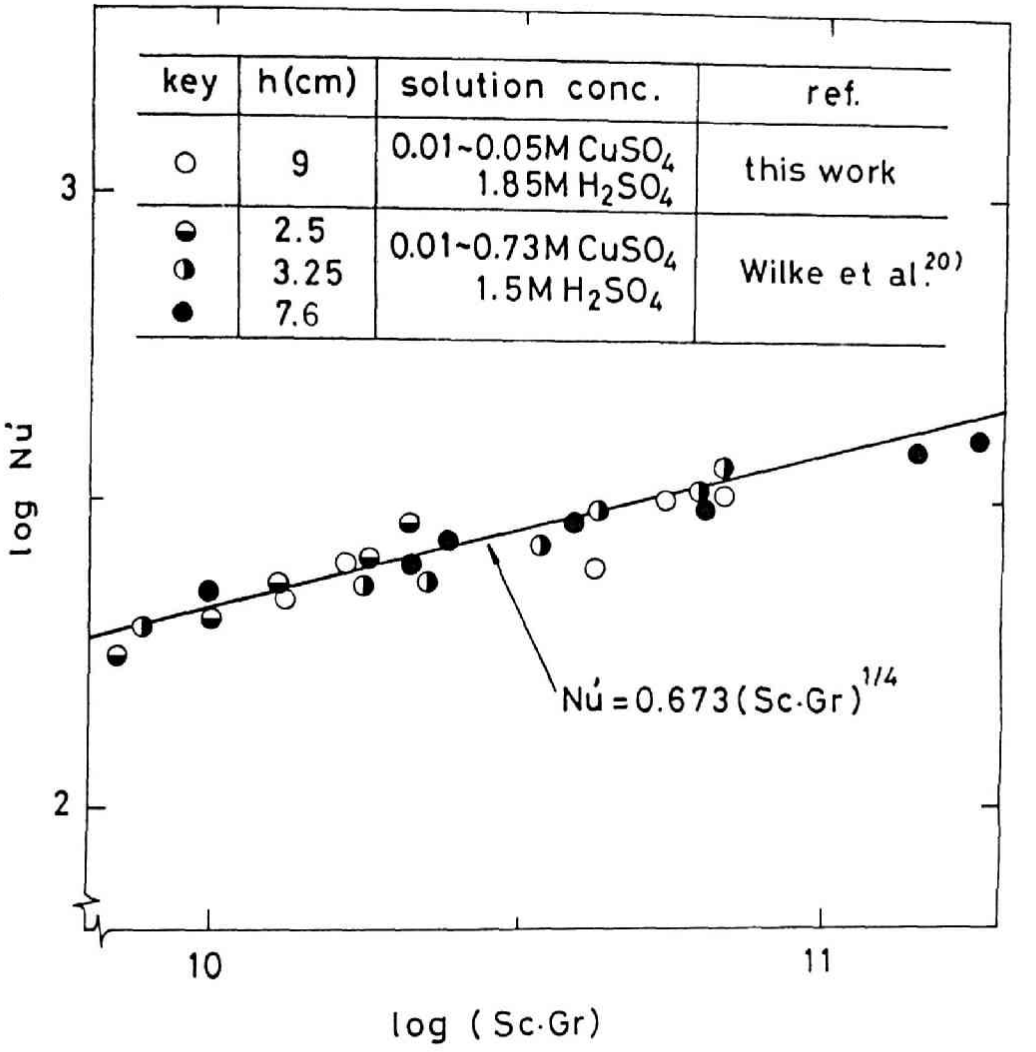

Fig. 4.30 Relationship between log Nu' and log(Sc·Gr)

Table 4.9 Average cathodic limiting current density and property constants used in the calculation of Nu'-Gr-Sc correlation

No.	$c_{H_2SO_4}$ (M)	c_{CuSO_4} (M)	H (cm)	$I_{d,av}$ (mA/cm^2)	μ (c.p.)	ρ (g/cm^3)	$k_l \times 10^{6*}$ (cm^2/sec)	α_l [22] (cm^3/mol)
1	1.85	0.01	9	0.284	1.261	1.1133	6.15	125
2	1.85	0.02	9	0.683	1.266	1.1149	6.04	125
3	1.85	0.03	9	0.910	1.273	1.1163	6.00	125
4	1.85	0.04	9	1.57	1.277	1.1177	5.96	125
5	1.85	0.05	9	1.96	1.283	1.1191	5.92	125

* see Appendix B

face is regarded as being zero at the cathodic limiting current density,[18,19] and the refractive index of the solution at the cathode surface shown in Fig. 4.25 represents the concentration of H_2SO_4. The concentration difference of H_2SO_4, $\Delta c_{H_2SO_4}$ between cathode surface and bulk-electrolyte was calculated from Fig. 4.25, and they were plotted against $CuSO_4$ concentration in the bulk-electrolyte, respectively. It is demonstrated in Fig. 4.31. As seen in this figure, $\Delta c_{H_2SO_4}$ is lowered with the decrease of $CuSO_4$ concentration. This tendency is predicted from Eq. (2.79). Furthermore, it is seen that the slope of $\Delta c_{H_2SO_4}$-curve decreases when $CuSO_4$ concentration in the bulk-electrolyte is lowered. This phenomenon may be explained as follows. The diffusivity of Cu^{2+} ion is lower in the solution of higher $CuSO_4$ concentrations[23] (see Appendix B). When the $CuSO_4$ concentration in the bulk-electrolyte becomes higher, the thickness of the diffusion layer of Cu^{2+} ion, δ_1, becomes thinner,[18] while the thickness of diffusion layer of H^+ ion, δ_2, is maintained to be virtually unvaried. As the results, the σ value in Eq. (4.23) increases, and the coefficient of $-\gamma\sigma(\omega_1/\omega_2)$ between θ_2 and θ_1 in Eq. (2.79) becomes higher when the $CuSO_4$ concentration is raised.

Brenner[3] measured the concentration of H_2SO_4 at the cathode surface by applying the freezing method during the electrodeposition of copper from a solution containing $CuSO_4$ and H_2SO_4. However, his experimental results cannot directly be compared with the present experimental results because of the different elec-

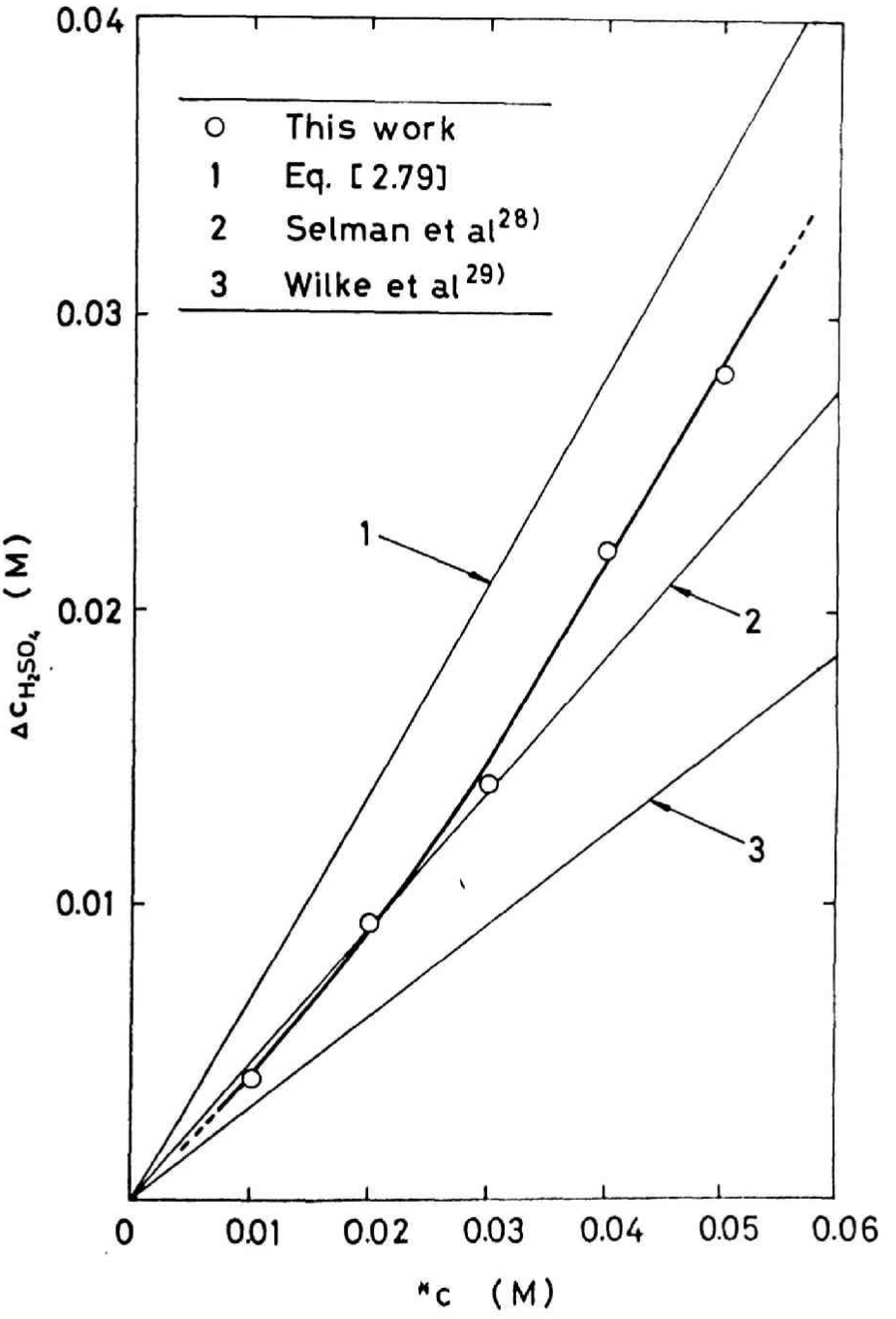

Fig. 4.31 Relationship between concentration difference of H_2SO_4 and concentration of $CuSO_4$ in the bulk-electrolyte, *c

trolytic conditions. The present experimental results were compared with the following theoretical values. First, the concentration difference of H_2SO_4, $\Delta c_{H_2SO_4}$, was calculated from Eq. (2.79) in which Θ_2 was replaced by $(1 + a)\Delta c_{H_2SO_4}$. At the cathodic limiting current density, Θ_1 is equal to the concentration of $CuSO_4$ in the bulk-electrolyte and both parameters ω_1 and ω_2 are assumed to be equal as the first approximation. The σ values of 1.14, 1.15, 1.16, 1.17 and 1.18 were employed in the electrolysis of 0.01, 0.02, 0.03, 0.04 and 0.05M $CuSO_4$ solutions containing 1.85M H_2SO_4, respectively, taking account of the ratios of the diffusivity of Cu^{2+} ion and the term $(i - {}^*t_1)$ in each solution to those of 0.6M $CuSO_4$-1.5M H_2SO_4 solution. Furthermore, the degree of the second stage dissociation of H_2SO_4 was assumed to be 0.31 (see Appendix C).

Selman and Newman,[27] on the other hand, obtained the numerical solution for the differential equation of mass transfer at the limiting current density in the cathodic diffusion layer of a solution containing $CuSO_4$ and an excessive amount of H_2SO_4. They obtained the following expression of $\Delta c_{H_2SO_4}$.

$$\Delta c_{H_2SO_4} = 0.46\,{}^*c_1 \tag{4.29}$$

where ${}^*c_1$ is $CuSO_4$ concentration in the bulk-electrolyte. It was assumed in their calculation that the concentration of $CuSO_4$ is lower and H_2SO_4 is completely dissociated into $2H^+$ and SO_4^{2-} ions.

Wilke et al.[28] also studied the mass transfer of Cu^{2+} ion in the cathodic diffusion layer at the limiting current density, and they derived the following expression for the concentration difference of H_2SO_4.

$$\Delta c_{H_2SO_4} = \Delta c_1 \cdot \left(\frac{D_1}{D_2}\right)^{3/4} \cdot \frac{{}^*t_2}{1 - {}^*t_1} \qquad (4.30)$$

The numerical values of

$$D_1 = 5.92 \text{ to } 6.15 \times 10^{-6} \ (cm^2/sec) \quad \text{(see Appendix B)}$$

and

$$D_2 = 2.1 \times 10^{-5} \ (cm^2/sec)^{29)}$$

were employed, and the values of transference numbers, ${}^*t_1$ and ${}^*t_2$, were calculated from the mobility of each ion at the infinited dilution.[24,25,26]

These calculated values of $\Delta c_{H_2SO_4}$ are also demonstrated in Fig. 4.31. It is seen that the calculated values from Eq. (2.79) are somewhat higher and those of Eq. (4.30) are somewhat lower as compared with the calculated values from Eq. (4.29), respectively. The measured values in the present work are in fairly good agreement with the calculation of Eq. (4.29) in which it was assumed that $CuSO_4$ and H_2SO_4 are completely dissociated into $Cu^{2+} + SO_4^{2-}$ and $2H^+ + SO_4^{2-}$ ions, respectively. However, it is unrealistic to presume that H_2SO_4 is completely dissociated into $2H^+ + SO_4^{2-}$ ions in the solution, and it is thought that the degree of the second stage dissociation of H_2SO_4 should be taken into considera-

tion on the studies of ionic mass transfer in the cathodic diffusion layer.

It may be also said that the difference between the measured values and the calculated ones from Eq. (2.79) may also be ascribed to the uncertainty in the estimation of the property constants such as the diffusivity of Cu^{2+} ion which was replaced by the diffusivity of $CuSO_4$ in the present work.

4.4 Summary

The measurement of the concentration profile of $CuSO_4$ in the cathodic diffusion layer which is accompanied by the upward natural convection is indispensable for studying the rate of mass transfer of cations through this layer. By applying the technique of holographic interferometry, it becomes feasible to measure the concentration profile because of the principle of common path interference employed in this technique. In the derivation of the profile of refractive index from the holographic interferogram, the effects of beam deflection in the cathodic diffusion layer were considered and the profile of refractive index obtained from the interferogram was corrected under the assumption of a linear variation of refractive index within the region of beam deflection in the cathodic diffusion layer.

The concentration profiles in the cathodic diffusion layer of the aqueous 0.05M and 0.1M $CuSO_4$ solutions were measured at various cathodic current densities below the limiting value and at various heights from the lower edge of the cathode.
It was disclosed from the experimental results that the concentration of $CuSO_4$ on the cathode surface is lowered and the thickness of the diffusion layer is decreased when the average current density is raised. It was also revealed that the thickness of the diffusion layer is increased in the upper portion of the vertical plane cathode at a constant cathodic current density.

In order to examine the validity of the theoretical expressions of Δc and δ_1 in the forms of Eq. (2.53) and (2.54), respectively, the dependances of the measured log Δc and log δ_1 on the logarithms of the current density and the height were examined, respectively, and those relationship were confirmed to be valid at the cathodic current densities far lower than the limiting value. At higher current densities, on the other hand, the experimental results start to deviate from the theoretical values. This is supposed to be caused by the unequal local cathodic current densities in the vertical direction. In order to further examine the theoretical relationships which were demonstrated in Eq. (2.59) and (2.60), respectively, the transport parameters which influence the concentration profile and the property constants of the solution were substituted in these equations, and the theoretical values were compared with the experimental results. It was shown that both theoretical and experimental values are in good agreement with each other in the region of the lower current densities.

It is also important to pursue the concentration profiles of $CuSO_4$ and H_2SO_4 in the cathodic diffusion layer for studying the electrodeposition of copper from an unstirred aqueous solution containing $CuSO_4$ and H_2SO_4 which often takes place in the industrial electrolytic refining and electroplating. As the first step toward this goal, the profile of the refractive index of the solution in the cathodic diffusion layer was measured by applying

holographic interferometry at various heights from the lower edge of the cathode and at various cathodic current densities up to the limiting value.

The theoretical expression of the difference of refractive index between the cathode surface and the bulk-electrolyte, Δn, was derived under the assumption of a uniform distribution of local current densities on the cathode surface. In order to verify this theoretical relationship, the dependances of the measured log Δn on the logarithms of current density and height from the lower edge of cathode were examined, respectively. At the cathodic current densities lower than the half-value of the limiting value, these relationships were satisfied. It was also disclosed that Δn is virtually unchanged in the vertical direction at the cathodic limiting current density. Furthermore, a generalized expression of Δn was derived in the form of Eq. (4.28), and after the distribution of the local cathodic current densities was obtained from the numerical analysis, the theoretical values of Δn were calculated. Both experimental and theoretical Δn values were in fairly good coincidence over the whole region of the cathodic current densities up to the limiting value, though the measured values were somewhat higher than the theoretical ones.

When the electrolysis takes place at the cathodic limiting current density, the concentration of $CuSO_4$ at the cathode surface is regard as being virtually zero. Under this experimental

condition, Δn was measured at a height of 4 cm from the lower edge of cathode in the aqueous solutions containing 1.85M H_2SO_4 and 0.01, 0.02, 0.03, 0.04 and 0.05M $CuSO_4$, respectively. From the above presumption that ${}^{o}c_1 = 0$ at the limiting current density, the concentration difference of H_2SO_4, $\Delta c_{H_2SO_4}$, was obtained from Δn. The $\Delta c_{H_2SO_4}$ value at the cathodic limiting current density decreases when $CuSO_4$ concentration in the bulk-electrolyte, ${}^{*}c_1$, is lowered. Furthermore, the slope of the curve of $\Delta c_{H_2SO_4}$, versus *c decreases as $CuSO_4$ concentration in the bulk-electrolyte is lowered. These experimental results were qualitatively explained by Eq. (2.79) and (4.23). The measured $\Delta c_{H_2SO_4}$ values were further compared with theoretical values. It was disclosed that the measured $\Delta c_{H_2SO_4}$ values are somewhat lower than the calculated values from Eq. (2.79) in which the incomplete dissociation of H_2SO_4 was presumed. The difference between the measured and calculated values may be ascribed to the uncertainty in the estimation of property constants used in the calculation such as the diffusivity of Cu^{2+} ion.

Reference to Chapter 4

1) V. G. Levich: "Physicochemical Hydrodynamics", Translated by Scripta Technica, Inc., p. 40, Prentice-Hall, Inc., Englewood Cliffs, N. J. (1962).

2) H. J. Read and A. K. Graham: Trans. Electrochem. Soc., 78 (1940) 279; 80 (1941) 329.

3) A. Brenner: Proc. Am. Electroplater's Soc., (1940) 95; (1941) 28.

4) T. Yannakopoulos and A. Brenner: J. Electrochem. Soc., 105 (1958) 521.

5) N. Ibl, B. Barrada and G. Trümpler: Helv. Chim. Acta, 37 (1954) 583.

6) N. Ibl and R. H. Müller: Z. Elektrochem., 59 (1955) 671.

7) A. Tvarusko and L. S. Watkins: Electrochim. Acta, 14 (1969) 1109.

8) A. Tvarusko and L. S. Watkins: J. Electrochem. Soc., 118 (1971) 248.

9) C. Knox, R. R. Sayano, E. T. Seo and H. P. Silverman: J. Phys. Chem., 71 (1967) 3102.

10) L. O. Heflinger, R. F. Werker and R. E. Brooks: J. Appl. Phys., 37 (1966) 642.

11) E. Yeager and A. J. Salkind: "Techniques of Electrochemistry", vol. 2, p. 144, John Wiley and Sons, Inc., New York (1973).

12) R. H. Müller: "Advances in Electrochemistry and Electrochemical

Engineering", vol. 9, p. 281, John Wiley and Sons, Inc., New York (1973).

13) K. W. Beach, R. H. Müller and C. W. Tobias: J. Opt. Soc. Am., 63 (1973) 559.

14) T. Mizushina, R. Ito, F. Ogino and H. Kojima: "Proceeding of the Symposium of Chemical Engineering", The Society of Chemical Engineering, Japan, p. 47, Osaka (1966).

15) B. Rossi: "Optics", p. 55, Addison-Wesley Publishing Co., London (1967).

16) N. Ibl and R. H. Müller: J. Electrochem. Soc., 105 (1958) 346.

17) G. H. Keulegan: J. Res. Nat. Bur. Stand., 47 (1951) 2240.

18) C. Wagner: J. Electrochem. Soc., 95 (1949) 161.

19) G. W. Tobias, M. Eisenberg and C. R. Wilke: J. Electrochem. Soc., 99 (1952) 359C.

20) C. R. Wilke, M. Eisenberg and C. W. Tobias: J. Electrochem. Soc., 100 (1953) 513.

21) N. Ibl, W. Rüegg and G. Trümpler: Helv. Chim. Acta, 36 (1953) 1624.

22) K. Asada, F. Hine, S. Yoshizawa and S. Okada: J. Electrochem. Soc., 107 (1960) 242.

23) W. G. Eversole, H. M. Kindsvater and J. D. Perterson: J. Phys. Chem., 46 (1942) 370.

24) R. C. Weast, "Handbook of Chemistry and Physics", 45th ed., p. D-80, The Chemical Rubber Co., Cleaveland (1964).

25) E. A. Moelwyn-Hughes, "Physical Chemistry", p. 859, Pergamon

Press, London (1961).

26) "Handbook of Electrochemistry", edited by The Electrochemical Soc. of Japan, p. 118, Maruzen Book Co., Tokyo (1964).

27) J. R. Selman and J. Newman: UCRL-20322 (1971).

28) C. R. Wilke, M. Eisenberg and C. W. Tobias: Chem. Eng. Progr., 49 (1953) 663.

29) E. A. Hollingshead and A. R. Gordon, J. Chem. Phys., 8 (1940) 423.

CHAPTER 5 MEASUREMENT OF LOCAL CATHODIC CURRENT DENSITIES ON VERTICAL PLANE CATHODE

5.1 Introduction

It is well known that not only the quality of electrodeposited metals but also the productivity in the industrial electrolytic refining and plating depend on the distribution of current densities on the cathode surface: it is very important and indispensable problem in the electrochemical industries to obtain uniform electrodeposited metals.

It is also known that the overall rate of the cathode reaction is affected by the process of ionic mass transfer in the cathodic boundary layer as mentioned in Chapter 1.[1,2,3] When copper is electrodeposited on a vertical plane cathode from an unstirred or gently stirred aqueous solution, an upward natural convective flow occurs along the cathode surface. It is caused by the lowered Cu^{2+} ion concentration in the cathodic diffusion layer.[4,5] Since the thickness of this hydrodynamic boundary layer and the diffusion layer of Cu^{2+} ion increase downstream along the vertical distance from the lower edge of cathode as men-

tioned in the previous chapters, the rate of mass transfer of Cu^{2+} ion in the cathodic diffusion layer is reduced in the upper portion of the cathode, and the distribution of the local current densities is formed in vertical direction. This effect of ionic mass transfer in the cathodic diffusion layer becomes more evident when the average cathodic current density is raised.

In order to examine the effect of ionic mass transfer in the cathodic diffusion layer on the cathodic current distribution in vertical direction, the velocity profile of natural convective flow near the vertical plane cathode and the concentration profile of ionic species in the cathodic diffusion layer were measured in Chapters 3 and 4 by applying the optical techniques under various experimental conditions, respectively: the dependances of the velocity profile of natural convective flow on the cathodic current density and on the height from the lower edge of cathode were examined in Chapter 3. The effects of the concentrations of $CuSO_4$ and H_2SO_4 as a supporting electrolyte on the velocity profile of natural convection were also discussed. Furthermore, the parameters ω, λ and η with which the measured velocity profiles are precisely described were determined.

The concentration profiles of ionic species in the cathodic diffusion layer were studied in Chapter 4. The effects of the average cathodic current density and the height from the lower edge of cathode on the concentration profiles in the cathodic diffusion layer were examined, and the accumulation of H_2SO_4 in the

cathodic diffusion layer was discussed during the electrolysis of aqueous solutions containing $CuSO_4$ and H_2SO_4 at the cathodic limiting current density.

The distribution of the local cathodic current densities in vertical direction which is more or less affected by the ionic mass transfer in the cathodic diffusion layer is studied in this chapter, and the experimental results are discussed on the bases of the velocity and concentration profiles in the cathodic boundary layer mentioned in Chapters 3 and 4, respectively.

It is known at the cathodic limiting current density that the concentration of Cu^{2+} ion is virtually zero on the cathode surface. Many theoretical and experimental works have been made in the past on the current distribution on the cathode surface under this experimental condition.[2,6,7,8] However, the majority of the industrial copper electrolysis is conducted at the cathodic current densities lower than the limiting value where the contributions of both the ionic mass transfer in the cathodic diffusion layer and the cathode reaction can not be ignored. Asada et al.[9] calculated the theoretical distribution of the local cathodic current densities on a vertical plane cathode in the region of the average cathodic current densities lower than the limiting value. They also measured the local cathodic current densities by weighing the horizontally sliced electrodeposited copper from an aqueous 0.1M $CuSO_4$-1.5M H_2SO_4 solution. However, the precision of their measurement is thought to be insufficient for the purpose of pre-

cisely comparing the experimental data with the calculation. In addition to this methode of measuring the local current densities, the measurement of the average cathodic limiting current densities on the vertical plane cathodes of different heights was also reported.[2,8)]

However, no attempts had been made to directly measure the local cathodic current densities before the recent proposal made by Lloyd et al.,[10)] in which a technique of measuring the local current densities at the cathodic limiting current was mentioned: they prepared a special plane cathode in which several miniature electrodes are imbedded in vertical direction and measured the cathodic local current densities by using these probes.

It is attempted in the present chapter to apply this experimental technique to measure the distribution of local current densities on a vertical plane copper cathode in the region below the cathodic limiting current density. It is also intended to compare the experimental data of the distribution of local cathodic current densities with the theoretical values.

5.2 Experimental Procedure

Four types of host bar of different dimensions were prepared from a deoxidized copper plate. As shown in Fig. 5.1, they were pierced with small holes of 0.33 cm in diameter. From the copper plate of the same quality, copper cylinders of 0.31 cm in diameter and 1 cm long were machined, and they were imbedded in the holes of the host bar after coating them with epoxy resin as the insulator: it is schematically illustrated in Fig. 5.2. The base planes of the miniature probe were filmed with camera, and the surface area was exactly measured on the photograph magnified 20 times. It was also found from this photograph that the thickness of the epoxy resin layer between host bar and miniature probe is 0.01 cm.

The back and side surfaces of the host bar were insulated with PVC resin, and the back surface and the joint of the miniature probe with the lead wire were imbedded in the epoxy resin. Each insulated host bar was installed one after another in a cathode holder made of acryl resin as shown in Fig. 5.3 so as to obtain a flat cathode surface of effective width of 5 cm. The local cathodic current densities were measured with the miniature probes located on the cathode surface at a space of 1 cm in vertical direction. The cathode holder loaded with host bars and a vertical plane anode, 21 cm high, 5.5 cm wide and 0.5 cm thick were installed in another acryl resin frame. The back and

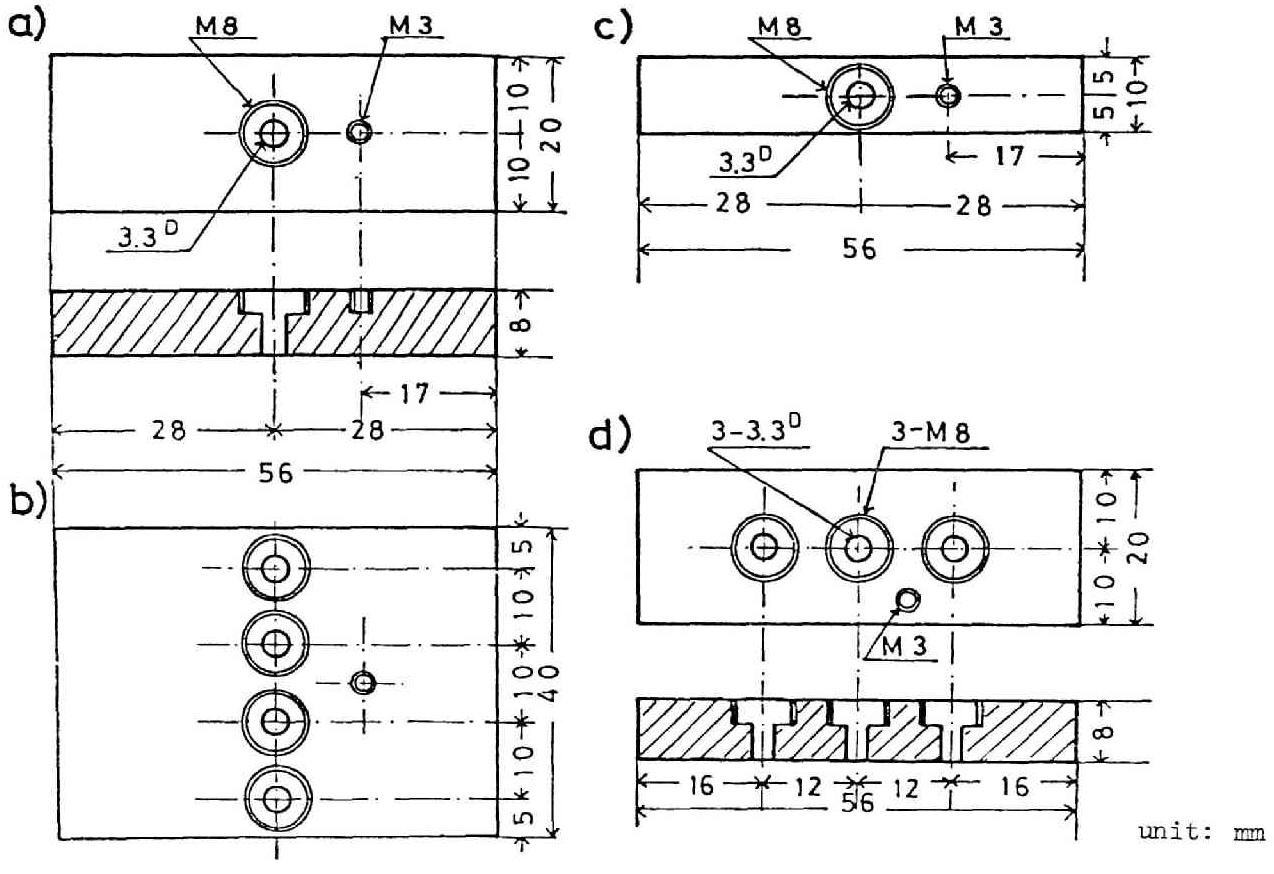

Fig. 5.1 Four types of host bar

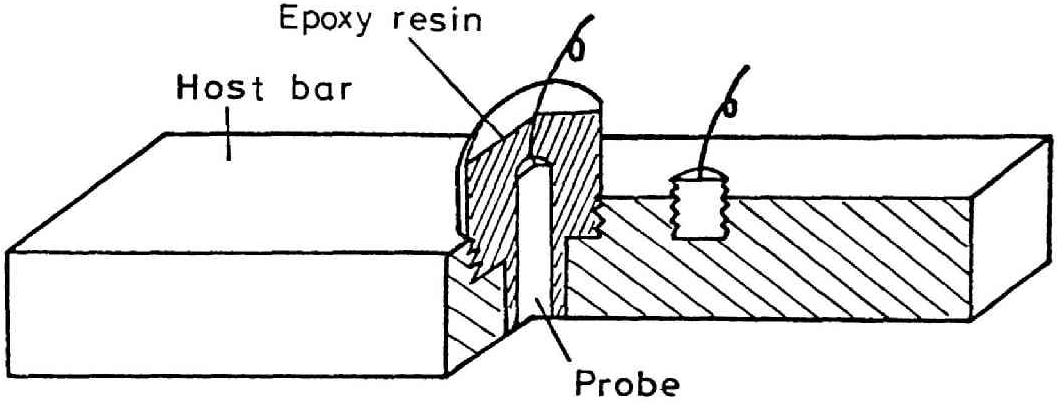

Fig. 5.2 Installation of miniature probe

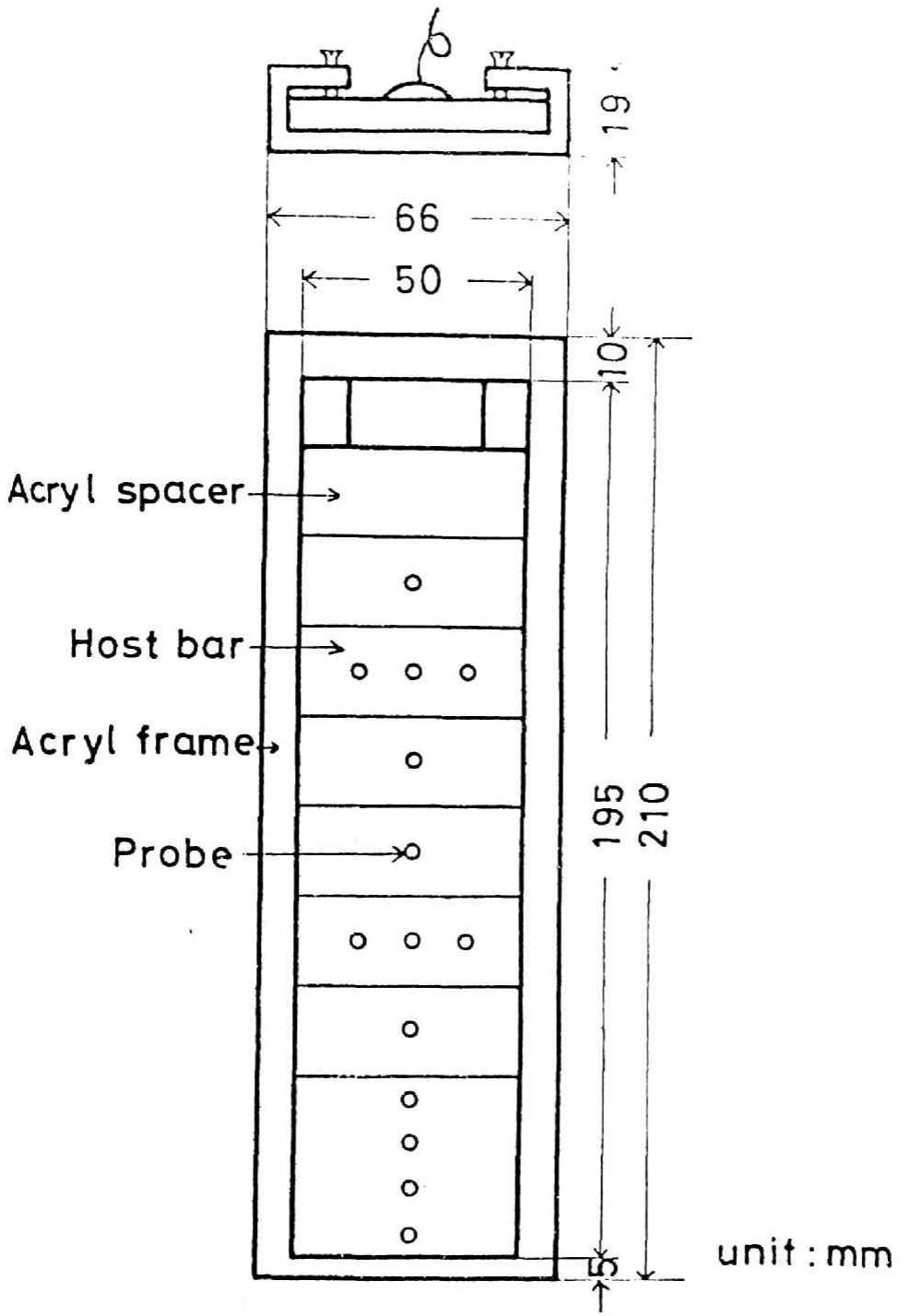

Fig. 5.3 Arrangement of cathode plate

side surfaces of the anode were also insulated with PVC resin. As the reference electrode for measuring the cathode potential, an enamelled copper wire of 0.18 cm in diameter was used: one end of this wire, about 1.5 cm long, was vertically bent toward the direction of the cathode surface, and the wire was fixed on a rack and pinion mechanism.

In a rectangular glass electrolytic cell of about 8.5 liter capacity maintained at 25°C in a thermostat, the acryl resin frame provided with electrodes and the reference electrode was placed, and the electrolysis was started. Analytical reagent grade $CuSO_4 \cdot 5H_2O$ and H_2SO_4 were used, and the aqueous $CuSO_4$-H_2SO_4 solutions were made up. Their compositions are summarized in Table 5.1.

The electric curcuit in the experimental arrangement is schematically illustrated in Fig. 5.4. By using a potentionstat, the cathode potential was maintained at a constant value during each experimental run. The electrolytic current was recorded on an electronic recorder. For the measurement of local cathodic current densities with the miniature probe, the probe was connected to a manganin wire resistor of known resistance, and the potential drop between both ends of the resistor was measured with a digital potentiometer. It is demonstrated in Fig. 5.4 that the local current density at the miniature probe P_3 is being measured. By using the change-over switch, S, it was possible to measure the local current density at 25 different positions on a

Table 5.1 Composition of electrolyte and the average cathodic limiting current density

No.	c_{CuSO_4} (M)	$c_{H_2SO_4}$ (M)	$\bar{i}_{d,av}$ (mA/cm^2)
1	0.1	1.85	4.1
2	0.1	1.00	5.2
3	0.1	0.10	6.9
4	0.1	0.01	8.7
5	0.1	0.00	9.8

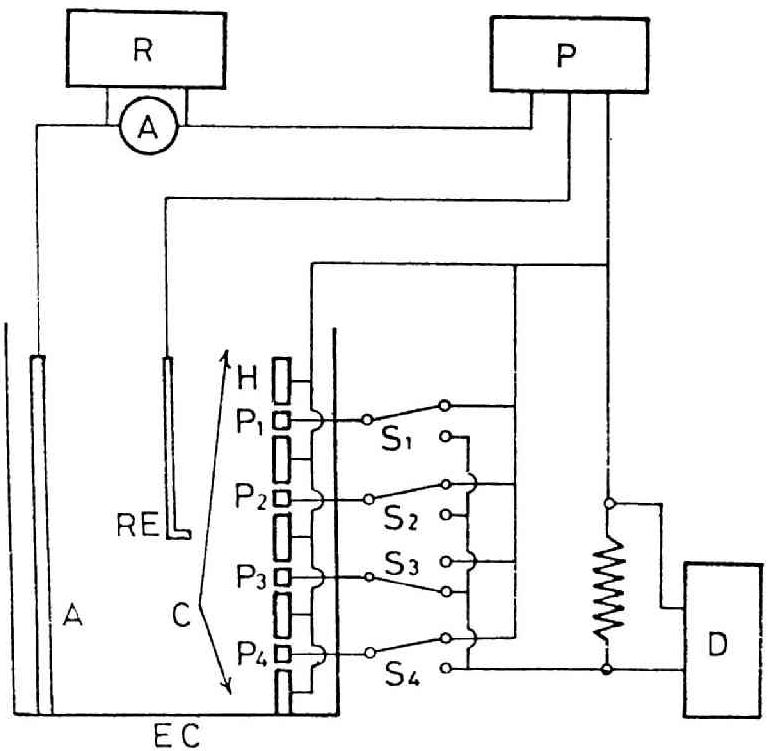

EC : Electrolytic cell
A : Anode
C : Cathode
Pi : Probe electrode
H : Host bar
RE : Reference electrode
P : Potentiostat
D : Digital voltmeter
R : Recorder
Si : Switch

Fig. 5.4 Schematic illustration of experimental arrangement

cathode plate one after another.

After the electrodes were placed in the electrolytic cell maintained at 25°C, they were left for about 30 min in order to minimize the turbulent flow in the bulk-electrolyte. After the electrolysis was started, it took 10 to 20 min to attain the steady electrolytic current. Then the measurement of local cathodic current densities was conducted within about 1 min by operating the change-over switch. It was observed that each local current density is unvaried during the period of the measurement.

Before the measurement of the local current densities, the current-potential curve of the solutions mentioned in Table 5.1 was measured. An example of the current-potential curve obtained with 0.1M $CuSO_4$-1.0M H_2SO_4 solution is illustrated in Fig. 5.5. As seen in this figure, the average cathodic current density gradually rises with the applied potential even after it reaches to the lower edge of the so-called "cathode plateau". This is probably because of the growth of rough electrodeposit on the cathode surface from the solution which contains no organic additives. Since it was difficult to exactly determine the average cathodic limiting current density from this current-potential diagram, the current density at the intersecting point of the two straight lines below and at the cathode plateau was obtained as the substitute of the cathodic limiting current density. They are also summarized in Table 5.1.

Prior to the measurement of the distribution of cathodic cur-

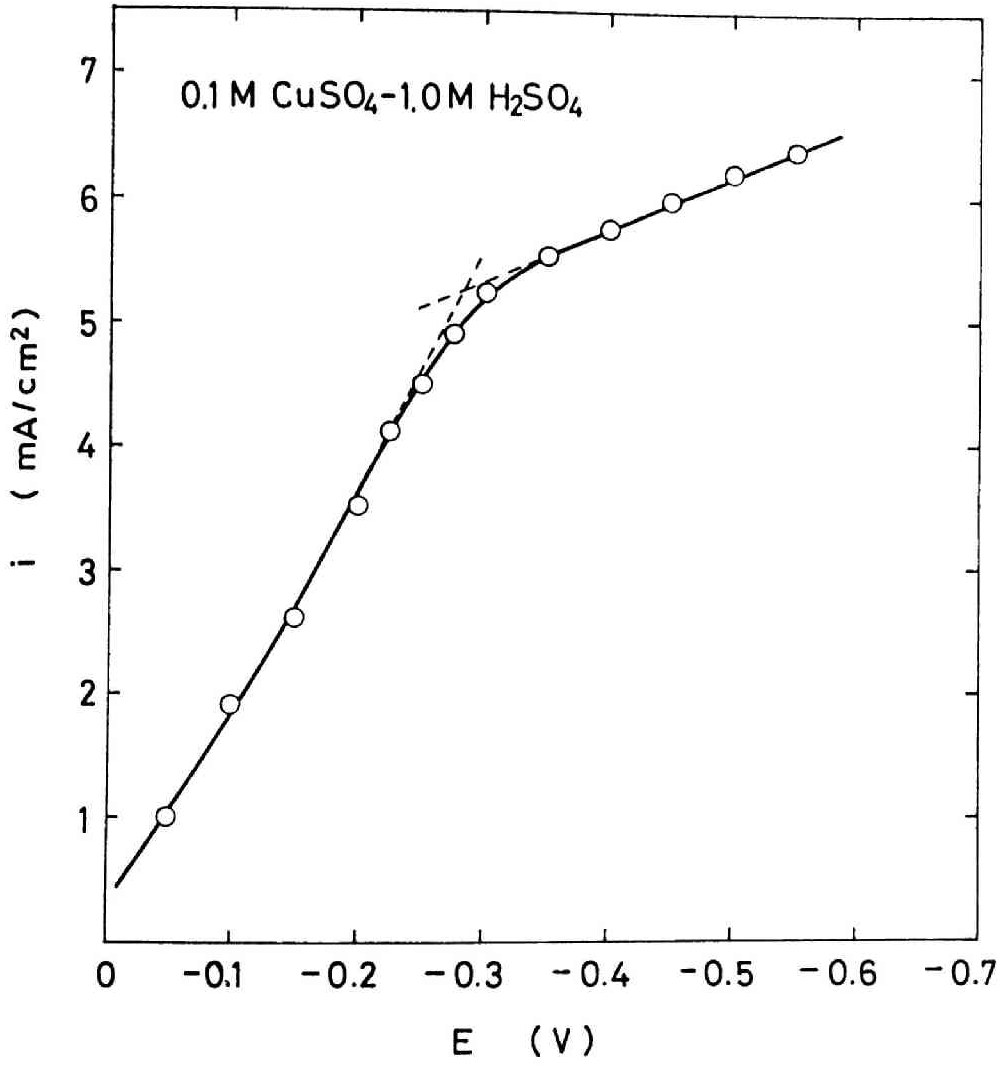

Fig. 5.5 Current potential curve with 0.1M $CuSO_4$-1.0M H_2SO_4 solution

rent densities in vertical direction on the cathode surface, the following preliminary tests were made. One possible problem in the measurement of local current densities by using the miniature probes is an unevenness of the potential between the host bar and the miniature probe which is connected to the additional manganin wire resistor: the cathodic potential of the miniature probe may become slightly higher than the host bar, and this may affect the overall rate of the cathode reaction. To examine this possible effect, the current density on the miniature probe was measured by using the manganin wire resistors of different resistances. The measurement was carried out at several average cathodic current densities at various heights from the lower edge of cathode. A solution of 0.1M $CuSO_4$-1.0M H_2SO_4 was used. The experimental results are demonstrated in Fig. 5.6. It is seen in this figure that the current density on the miniature probe was slightly elevated when the manganin wire resistors of lower resistance were used, and no significant variation was observed in the current densities of the miniature probe when the manganin wire resistors of less than 10 ohm were used. Based on this experimental result, one of the manganin wire resistors of 3.38, 5.03 and 10.04 ohm was chosen and used in the measurement of the local cathodic current densities according to the experimental conditions.

It was observed during the electrolysis of 0.6M $CuSO_4$-1.5M H_2SO_4 solution with a horizontal plane cathode facing downward that the average cathodic current densities of the host bar and

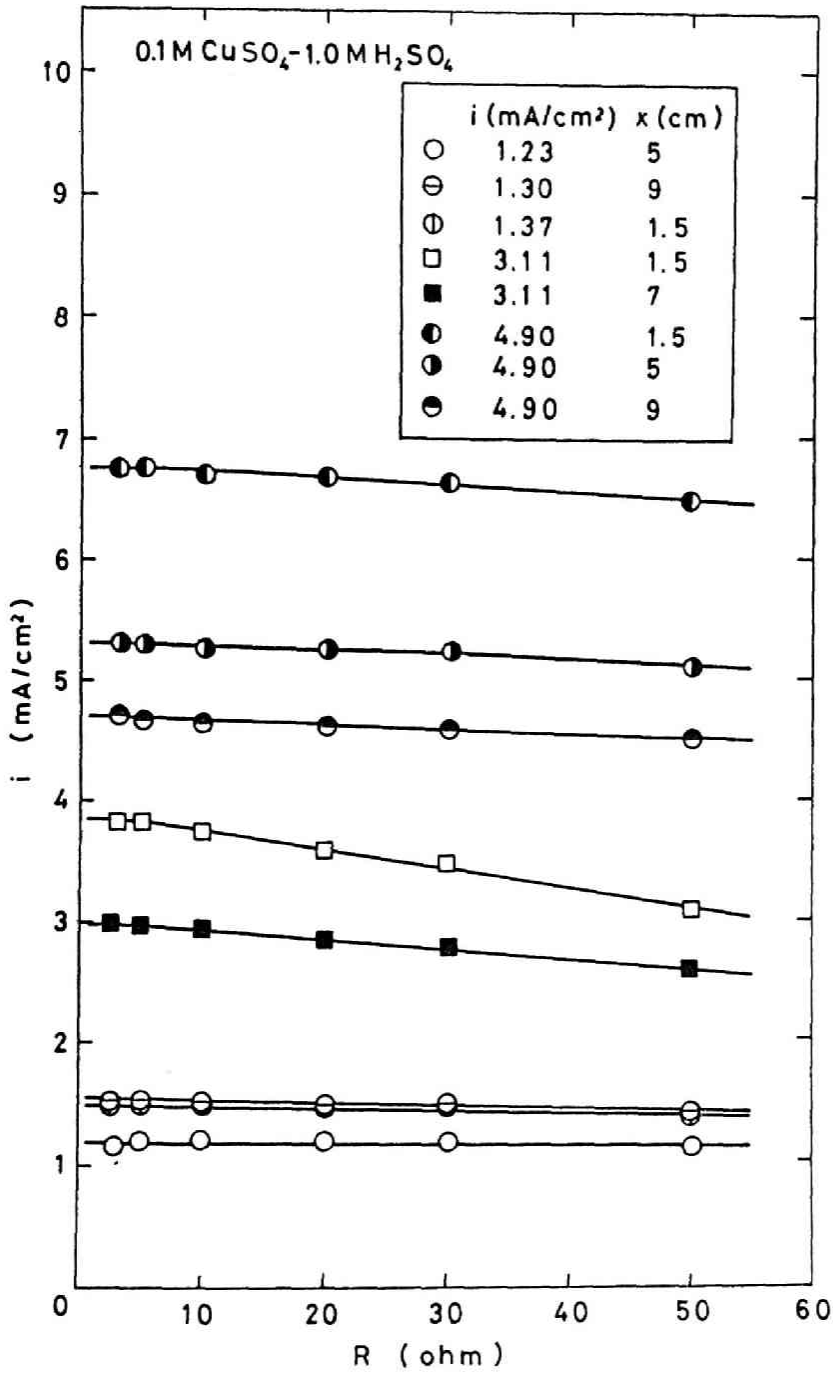

Fig. 5.6 Relationship between current density on probe surface and resistance of probe circuit

the miniature probe were in good accordance with each other; the natural convective flow along the cathode surface does not occur with this arrangement of the cathode surface. Furthermore, a similar experiment was carried out with a vertical plane cathode along which the upward natural convection occurs, and it was identified that both average cathodic current densities measured with the host bar and with the miniature probe are in good agreement. The vertical distribution of the cathodic current densities was measured by changing the distance between both electrodes at 5, 10 and 15 cm, respectively. No significant difference was observed, and the distance between both electrodes was maintained at 15 cm in following experiments.

It was also supposed that the lines of electric force are expanded when the vertical distance between the upper edge of the cathode and the surface of the aqueous solution is larger. The vertical distribution of cathodic current densities on the surface of a plane cathode of 8 cm height was measured in a solution of 0.1M $CuSO_4$-1.0M H_2SO_4. The distance between the upper edge of the cathode and the surface of the aqueous solution was maintained at 2 and 0.5 cm, respectively. The results are summarized in Fig. 5.7. As seen in this figure, the effect of the expanded lines of electric force in the upper portion of the solution is evident and this effect can virtually be eliminated when the vertical distance between the upper edge of cathode and the surface of solution is maintained at 0.5 cm or less.

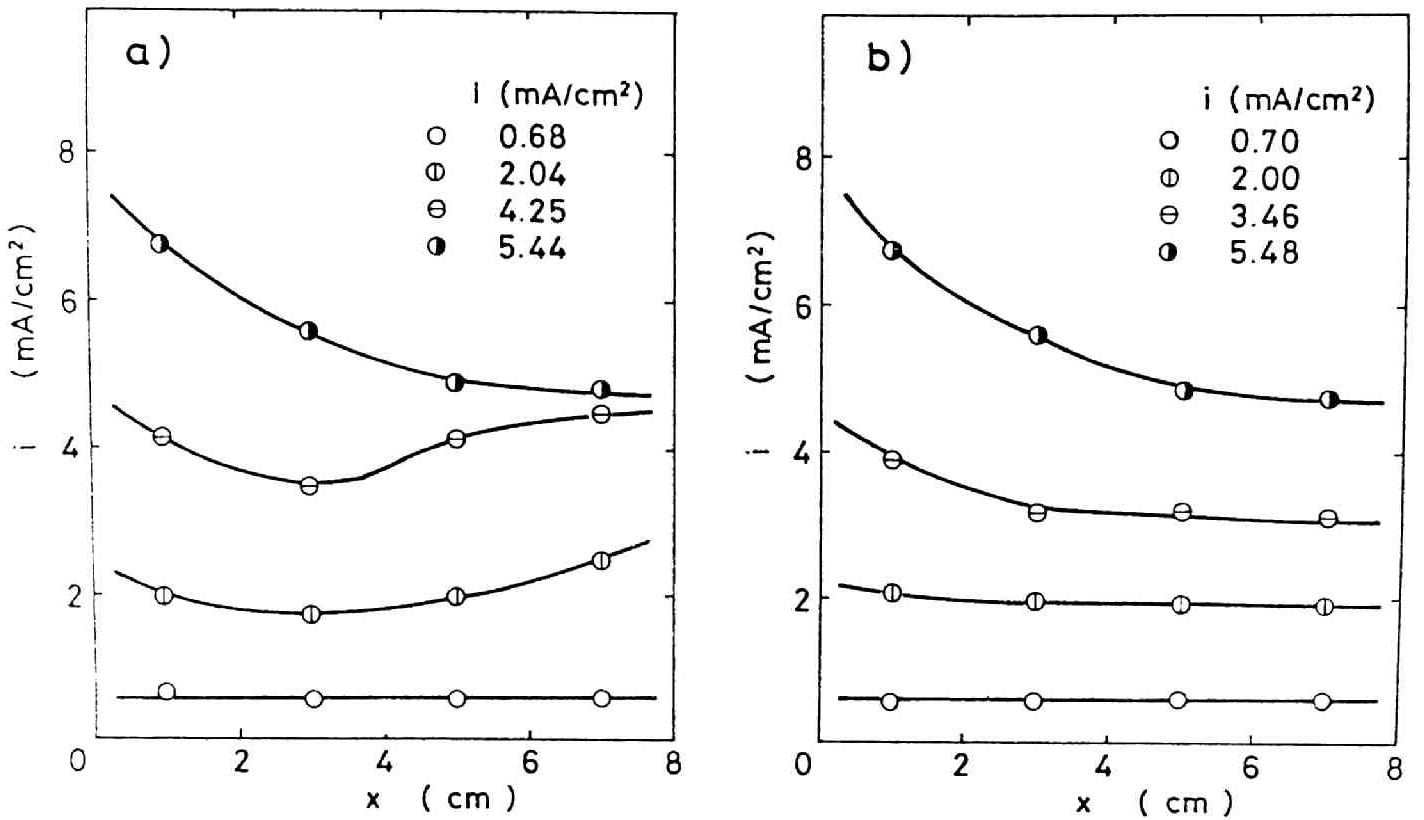

Fig. 5.7 Distribution of cathodic current density. The distance between the upper edge of cathode and the surface of solution was mentioned at (a) 2 cm and (b) 0.5 cm, respectively

The horizontal distribution of the cathodic current densities on a vertical plane cathode was also measured. When a host bar shown in Fig. 5.1(d) is used, the horizontal distance in which the local cathodic current densities are measured is 2.73 cm. It was clarified from the measurement that the local current densities within this horizontal distance are uniform. Furthermore, the possible effect of the side wall of acryl resin frame on the local cathodic current densities was examined: the effective width of the cathode was reduced to 3 cm by inserting the additional acryl plates of 1 cm thickness on both sides of the cathode plate. When a host bar of Fig. 5.1(d) is used, the distance between the edge of this acryl plate and the miniature probe is 0.135 cm. From the measurement of the horizontal distribution of the cathodic current densities with this experimental arrangement, it was revealed that the local cathodic current densities are uniform in horizontal direction when the horizontal distance between the miniature probe and the side wall is larger than 0.135 cm.

5.3 Experimental Results

After the above-mentioned preliminary tests were made with the miniature probes, the vertical distribution of cathodic current densities on a vertical plane copper cathode of 16 cm height was measured. The aqueous solutions mentioned in Table 5.1 were used. Measurement was conducted in the region of the average cathodic current densities up to the limiting value shown in the same table. The experimental results are illustrated in Fig. 5.8 through 5.12, respectively. It is seen in these figures that the local cathodic current densities are uniform in the region of the current density far lower than the limiting value. When the average cathodic current density becomes higher than a half of the limiting value, the local cathodic current densities in the lower portion of the cathode preferentially increase, and they become unequal in the vertical direction.

It was also observed in the electrolysis of the aqueous solutions whose H_2SO_4 concentration is lower than 0.1M that the local cathodic current densities in the upper portion of the cathode start to irregularly oscillate during the electrolysis at the average cathodic current densities near the limiting value. The range of variation is indicated with arrow in the diagrams. The electrodeposited copper in this upper portion of the cathode is very rough and is faded to reddish color which is different from the other portion of the cathode.

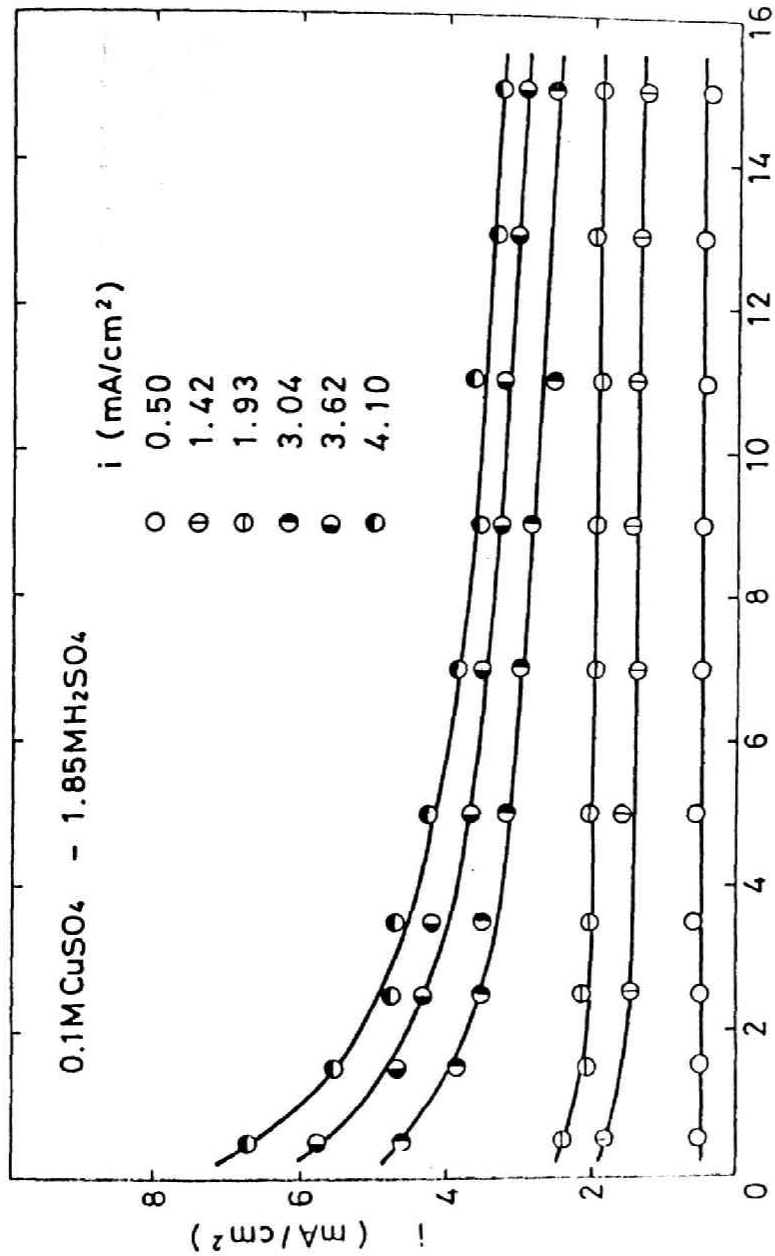

Fig. 5.8 Distribution of cathodic current density in the electrolysis of 0.1M $CuSO_4$-1.85M H_2SO_4 solution

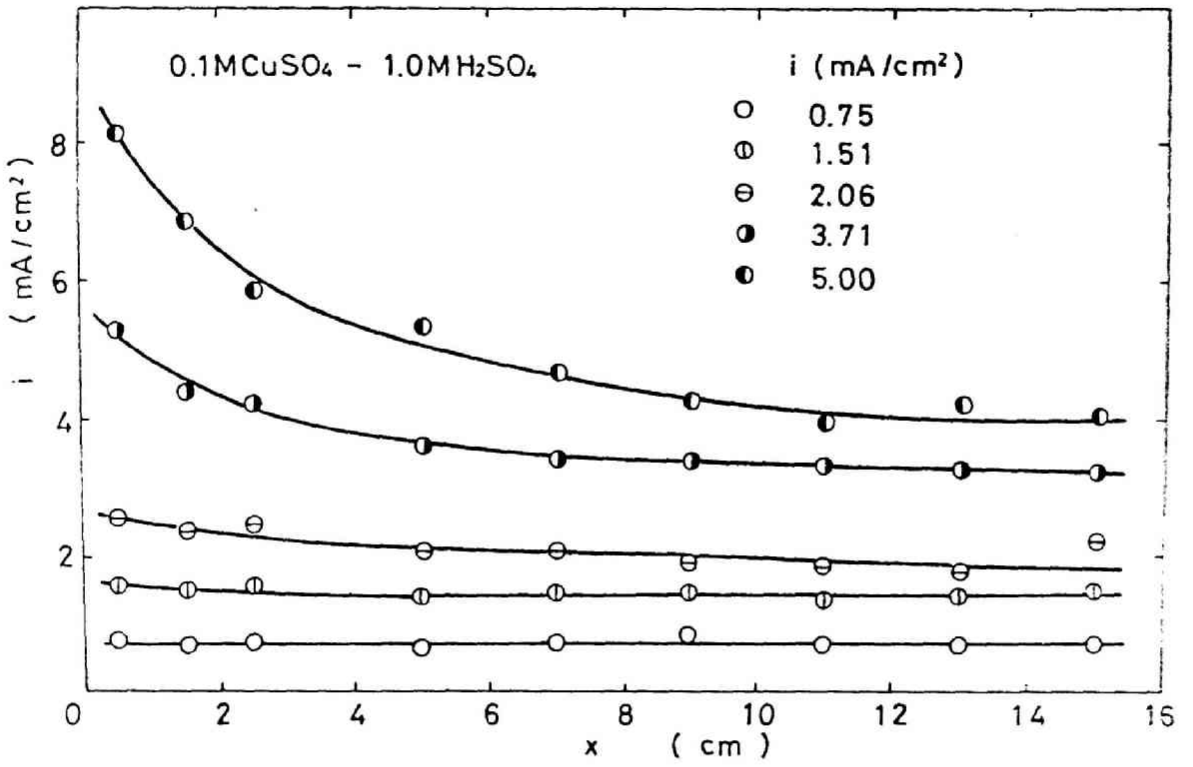

Fig. 5.9 Distribution of cathodic current density in the electrolysis of 0.1M $CuSO_4$-1.0M H_2SO_4 solution

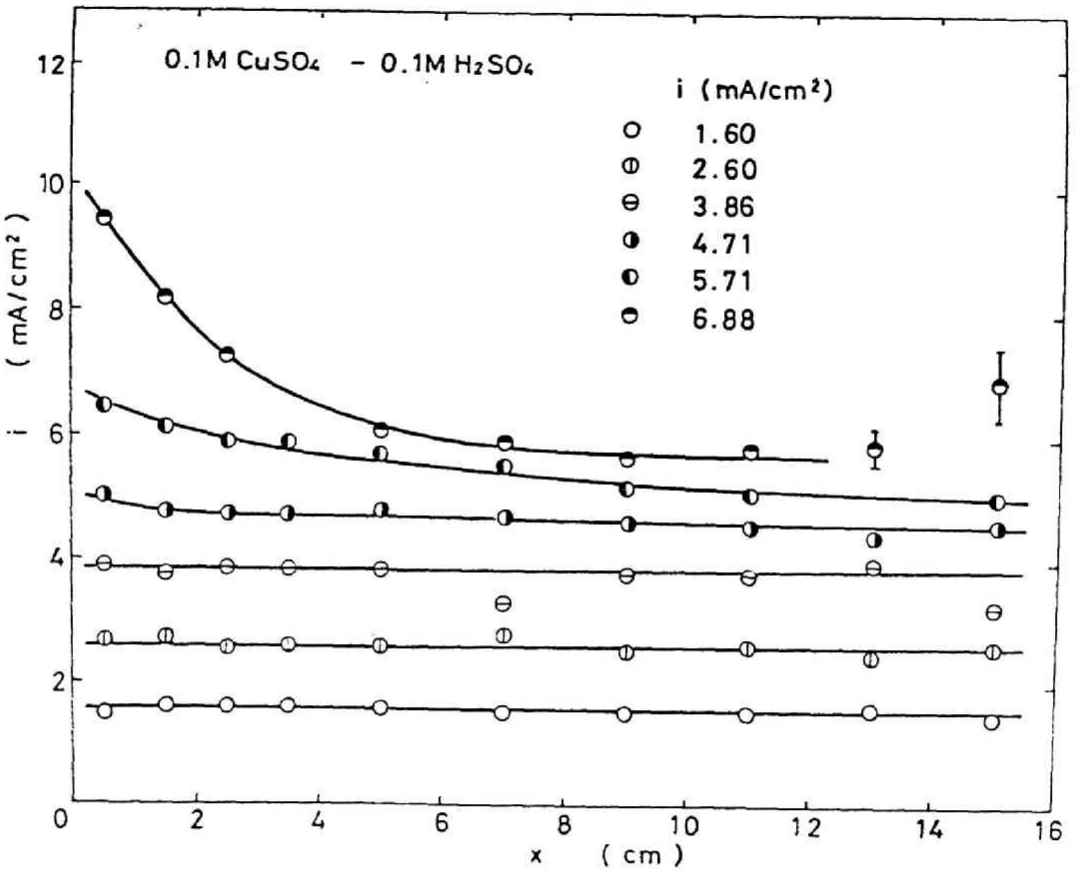

Fig. 5.10 Distribution of cathodic current density in the electrolysis of 0.1M $CuSO_4$-0.1M H_2SO_4 solution

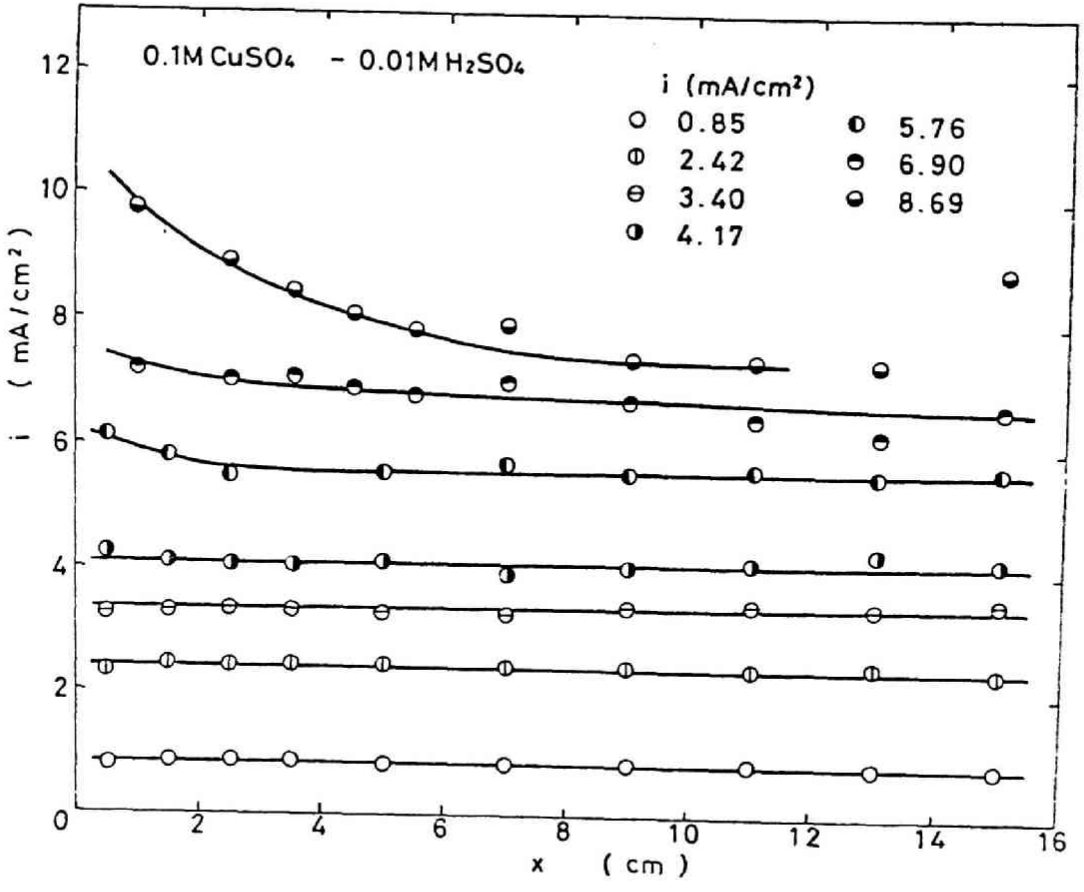

Fig. 5.11 Distribution of cathodic current density in the electrolysis of 0.1M $CuSO_4$-0.01M H_2SO_4 solution

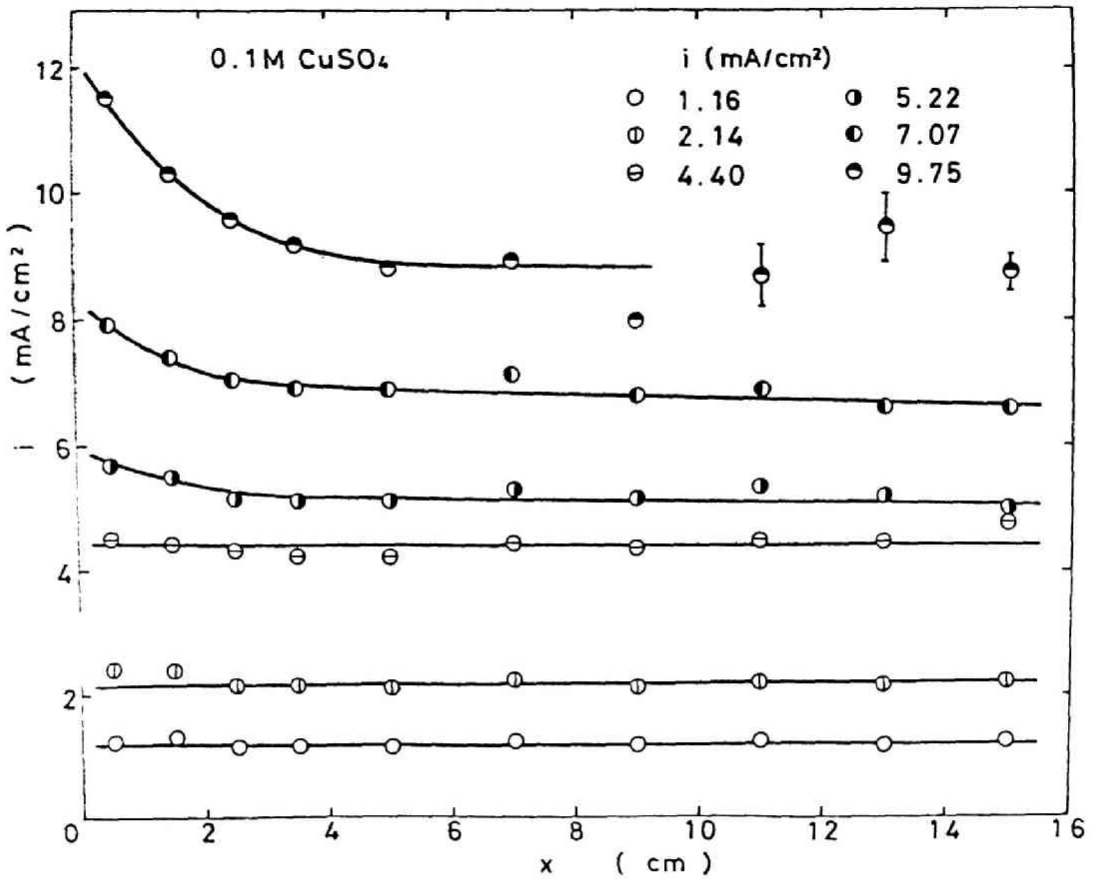

Fig. 5.12 Distribution of cathodic current density in the electrolysis of aqueous 0.1M $CuSO_4$ solution

5.4 Discussion

In order to further study the distribution of the local cathodic current densities in the vertical direction on a vertical plane cathode installed in the unstirred aqueous solution, the logarithm of the local current density was plotted against the logarithm of the height from the lower edge of cathode, and they are illustrated in Fig. 5.13 through 5.17. It is seen in Fig. 5.13 and 5.14 that the variation of the plots is more conspicuous at the lower average cathodic current densities. This is caused by the amplified measuring error of the lower local current densities on the logarithmic scale.

It is also noted from Fig. 5.13 and 5.14 which were obtained with the aqueous solutions containing $CuSO_4$ and H_2SO_4 whose concentration is higher that the slope of straight lines becomes gradually steeper with the rise of the average cathodic current density and it approaches to -1/4 in the vicinity of the cathodic limiting current density: it is in excellent coincidence with the theoretical calculation[2,6] mentioned in Chapter 2 concerning the distribution of the local cathodic limiting current densities in vertical direction.

It is seen, on the contrary, from Fig. 5.15 through 5.17 which were obtained from the measurement with the aqueous solutions of lower H_2SO_4 concentrations that the distribution of the local cathodic current densities is uniform in the region below

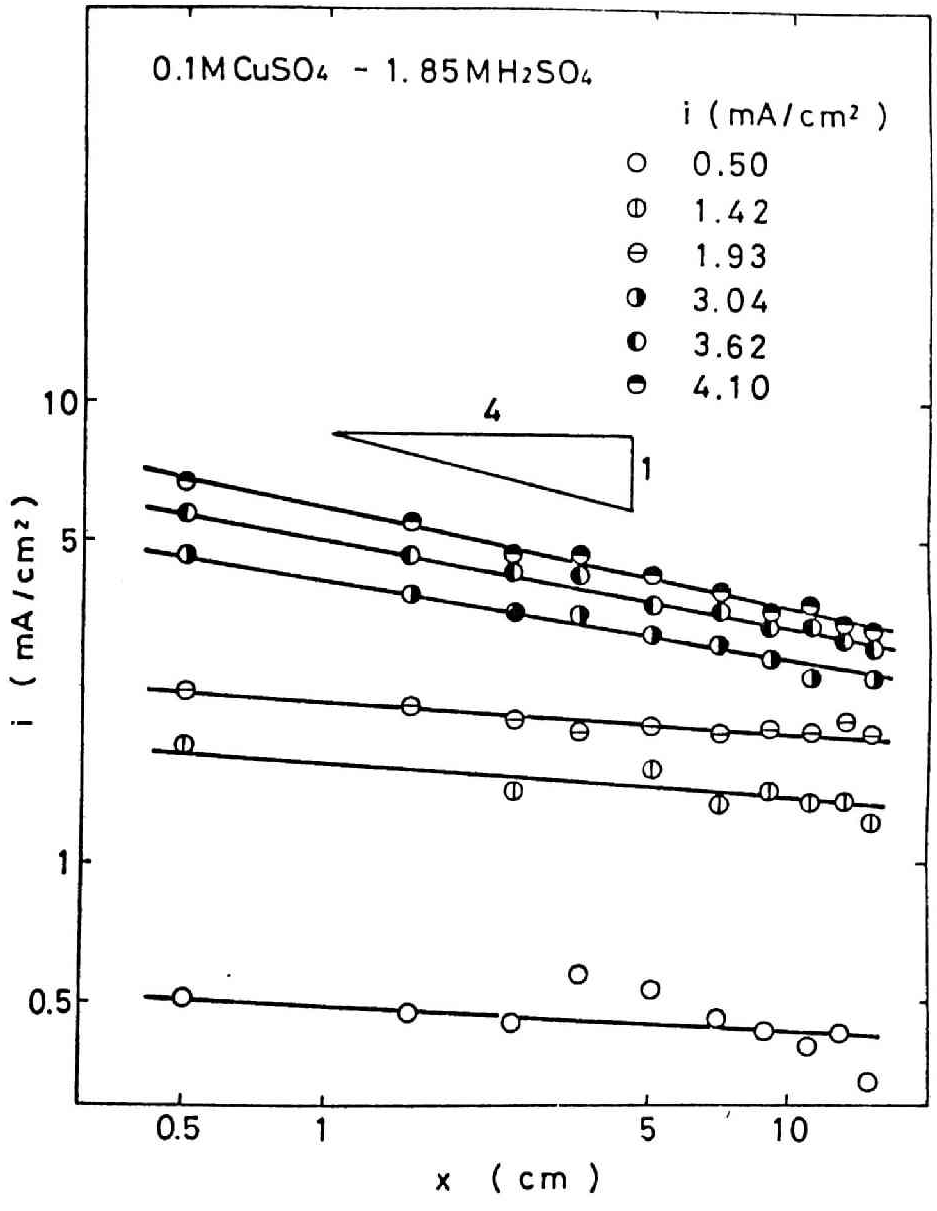

Fig. 5.13 Relationship between cathodic current density and height from lower edge of cathode ($0.1M\ CuSO_4$-$1.85M\ H_2SO_4$ solution)

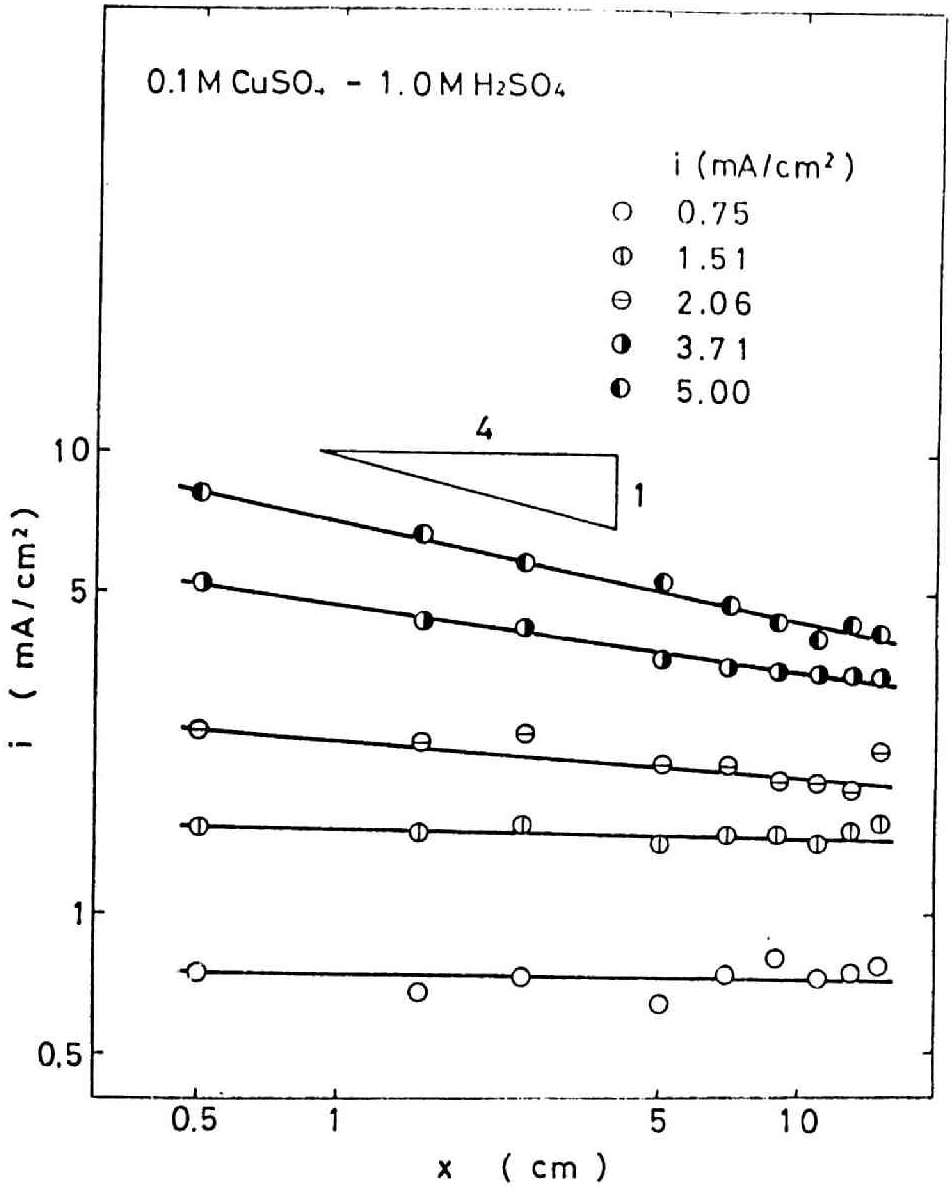

Fig. 5.14 Relationship between cathodic current density and height from lower edge of cathode ($0.1M\ CuSO_4$-$1.0M\ H_2SO_4$ solution)

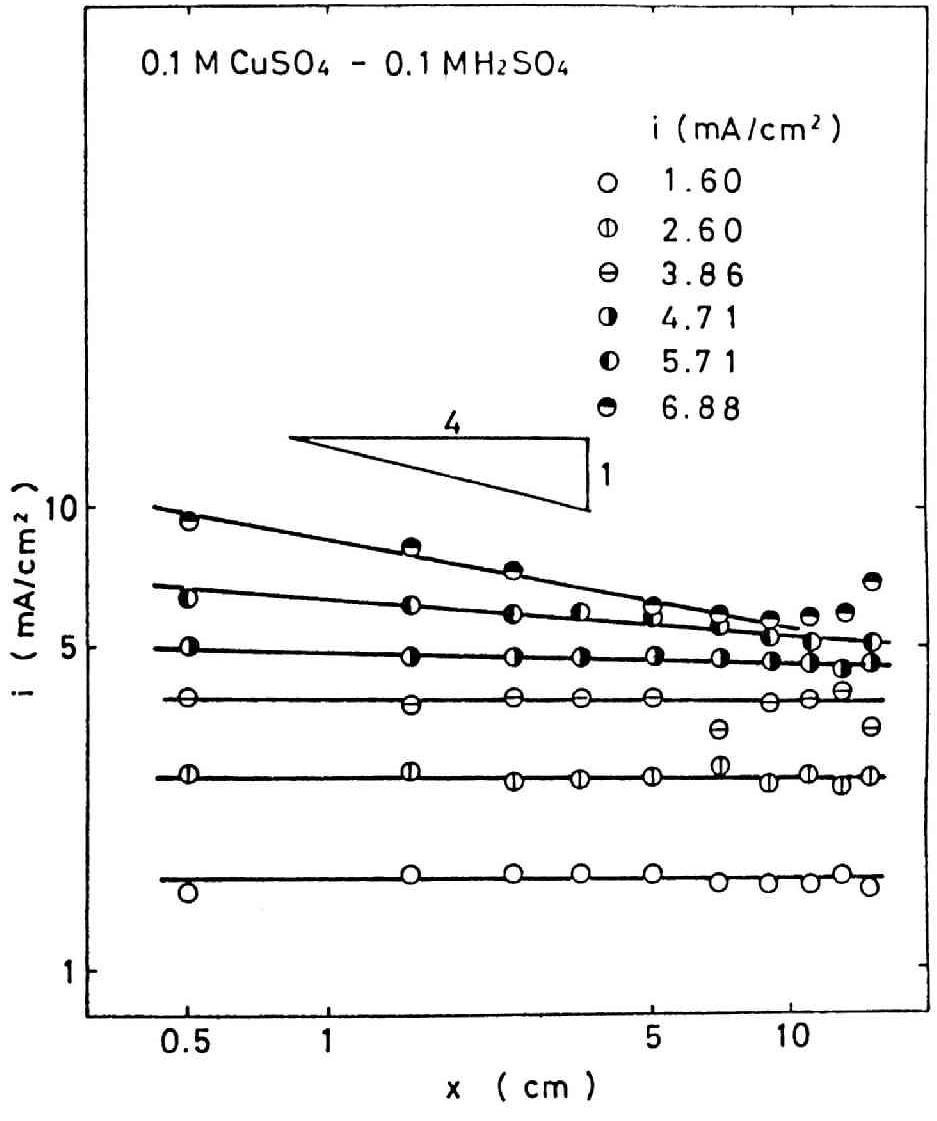

Fig. 5.15 Relationship between cathodic current density and height from lower edge of cathode ($0.1M\ CuSO_4$-$0.1M\ H_2SO_4$ solution)

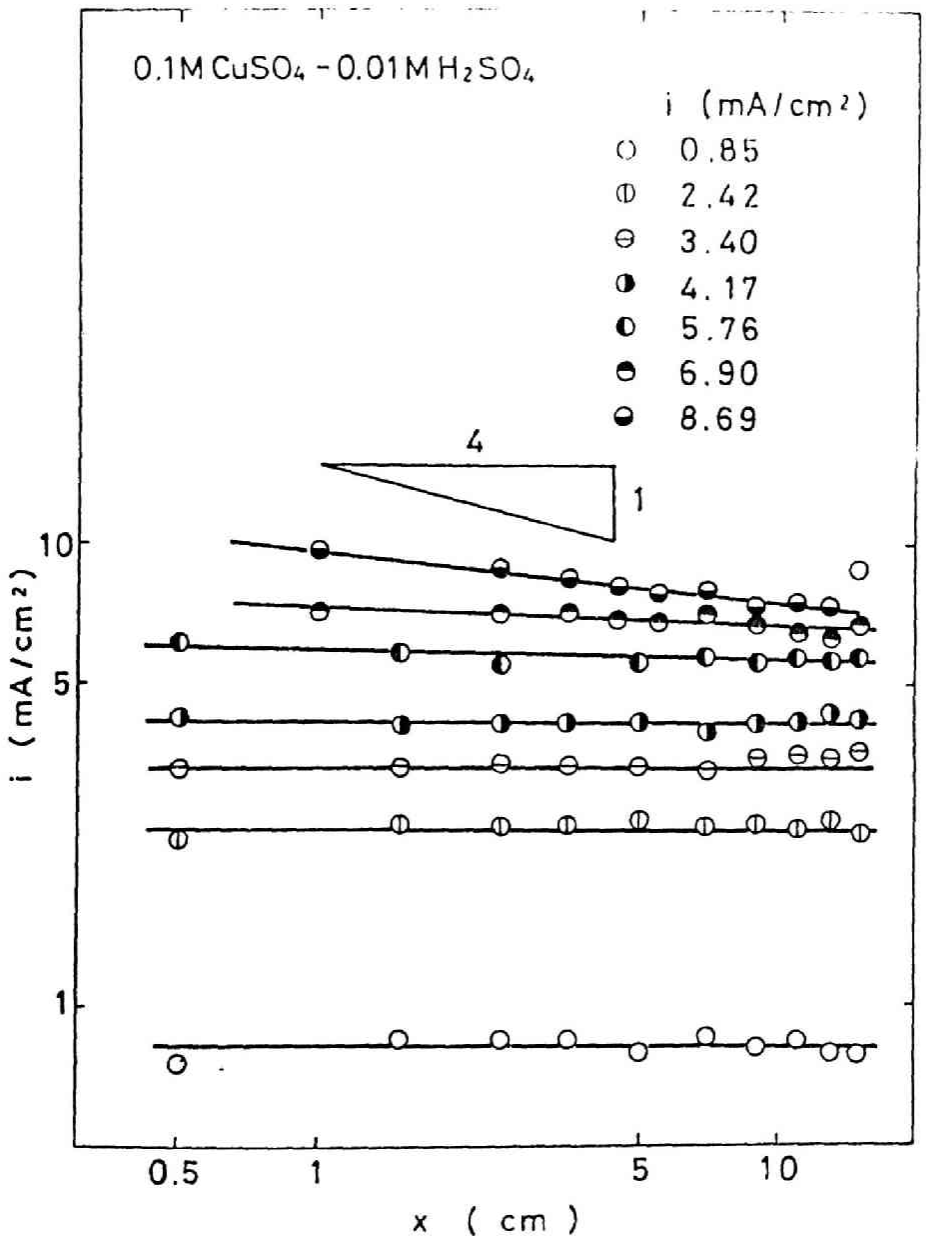

Fig. 5.16 Relationship between cathodic current density and height from lower edge of cathode ($0.1M\ CuSO_4$-$0.01M\ H_2SO_4$ solution)

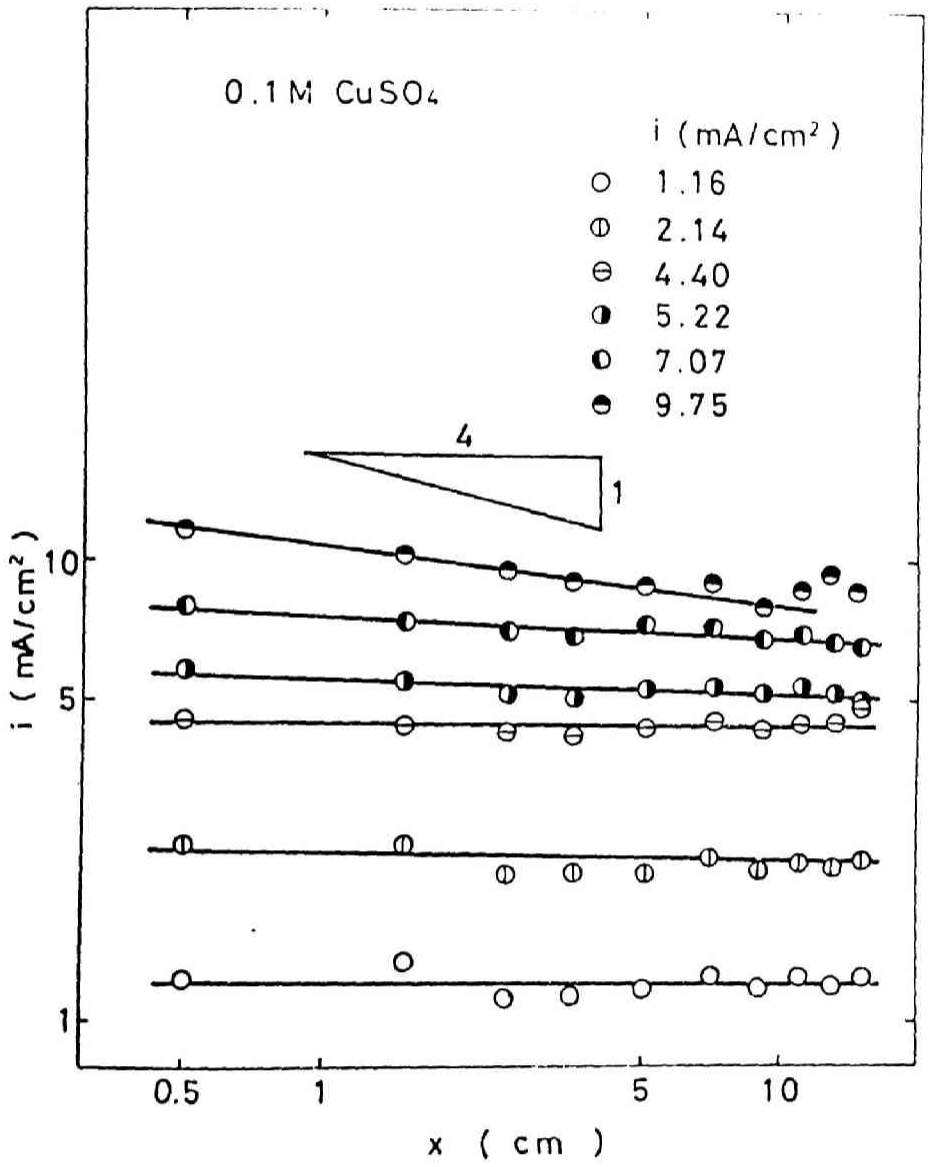

Fig. 5.17 Relationship between cathodic current density and height from lower edge of cathode (aqueous 0.1M $CuSO_4$ solution)

one half of the limiting current density. The electric conductivity is lower in these solutions, and it is thought that the effect of concentration polarization in the cathodic boundary layer is relatively minor as compared with the ohmic potential drop within the bulk-electrolyte. Then the distribution of local current densities on the cathode surface which is affected both by the resistivity of the bulk-electrolyte and by the concentration polarization in the cathodic diffusion layer becomes more uniform.

Furthermore, when the variation of $CuSO_4$ concentration at the cathode surface due to the change of the cathodic current density in the aqueous 0.05M $CuSO_4$ solution is precisely compared with the dependance of refractive index of solution at the cathode surface on the cathodic current density in the 0.05M $CuSO_4$-1.85M H_2SO_4 solution, both mentioned in Chapter 4, it is seen that the experimental results with the aqueous 0.05M $CuSO_4$ solution is in better coincidence than in 0.05M $CuSO_4$-1.85M H_2SO_4 solution with the theoretical calculations which were derived on the assumption of uniform distribution of cathodic current densities within a wider range of the ratio of applied cathodic current density to the limiting value. This experimental result indirectly indicates the appropriateness of the above-mentioned experimental results of the current distribution.

It is also seen in Fig. 5.15 through 5.17 that the slope of straight lines becomes steeper with the rise of the average cathod-

ic current density. However, it is fairly lower than the theoretical value of -1/4 even in the vicinity of the limiting value. This tendency is particularly evident in 0.1M $CuSO_4$-0.01M H_2SO_4 and 0.1M $CuSO_4$ solutions. Furthermore, it was observed during the electrolysis of the aqueous solutions whose H_2SO_4 concentration is lower than 0.1M that the plots tend to deviate from the straight line in the upper portion of the cathode and that the local cathodic current densities in this portion of the cathode start to irregularly oscillate at the average cathodic current densities near the limiting value. These phenomena are thought to be due to the very rough reddish electrodeposit in the upper portion of the cathode which may cause a short-circuit between host bar and miniature probe or due to the development of the natural convection into a turbulent flow in this portion of the cathode surface.

In order to further pursue the possible causes, the distribution of local cathodic current densities was measured with 0.6M $CuSO_4$-1.85M H_2SO_4 solution by using a vertical plane cathode of 16 cm height. The experimental results are illustrated in Fig. 5.18. It was observed during the experiment that the laminar natural convective flow starts to slightly wave at the vertical distance of more than about 10 cm from the lower edge of cathode at the average cathodic current density of 10 mA/cm^2 which is roughly equivalent to the average cathodic limiting current density in the aqueous 0.1M $CuSO_4$ solution. The obtained elec-

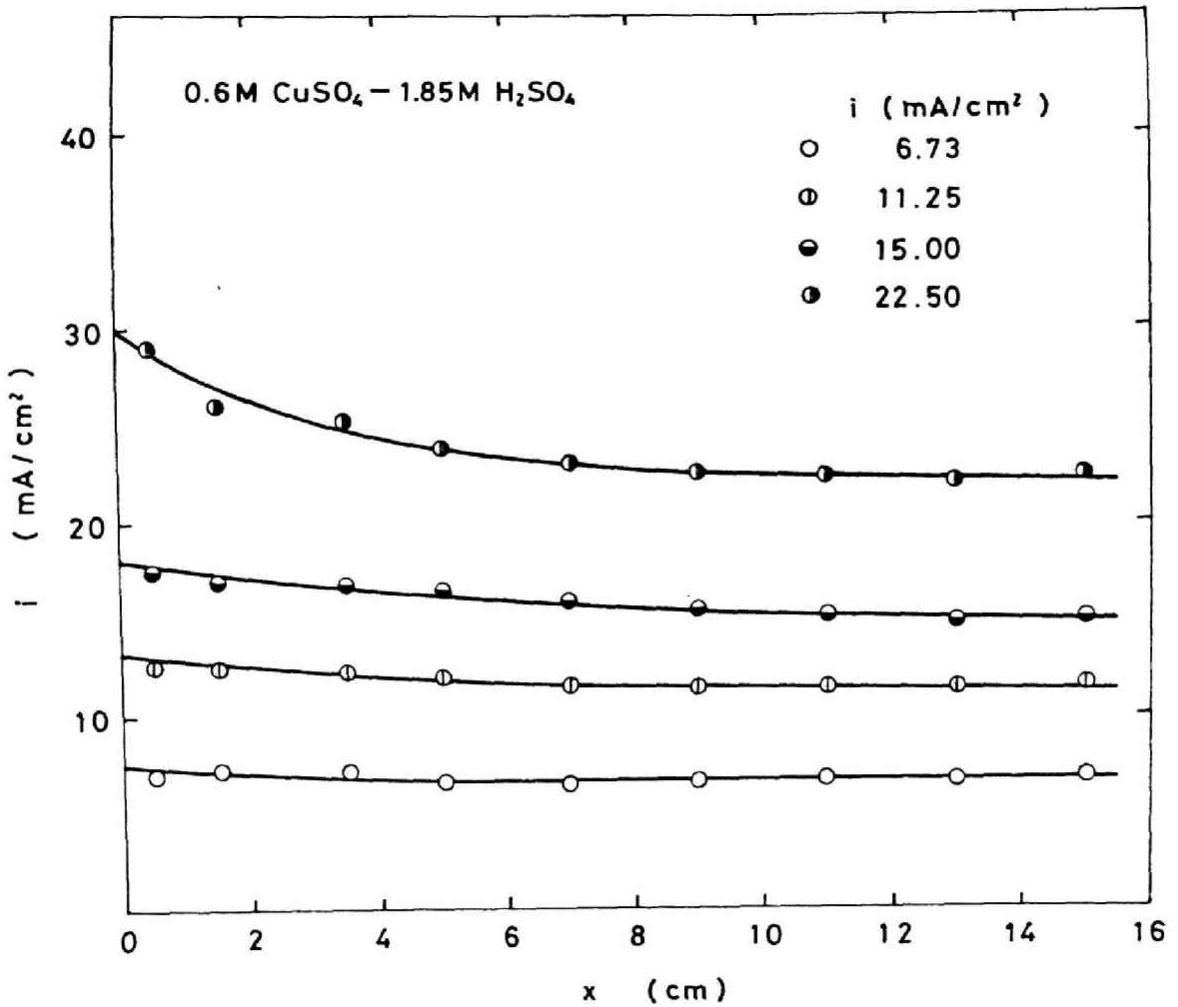

Fig. 5.18 Distribution of cathodic current density in the electrolysis of 0.6M $CuSO_4$-1.85M H_2SO_4 solution

trodeposit is uniform over the whole vertical distance of the cathode surface. Furthermore, it is seen in Fig. 5.18 that the irregular oscillation of the local cathodic current density in the upper portion of cathode was not observed even at the average cathodic current density of 20 mA/cm^2 which is twice larger than the average cathodic limiting current density of the aqueous 0.1M $CuSO_4$ solution. In addition, the natural convective flow in the upper portion of the cathode surface was carefully observed during the electrolysis of the aqueous 0.1M $CuSO_4$ solution at the average cathodic limiting current density, and it was found that the natural convective flow becomes fully turbulent at the height of more than about 10 cm from the lower edge of cathode.

From the above-mentioned observations it may be said that the waving flow of the natural convection is developed in the upper portion of cathode to the fully turbulent flow due to the hydrodynamic resistance of the rough surface of the electrodeposit during the electrolysis of the aqueous solutions containing H_2SO_4 of lower concentration when the average cathodic current density approaches to the limiting value. It is thought that the irregular oscillation of the local cathodic current density in the upper portion of cathode is caused by the disturbance of the ionic mass transfer toward the cathodic surface by the developed turbulent flow of natural convection.

In the next place, the measured distribution of the local cathodic current densities were compared with the theoretical dis-

tribution of the local cathodic current densities. In order to carry out the comparison, the numerical solution of the simultaneous Eq. (2.95), (2.96) and (2.97) was obtained by applying a technique of successive approximation, and the numerical values of $i_c(x)$ which satisfy these equations were determined. This calculation of the distribution of local cathodic current densities in the vertical direction was carried out with an aqueous 0.1M $CuSO_4$-1.85M H_2SO_4 solution by using a digital computer. The property constants and the transfer parameters used in the calculation are summarized in Table 5.2. The calculated distribution of cathodic current densities at each average current density are illustrated in Fig. 5.19 together with the experimental results demonstrated in Fig. 5.13. By comparing the theoretical and experimental distributions of the cathodic current densities, it is seen that the theoretical values are in excellent agreement with the experimental ones.

A similar calculation was also carried out with the aqueous 0.1M $CuSO_4$ solution by using Eq. (2.66), (2.68) and (2.69). The calculation was successful at the average cathodic current densities below one half of the limiting value. However, the calculation was not successful at the higher current densities above the half-value of the cathodic limiting current density. From the theoretical distribution of the local current densities calculated at the lower average cathodic current densities, it was

Table 5.2 Property constants used in the calculation

κ	(1/ohm cm)[12]	0.600
k_1	(cm^2/sec)	5.43×10^{-6}*
ν	(cm^2/sec)	1.163×10^{-2}
$*t_1$	(-)[13,14,15]	0.0066
α	(-)[9]	0.5
i_e	(A/cm^2)[11]	1×10^{-4}
α_1	(cm^3/mol)[9]	120.6
α_2	(cm^3/mol)[9]	40.9**
σ	(-)	1.30
ω	(-)	2.30
λ	(-)	2.95
η	(-)	3.15
ε	(-)	10
α	(-)	0.31***

* see Appendix B
** see Appendix D
*** see Appendix C

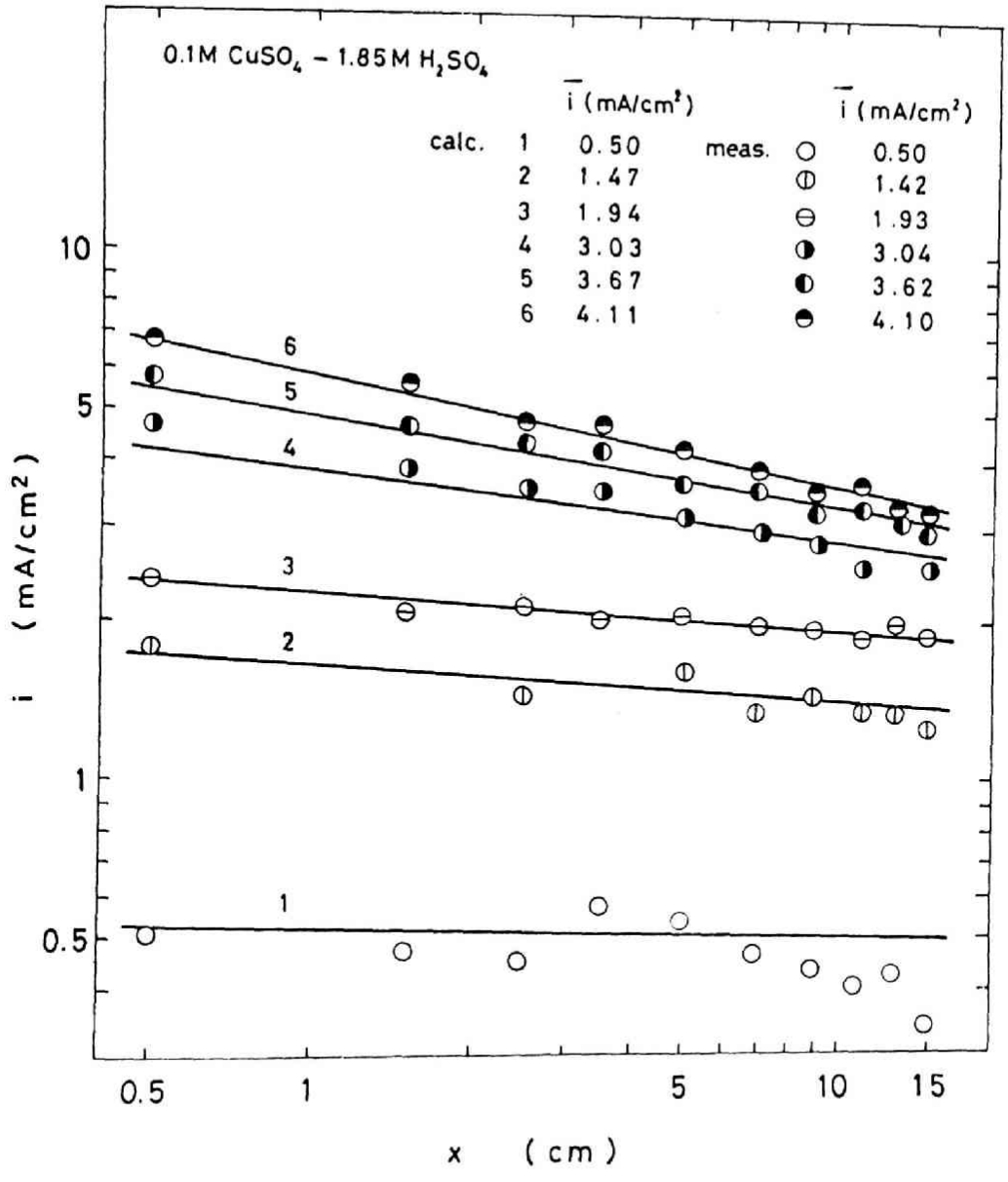

Fig. 5.19 Comparison of calculated and measured current density distribution on the cathode surface in the electrolysis of 0.1M $CuSO_4$-1.85M H_2SO_4 solution

revealed that the distribution of local cathodic current densities are virtually uniform in vertical direction, and they are in good agreement with the experimental data. Among the probable reasons of the unsuccessful theoretical calculation with the aqueous 0.1M $CuSO_4$ solution at higher current densities, it can be said that the electric conductivity of the 0.1M $CuSO_4$ solution is far lower than the 0.1M $CuSO_4$-1.85M H_2SO_4 solution.

As shown in Fig. 5.13 through 5.17, the slope of straight lines in the diagram of log i versus log x becomes steeper with the rise of the average cathodic current density. In order to further investigate this experimental result, the experimental slopes were plotted against the fractional cathodic current density which is the ratio of the average cathodic current density to the cathodic limiting current density, $i_{av}/i_{d,av}$, in Fig. 5.20. The curve shown in the same figure demonstrates the relationship between the theoretical slope and the fractional cathodic current density calculated with the 0.1M $CuSO_4$-1.85M H_2SO_4 solution. As seen in this figure, the experimental slopes obtained with the solutions of 0.1M $CuSO_4$-1.85M $CuSO_4$ and 0.1M $CuSO_4$-1.0M $CuSO_4$ are fairly well coincident with the theoretical value which decreases with the rise of average cathodic current density to -1/4 at the cathodic limiting current density.

The experimental slopes obtained with the aqueous solutions containing 0.1M $CuSO_4$ and H_2SO_4 whose concentration is 0.1, 0.01 and 0M, respectively, are, on the other hand, scattered in the

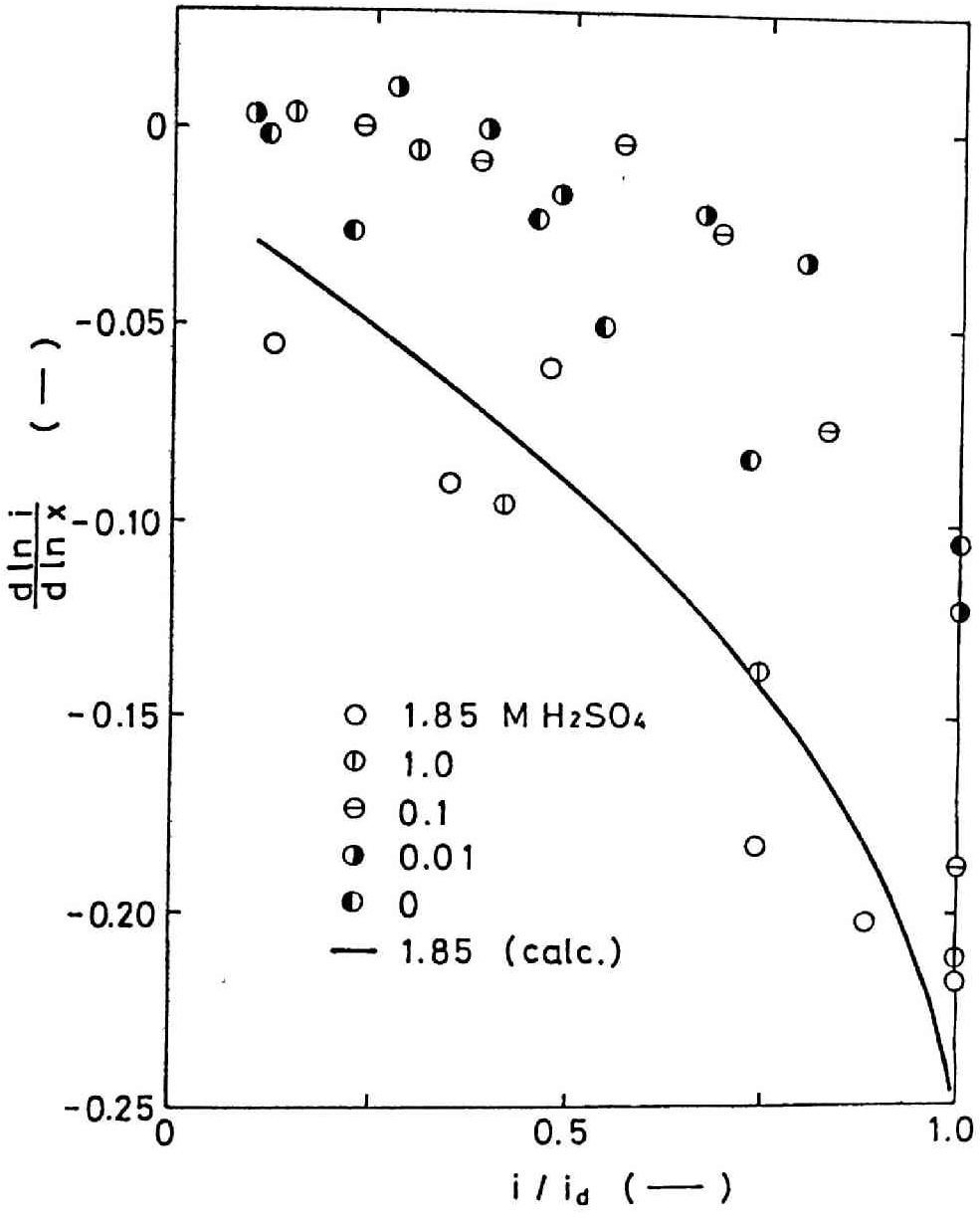

Fig. 5.20 Relationship between dlni/dlnx and i/i_d

neighborhood of zero in the region of the average cathodic current density lower than one half of the limiting value. It is again indicated that the local cathodic current densities are uniform. Furthermore, it is observed that the slope decreases with the rise of the average cathodic current density above the half-value of the limiting current density, and they are fairly higher than the theoretical value of -1/4 in the vicinity of the limiting current density.

From the observation mentioned before that the "burnt" deposit is obtained in the upper portion of cathode when the electrolysis of the aqueous solutions of lower H_2SO_4 concentration takes place in the vicinity of cathodic limiting current density, it is evident that the local Cu^{2+} ion concentration in the cathodic diffusion layer in the upper portion of the cathode is preferentially lowered to zero due to the development of the upward natural convective flow. It was also mentioned before that the local current densities in the upper portion of cathode measured with the miniature probes irregularly oscillate in the vicinity of the average cathodic limiting current density. In this portion of the cathode, the local current density is higher than the theoretical local cathodic limiting current density because of the developed turbulent flow of natural convection. These oscillating values of local current densities in the upper portion of cathode were omitted in the estimation of the experimental slopes in Fig. 5.20. The local cathodic current densities in the

lower portion of cathode which were used in the estimation are, on the contrary, below the theoretical local cathodic limiting current density even in the vicinity of the average cathodic limiting current density, and it is supposed that the higher values of the slope than -1/4 were obtained at the average limiting current density.

5.5 Summary

The local cathodic current densities on the surface of a vertical plane copper cathode installed in the unstirred aqueous solutions containing $CuSO_4$ and H_2SO_4 were measured by applying the technique proposed by Lloyd et al.[10] In this technique, the local cathodic current densities were measured with the miniature probes imbedded in the plane cathode. Each miniature probe is connected with a manganin wire resistor of a constant resistance, and the potential difference between both ends of the resistor was meausred. The possible effects of the resistance of the used resistor, the distance between both electrodes, the unevenness of the lines of electric force in the portion of the solution higher than the electrodes, the hydrodynamic resistance due to the side wall of the acryl resin frame, etc. were examined, and the appropriate experimental conditions were established. The measurement of the distribution of local current densities in vertical direction on the plane cathode was carried out at 25°C with the aqueous solutions containing 0.1M $CuSO_4$ and 1.85, 1.0, 0.1, 0.01 and 0M H_2SO_4, respectively.

During the electrolysis of the aqueous 0.1M $CuSO_4$-1.0M H_2SO_4 and 0.1M $CuSO_4$-1.85M H_2SO_4 solutions, the local cathodic current densities are uniform in vertical direction at lower average cathodic current densities. The local current densities decrease along the vertical distance from the lower edge of cathode when

the average cathodic current density is raised. It is proportional to the -1/4th power of the vertical distance in the vicinity of the average cathodic limiting current density. This experimental result is in good agreement with the results of previous workers. The theoretical distribution of the local cathodic current densities in vertical direction in the aqueous 0.1M $CuSO_4$-1.85M H_2SO_4 solution was calculated by the procedure mentioned in Chapter 2, and it was revealed that the theoretical distribution is in excellent agreement with the measurement.

From the measurement with the aqueous 0.1M $CuSO_4$ solutions containing H_2SO_4 whose concentration is lower than 0.1M, it was found that the distribution of the local cathodic current densities is uniform in vertical direction in the region of the average cathodic current density lower than one half of the limiting value. It is because the concentration polarization in the cathodic diffusion layer is relatively minor as compared with the ohmic potential drop in the bulk-electrolyte of lower electric conductivity. In the region of the average cathodic current density higher than one half of the limiting value, the local current densities become dependent on the vertical distance from the lower edge of cathode. However, this experimental dependance of the local cathodic current densities on the vertical distance is fairly lower than the theoretical relationship that the local cathodic current density is proportional to the -1/4th power of the height at the average cathodic limiting current density. Furthermore, the local

cathodic current densities in the upper portion of the cathode are higher and irregularly oscillate in the vicinity of the average limiting current density. It is probably because the natural convective flow becomes fully turbulent in this portion of the cathode due to the rough electrodiposit obtained from the aqueous solutions of lower H_2SO_4 concentration near the limiting current density. Then the local cathodic current densities at the lower portion of cathode are below the limiting value. It is supposed that the measured dependance of the current distribution on the vertical distance from the lower edge of cathode become fairly lower than the theory.

Reference to Chapter 5

1) J. N. Ager: Discussions Faraday Soc., 1 (1947) 26.

2) C. Wagner: J. Electrochem. Soc., 95 (1949) 161; 104 (1957) 129.

3) G. H. Keulegan: J. Res. Nat.Bur. Stand., 47 (1951) 2240.

4) N. Ibl and R. H. Muller: A. Elecktrochem., 59 (1955) 671.

5) N. Ibl and R. H. Muller: J. Electrochem. Soc., 105 (1958) 346.

6) C. R. Wilke, M. Eisenberg and C. R. Tobias: J. Electrochem. Soc., 100 (1953) 513.

7) C. R. Wilke, M. Eisenberg and C. W. Tobias: Chem. Eng. Prog., 49 (1953) 663.

8) Y. Maru, S. Ito, S. Oyama and Y. Kondo: Denki Kagaku, 38 (1970) 343.

9) K. Asada, F. Hine, S. Yoshizawa and S. Okada: J. Electrochem. Soc., 107 (1960) 242.

10) J. R. Lloyd, E. M. Sparrow and E. R. G. Eckert: J. Electrochem. Soc., 119 (1972) 702.

11) J. M. West: "Electrodeposition and Corrosion Processes", p. 47, D. Van Nostrand Co., Ltd., London (1965).

12) H. K. Richardson and F. D. Taylor: Trans. Am. Electrochem. Soc., 20 (1911) 179.

13) "Handbook of Electrochemistry", edited by The Electrochemical Soc. of Japan, p. 118, Maruzen Book Co., Tokyo (1964).

14) R. C. Weast: "Handbook of Chemistry and Physics", 45th Ed., p. D-80, The Chemical Rubber Co., Cleaveland (1964).

15) E. A. Moelwyn-Hughes: "Physical Chemistry", p. 859, Pergamon Press, London (1961).

CHAPTER 6 SUMMARY AND CONCLUSION

The electrolytic refining and winning have widely been employed in the hydrometallurgical process for the extraction of common metals. These electrolytic processes possess an advantage over the pyrometallurgical process that the metals of high purity can easily be obtained at low temperature by applying the electric energy. However, one of the important engineering problems in the electrolytic process is that the productivity of metals per unit area of the electrolytic bath is lower.

Recently, the problem of lower productivity in the electrolytic process was recognized, and many attempts have been made to cope with this problem: the electrolytic refining and winning at higher current densities were studied, and they have been brought into practice at various electrolytic plants. It is known that the current distribution on the surface of an electrode usually becomes uneven at higher current densities. It may cause an undesirable side reaction at the portions of higher current densities. Then it is desired that the electrolytic process is conducted at a current density of uniform distribution to the possible extent.

Many theoretical and experimental works have been made on the current distribution on the electrode surface since more than thirty years ago. Among these works, the major interest of the earlier workers was directed to the primary and secondary current distributions; the primary current distribution is determined solely by the geometric factors of the electrolytic cell and electrodes, and the secondary current distribution is related to the geometric factors and the chemical polarization at the electrode surface. These theoretical current distributions are valid for the electrolysis under the electrolytic condition that the composition of the electrolyte is uniform throughout the electrolytic cell.

It is known, on the other hand, that a very thin liquid film of different composition from the bulk-electrolyte is formed at the electrode surface during the electrolysis. This thin liquid film is called as the diffusion layer. The current distribution on the electrode is also affected by the ionic mass transfer in this diffusion layer. The electrolytic refining, winning and plating often take place on a vertical plane cathode in the unstirred or gently stirred aqueous solutions. Under this electrolytic condition, the concentration gradient in the cathodic diffusion layer yields an upward natural convective flow along the cathode surface, and this natural convective flow should also be taken into consideration in the studies of the ionic mass transfer in the cathodic diffusion layer. It goes without saying that

it is very important from the industrial viewpoint to disclose the mechanism of ionic mass transfer in the cathodic diffusion layer which is accompanied by the natural convection in vertical direction.

The industrial electrolytic refining of copper is conducted in the aqueous solutions containing $CuSO_4$ and H_2SO_4; H_2SO_4 is added to the solution to raise the electric conductivity. During the electrolysis of this aqueous solution, H^+ ion migrates from the bulk-electrolyte toward the cathode surface and is accumulated in the cathodic diffusion layer. The accumulation of H_2SO_4 may have an additional effect on the natural convective flow and the ionic mass transfer in the cathodic boundary layer.

Since it was recognized that the natural convection along the surface of a vertical plane cathode plays an important role in the electrolysis of an unstirred electrolyte, many theoretical and experimental studies have been made on the ionic mass transfer in the cathodic boundary layer which is accompanied by the natural convection. The majority of these studies concerned the cathodic limiting current density, and only a few theoretical and experimental works have been made on the ionic mass transfer in the cathodic diffusion layer and the resultant distribution of the local current densities in the region where the average cathodic current densities are lower than the limiting value. It should be noted that the industrial electrolytic refining, winning and plating are usually conducted below the cathodic limiting current

density.

It was intended in the present work to study the ionic mass transfer and the natural convection in the boundary layer near the surface of a vertical plane cathode during the electrolysis of the unstirred aqueous $CuSO_4$ and $CuSO_4$-H_2SO_4 solutions at the cathodic current densities below and at the limiting value.

The theoretical solutions of the ionic mass transfer in the cathodic diffusion layer and the current distribution on the surface of a vertical plane cathode were derived under various electrolytic conditions in Chapter 2. In order to derive these theoretical expressions, the basic equations regarding the natural convective flow, the ionic mass transfer and the charge transfer were established. These simultaneous equations were solved together with the rate equation of electrode reaction. Under the assumptions that the width of electrodes is infinite and that the electrolysis is conducted at the steady state, these basic differential equations were simplified. The integration of the Navier-Stokes equation and the equations of ionic mass transfer in the cathodic boundary layer were carried out by applying the method proposed by von Kármán and Pohlhausen. In addition, the generalized functions in which the parameters ω, λ, η and ε are involved were used to express the velocity profile of natural convection and the concentration profile of Cu^{2+} and H^+ ions in the cathodic diffusion layer, respectively. From these equations, furthermore, the expressions regarding the maximal velocity

of natural convective flow, the concentration difference of ionic species between bulk-electrolyte and cathode surface, the thickness of diffusion layer and the resultant distribution of local cathodic current densities were derived under the following electrolytic conditions, respectively.

1) Electrolysis at the cathodic limiting current density
2) Electrolysis at the cathodic current densities of uniform distribution
3) Electrolysis in the intermediate region between the cathodic limiting current density and the uniform current densities

These theoretical expressions were derived for the electrolysis of the aqueous $CuSO_4$ solution and of the aqueous $CuSO_4$-H_2SO_4 solution, respectively. In the derivation of the theoretical expressions regarding the aqueous $CuSO_4$-H_2SO_4 solution, the incomplete dissociation of HSO_4^- ion into H^+ and SO_4^{2-} ions in the second stage dissociation of H_2SO_4 was taken into consideration.

The upward natural convective flow along the cathode surface was studied in Chapter 3. The velocity profile of the natural convective flow was measured in aqueous $CuSO_4$ and $CuSO_4$-H_2SO_4 solutions by filming the motion of small colophonium particles suspended in the solution and dragged along by the natural convective flow near the cathode surface. The measurement was carried out at 23°C with the aqueous 0.6M $CuSO_4$, 0.1M $CuSO_4$ and 0.6M $CuSO_4$-1.5M H_2SO_4 solutions, respectively. It was measured at vari-

ous heights from the lower edge of cathode and at various cathodic current densities below 4 mA/cm^2 where the vertical distribution of local current densities was presumed to be uniform.

It was revealed from the experimental results with aqueous $CuSO_4$ solutions that the non-dimensional theoretical correlations derived in Chapter 2 between $(u_m x/D_1)$ and $(Sc \cdot Gr^*)$ and between (τ/x) and $(Sc \cdot Gr^*)$ were satisfied under the electrolytic conditions of uniform distribution of cathodic current densities.

In order to examine the effect of $CuSO_4$ concentration on the velocity profile, the experimental results with aqueous 0.1M $CuSO_4$ solution were compared with those of aqueous 0.6M $CuSO_4$ solution. It was revealed from this comparison that u_m is lower in 0.1M $CuSO_4$ solution, which was unable to be explained from the difference of property constants of these two solutions. The parameter $\eta(= \delta_1/\tau)$ was larger in 0.1M $CuSO_4$ solution, and the other parameters ω_1, λ and ε were unvaried in both solutions. Since τ is virtually unvaried in both solutions, the higher value of η in 0.1M $CuSO_4$ solution indicated that the thickness of diffusion layer, δ_1, is larger in this solution. From a simple calculation it was shown that the larger δ_1-value in 0.1M $CuSO_4$ solution is mainly attributed to the higher diffusivity of $CuSO_4$ in this solution of lower $CuSO_4$ concentration.

Next, the experimental results with the aqueous 0.6M $CuSO_4$-1.85M H_2SO_4 solution was found to satisfy the theoretical expressions of u_m and τ in $CuSO_4$-H_2SO_4 solutions derived in Chapter 2.

The parameters ω_1, λ, η and ε involved in these equation were determined according to the procedure proposed by Ibl. In this calculation the incomplete dissociation of H_2SO_4 was taken into consideration, and the ratio of the thickness of diffusion layers of H^+ ion and Cu^{2+} ion was obtained at 1.54 in 0.6M $CuSO_4$-1.5M H_2SO_4 solution. From the comparison of velocity profiles of natural convective flow in aqueous 0.6M $CuSO_4$ and 0.6M $CuSO_4$-1.5M H_2SO_4 solutions, it was revealed that both u_m and τ are reduced in the latter solution. In order to clarify the reduced τ-value in the acidified $CuSO_4$ solution, the density distribution in the cathodic diffusion layer was calculated in $CuSO_4$ and $CuSO_4$-H_2SO_4 solutions, respectively. It was disclosed that the buoyancy force acts in the upward direction in the whole region of the diffusion layer in the former solution. On the contrary, the buoyancy force acts in the upward direction in the inner portion of the diffusion layer and the gravitational force acts downward in the outer portion of the diffusion layer in the latter solution because of the inverse concentration profile of H^+ ion. Then the upward natural convection is depressed by the gravitational force in the outer portion of the cathodic diffusion layer in the acidified $CuSO_4$ solution which is caused by the accumulation of H^+ ion.

The measurement of the concentration profile of $CuSO_4$ in the cathodic diffusion layer which is accompanied by the upward natural convection is very important for the studies of the ionic mass

transfer in this layer. This concentration profile was pursued in Chapter 4. It was feasible to measure the concentration profile by applying the technique of holographic interferometry. In the derivation of the profile of refractive index of solution from the holographic interferograms, the effects of beam deflection in the cathodic diffusion layer were considered, and the interferograms were corrected under the assumption of a linear change of refractive index in the region of beam deflection in the cathodic diffusion layer. The concentration profile of $CuSO_4$ in the cathodic diffusion layer was obtained from this corrected profile of refractive index of the solution.

First the concentration profiles in the cathodic diffusion layer of the aqueous 0.05M and 0.1M $CuSO_4$ solutions were measured at various cathodic current densities below the limiting value and at various heights from the lower edge of cathode. The experimental temperature was maintained at 23°C. It was disclosed from the measurement that the concentration difference of $CuSO_4$ between bulk-electrolyte and cathode surface, Δc, is increased and the thickness of the diffusion layer, δ_1, is decreased when the average current density is raised. It was also revealed that δ_1 is increased in the upper portion of the cathode.

Furthermore, it was revealed from the experiment that the theoretical dependances of Δc and δ_1 on the current density and on the vertical distance from the lower edge of cathode were satisfied in the region of lower current densities below one half of

the limiting value. However, the experimental values start to deviate from the theory at higher current densities. This is supposed to be caused by the unequal local cathodic current densities in the vertical direction.

It is also important to pursue the concentration profiles of $CuSO_4$ and H_2SO_4 in the cathodic diffusion layer for studying the electrodeposition of copper from the unstirred aqueous solution containing $CuSO_4$ and H_2SO_4, which often takes place in the industrial electrolytic refining and plating. As the first step toward this goal, the profile of the refractive index of solution in the cathodic diffusion layer was measured at various heights from the lower edge of cathode and at various cathodic current densities up to the limiting value. The theoretical expression of the difference of refractive index between bulk-electrolyte and cathode surface, Δn, was derived under the assumption of a uniform distribution of local current densities on the cathode surface. At the cathodic current densities lower than a half of the limiting value, the experimental results satisfied both theoretical relationships between Δn and the height from the lower edge of cathode and between Δn and the average cathodic current density. It was also disclosed that Δn is virtually unchanged in vertical direction at the cathodic limiting current density.

Furthermore, a generalized expression of Δn which holds in the whole region of the cathodic current densities up to the limiting value was derived in the form of Eq. (4.28). After the

theoretical distribution of the local cathodic current densities was obtained by using a technique of numerical analysis, the theoretical Δn values were calculated. Both experimental and theoretical Δn values were in fairly good coincidence over the whole region of the cathodic current densities, though the measured values were somewhat higher than the theoretical ones.

When the electrolysis takes place at the cathodic limiting current density, the concentration of $CuSO_4$ is regarded as being virtually zero on the cathode surface. Under this experimental condition, Δn at a height of 4 cm from the lower edge of cathode was measured at 23°C with the aqueous solutions containing 1.85M H_2SO_4 and 0.01, 0.02, 0.03, 0.04 and 0.05M $CuSO_4$, respectively, and the concentration difference of H_2SO_4 between cathode surface and bulk-electrolyte, $\Delta c_{H_2SO_4}$, was obtained. The $\Delta c_{H_2SO_4}$ value at the cathodic limiting current density decreases when $CuSO_4$ concentration in the bulk-electrolyte, $^*c$, is lowered. Furthermore, the slope of the curve of $\Delta c_{H_2SO_4}$ versus $^*c$ also decreases when $CuSO_4$ concentration in the bulk-electrolyte is lowered. These experimental results were explained by Eq. (2.79) and (4.23). The measured $\Delta c_{H_2SO_4}$ values were further compared with theoretical ones. It was disclosed that the measured $\Delta c_{H_2SO_4}$ values were somewhat lower than the calculated values from Eq. (2.79) in which the incomplete dissociation of H_2SO_4 was considered. This difference between the measured and calculated values may be ascribed to the uncertainty in the estimation of property constants used in

the calculation such as the diffusivity of Cu^{2+} ion.

Finally, the distribution of local current densities in the vertical direction on a plane cathode was studied in Chapter 5. The measurement of local cathodic current densities was made by using the miniature probes imbedded in the plane cathode. Measurement was carried out at 25°C with the aqueous solutions containing 0.1M $CuSO_4$ and 1.85, 1.0, 0.1, 0.01 and 0M H_2SO_4, respectively.

From the electrolysis of the aqueous solutions containing 0.1M $CuSO_4$ and H_2SO_4 whose concentration is higher than 1.0M, it was revealed that the local cathodic current densities are uniform at the lower average current densities. It decreases along the vertical distance from the lower edge of cathode when the higher average current densities are applied. It was proportional to the -1/4th power of the vertical distance from the lower edge of cathode in the vicinity of the cathodic limiting current density. This experimental result at the limiting current was in good agreements with the theoretical result mentioned in Chapter 2. The theoretical distribution of cathodic current densities in vertical direction was calculated in the wide region of cathodic current densities up to the limiting value with the aqueous 0.1M $CuSO_4$-1.85M H_2SO_4 solution. It was revealed that the theoretical distribution is in good agreement with the experimental results.

In the electrolysis of the aqueous solutions containing 0.1M

$CuSO_4$ and H_2SO_4 whose concentration is lower than 0.1M, the measured distribution of local cathodic current densities was uniform in the region of the average current density lower than a half of the limiting value. This is because the concentration polarization in the cathodic diffusion layer is relatively minor as compaired with the ohmic potential drop in the bulk-electrolyte of lower electric conductivity. In the region of the average cathodic current densities higher than a half of the limiting value, it was revealed that the local current densities become dependent on the vertical distance from the lower edge of cathode. However, the experimental dependance of local current densities on the vertical distance was fairly lower in the vicinity of the cathodic limiting current density than the theoretical relationship that the local cathodic current density is proportional to the -1/4th power of the vertical distance from the lower edge of cathode.

It was also observed that the local cathodic current density in the upper portion of the cathode surface is higher than the theoretical value and it irregularly oscillates in the vicinity of the limiting current density. It is presumably because the natural convective flow is developed in this portion of the cathode to the turbulent flow due to the hydrodynamic resistance at the surface of the rough electrodeposit obtained from the aqueous solution of lower H_2SO_4 concentration near the average cathodic limiting current density. It was also supposed that the local

cathodic current densities in the lower portion of cathode are not attained at the limiting value. It may be said that the measured dependance of the local cathodic current density on the vertical distance from the lower edge of cathode becomes fairly lower than the theoretical one in the vicinity of the limiting current density.

As mentioned above, the ionic mass transfer and the natural convective flow in the boundary layer of a vertical plane cathode and the resultant current distribution on the cathode surface were fairly well disclosed in the present work under the experimental conditions that the natural convective flow is laminer. However, it should be mentioned that the following problems should further be clarified in the future works.

The concentration profiles of Cu^{2+} and H^{+} ions in the cathodic diffusion layer were not measured in the present work during the electrolysis of the solution containing $CuSO_4$ and H_2SO_4. The present discussion was referred only to the profile of the refractive index of solution in the cathodic diffusion layer and the concentration difference of H_2SO_4 between cathode surface and bulk-electrolyte at the limiting current density. In order to further study this problem, it may be a very important clue to apply the colorimetric method.

Industrial electrolytic refining and winning are conducted by employing the large vertical plane cathode of about 1 m height. The natural convective flow in the major portion of the vertical plane cathode higher than 10 to 20 cm from the lower edge of

cathode is thought to become turbulent. In order to study the electrolysis which takes place at higher current densities, it is desirable to investigate an ionic mass transfer in the cathodic diffusion layer which is accompanied by the turbulent natural convective flow.

The prevention of passivation of anode is important to carry out the industrial electrolysis at higher current densities. Many attempts have been made to overcome the problem. Among them the application of periodic reverse current of higher density to the industrial electrolytic refining of copper is proposed. However, the basic studies have rarely been made on the electrolysis with the periodic reverse current. It is thought to be important to study the ionic mass transfer and the natural convective flow in the anodic boundary layer during the unsteady electrolysis.

Appendix A. Relationship between Concentration Gradients of Cu^{2+} and H^{+} Ions at the Cathode Surface

When the electrodeposition takes place on the surface of a vertical plane cathode installed in an unstirred or gently stirred aqueous solution containing $CuSO_4$ and H_2SO_4, we are primarily interested in the concentration of Cu^{2+} ion which is lowered on the cathode surface. In addition, our interest also concerns both the increased concentration of unreacted H^{+} ion which migrates toward the cathode surface and is accumulated in the cathodic diffusion layer due to the applied potential difference between both electrodes and the decreased concentration of HSO_4^{-} and SO_4^{2-} ions which migrate away from the cathode surface. Then it is required to disclose the interrelationship among the concentration gradients of these ions at the cathode surface.

The flux of an ion i passing through a cross-sectional area A in the cathodic diffusion layer toward the cathode surface is expressed as

$$\frac{dn_i}{dt} = -Ak_i \frac{dc_i}{dy} - Ac_i u_i \frac{d\phi}{dy} + Ac_i v \qquad (A.1)$$

Furthermore, we denote the symbol s_i as the number of moles of an

ion i which reacts on the cathode surface per unit Faraday, F. Negative sign of s_i indicates that this ion is formed due to the cathode reaction. Since the velocity component of the natural convective flow toward the cathode surface, v, is zero at the cathode surface, Eq. (A.1) is rewritten at y = 0 as

$$\frac{dn_i}{dt} = \frac{s_i I}{F} = -Ak_i\left(\frac{dc_i}{dy}\right)_{y=0} = -Ac_i u_i\left(\frac{d\phi}{dy}\right)_{y=0} \tag{A.2}$$

where the symbol I represents the electric current.

Upon adding Eq. (A.2) regarding each ion after being multiplied by a term (z_i/k_i), respectively, the resultant term in which the concentration gradients are involved, $A\Sigma z_i\left(\frac{dc_i}{dy}\right)_{y=0}$, disappears because of the condition of electroneutrality:

$$\sum_i z_i c_i = 0 \tag{A.3}$$

Then the potential gradient at the cathode surface becomes

$$\left(\frac{d\phi}{dy}\right)_{y=0} = -\frac{I}{AF}\,\frac{\sum_i (z_i s_i/k_i)}{\sum_i (z_i c_i u_i/k_i)_{y=0}} \tag{A.4}$$

Substitution of Eq. (A.4) in Eq. (A.2) regarding an ion j yields the expression of concentration gradient of this ion as

$$\left(\frac{dc_j}{dy}\right)_{y=0} = -\frac{I}{AF}\left\{\frac{s_j}{k_j} - c_j\,\frac{u_j}{k_j}\,\frac{\sum_i (z_i s_i/k_i)}{\sum_i (z_i c_i u_i/k_i)}\right\}_{y=0} \tag{A.5}$$

The diffusivity of an ion i, k_i and the ionic mobility, u_i, are interrelated with each other by the well-known Nernst-Einstein

equation of

$$k_i = \frac{u_i}{z_i e_0} kT \tag{A.6}$$

where the symbols k and T are the Boltzmann constant and the absolute temperature, respectively. Substituting Eq. (A.6) in Eq. (A.5), we have

$$\left(\frac{dc_j}{dy}\right)_{y=0} = -\frac{I}{AF}\left\{\frac{s_j}{k_j} - c_j z_j \frac{\sum_i (z_i s_i / k_i)}{\sum_i (z_i^2 c_i)}\right\}_{y=0} \tag{A.7}$$

Furthermore we consider, for example, the electrolysis of an aqueous $CuSO_4$ solution containing H_2SO_4. Presuming the subscripts 1, 2, 3 and 4 to represent the ions Cu^{2+}, H^+, HSO_4^- and SO_4^{2-}, respectively, we have

$$\left.\begin{aligned} s_1 &= 1/2,\ s_2 = s_3 = s_4 = 0 \\ z_1 &= 2,\ z_2 = 1,\ z_3 = -1,\ z_4 = -2 \end{aligned}\right\} \tag{A.8}$$

Substitution of Eq. (A.8) in Eq. (A.7) yields

$$\left(\frac{dc_1}{dy}\right)_{y=0} = -\frac{I}{2AFk_1}\left\{\frac{c_2+c_3+c_4}{4c_1+c_2+c_3+4c_4}\right\}_{y=0} \tag{A.9}$$

$$\left(\frac{dc_2}{dy}\right)_{y=0} = \frac{I}{2AFk_1}\left\{\frac{2c_2}{4c_1+c_2+c_3+4c_4}\right\}_{y=0} \tag{A.10}$$

$$\left(\frac{dc_3}{dy}\right)_{y=0} = -\frac{I}{2AFk_1}\left\{\frac{2c_3}{4c_1+c_2+c_3+4c_4}\right\}_{y=0} \tag{A.11}$$

$$\left(\frac{dc_4}{dy}\right)_{y=0} = -\frac{I}{2AFk_1}\left\{\frac{4c_4}{4c_1+c_2+c_3+4c_4}\right\}_{y=0} \tag{A.12}$$

respectively.

Furthermore it is assumed that the dissociation of $CuSO_4$ into Cu^{2+} and SO_4^{2-} ions and the first stage dissociation of H_2SO_4 into H^+ and HSO_4^- ions are complete, and the dissociation of HSO_4^- ion into H^+ ion and SO_4^{2-} ion is incomplete. Denoting the degree of dissociation of HSO_4^- by a, we have the following equations.

$$c_3 = \frac{1-a}{1+a} c_2 \tag{A.12}$$

$$c_4 = c_1 + \frac{a}{1+a} c_2 \tag{A.13}$$

Then the substitution of Eq. (A.12) and (A.13) in Eq. (A.9) through (A.12) yields

$$\left(\frac{dc_2}{dy}\right)_{y=0} = -\left\{\frac{(1+a)c_2}{2(1+a)c_1 + (1+2a)c_2}\right\}_{y=0} \cdot \left(\frac{dc_1}{dy}\right)_{y=0} \tag{A.14}$$

$$\left(\frac{dc_3}{dy}\right)_{y=0} = \left\{\frac{(1-a)c_2}{2(1+a)c_1 + (1+2a)c_2}\right\}_{y=0} \cdot \left(\frac{dc_1}{dy}\right)_{y=0} \tag{A.15}$$

$$\left(\frac{dc_4}{dy}\right)_{y=0} = 2\left\{\frac{(1+a)c_1 + a c_2}{2(1+a)c_1 + (1+2a)c_2}\right\}_{y=0} \cdot \left(\frac{dc_1}{dy}\right)_{y=0} \tag{A.16}$$

When we consider the electrolysis of $CuSO_4$ solution containing an excessive amount of H_2SO_4 at the cathodic limiting current and it is assumed that the degree of the second stage dissociation of H_2SO_4 is complete, or, a = 1, it is seen that Eq. (A.14) through (A.16) are in coincidence with the following equations which were derived by Wagner.[1)]

$$\left(\frac{dc_2}{dy}\right)_{y=0} = -\frac{2}{3}\left(\frac{dc_1}{dy}\right)_{y=0} \qquad (A.17)$$

$$\left(\frac{dc_4}{dy}\right)_{y=0} = \frac{2}{3}\left(\frac{dc_1}{dy}\right)_{y=0} \qquad (A.18)$$

Reference to Appendix A

1) C. Wagner: J. Electrochem. Soc., 95 (1947) 161.

Nomenclature to Appendix A

A	surface area of electrode	(cm^2)
a	degree of dissociation of HSO_4^- ion	(-)
c_i	concentration of ionic species i	(mol/cm^3)
e_o	elementary electric charge	(= 1.602×10^{-19} coulomb)
F	Faraday constant	(= 96,500 coulombs/g-equiv.)
I	total electric current	(A)
k	Boltzmann constant	(= 1.3805×10^{-16} erg/K)
k_i	diffusivity of ionic species i	(cm^2/sec)
n_i	number of moles of ionic species i	(mol)
s_i	number of moles of ionic species i which reacts on the cathode surface per one Faraday	(mol/F)
T	absolute temperature	(K)
t	time	(sec)
u_i	ionic mobility of species i	($cm^2/sec \cdot volt$)
v	velocity of natural convective flow in horizontal direction	(cm/sec)
y	holizontal distance from cathode surface	(cm)
z_i	valency of ionic species i	(-)

Greek Letters

ϕ	potential	(volt)

subscripts

1	Cu^{2+} ion
2	H^{+} ion
3	HSO_4^{-} ion
4	SO_4^{2-} ion

Appendix B. Measurement of Diffusivity of $CuSO_4$ in Aqueous $CuSO_4$ and $CuSO_4$-H_2SO_4 Solutions

1. Introduction

Among the basic transport parameters used in the mass transfer calculation, the measurement and estimation of diffusivity in liquid are supposed to be less developed than the other parameters. In contrast to the diffusivity in a gas mixture which is independent of the partial pressure of the diffusing gas component and is precisely estimated by the Chapman-Enskog equation,[1] the diffusivity in liquid is usually dependent on the concentration of diffusing species because of the interaction with solvent, and the estimation is extremely difficult: it may only be possible to estimate the diffusivity in the extremely lower concentration region.[2] In the higher concentration region, on the other hand, no appropriate procedure of estimation has been proposed, and it may be a wise way to measure them rather than to hope to estimate from the theory.

In the electrolytic refining of copper, the aqueous solution containing $CuSO_4$ and H_2SO_4 is employed, and the cathodic current

density is affected by the rate of mass transfer of $CuSO_4$ in the cathodic diffusion layer.[3,4] Then it is indispensable to obtain the diffusivity of $CuSO_4$ for studying the distribution of cathodic current densities.

Among various experimental procedures of measuring the diffusivity, optical methods such as Schlieren[5] and interferometric methods[6] are prevalent and reliable. A modified Lamm scale method[7] using moiré pattern[8] was employed in the present work. The obtained moiré pattern represents the profile of the gradient of refractive index in the solution caused by the gradient of concentration of diffusing species, and the diffusivity at various concentrations is easily obtained.

2. Theoretical

When the diffusivity is dependent on the concentration of the diffusing species, Fick's second law of diffusion is represented in the form of

$$\frac{\partial c}{\partial t} = \frac{\partial}{\partial x}\left(D \frac{\partial c}{\partial}\right) \tag{B.1}$$

By applying the Boltzmann parameter[9] of

$$z' = x/\sqrt{t} \tag{B.2}$$

under the following initial and boundary conditions

$$c = c_1 \ (x < 0), \quad c = c_2 \ (x > 0) \quad \text{at } t = 0 \tag{B.3}$$

$$c = c_1 \ (x \to -\infty), \quad c = c_2 \ (x \to \infty) \quad \text{at } t = t \tag{B.4}$$

Eq, (B.1) is rewritten as

$$D = -\frac{1}{2}\frac{dz'}{dc}\int_{c_1}^{c_2} z'dc \tag{B.5}$$

or

$$D = -\frac{1}{2t\left(\frac{dc}{dx}\right)_{x=x'}}\int_{-\infty}^{x'} x\left(\frac{dc}{dx}\right)dx \tag{B.6}$$

It is seen from Eq. (B.6) that the diffusivity of the diffusing species is calculated from the profile of its concentration gradient which is established during the course of diffusion under the experimental conditions of Eq. (B.3) and (B.4).

A moiré pattern is composed of the points of intersection between two groups of parallel lines. When two groups of the parallel lines a_i and A_i are placed in a slanted position of a small angle θ as shown in Fig. B.1, moiré pattern is observed as a linear striped pattern represented by the line BB´. When a solution having a gradient of refractive index is placed between both groups of lines A_i and a_i at right angles to the lines a_i, the lines a_i are shifted to a new position of a_i', and the points of intersection are moved: for example, point P is shifted to point P´. Consequently, the curved moiré pattern of line BC is observed. The deviation, v, of the point of intersection from P to P´ is related to the local gradient of the refractive index, n, in the solution as[10]

$$v = k\frac{dn}{dx} \tag{B.7}$$

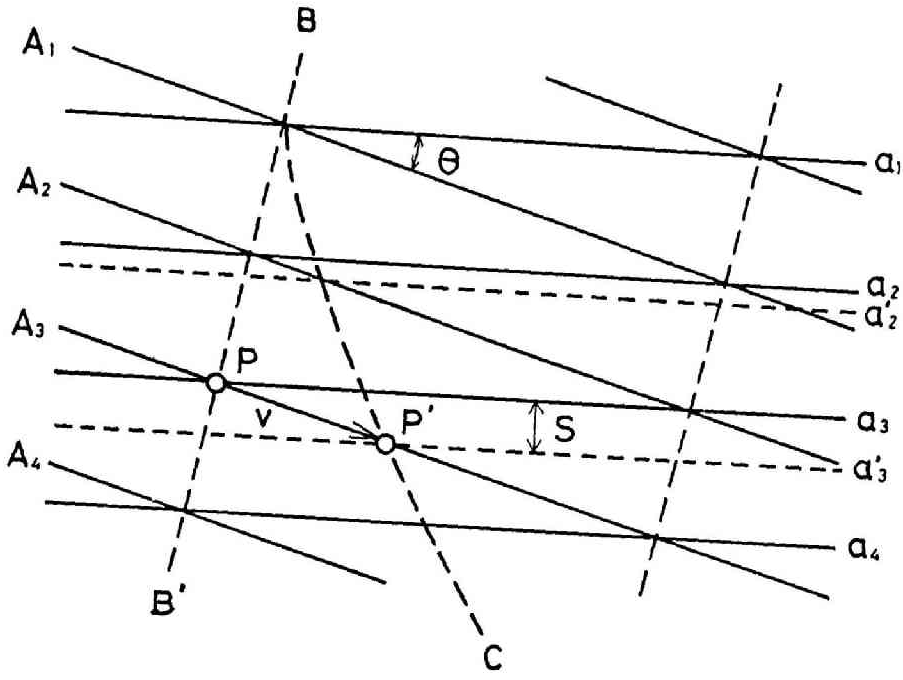

Fig. B.1 Principle of moiré pattern

where k is a constant. Presuming a linear relationship between the refractive index of the solution and the concentration of the diffusing species, the deviation v is proportional to the local concentration gradient of the species.

Substituting the numerical values of v measured from the moiré pattern in Eq. (B.6), the diffusivity of the species at a position x' is obtained: the local concentration gradient of the diffusing species at a position x' is related with the deviation v as

$$v = k' \frac{dc}{dx} \tag{B.8}$$

Then the integration of Eq. (B.8) under the following boundary conditions

$$\left.\begin{aligned} x &= -\infty \quad c = c_1 \\ x &= x' \quad c = c_{x'} \end{aligned}\right\} \tag{B.9}$$

yields

$$c_{x'} - c_1 = \frac{1}{k'} \int_{-\infty}^{x'} v\,dx \tag{B.10}$$

Furthermore, by integrating Eq. (B.8) between the concentration c_1 and c_2, we have

$$c_2 - c_1 = \frac{1}{k'} \int_{-\infty}^{\infty} v\,dx \tag{B.11}$$

Eliminating k' from Eq. (B.10) and (B.11), the following equation regarding the concentration of the diffusing species at $x = x'$ is obtained.

$$c_{x'} = c_1 + (c_1 - c_2) \cdot \frac{\int_{-\infty}^{x'} v\, dx}{\int_{-\infty}^{\infty} v\, dx} \qquad \text{(B.12)}$$

The denominator of the second term on the right hand side of Eq. (B.12) represents the area between the linear striped moiré patterns before and after the start of diffusion.

3. Experimental

3.1 Experimental Apparatus and Procedure

The experimental arrangement is schematically illustrated in Fig. B.2. It is composed of an optical system and a thermostat in which the diffusion cell is installed. The beam emitted from a laser light source was enlarged to a parallel beam of about 60 mm in diameter and transmitted to the diffusion cell. A helium-neon gas laser emitter of 1 mW output was used. Two transparent gratings of 100 lines per inch spacing were placed just in front of and in back of the windows of the thermostat at a slanted position of about 7° to 10° with each other, and their overlapped image forms a moiré pattern on a frosted glass plate located behind the second grating.

In order to avoid any vibration of the diffusion cell immersed in the thermostat, water of constant temperature was circulated through the thermostat from a separate heater. The diffusion

L : Laser Emitter
A,B : Lenses
P : Pinhole
G_1,G_2 : Gratings
D : Diffusion Cell
W : Water Bath
FG : Frosted Glass Plate
C : Camera

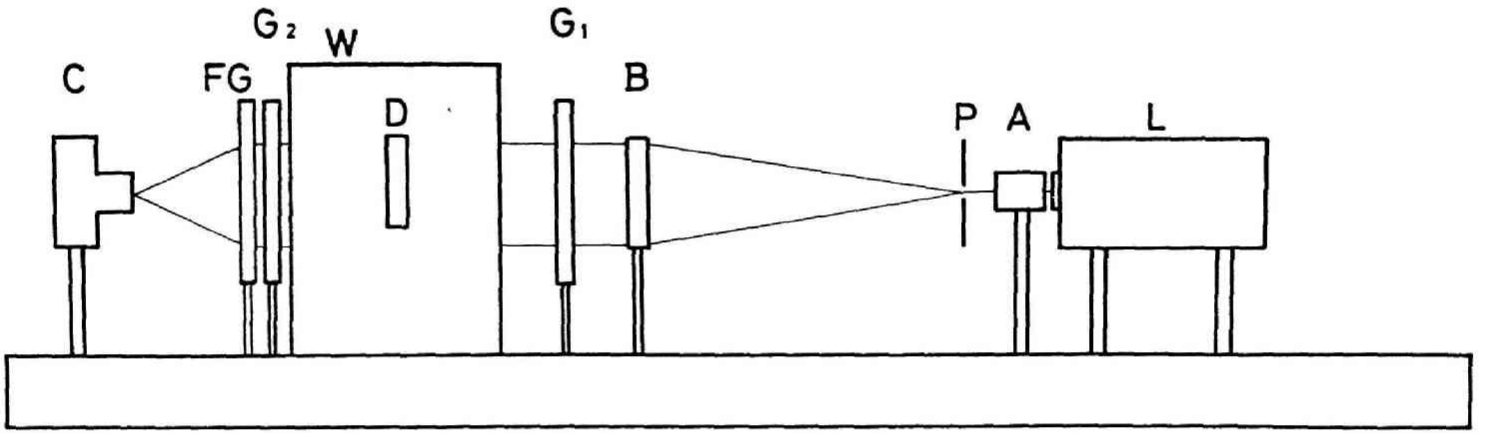

Fig. B.2 Experimental apparatus

cell used in this work is shown in Fig. B.3. It is composed of a rectangular cell of 6 cm high, 4 cm wide and 0.6 cm thick and a cylindrical glass reservoir of about 14 ml capacity: these cell and reservoir are linked together with a glass capillary of 0.1 cm inner diameter. Another glass capillary of 0.03 cm inner diameter and 50 cm long was connected to the upper end of the glass valve of the diffusion cell as an additional hydrodynamic resistance in order to reduce the transferring rate of solution from the glass reservoir to the diffusion cell. This is for minimizing the mixing of the solution near the two-solution interface.

Prior to the diffusivity measurement, two aqueous solutions of different $CuSO_4$ concentrations were prepared and maintained in the thermostat. The solution of lower concentration was poured into the diffusion cell to a half height, and the reservoir was filled with the solution of higher concentration. A small air bubble was left in the glass capillary between diffusion cell and reservoir in order to avoid the contact of both solutions. By adjusting the opening of the glass valves, the latter solution was gently transferred through the capillary from the reservoir to the cell due to the difference of static pressure. The solution in the cell was pushed up, and the two-solution interface was formed. Thus the diffusion of $CuSO_4$ in the upward direction was started. The moiré pattern of the solution was filmed at proper time intervals.

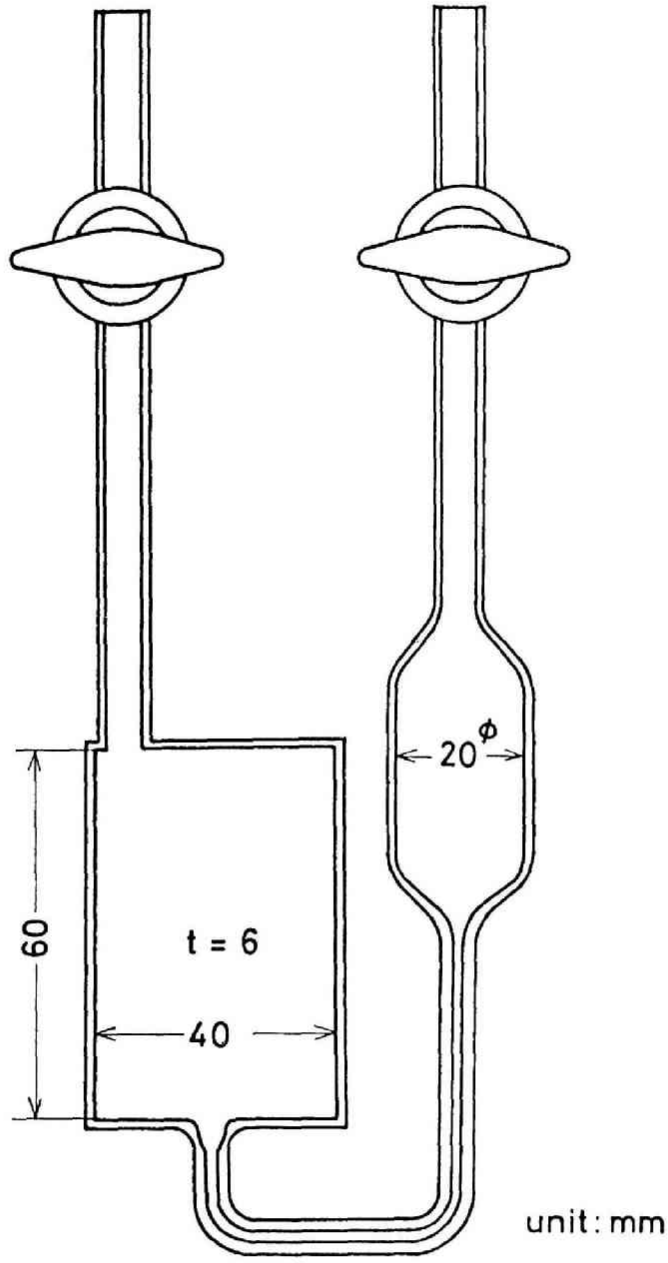

Fig. B.3 Diffusion cell

Analytical reagent grade H_2SO_4 and $CuSO_4 \cdot 5H_2O$ and deionized water were used, and the measurement of diffusivity was conducted with the solutions mentioned in Table B.1. Experimental temperature is also shown in the same table.

3.2 Experimental Results

An example of the moiré pattern is illustrated in Fig. B.4 which was filmed during Run 12 shown in Table B.1. The duration of diffusion was 24,000 sec. The curve that appears on the moiré pattern represents the local gradient of refractive index in the solution. The refractive index of aqueous $CuSO_4$ and $CuSO_4$-H_2SO_4 solutions of various concentrations was measured by using the Abbé refractometer at the temperatures of 25°, 40° and 55°C prior to the experiment of diffusion, respectively. It is seen from Fig. B.5 that the relationship between the refractive index of the aqueous solution and the concentration of $CuSO_4$ is linear. Similar linear relationship was obtained in the $CuSO_4$-H_2SO_4 solution at each temperature. Thus it is possible to calculate the diffusivity of $CuSO_4$ from the moiré pattern by applying Eq. (B.6).

An example of the concentration profile of $CuSO_4$ is calculated from Eq. (B.12) and shown in Fig. B.6. A graphical integration of the concentration profile as

$$q_x = \int_{-\infty}^{x} (c - c_1)dx \qquad (B.13)$$

Table B.1 Diffusion couples

Run	Composition of higher concentration solution		Composition of lower concentration solution		Temp. (°C)
	$CuSO_4$(M)	H_2SO_4(M)	$CuSO_4$(M)	H_2SO_4(M)	
11	1.0	0	0	0	25
12	1.0	0.6	0	0.6	25
13	0.8	1.2	0	1.2	25
14	0.72	1.85	0	1.85	25
15	1.2	0	0.6	0	25
21	0.8	0	0	0	40
22	0.8	0.6	0	0.6	40
31	0.8	0	0	0	55
32	0.8	0.6	0	0.6	55

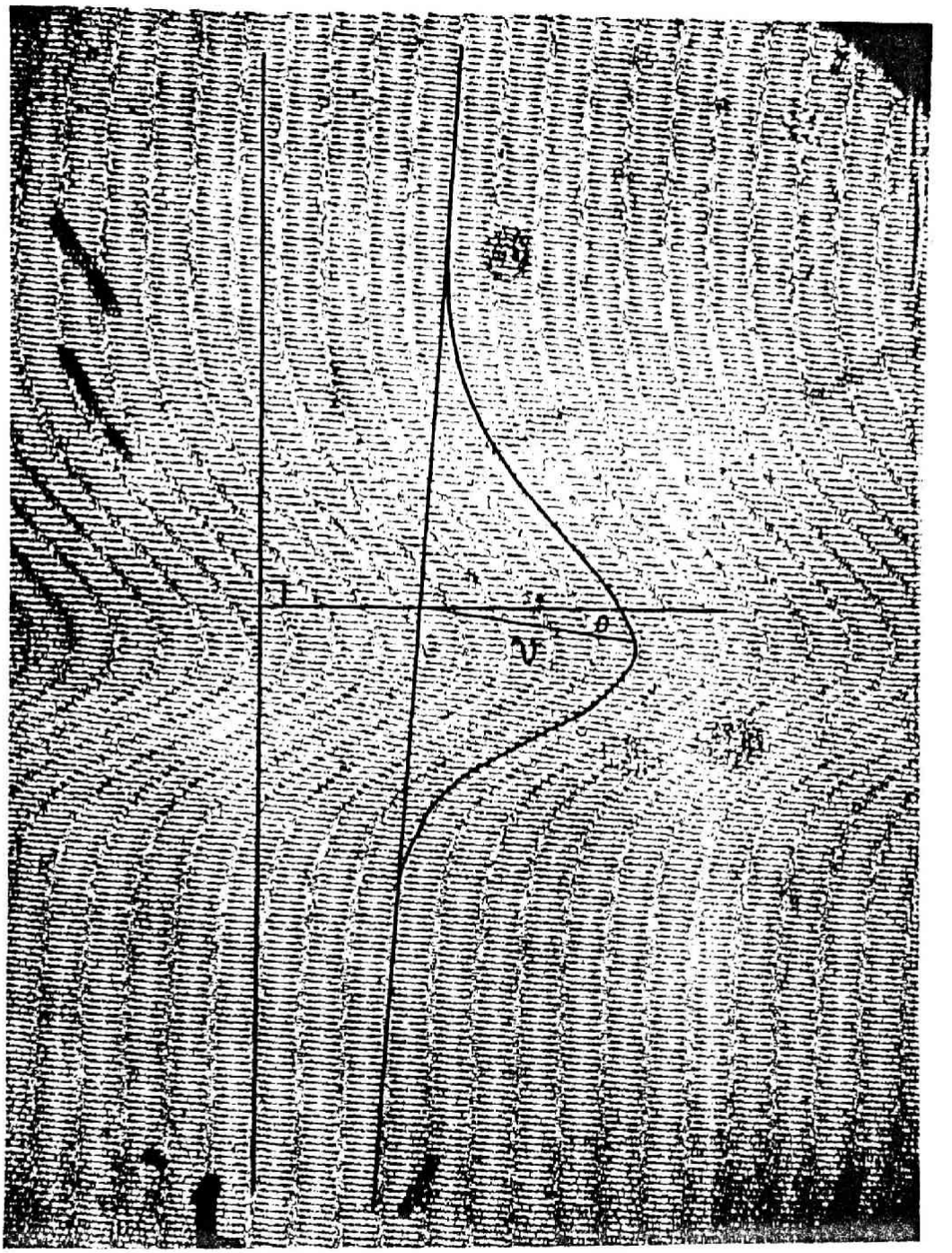

Fig. B.4 Moiré pattern

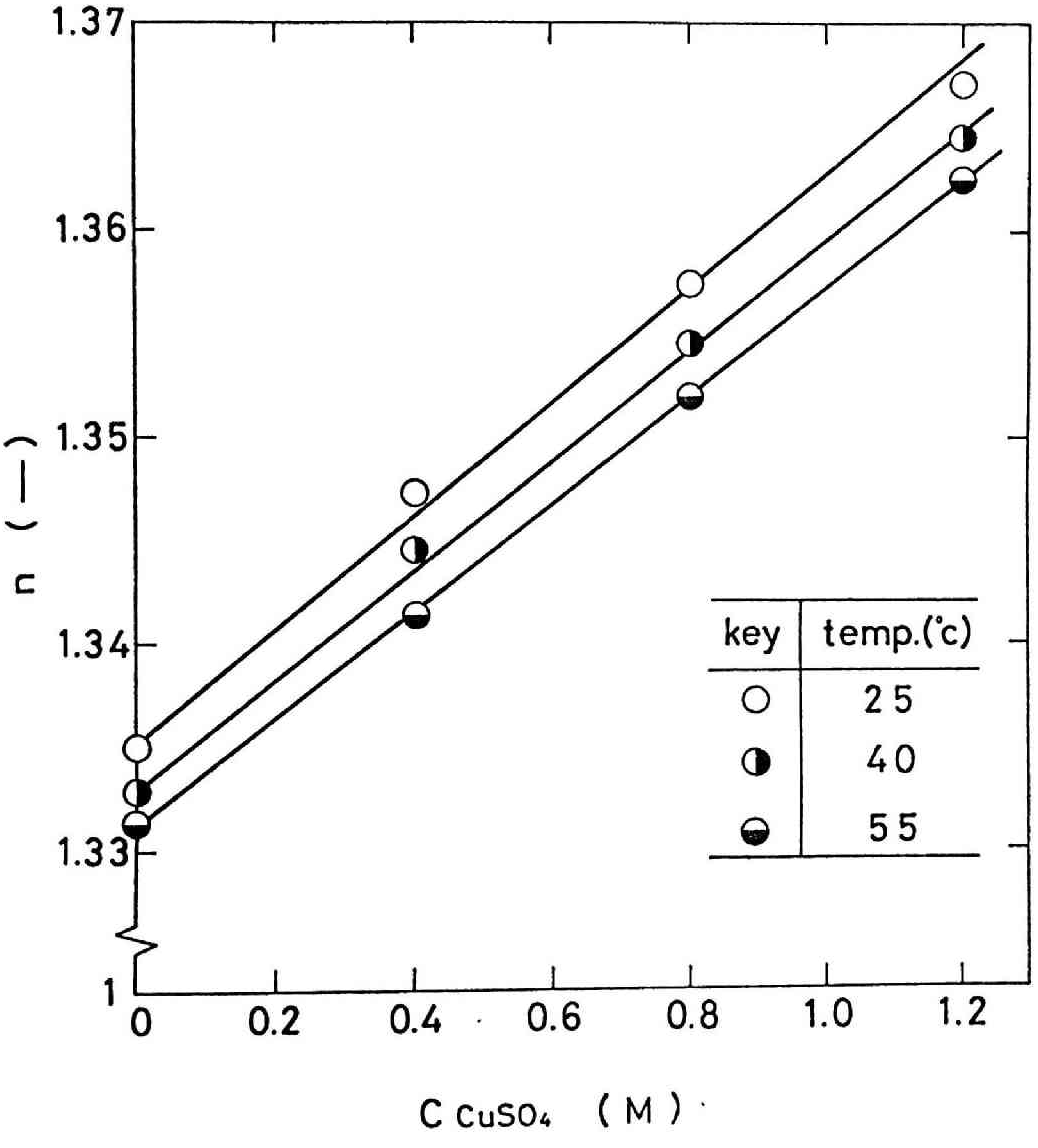

Fig. B.5 Relationship between refractive index of aqueous $CuSO_4$ solution and $CuSO_4$ concentration

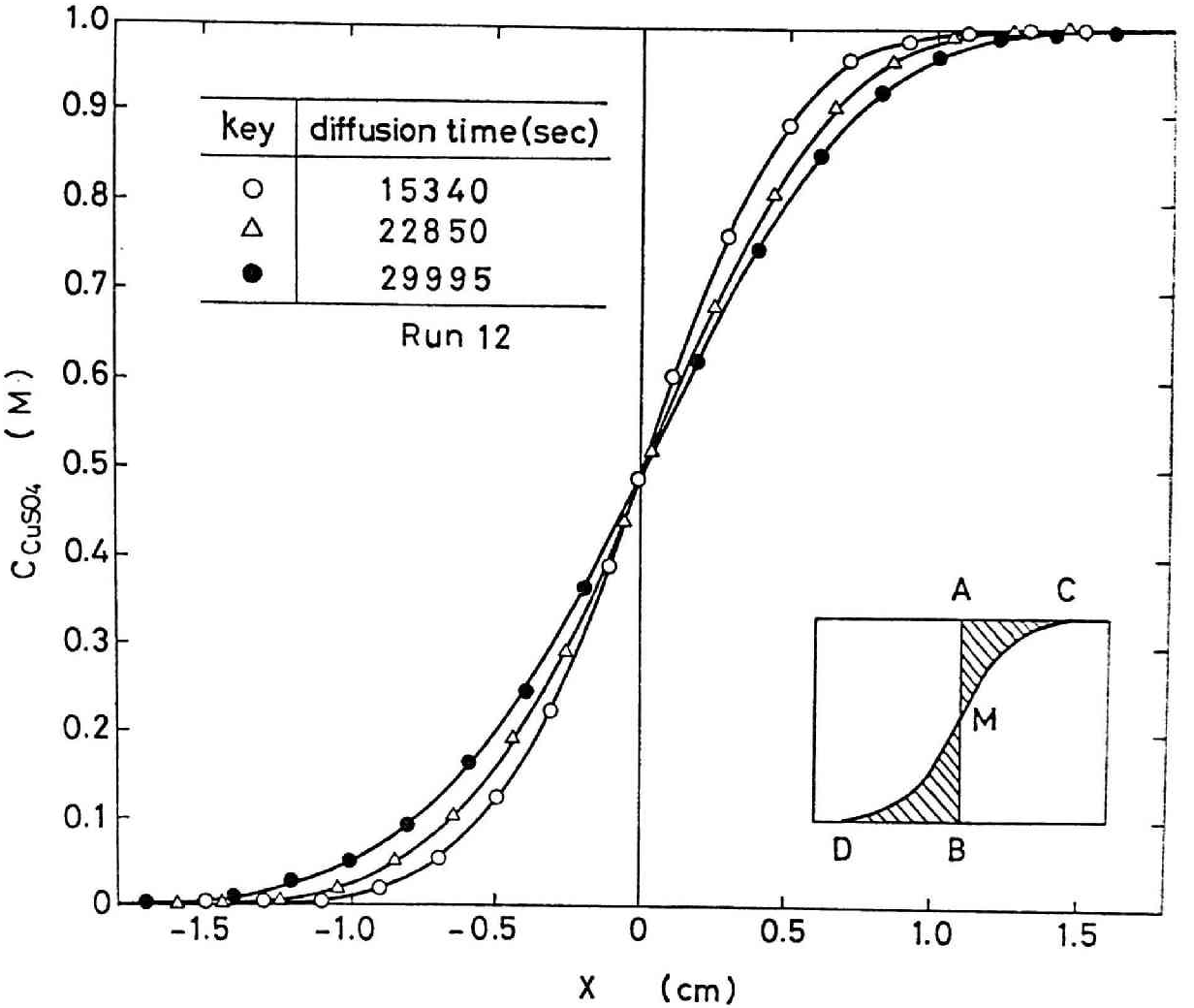
key
diffusion time(sec)
○ 15340
△ 22850
● 29995
Run 12
C_{CuSO_4} (M)
X (cm)
A
C
M
D
B

yields the amount of $CuSO_4$ transferred per unit area at a position x. The origin x = 0 is determined from the following mass balance equation

$$\int_{-\infty}^{0} (c - c_1)dx = \int_{0}^{\infty} (c_2 - c)dx \qquad (B.14)$$

which is also schematically illustrated in Fig. B.6.

The concentration profile shown in Fig. B.6 is further transformed into a curve shwon in Fig. B.7 in which $CuSO_4$ concentration and $z' = x/\sqrt{t}$ are taken as the ordinate and abscissa, respectively. It is evident from this figure that all concentration profiles shown in the figure are represented by a single curve, and the concentration is a function of $(x/\sqrt{t})$. Then

$$\frac{x}{\sqrt{Dt}} = k'' \qquad (B.15)$$

at a fixed concentration. In this equation, k'' is a constant.

The starting time of diffusion was corrected because of the unavoidable mixing of the two solutions near the interface at the start of diffusion where the solution of higher concentration was transferred from the glass reservoir to the diffusion cell.

In order to compensate the possible error in the determination of the origin x = 0, the following procedure was employed. Presuming that the determined origin is deviated a distance Δx from the true origin, the diffusion lengths $(x_A + \Delta x)$ and $(x_B + \Delta x)$ are obtained at two different levels of concentration c_A and c_B, respectively. Substitution of these diffusion lengths in

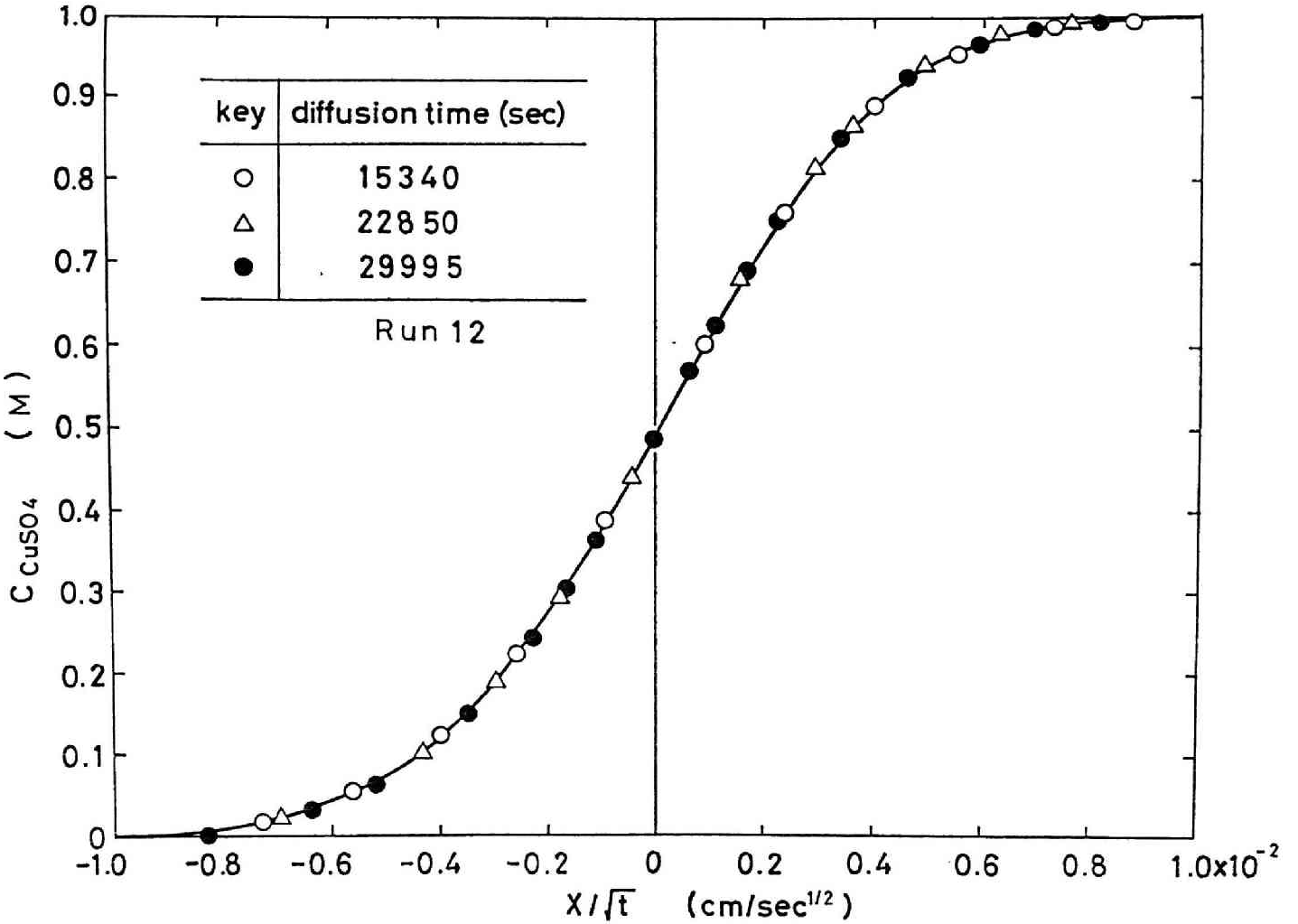

Fig. B.7 $CuSO_4$ concentration vs. Boltzmann parameter

Eq. (B.15) yields

$$\frac{x_A + \Delta x}{\sqrt{D_A t}} = k_A'' \tag{B.16}$$

and

$$\frac{x_B + \Delta x}{\sqrt{D_B t}} = k_B'' \tag{B.17}$$

respectively. From Eq. (B.16) and (B.17),

$$x_A - x_B = (k_A''\sqrt{D_A} - k_B''\sqrt{D_B})\sqrt{t} \tag{B.18}$$

in which the deviation Δx is not involved. Then it is possible to correct the starting time by using the linear relationship between $(x_A - x_B)^2$ and t shown in Fig. B.8: the group of straight lines obtained at various combinations of $CuSO_4$ concentration pass through a common intercept which is apart from the time origin by Δt. By adding Δt to the measured diffusion time, the diffusivity was calculated.

The measured diffusivities in the solutions mentioned in Table B.1 are summarized in Fig. B.9, B.10 and B.11.

4. Discussion

In order to ascertain the reliability of the measurement in the present work, it is necessary to investigate the correction of the starting time. The obtained time corrections Δt are summarized in Table B.2. In order to further examine these time corrections, holographic interferograms[11] were filmed in the vicinity of the two-solution interface. It is demonstrated

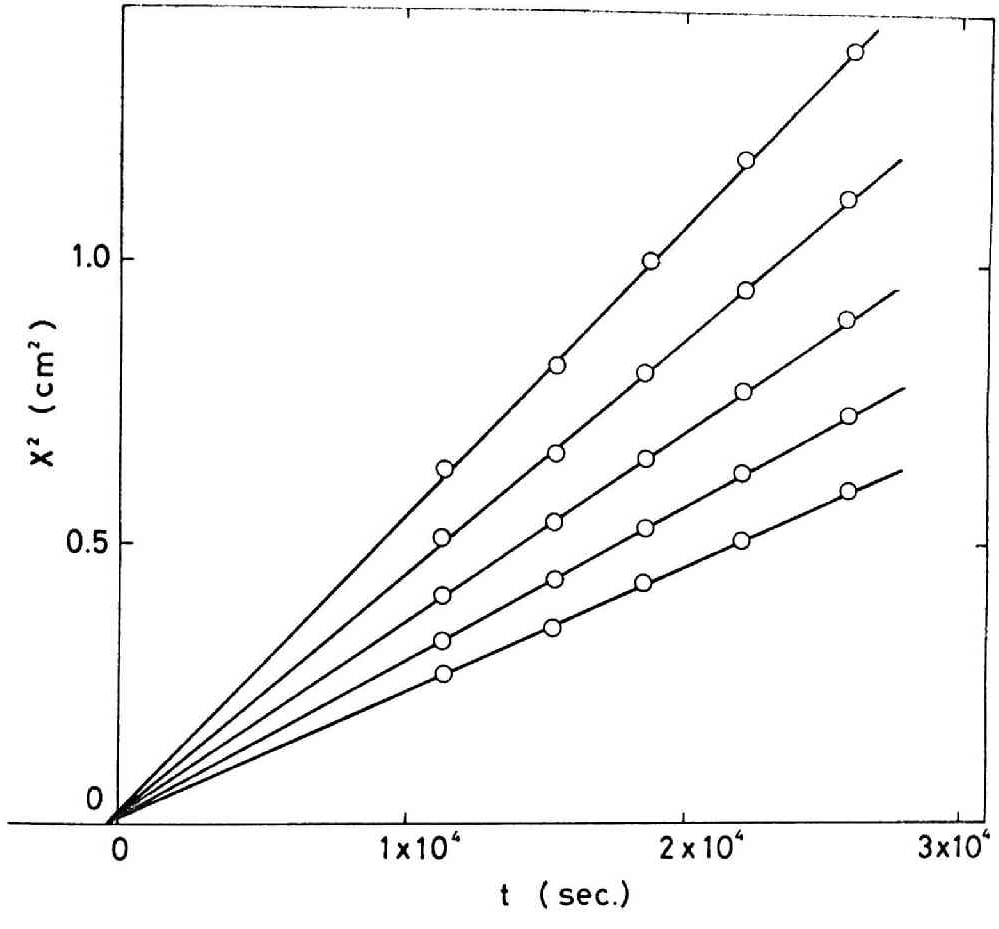

Fig. B.8 Determination of the time origin

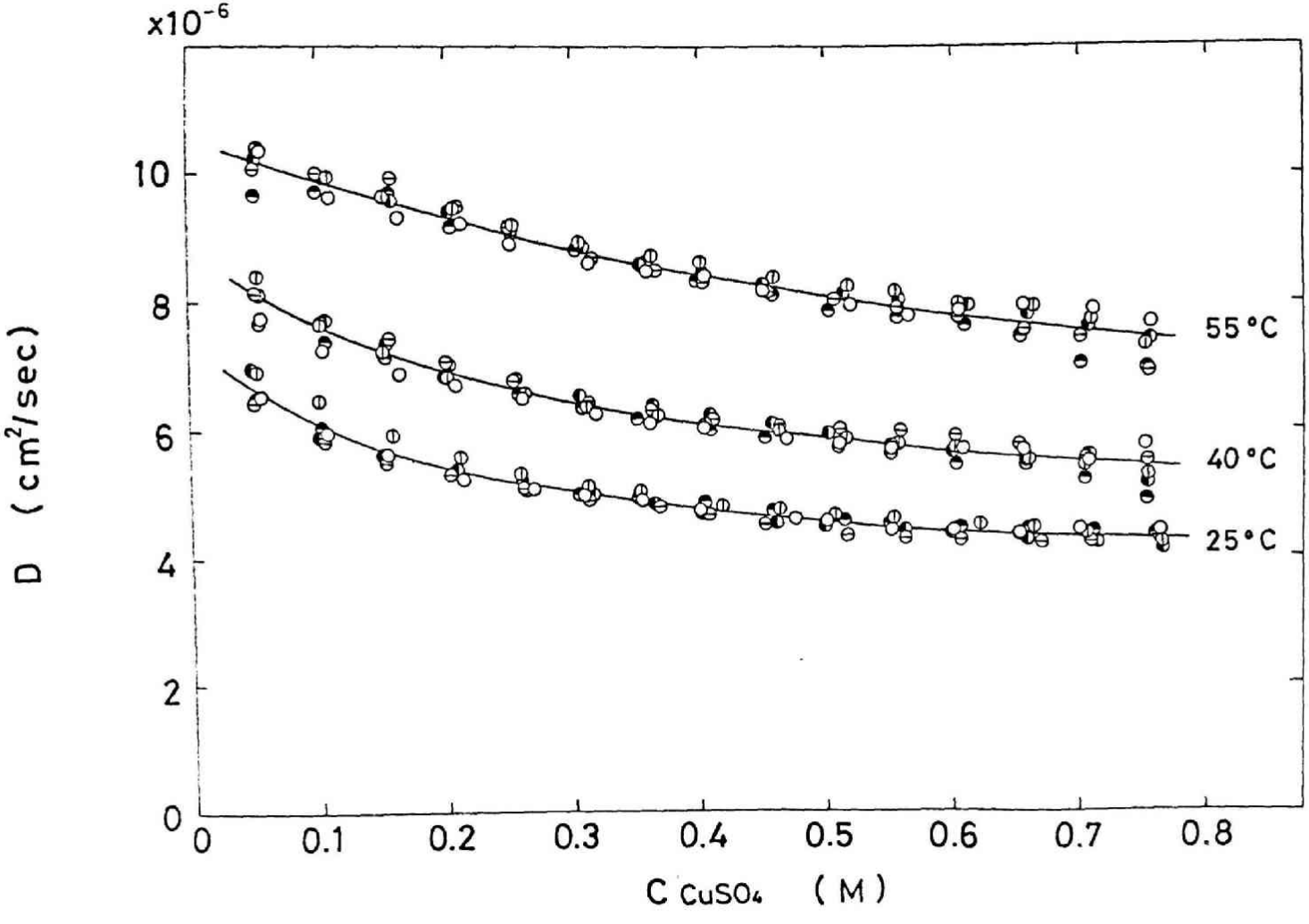

Fig. B.9 Diffusivity of $CuSO_4$ in aqueous $CuSO_4$ solution (Run 11, 21, 31)

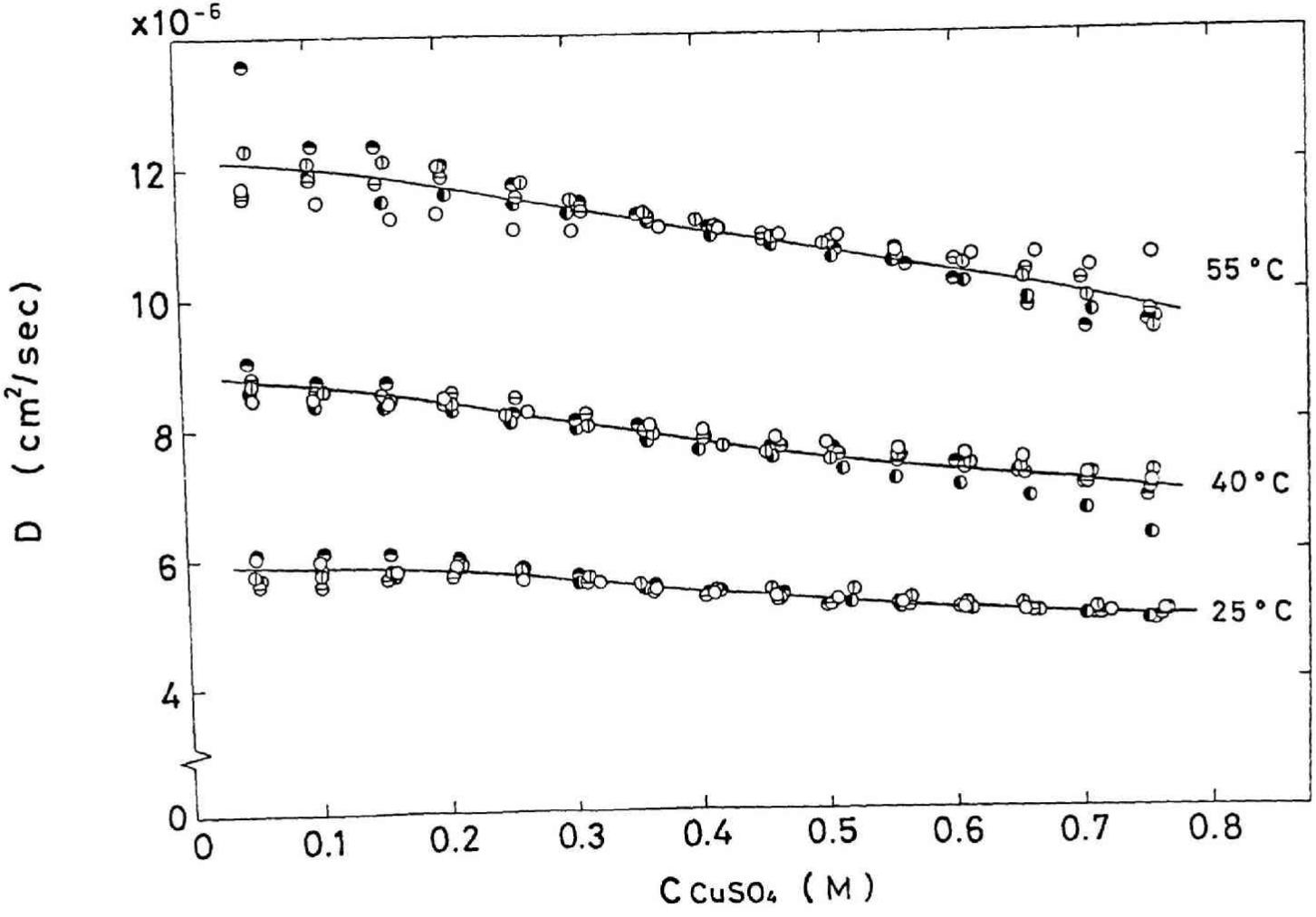

Fig. B.10 Diffusivity of $CuSO_4$ in aqueous $CuSO_4$-0.6M H_2SO_4 solution

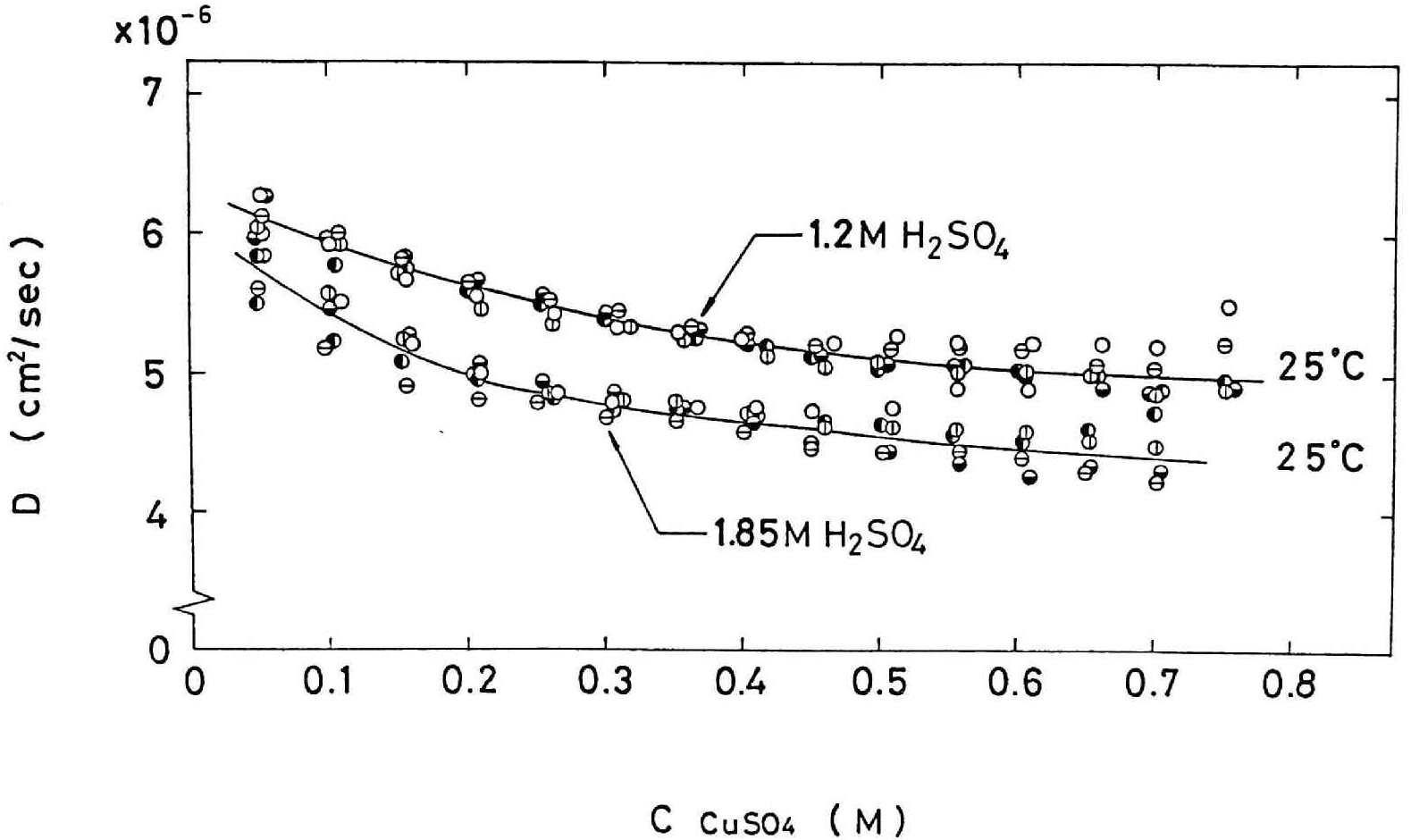

Fig. B.11 Diffusivity of $CuSO_4$ in aqueous $CuSO_4$-1.2M H_2SO_4 and $CuSO_4$-1.85M H_2SO_4 solutions (Run 13, 14)

Table B.2 Time correction

Run	Δt (sec)
11	-92
12	-223
13	-829
14	-2292
15	-79
21	-702
22	-396
31	-609
32	-139

in Fig. B.12 through B. 14.

Figure B.12 was filmed just after the passage of the air bubble through the diffusion cell: it is seen that the air bubble is escaping from the center of solution surface. A trivial disturbance of interference fringes is observed along the rising path of the bubble: this is caused by the mixing of the solution of higher concentration accompanied by the air bubble. Figure B.13 was filmed at 32 sec after the passage of the bubble. It is seen that the disturbance of fringes almost disappears and that the two-solution interface is being formed: curved fringes are observed at the bottom of the diffusion cell. Third holographic interferogram was taken at 240 sec after the passage of bubble and is illustrated in Fig. B.14. It is seen that a diffusion zone of 0.5 to 0.6 cm thickness is formed at the interface.

It is possible to estimate an approximate value of Δt from the holographic interferograms under the assumption that the diffusivity is unvaried. An enlarged holographic interferogram of the diffusion zone is demonstrated in Fig. B.15 which was filmed at 4,800 sec after the start of diffusion. With the procedure shown in this figure, the distance x which corresponds to a constant concentration difference was measured at different diffusion times between 600 and 36,000 sec, and x^2 was plotted against t. By applying the least squares method, the intercept at $x = 0$ was calculated, and $\Delta t = -138$ sec was obtained. This value of time correction is in the same order of magnitude

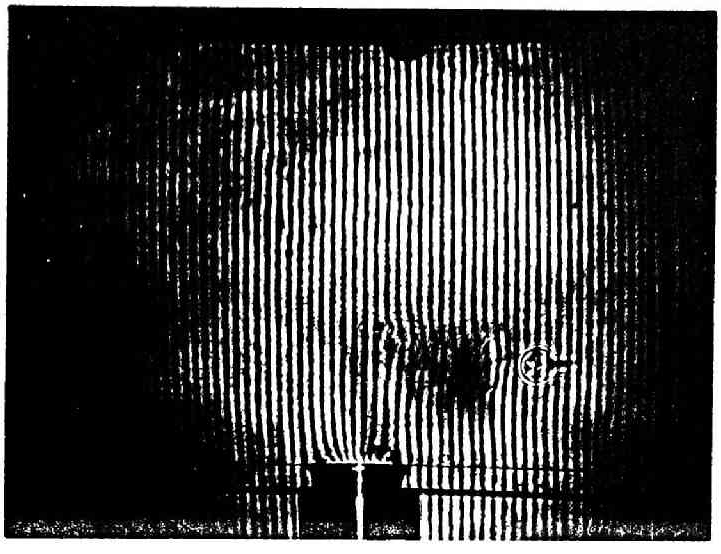

Fig. B.12 Holographic interferogram at the start of diffusion

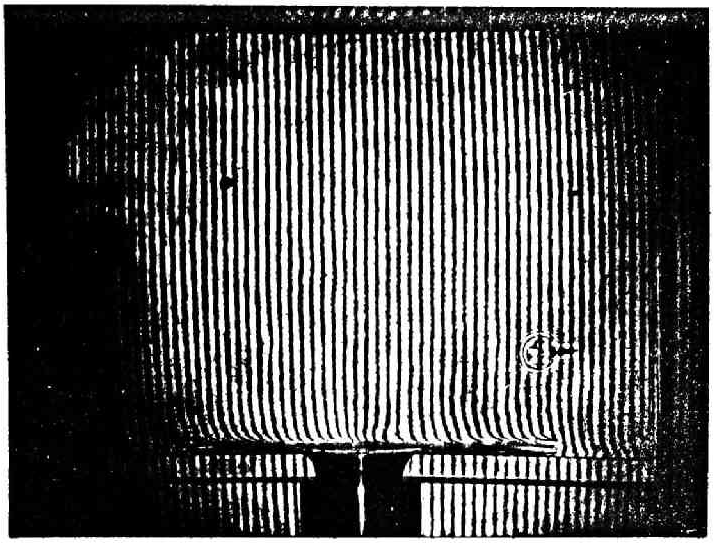

Fig. B.13 Holographic interferogram

(after 32 sec)

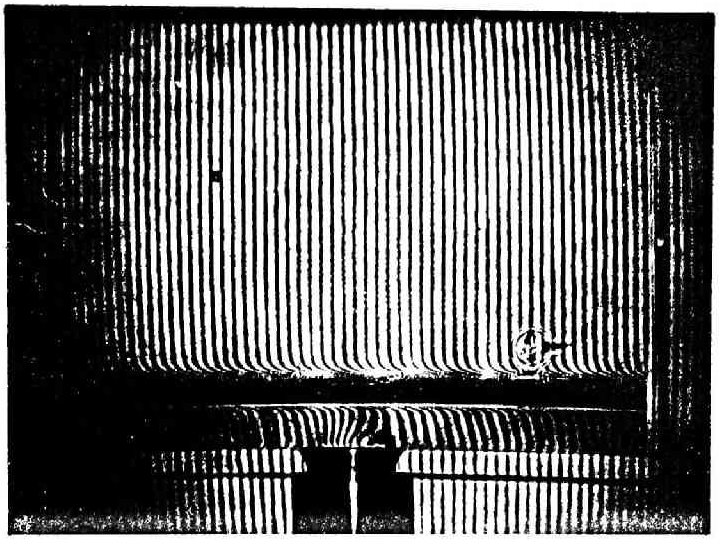

Fig. B.14 Holographic interferogram

(after 240 sec)

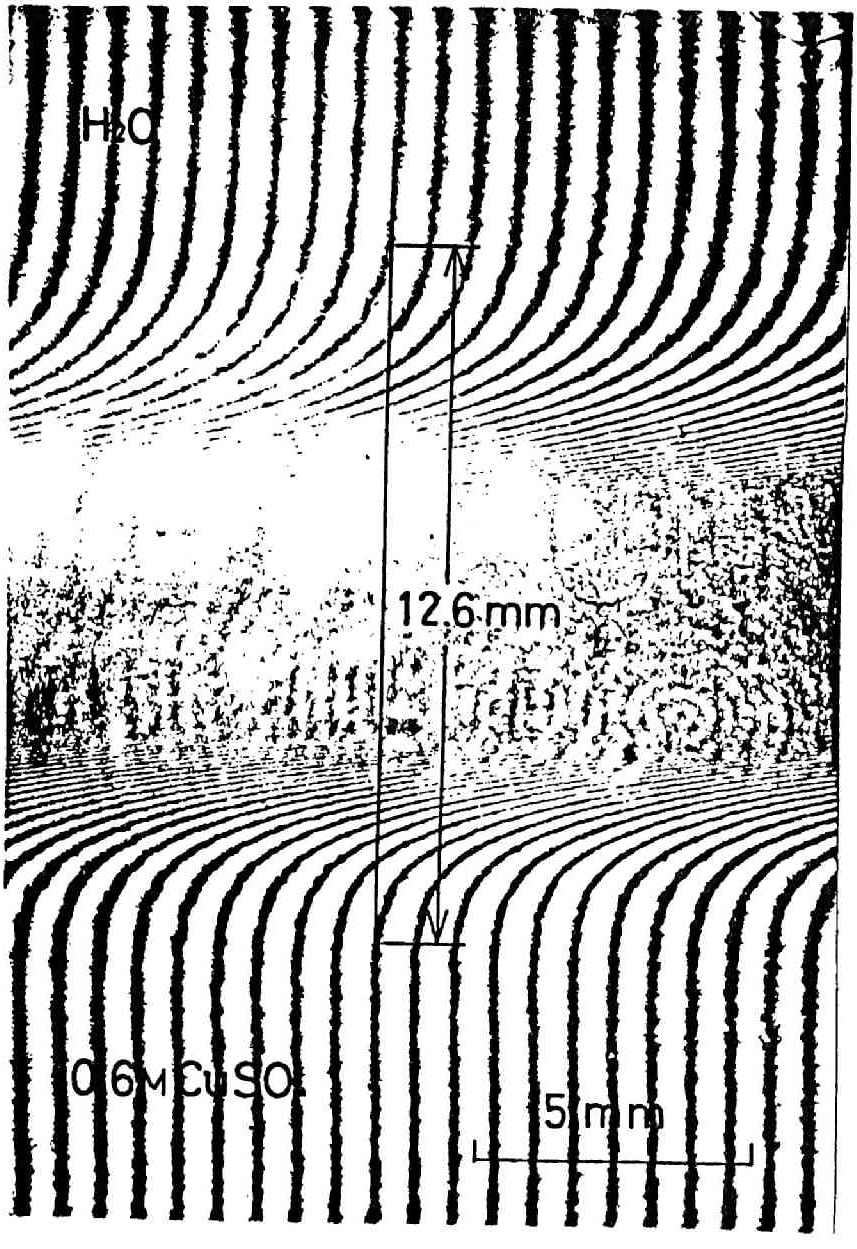

Fig. B.15 Enlarged holographic interferogram near the interface (after 4,800 sec)

as those mentioned in Table B.2. It may be said that the obtained values of time correction are reasonable.

It was already mentioned that the graphical integration of a moiré pattern was carried out in order to obtain the diffusivity. The precision of this graphical integration was also examined: the deviation of moiré pattern was independently measured by three individuales, and the obtained diffusivities were comapred with each other. It was revealed that these diffusivities coincided very well within the experimental error.

It was also supposed that the precision of the deviation measurement is lowered in the region where the concentration gradient is small. In order to examine this, the diffusivity was tried to be measured with two diffusion couples of 0.6M $CuSO_4$ solution-1.2M $CuSO_4$ solution (Run 15) and H_2O-1.0M $CuSO_4$ solution (Run 11), and the obtained diffusivities were compared. As seen in Fig. B.16, the difference of diffusivities at about 0.6M $CuSO_4$ is very minor, and the possible error of measurement in the region of small concentration gradient is omitted.

As seen in Fig. B.9, B.10 and B.11, the diffusivity of $CuSO_4$ is more dependent on $CuSO_4$ concentration in the lower concentration region in aqueous $CuSO_4$ solution than in the higher concentration region: the numerical values of diffusivity are in good coincidence with the diffusivity obtained by Cole[12] using a sintered glass disphragm in the lower concentration region.

It is also seen that the diffusivity of $CuSO_4$ in the aqueous

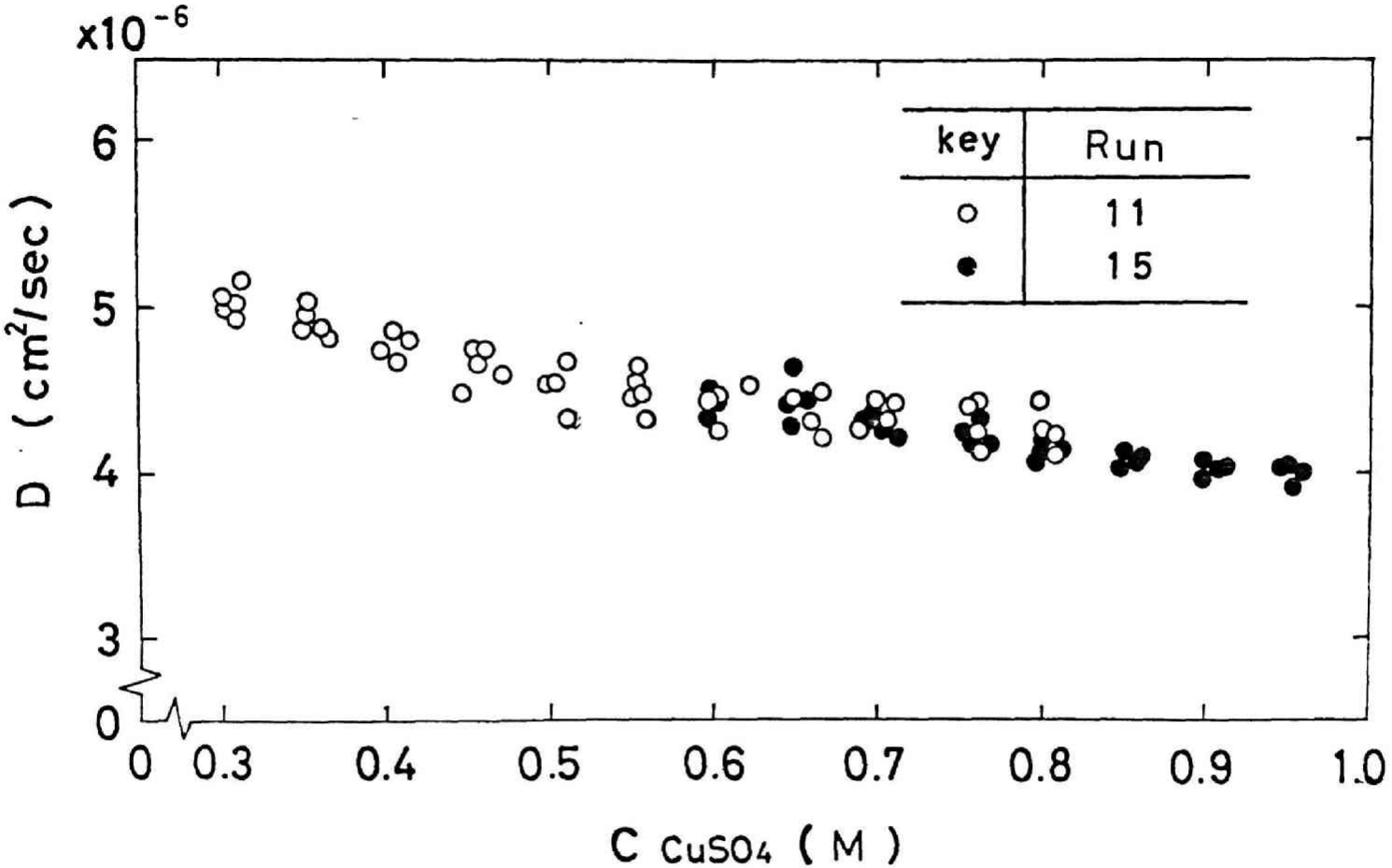

Fig. B.16 Diffusivity of $CuSO_4$ obtained from Runs 11 and 15

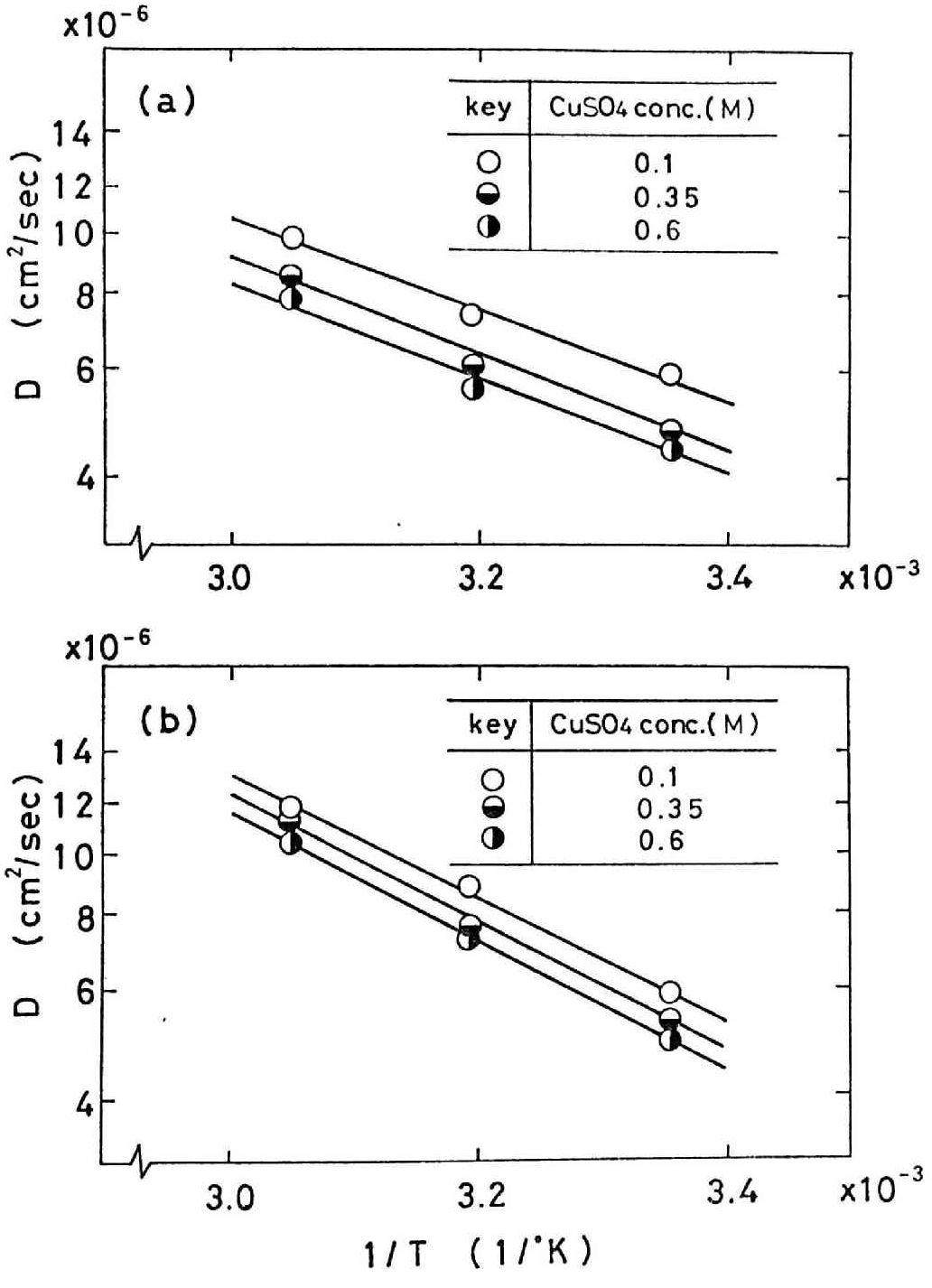

Fig. B.17 Arrhenius plot of diffusivity
(a): aqueous $CuSO_4$ solution
(b): aqueous $CuSO_4$-0.6M H_2SO_4 solution

$CuSO_4$-H_2SO_4 solutions whose H_2SO_4 concentration is 0.6 and 1.2M, respectively, is higher than the diffusivity in the aqueous $CuSO_4$ solution. The higher diffusivity in aqueous $CuSO_4$-H_2SO_4 solutions is thought to be attributed to the presence of large amount of H^+ ion in the solution; the local electroneutrality accompanied by the diffusion of Cu^{2+} ion is easily attained, and the interaction between Cu^{2+} and SO_4^{2-} ions is reduced.

When H_2SO_4 concentration is further raised, on the contrary, the diffusivity is lowered: the diffusivity in the solution containing $CuSO_4$ and 1.85M H_2SO_4 solution is slightly lower. This phenomenon was also observed by Cole.[12] The lowered diffusivity in this solution is supposed to be caused by the increased viscosity.

In order to obtain the activation energy, the diffusivity of $CuSO_4$ was measured at 25°, 40° and 55°C in the aqueous $CuSO_4$ and $CuSO_4$-0.6M H_2SO_4 solutions, respectively. Arrhenius plots are demonstrated in Fig. B.17. The activation energies in these two solutions are 3.6 and 4.6 kcal/mol, respectively, which are again in good coincidence with the reported values.[6,13]

5. Summary

The diffusivity of $CuSO_4$ in the aqueous solutions containing $CuSO_4$ and $CuSO_4$-H_2SO_4 was measured by the modified Lamm scale method using moiré pattern. In order to reduce the error of

the measurement, a few improvements were made.

Firstly, an additional hydrodynamic resistance was attached to the diffusion cell in order to reduce the transferring rate of the solution to the cell, thus minimizing the mixing of solutions near the two-solution interface. It was confirmed with the holographic interferometry that the mixing of the solutions at the start of diffusion was reduced to a large extent. The time correction Δt was calculated from the plot of $(x_A - x_B)^2$ vs. t in which the possible deviation Δx was not involved. Thus the reproducibility of the measurement was significantly improved.

Secondly, the precision in the graphical integration of the moiré pattern was examined: it was revealed that the diffusivities independently calculated by three individuals coincided very well within the experimental error and that the possible error of the measurement in the region of small concentration gradient was very minor.

The obtained diffusivities were in excellent agreement with those of the previous workers. The diffusivity becomes higher when H_2SO_4 is added to the aqueous $CuSO_4$ solution, and it decreases again when the H_2SO_4 concentration is higher. The obtained activation energies of diffusion were 3.6 and 4.6 kcal/mol in the aqueous $CuSO_4$ and $CuSO_4$-0.6M H_2SO_4 solutions, respectively, which are again in good coincidence with those of previous workers.

Reference to Appendix B

1) R. B. Bird, W. E. Stewart and E. N. Lightfoot: "Transport Phenomena", p. 510 (1960), John Wiley and Sons, Inc., New York.

2) C. R. Wilke and P. Chang: AIChE Journ., 1 (1955) 264.

3) C. Wagner: J. Electrochem. Soc., 95 (1949) 161.

4) G. H. Keulegan, J. Res. National Bur. Standards, 47 (1951) 156.

5) T. Takamatsu, S. Hiraoka, Y. Inoue and A. Osugi: Kagaku Kogaku, 28 (1964) 451.

6) R. N. O'Brien and C. Rosenfield: J. Phys. Chem., 67 (1963) 643.

7) H. Nuerath: Chem. Rev., 30 (1942) 357.

8) K. Sato, S. Hoshino and K. Miyamoto: Kagaku Kogaku, 28 (1964) 445.

9) L. Boltzmann: Ann. Physik, Leibzig, 53 (1849) 959.

10) E. Münter: Ann. Physik, 11 (1931) 558.

11) E. Yeager and A. J. Salkind: "Techniques of Electrochemistry", vol. 2, p. 144 (1973), John Wiley and Sons, Inc., New York.

12) A. F. W. Cole and A. R. Gordon: J. Phys. Chem., 40 (1936) 736.

13) Y. Maru, S. Ito, S. Oyama and Y. Kondo: Denki Kagaku, 38 (1970) 343.

Nomenclature to Appendix B

c	concentration of $CuSO_4$	(mol/cm^3)
c_1	concentration of $CuSO_4$ in the solution of lower concentration	(mol/cm^3)
c_2	concentration of $CuSO_4$ in the solution of higher concentration	(mol/cm^3)
$c_{x'}$	concentration of $CuSO_4$ at $x = x'$	(mol/cm^3)
D	diffusivity of $CuSO_4$	(cm^2/sec)
D_A	diffusivity of $CuSO_4$ at $c = c_A$	(cm^2/sec)
D_B	diffusivity of $CuSO_4$ at $c = c_B$	(cm^2/sec)
k	proportionality constant between v and local gradient of refractive index	(cm^2)
k'	proportionality constant between v and local gradient of concentration	(cm^3/mol)
k_A'', k_B''	constants	(-)
n	refractive index of solution	(-)
t	time	(sec)
v	deviation from a linear striped moiré pattern	(cm)
x	vertical distance from two-solution interface	(cm)
x'	vertical distance at $c = c_{x'}$ from two-solution interface	(cm)
x_A	diffusion length at $c = c_A$	(cm)
x_B	diffusion length at $c = c_B$	(cm)
Δx	possible error in the determination of origin	(cm)

z' Boltzmann parameter $(cm/sec^{1/2})$

Appendix C. Dissociation of H_2SO_4

Complete dissociation of H_2SO_4 into H^+ and SO_4^{2-} ions was often assumed in the previous works[1,2] on the ionic mass transfer in the cathodic diffusion layer during the electrolysis of aqueous solution containing $CuSO_4$ and H_2SO_4. It is well known, on the other hand, that H_2SO_4 is dissociated in two steps among which the first stage dissociation of H_2SO_4 into H^+ and HSO_4^- ions is complete and the second stage dissociation of HSO_4^- into H^+ and SO_4^{2-} ions is incomplete in the aqueous H_2SO_4 solution of higher concentrations. Since the dissociation of H_2SO_4 plays an important role in the studies on the ionic mass transfer in the cathodic diffusion layer of aqueous $CuSO_4$-H_2SO_4 solution, the dissociation of H_2SO_4 was further studied in the present work in the aqueous $CuSO_4$-H_2SO_4 solutions on the basis of the works of Young et al.[3] and Hsueh and Newman.[4]

The dissociation constant of HSO_4^- ion into H^+ and SO_4^{2-} ions defined by the following equation is reported as[4]

$$K_{HSO_4^-} = \frac{a_{H^+} a_{SO_4^{2-}}}{a_{HSO_4^-}} = 0.01 \qquad (C.1)$$

at 25°C. The dissociation constant, $K_{HSO_4^-}$, in this equation

is a thermodynamic dissociation constant and it is related to the apparent dissociation constant expressed with the ionic concentration as

$$K'_{HSO_4^-} = \frac{c_{H^+} \cdot c_{SO_4^{2-}}}{c_{HSO_4^-}} \tag{C.2}$$

and

$$K'_{HSO_4^-} = K_{HSO_4^-} \cdot \frac{f_{HSO_4^-}}{f_{H^+} \cdot f_{SO_4^{2-}}} \tag{C.3}$$

where f_i is the activity coefficient of the ionic species i. Then $K'_{HSO_4^-}$ is a function of the true ionic strength of the solution in the form of

$$I_r = \frac{1}{2} \Sigma c_i z_i^2 \tag{C.4}$$

where c_i is the equilibrium concentration of the ionic species i which is determined by the dissociation equilibrium of HSO_4^-.

Young et al.[3] measured the concentration of HSO_4^- in the aqueous H_2SO_4 solution of various concentrations by applying a technique of Raman spectral analysis. Hsueh and Newman[4] correlated $K'_{HSO_4^-}$ obtained from the Raman spectral analysis with the true ionic strength in the form of the following expression. It is

$$\ln \frac{K'_{HSO_4^-}}{K_{HSO_4^-}} = \frac{5.29\sqrt{I_r}}{1 + 0.56\sqrt{I_r}} \tag{C.5}$$

By applying Eq. (C.5), the degree of the second stage dissociation

of H_2SO_4 in the aqueous solutions employed in the present work was calculated. The results of calculation are summarized in Table C.1. In this table the notation a represents the degree of the second stage dissociation of HSO_4^-. It was further assumed in this calculation that H_2SO_4 is completely dissociated into H^+ and HSO_4^- ions in the first stage of dissociation.

It is seen from this table that HSO_4^- ion is not completely dissociated but the degree of the second stage dissociation is only about 0.3.

Table C.1 The apparent dissociation constant of HSO_4^- ion into H^+ and SO_4^{2-} ions and the degree of dissociation of HSO_4^- ion in aqueous $CuSO_4$-H_2SO_4 solutions of various compositions

No.	$c_{H_2SO_4}$ (M)	c_{CuSO_4} (M)	K_2' (M)	I_r (M)	a (-)	Ref.
1	1.5	0.6	1.80	4.76	0.29	Chapter 3
2	1.85	0.01	1.09	3.04	0.31	Chapter 4
3	1.85	0.02	1.11	3.08	0.31	
4	1.85	0.03	1.13	3.11	0.31	
5	1.85	0.04	1.15	3.13	0.31	
6	1.85	0.05	1.17	3.21	0.31	
7	1.85	0.1	1.26	3.39	0.31	Chapter 5
8	1.473	0.0999	0.97	2.73	0.30	Hsueh and Newman[4]
9	2.95	0	1.92	4.89	0.33	Young et al.[3] (the experimental data of Raman spectroscopy)
10	1.85	0	1.08	3.00	0.33	
11	1.47	0	0.816	2.35	0.30	

Reference to Appendix C

1) C. Wagner: J. Electrochem. Soc., 95 (1947) 161.

2) K. Asada, F. Hine, S. Yoshizawa and S. Okada: J. Electrochem. Soc., 107 (1960) 242.

3) T. F. Young, L. F. Maranville and H. M. Smith: "The Structure of Electrolytic Solutions", ed. by W. J. Hamer, p. 35, Wiley and Sons, New York (1959).

4) L. Hsueh and J. Newman: Ind. Chem. Fund., 10 (1971) 615.

Nomenclature to Appendix C

a	degree of dissociation of HSO_4^- ion	(-)
a_{n^+}	activity of H^+ ion	(mol/l)
$a_{HSO_4^-}$	activity of HSO_4^- ion	(mol/l)
$a_{SO_4^{2-}}$	activity of SO_4^{2-} ion	(mol/l)
c_i	concentration of ionic species i	(mol/l)
c_{H^+}	concentration of H^+ ion	(mol/l)
$c_{HSO_4^-}$	concentration of HSO_4^- ion	(mol/l)
$c_{SO_4^{2-}}$	concentration of SO_4^{2-} ion	(mol/l)
f_{H^+}	activity coefficient of H^+ ion	(-)
$f_{HSO_4^-}$	activity coefficient of HSO_4^- ion	(-)
$f_{SO_4^-}$	activity coefficient of SO_4^{2-} ion	(-)
I_r	true ionic strength	(mol/l)
$K_{HSO_4^-}$	thermodynamic dissociation constant	(mol/l)
$K'_{HSO_4^-}$	apparent dissociation constant	(mol/l)
z_i	valency of ionic species i	(-)

Appendix D. Densification Coefficient of H^+ Ion in the Integrated Navier-Stokes Equation

When the electrolysis takes place with the vertical plane electrodes installed in an unstirred solution containing $CuSO_4$ and H_2SO_4, the integrated Navier-Stokes equation for the natural convective flow along the cathode surface is expressed by the following equation. It is

$$\frac{d}{dx}\int_0^{\ell} u^2 dy = \alpha_1 g \int_0^{\ell} (c_1 - {}^*c_1)dy + \alpha_2 g \int_0^{\ell} (c_2 - {}^*c_2)dy - {}^*\nu\left(\frac{du}{dy}\right) \tag{D.1}$$

where the subscripts 1 and 2 denote Cu^{2+} and H^+ ions, respectively. The first and second terms on the right-hand side of Eq. (D.1) represent the buoyancy force acting on an infinitesimal volume element of the solution in the cathodic diffusion layer. The buoyancy force is determined solely by the density difference of the solution between the diffusion layer and the bulk-electrolyte.

The density of an aqueous solution is a function of the composition of this solution. With regard to an aqueous solution containing $CuSO_4$ and H_2SO_4, the density is determined by the concentrations of Cu^{2+} ion and H^+ ion even though the solution con-

tains four types of ions, Cu^{2+}, H^{+}, HSO_4^{-} and SO_4^{-}. It is because the concentrations of these ions are to satisfy the relationships of the electroneutrality and the dissociation equilibrium of HSO_4^{-} into H^{+} and SO_4^{-} ions.

The densification coefficients with which the concentration of a certain species is related to the density of the solution are measured and represented by the salt concentration such as c_{CuSO_4} and $c_{H_2SO_4}$: they are defined as follows.

$$\beta_{CuSO_4} = \frac{\partial \ln \rho}{\partial c_{CuSO_4}}$$
$$\beta_{H_2SO_4} = \frac{\partial \ln \rho}{\partial c_{H_2SO_4}} \qquad (D.2)$$

Assuming that the dissociation of $CuSO_4$ is complete, the densification coefficient of Cu^{2+} ion, α_1, is demonstrated as

$$\alpha_1 = \beta_{CuSO_4} \qquad (D.3)$$

It is known, on the other hand, regarding H_2SO_4 that the first stage dissociation is complete and the second stage dissociation is incomplete. Presuming that the degree of the second stage dissociation is denoted by a, the densification coefficient of H^{+} ion, α_2, is related to $\beta_{H_2SO_4}$ as

$$\alpha_2 = \frac{1}{1+a} \beta_{H_2SO_4} \qquad (D.4)$$

Nomenclature of Appendix D

a	degree of dissociation of HSO_4^- ion	(-)
c_1	concentration of Cu^{2+} ion	(mol/cm^3)
c_2	concentration of H^+ ion	(mol/cm^3)
$^*c_1$	concentration of Cu^{2+} ion in the bulk-electrolyte	(mol/cm^3)
$^*c_2$	concentration of H^+ ion in the bulk-electrolyte	(mol/cm^3)
c_{CuSO_4}	concentration of $CuSO_4$	(mol/cm^3)
$c_{H_2SO_4}$	concentration of H_2SO_4	(mol/cm^3)
g	gravitational acceleration	(= 980 cm/sec^2
ℓ	thickness of hydrodynamic boundary layer	(cm)
u	velocity of upward natural convective flow	(cm/sec)
x	height from lower edge of cathode	(cm)
y	horizontal distance from cathode surface	(cm)

Greek Letters

α_1	densification coefficient of Cu^{2+} ion (= $d\ln\rho/dc_1$)	(cm^3/mol)
α_2	densification coefficient of H^+ ion (= $d\ln\rho/dc_2$)	(cm^3/mol)
β_{CuSO_4}	densification coefficient of $CuSO_4$ (= $d\ln\rho/dC_{CuSO_4}$)	(cm^3/mol)

$\beta_{H_2SO_4}$	densification coefficient of H_2SO_4 (= $d\ln\rho/dC_{H_2SO_4}$)	(cm^3/mol)
*ν	kinematic viscosity of bulk-electrolyte	(cm^2/sec)
ρ	density of solution at a distance y	(g/cm^3)